UiT The Arctic University of Norway

Faculty of Health Sciences

Activity-Based Protein Profiling (ABPP) and functional validation of uncharacterized enzymes in bacterial pathogens *Staphylococcus aureus* and *Klebsiella pneumoniae*

Md Jalal Uddin

A dissertation for the degree of Philosophiae Doctor - May 2024

A dissertation for the degree of Philosophiae Doctor

Activity-Based Protein Profiling (ABPP) and functional validation of uncharacterized enzymes in bacterial pathogens *Staphylococcus aureus* and *Klebsiella pneumoniae*

MD JALAL UDDIN

May 2024

Research Group for Host-Microbe Interactions

Department of Medical Biology

Faculty of Health Sciences

UiT- The Arctic University of Norway

Acknowledgments

This research project has been carried out in the research group of Host-Microbe Interaction (MHI), Faculty of Health Sciences, the Institute of Medical Biology, UiT, The Arctic University of Norway. I express my sincere gratitude to CANS (Centre for New Antibacterial Strategies) for providing financial support for this work. I also thank BioCat and IBA School for providing travel grants for attending courses, conferences, and research stays.

First and foremost, I would like to thank my supervisory team (Associate Professor Christian Lentz, Professor Mona Johannessen, Professor Pål J. Johnsen, and Associate Professor Veronika K. Pettersona) for their valuable feedback and support throughout my PhD journey.

I would like to express my deepest and sincerest gratitude to my main supervisor, Christian Lentz, for the extraordinary opportunity to be a part of his research team. His patience, encouragement, and unwavering support have been pivotal throughout my PhD journey. I really appreciate his consistently maintained open-door policy, whether for small or large discussions. I will always be thankful for his allowing me the freedom to explore my own ideas while ensuring I had the resources to grow into an independent researcher. I am deeply thankful for his trust in my capabilities and his invaluable contributions to my papers and this thesis. Thank you very much, Christian, for everything.

I am also immensely grateful to my co-supervisor, Mona Johannessen, for her enriching discussions, continuous support, and the sharing of her expertise. I am truly grateful for her openness and accessibility throughout this work. Her support, both academic and personal, has been invaluable to me. Thank you for everything.

I would also like to thank my co-supervisors Veronika K. Petterson and Pål J. Johnsen for their contributions, comments, and encouragement during this work.

While working towards a PhD can be an isolating and harrowing experience, I have been fortunate to have a vast network of support. I am grateful to all those with whom I have had the pleasure of working during this project.

My thanks go to all members of HMI, associates, and Labgang for creating such a wonderful work atmosphere. Thanks to the past members of Labgang (Jessin, Mushtaq, Bishnu, Diana, Theresa, Clement). Special thanks to Jessin for being one of the nicest person to me and Didi. A big thanks to all my fellow PhD students (Martin, Gaute, Ken, Srijana, Jeanette, Nadia, Ahmed). Thanks to Martin and Gaute for being such dear friends – sharing all the coffee and movies throughout my journey. Thanks to Ken for discussing *Klebsiella*; I look forward to continuing our discussions and appreciate your help. Thanks to Srijana and Jeanette for all our nice memories. Thanks to Nadia for learning and taking Norwegian classes together and for good memories.

Thanks go to our seniors, PIs, and postdocs for the constructive suggestions and scientific discussions. Thanks to Stephen, Roni, Jonathan, and Hermione for good scientific discussions and motivation.

I would like to thank all lab engineers (Kjersti, Bhupender, and Julia) for their excellent support in ordering chemicals/reagents on time and troubleshooting every lab instrument. Kjersti, thank you very much from the bottom of my heart for your kindness and for being so nice to me. You will always be in my heart. Thanks to all the past and current students in our lab (Wasifa, Sonja, Caroline, Knut, Thomas, Jasmin, Arshad, Balqees, Lukas) and interns. Thanks to Thomas for joining the coffee breaks with us and all the training lessons. I did not have to share an office with my fellow mates, but thanks to my current officemate Kristin Hegstad; your hard work, kindness, and focus on research always motivated me to pursue science.

Heartfelt thanks go to our collaborators at UMC Utrecht, especially Rob Willems, for allowing me to visit your lab to explore and learn about organoids. Thank you, Marcel and Janetta Top, for providing me with new ideas and listening to my thoughts. Thanks to Marco for guiding me through the laboratory facilities and techniques, and for sharing your knowledge during my stay. Julian, Leire, Frerich, Coco, Jesse, Tristan, Leo, Matteo, Michal, and Julia, you were all amazing. Thanks for all the sharing, caring, and birthday celebrations, and for making my stay abroad memorable.

Sincere thanks go to the UiT Proteomics Platform (Jack-Ansgar Bruun and Toril Anne Grønset) and the Imaging Platform (Roy Andre Lysså and Kenneth Bowitz Larsen) for their help and support.

Tromsø, charming as it is, would have been unbearable without the support of those who helped me find my footing and move from one housing to another on this island after losing both of my parents and during the COVID-19 period. I extend my heartfelt thanks to everyone I met and spoke with during this journey. In particular, I am deeply grateful to the Bengali families in Tromsø, some of whom are no less than my family. Jazakallah for everything.

Finally, my heartfelt gratitude goes to my family, and my prayers are for the souls of my father and mother, the most remarkable, supportive, and faithful people in my life. I know you, Baba, would be more than happy, as I have achieved what you always wished for me.

Above all, all praise, thanks, and gratitude go to Allah (SWT), the Almighty and the Most Merciful, for His showers of blessings and guidance throughout my journey and all my hardships.

Tromsø, May 2024

Jalal

Table of Contents

List of Tables

List of Figures

Abbreviations

ABP	Activity-based probe
ABPP	Activity-based protein profiling
FP	Fluorophosphonate
TAMRA	Tetramethylrhodamine
Cy3	Cyanine 3
BODIPY	4,4-difluoro-4-bora-3a,4a-diaza-s-indacene
SHs	Serine hydrolases
GHs	Glycoside hydrolases
TMT	Tandem mass-tag
SILAC	Stable isotope labeling by amino acids in cell culture
LC	Liquid chromatography
MS	Mass spectrometry
CRISPRi	Clustered regularly interspersed short palindromic repeats interference
EPS	Extracellular polymeric substance
ECM	Extracellular matrix
eDNA	Extracellular DNA
CPS	Capsular polysaccharide
LPS	Lipopolysaccharides
TLR	Toll-like receptor
IL	Interleukin
AMR	Antimicrobial resistance
AMP	Antimicrobial peptide
5 FU	5-Fluorouracil
SDS	Sodium dodecyl sulfate

List of papers

Paper I

Md Jalal Uddin, Hermen S. Overkleeft and Christian S. Lentz. **Activity-Based Protein Profiling in Methicillin-Resistant *Staphylococcus aureus* Reveals the Broad Reactivity of a Carmofur-Derived Probe**. Chembiochem. 2023 Nov 2;24(21):e202300473. doi: 10.1002/cbic.202300473. Epub 2023 Aug 29.

Paper II

Md Jalal Uddin, Hermen S. Overkleeft, Mona Johannessen and Christian S. Lentz. **Activity-Based Protein Profiling Identifies an Alpha-amylase Family Protein Contributing to the Virulence of Methicillin-Resistant *Staphylococcus aureus*.**

(Manuscript)

Paper III

Md Jalal Uddin, George Randall, Jiyun Zhu, Tulsi Upadhyay, Laura van Eijk, Paul B. Stege, Frerich M. Masson, Marco C. Viveen, Matthew Bogyo, Matthias Fellner, Marcel R. de Zoete, Mona Johannessen and Christian S. Lentz. **Activity-Based Protein Profiling Identifies *Klebsiella pneumoniae* Serine Hydrolases with Potential Roles in Host-Pathogen Interactions.**

(Manuscript)

Summary

S. aureus and *K. pneumoniae* often reside in the human body as harmless commensal bacteria but can cause various infections once they breach the host's immune defenses. These pathogens are increasingly difficult to treat due to the emergence of antibiotic-resistant strains such as methicillin-resistant *S. aureus* (MRSA) and carbapenem-resistant *K. pneumoniae*. Activity-based protein profiling (ABPP) is a powerful chemoproteomic method to uncover potential new druggable targets and to identify off-target effects of drugs. It uses functionalized covalent enzyme inhibitors called activity-based probes (ABPs) for directly capturing enzyme activity changes within their native biological systems. To search for new putative targets of antimicrobial drugs, this study aimed to identify active enzymes in these pathogens using ABPP and to validate them in the context of bacterial physiology and host-pathogen interactions.

In Paper I, multiple classes of enzymes were identified in MRSA using an ABP derived from carmofur, which is registered as an anti-neoplastic agent and also possesses antimicrobial and anti-biofilm properties. The broad reactivity and somewhat promiscuous nature of the carmofur probe suggest potential side effects and therapeutic implications in clinical settings due to the inactivation of multiple enzymes in both humans and microbes.

In Paper II, two previously uncharacterized glycosidases were identified in MRSA. Functional studies using CRISPRi-induced gene silencing showed that a protein from the α-amylase family, trehalase C (TreC), plays a role in bacterial virulence during infections of wax moth larvae *Galleria mellonella.*

In Paper III, seven previously uncharacterized serine hydrolases were identified in *K. pneumoniae*, most of which show little or no homology with the proteomes of gut commensal bacteria and humans. Functional validation using transposon mutants deficient in either of the putative lysophospholipase PldB, esterase YjfP, and patatin-like phospholipase YchK revealed pronounced growth defects in human-derived colonic organoid co-culture models and reduced virulence in *G. mellonella* infection models.

Overall, this study provides substantial insights into the molecular mechanisms underlying the virulence and cellular physiology of *S. aureus* and *K. pneumoniae,* offering promising targets such as TreC, PldB, YjfP, and YchK for developing new antimicrobial strategies. Inhibiting these enzymes could synergize with existing antibiotics and augment human immune defenses

1. Introduction

The rapid spread and emergence of antibiotic resistance among pathogenic bacteria to conventional chemotherapy is a significant global health concern due to the scarcity of novel antibacterial drug developments. Understanding the molecular mechanisms behind bacterial pathogenesis and virulence is crucial for both academic and clinical purposes, especially in light of the increasing resistance to existing antibiotics and antibacterial agents. Activity-based protein profiling (ABPP), a chemoproteomic technique, has recently become an attractive approach for dissecting the basis of these dynamic processes. It uses small molecules functionalized covalent enzyme inhibitors called activity-based probes to identify and characterize (unknown) protein functions, study key regulators and visualization of enzymatic activity in various disease states and discover and evaluate potential new enzyme inhibitors.

This thesis focuses on screening and identifying novel functional enzymes using ABPP within the bacterial pathogens *Staphylococcus aureus* and *Klebsiella pneumoniae*. Additionally, validates the role of some previously uncharacterized enzymes within bacterial physiology and the dynamics of host-pathogen interactions. This study will increase the understanding of the importance of using small molecule probes to search for new antibacterial targets that might work in combination with existing antibiotics and human immune defenses to combat bacterial infections.

1.1 Bacterial pathogens

Infectious diseases represent a considerable threat to the humankind, contributing to the global burden of diseases and ranking among the top three causes of death worldwide, alongside cancer and cardiovascular diseases[1-4] . The rapid spread of these diseases is exacerbated by globalization, overpopulation, and the interconnectedness of communities, posing serious public health concerns, especially in low-resource settings with inadequate infrastructure and poor healthcare access[4,5].

Bacterial pathogens, mainly those resistant to multiple drugs, play a significant role in this threat, accounting for about 54% of all emerging infectious diseases[6]. Among these, the ESKAPE pathogens (*Enterococcus faecium*, *Staphylococcus aureus*, *Klebsiella pneumoniae*, *Acinetobacter baumannii*, *Pseudomonas aeruginosa*, and *Enterobacter* species) are especially notorious for their drug resistance and the challenges they pose to healthcare systems[7]. *Staphylococcus aureus* and *Klebsiella pneumoniae*, two of the most formidable among these,

exemplify the difficulties in combating bacterial infections due to their ability to develop resistance to multiple antibiotics, leading to severe and often fatal infections[8,9].

The misuse of antibiotics, together with inadequate public health infrastructure and disease surveillance, especially in resource-limited countries, hampers the effective response and management of infectious diseases[10,11]. This situation is further complicated by global trade and intensive livestock systems that facilitate disease transmission between species, and the movement of people and goods across borders, making disease containment increasingly challenging[12] (reviewed in [13]). Therefore, there is an urgent need for improved diagnostics, treatments, and management strategies to combat infectious diseases.

1.1.1 *Staphylococcus aureus*

Staphylococcus aureus was first reported by Scottish physician Sir Alexander Ogston in 1880 from surgical abscess fluid[14]. He observed unique micrococci clustering together like grapes; thereby, he coined the organism *Staphylococcus*, a term originated from the Greek words 'Staphyle' and 'kokkos,' denoting 'bunch of grapes' and 'berries,' respectively[15,16]. A few years later, in 1884, Rosenbach successfully identified and cultivated staphylococci from individuals and was given the name *Staphylococcus aureus* due to its unique yellowish pigmentation of colonies derived from the production of staphyloxanthin[17,18]. *S. aureus* is a versatile Gram-positive bacterium with the unique ability to live as harmless commensals but has the potential to cause infections in both humans and animals. These bacteria are typically 0.5-1.0 μm in diameter, aerobic and/or facultatively anaerobic, catalase positive, oxidase negative, coagulase-positive, and non-spore-forming, with some strains even capable of forming capsules[19-21]. The cell wall of *S. aureus* is primarily composed of peptidoglycan (PG) and wall teichoic acid (WTA), which create a rigid, insoluble, heterogeneous matrix[22,23]. This bacterium can grow in high-salt conditions with up to 10% NaCl concentration[24]. Additionally, it can produce a range of toxins, including α, β, γ, δ, exfoliative, and enterotoxins, leading to hemolytic and cytolytic activities[25,26]. Nearly 140 years since its discovery, *S. aureus* remains a major cause of human disease and is extensively studied staphylococcal species alongside *Staphylococcus epidermidis*[27].

1.1.3 Colonization and/or infection of *S. aureus*

S. aureus is a versatile and opportunistic bacterium that resides in different parts of the human body as a harmless commensal, yet it also has the potential to become a formidable pathogen,

capable of causing a wide range of infections[27]. Humans are frequently colonized by *S. aureus* either for short or long periods at various stages throughout life[28]. The primary site of *S. aureus* colonization in humans is the anterior nares (nostrils). Around 20-30% of the healthy adult population asymptomatically carries *S. aureus* in their nostrils as a part of their normal flora[29,30]. However, it can also temporarily colonize other parts of the body, including the skin, throat, perineum, vagina, and gastrointestinal tract[31-33].

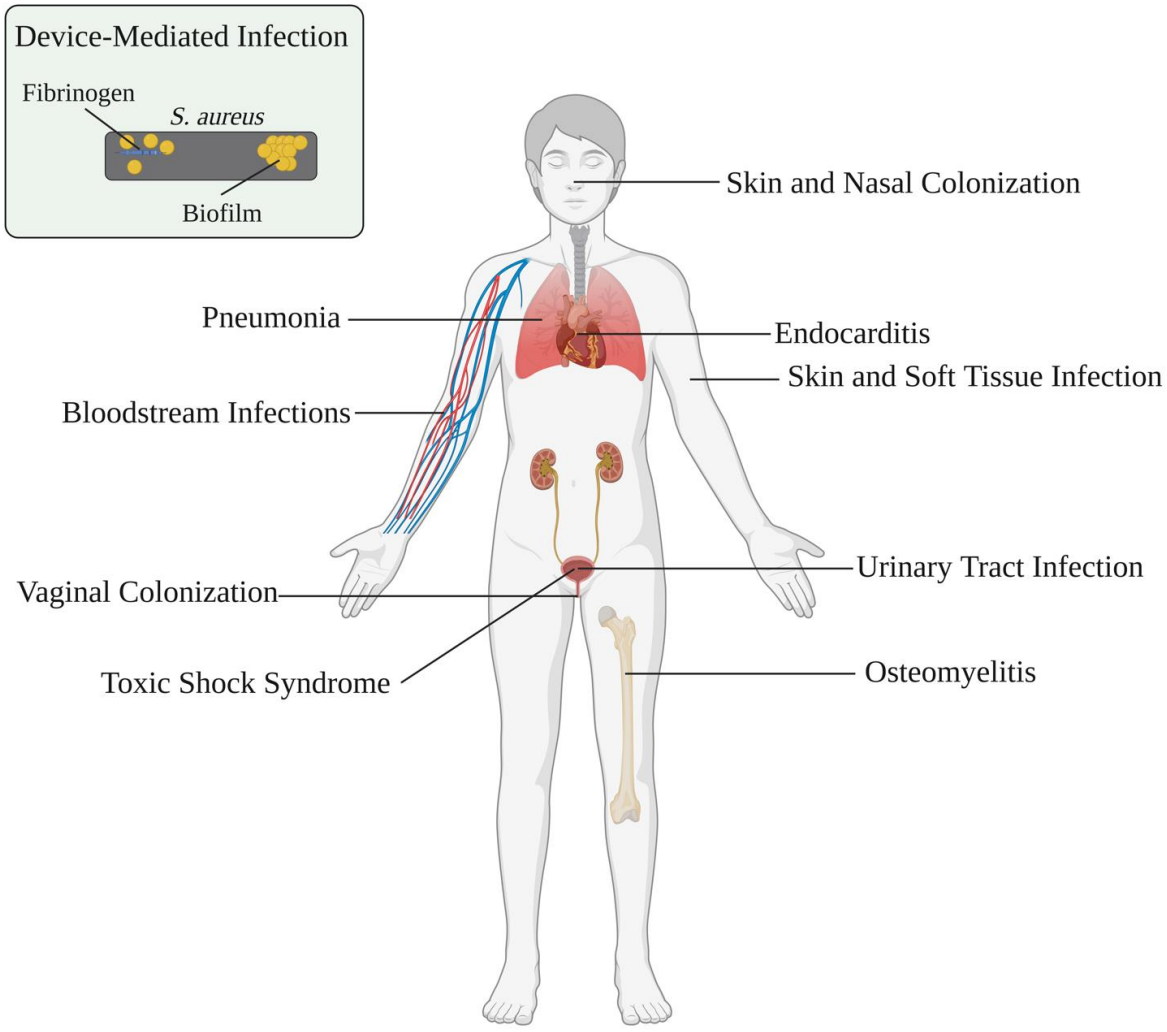

Figure 1. *S. aureus* colonizes asymptomatically but can cause various infections. *S. aureus* has the capability to attach to and invade various human body tissues. The colonization of the skin and nasal passages increases the likelihood of developing pneumonia, sepsis, endocarditis, infections of the urinary tract, osteomyelitis, and infections of the skin and soft tissues. Infections related to medical devices can happen when these devices are covered with host substances like fibrinogen, creating a perfect environment for *S. aureus* to attach, colonize, and form biofilms. The figure was created with biorender.com. and adapted from [34].

Colonization is recognized as a critical risk factor for the onset of *S. aureus* infections, notably in individuals who have compromised skin integrity or weakened immune systems[35]. The likelihood of colonization and the progression to infection is influenced by many factors, including the various bacterial adhesion and immune-modulating proteins, host factors, and the presence of local microbiota. At the interface between host and microbe, there is a constant battle between the host's immune defenses and the pathogenic capabilities of the bacteria. Humans are defended against bacterial infection through innate and adaptive immune responses, and physical barriers like skin, epithelial layers, and mucous membranes. The skin barrier, protected by the secretion of antimicrobial peptides such as defensins and cathelicidins, usually prevents *S. aureus* from penetrating[29,36]. However, any breach of these barriers significantly increases the risk of infection, which can vary from minor skin and soft-tissue infections (SSTI) to life-threatening conditions, including endocarditis, meningitis, osteomyelitis, hemolytic pneumonia, bacteremia, toxic shock syndrome, and device-related infections[27,37].

1.1.4 Virulence factors of *S. aureus*

The term "virulence" originates from the Latin "virulentus" which means "full of poison". It describes a pathogen´s capacity to cause disease or infection, effectively quantifying its pathogenicity[38,39]. Bacteria possess various virulence factors that enhance their ability to cause disease[40,41]. These factors are important for successful colonization and proliferation, leading to tissue damage and infection, and they play an essential role in evading host defense mechanisms (reviewed in [42,43])[44]. These virulence factors are encoded by genes located both on the bacterial chromosome and extrachromosomal elements, often present on mobile genetic elements (MGEs) such as plasmids, pathogenic islands, or bacteriophages[45,46].

S. aureus can produce various virulence factors, which are crucial for its ability to adhere, invade, and cause disease within the host. These include over 24 cell wall-anchored (CWA) proteins, a plethora of toxins, and extracellular enzymes that facilitate host colonization and infection (**Table 1**) (reviewed in[34,47-49]). Among the cell wall-anchored proteins, key components are the microbial surface components recognizing adhesive matrix molecules (MSCRAMMs), including fibronectin-binding proteins, clumping factors, and Protein A, which are vital for initial adhesion to host tissues. Additionally, *S. aureus* produces multiple toxins contributing to tissue damage and the immune system disruption. The secreted proteins encompass various extracellular enzymes, such as proteases, lipases, and hyaluronidases,

crucial for penetrating host tissues, evading the immune response, and promoting bacterial proliferation.

Table 1. Examples of *S.* aureus virulence factors involved in pathogenesis. The table is based on [34,47,48].

Process involved with virulence	Protein/protein group	Associated molecule(s)/Bacterial determinant(s)	Abbreviation	Role in pathogenesis (examples)	References
Adhesion	CWA-MSCRAMM	Fibronectin binding protein A, B	FnBPA, FnBPB	Aids cell adhesion and host cell internalization	[50,51] & reviewed in[47]
	CWA-MSCRAMM	Clumping factor A, B	ClfA, ClfB	Facilitates the nasal colonization and immune evasion	[52,53] & reviewed in[47]
	CWA-MSCRAMM	Serine-aspartate repeat proteins C, D, E	SdrC, SdrD, SdrE	Binding to desquamated nasal epithelial cells and/or keratinocytes *in vitro*	[54,55]& reviewed in[34,47]
	CWA-MSCRAMM	Bone sialoprotein-binding protein	Bbp	Adhesion to ECM	[56] & reviewed in[47]
	CWA-MSCRAMM	Collagen	Cna	Adhesion to collagen-rich tissue	[57,58]
	CWA-NEAT motif Family	Iron-regulated surface determinant A, B, H	IsdA, IsdB, IsdH	Iron acquisition and immune evasion	[59-62]
	CWA- G5-E repeat Family	*S. aureus* surface protein G	SasG	Binding to desquamated nasal epithelial cells *in vitro*	[63,64]
	CWA structurally uncharacterized	*S. aureus* surface protein X	SasX	Biofilm formation, cell aggregation, and squamous cell adhesion	[65] & reviewed in[47]
	Tandemly repeated three-helical bundles family	Protein A	SpA	Inhibition of opsonophagocytosis and inflammation	[66,67]& reviewed in[34,47]
	SERAM	Extracellular adhesive protein	Eap	Impaired function in neutrophil and block complement activation	[68,69]
	SERAM	Coagulases	Coa, vWbp	Ability to evade the host's immune response and protect the bacterium during abscess development and sepsis	[70-72]
	Cell-wall component	Wall teichoic acid	WTA	Facilitates the nasal colonization	Reviewed in [73] &[74]
	Noncovalent attached cell proteins / major murein hydrolase	Autolysin	Atl	Aids host cell internalization and biofilm formation	[75,76]
	Cytotoxin	α-hemolysin/ α-Toxin	Hla	Enhanced host survival, inflammation, and tissue injuries	[77-79]
	Exotoxins	Enterotoxins	SEs	Causes food poisoning and tissue injuries	[80,81] & reviewed in[82]
	Exotoxin	Toxic shock syndrome toxin-1	TSST-1	Inhibit host immune responses	[83-85]
	Secreted enzyme	Hyaluronidase	HysA	Enhanced intracellular survival and inhibition of proinflammatory cytokine expression	[86-88]

Ability to produce toxins and enzymes	Exoenzyme	Staphylokinase	Sak	Activates host plasminogen and promotes bacterial dissemination	[89,90] & reviewed in[48]
	Serine protease	V8 protease or GluV8	SspA	Contributes to *S. aureus* immune evasion and dissemination by breaking down self and host proteins	[91,92] & reviewed in[48]
	Metalloprotease	Aureolysin	Aur	Contributes to *S. aureus* immune evasion and prevent complement activation	[93-95]
	Cysteine proteases	Staphopain A, B	ScpA, SspB	Prevents *S. aureus* from phagocytosis and thrives intracellularly in macrophages and dendritic cells	[96-98]
	Serine proteases	Serine protease-like proteins A to F	SplA to SplF	Role in shaping the *S. aureus* proteome	[99,100]
	Phospholipases	β-toxin and phospholipase C	PI-PLC	Promote survival of *S. aureus* in human blood and neutrophils	[101-103]
	Glycerol ester hydrolases	lipases 1 and 2	SAL1 and SAL2	Promote bacterial survival in biofilms and abscesses	[104,105]
	Acetyl esterase/lipase	Fluorophosphonate-binding hydrolases B	FphB	Reducing the colonization efficiency of *S. aureus* in a mouse model	[106]

CWA: Cell wall anchored protein, ECM: Extracellular Matrix, MSCRAMM: microbial surface component recognizing adhesive matrix molecule, NEAT: near iron transporter family, SERAM: secreted expanded repertoire adhesive molecules.

The expression of these virulence factors is highly adaptive and depends on the pathogen's requirements at various stages of infection; for example, adhesion proteins are predominantly expressed during the initial colonization stages, whereas the production of toxins becomes more pronounced during later stages of infection. Moreover, these factors support the bacteria's long-term persistence within the host by enabling it to evade detection or killing by the immune systems. The regulation of these virulence factors is precise and coordinated, changing with growth factors and conditions[107]. Altogether, the extensive array of virulence factors produced by *S. aureus* underscores its versatility as a pathogen and its capacity to cause diverse human infections.

1.1.5 *S. aureus* biofilm

A biofilm is often described as a complex, heterogeneous microbial community where cells adhere to a surface or to other cells and are surrounded by a protective extracellular polymeric substance (EPS)[108-110]. This substance, also known as the extracellular matrix (ECM), varies in composition based on environmental factors and bacterial strain. It generally comprises elements like host factors, polysaccharides, proteins, and extracellular DNA (eDNA)[111-113]. The recent perspective on biofilm formation highlights its dynamic nature, noting that biofilms do

not always conform to the classic mushroom-shaped structure and exhibit diverse formation scenarios. Biofilms can appear as either single or multiple discrete aggregates, or as more continuous films. These formations consist of microbial aggregates that are either attached to or associated with a surface (outstanding reviewed in [114]). Biofilms can form on various surfaces, including medical devices, industrial or potable water systems, and human tissues[115,116].

Biofilms act as formidable barriers against immune system attacks and antibiotic treatments during infections. The biofilm matrix can prevent the penetration of immune cells, leading to inefficient phagocytosis and increasing the bacteria's ability to resist antibiotics[117,118]. Additionally, cells within a biofilm can survive exposure to antibiotics without developing inheritable genetic resistance, termed as antibiotic tolerance, which reverts to normal sensitivity when they return to the planktonic state[119]. This tolerance may result from limited antibiotic diffusion within the biofilm or the presence of metabolically dormant persister cells that are inherently resistant to antibiotics[119,120]. The ability of *S. aureus* to develop biofilms is closely linked to its involvement in various chronic infections, such as osteomyelitis and endocarditis. Moreover, *S. aureus* has become particularly notorious for its ability to establish biofilms on indwelling medical devices, significantly complicating clinical outcomes by increasing morbidity and mortality rates associated with biofilm-related infections (reviewed in[121]). The challenge in treating *S. aureus* biofilm infections lies in their resilience; often, eradicating the infection requires not only the use of antibiotics but also the physical removal of the infected device or tissue[121].

The development of a biofilm is traditionally characterized by three major events: initial attachment of planktonic cells to a surface; maturation of the biofilm as cells proliferates and produce an extracellular matrix; and eventual dispersal, where cells revert to a planktonic state, enabling the seed new sites for biofilm formation[122,123]. Moormeier et al. have proposed the addition of two stages, multiplication, and exodus, to outline a five-stage process in *S. aureus* biofilm development: attachment, multiplication, exodus, maturation, and dispersal[124,125].

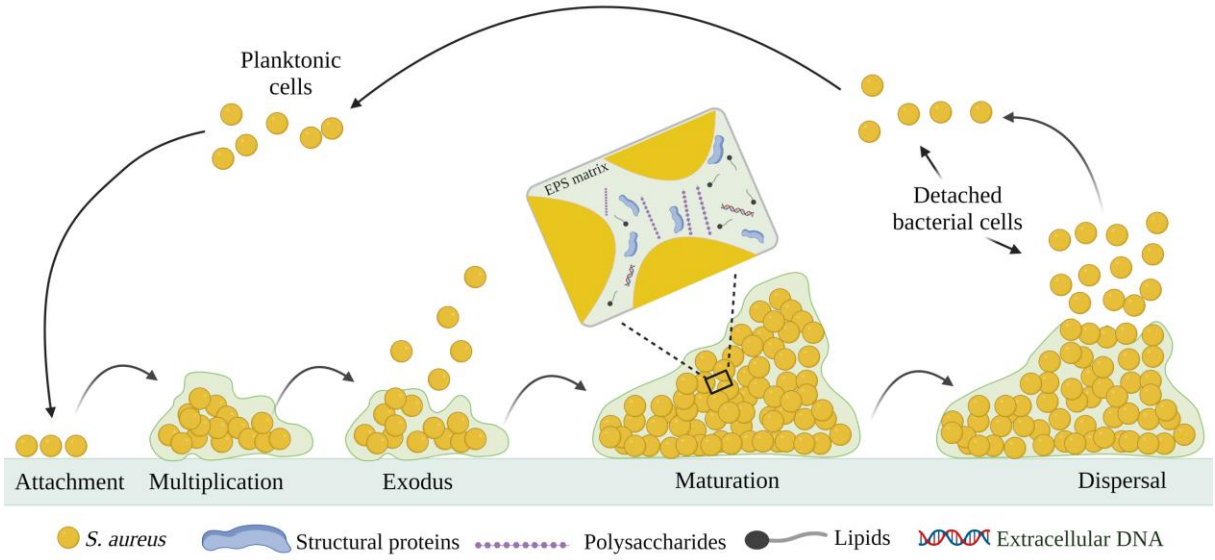

Figure 2. The development of *S. aureus* biofilms is characterized by five distinct stages. Initially, planktonic *S. aureus* adheres to either living (biotic) or non-living (abiotic) surfaces. Following attachment, the cells form a confluent 'mat', encapsulated within an extracellular matrix made of proteins and extracellular DNA (eDNA). A phase of exodus occurs next, during which a subpopulation of cells is detached from the main biofilm body. In the maturation stage, cells become interconnected through adhesive forces, leading to the substantial formation of the extracellular matrix and three-dimensional microcolonies. Finally, regulatory mechanisms trigger cell dispersal through the activation of proteases and/or phenol soluble modulins (PSM), facilitating the spread of cells to new locations and potentially initiating new biofilm formations. The figure was created with biorender.com. and modified based on[124].

Attachment involves the adhesion of *S. aureus* cells to both biotic and abiotic surfaces. On biotic surfaces (such as host tissues), this process is facilitated by cell-wall anchored proteins that recognize specific host matrix molecules. For abiotic surfaces, like medical devices, attachment is influenced by the surface properties of the bacteria and the physiochemical characteristics of the device[126]. Studies have shown that the net charge of teichoic acids, along with specific surface proteins such as the major autolysin of *S. aureus*, known as Atl, which is essential for daughter cells separation during cell division, plays a role in the initial phase of biofilm formation[75,127,128]. Among the key proteins involved in attachment are MSCRAMMs, which bind to various host matrix components, including fibronectin, fibrinogen, and collagen, playing a vital role in the binding of cells to host tissues (outstanding reviewed in[129]). These proteins, alongside others such as fibronectin-binding proteins (FnBPA and FnBPB)[130], clumping factors (ClfA and ClfB)[131], and serine-aspartate repeat family proteins (SdrC, SdrD, and SdrE)[54] initiate cell adherence and biofilm development.

Following the initial attachment, *S. aureus* cells enter a multiplication phase in the presence of sufficient nutrients, during which the adherent cells divide and aggregate, aided by factors that promote cell-to-cell interactions[124]. Some proteins, including the MSCRAMMs, FnBPs, and ClfB, serve dual purposes in both attachment and multiplication phases[124,132], whereas other CWA proteins, such as Protein A[133], SasC[134], and Bap[135], are shown to play roles in biofilm multiplication. The exodus phase represents an early dispersal event characterized by the release of cell subpopulations and the restructuring of the biofilm[124]. This is facilitated by the regulated, nuclease-dependent degradation of eDNA. This phase highlights the transition in biofilm integrity from protein-dependent biofilm structure to both proteins and eDNA[124,125].

An essential event in the maturation process of biofilms across bacterial species involves the development of microcolony structures. These structures enhance the surface area available for nutrient uptake and waste removal and facilitate the spread of biofilm cells to distant sites[136,137]. Most of the ECM is produced during this phase, forming a three-dimensional structure around the biofilm cells[125,138-140]. Studies have shown that the production of the exopolysaccharide poly-N-acetylglucosamine (PNAG), also known as polysaccharide intercellular adhesin (PIA), encoded by the *ica*ADBC genes, plays an important role in biofilm maturation[110,141]. The ica regulator (icaR) negatively regulates these genes expression, with most clinical *S. aureus* isolates containing the ica operon[142,143]. However, ica-independent mechanisms also contribute to biofilm formation, involving components like teichoic acids and MSCRAMMs, as well as reliance on proteins such as Atl and fibronectin-binding proteins (FnBPs)[144].

Dispersal, the final phase of biofilm formation, involves the partial degradation of the ECM by nucleases and proteases, allowing cells to detach and potentially establish infections elsewhere or cause acute conditions such as sepsis[122,145,146]. Several studies have shown that the dispersal of *S. aureus* biofilms is predominantly regulated by the agr quorum sensing system[147-149].

1.1.6 *Klebsiella pneumoniae*

Carl Friedlander first reported *K. pneumoniae* in 1882 as a bacterium from the lungs of patients who had died from pneumonia[150]. *K. pneumoniae* is a member of the Gram-negative *Enterobacteriaceae* family, along with other well-known pathogens, such as *Escherichia coli*, *Salmonella*, and *Shigella*[151]. It is a rod-shaped, facultative anaerobic, encapsulated, and non-motile bacteria, measuring between 0.3 to 2.0 μm in width and 0.6 to 6.0 μm in length, and often shows a slimy, mucoid appearance when grown on agar plates. Biochemically, it is

distinguished by its ability to ferment lactose, catalase-positive, and cytochrome oxidase-negative[152] (reviewed in[153]) .

K. pneumoniae is capable of inhabiting various animal hosts as well as plants. It can also be found in different environments, such as soil, water, and drains. Moreover, *K. pneumoniae* can colonize different body parts including the respiratory tract, gut, nasopharynx, oropharynx, and skin[154,155]. A key feature of *K. pneumoniae* is its encapsulated morphology. It produces a thick extracellular layer of polysaccharides known as a capsule[156]. The capsule promotes immune evasion by hindering host clearance through phagocytosis, enhancing bacterial resistance to intracellular killing, and mimicking host glycans[157-159]. The capsule production is controlled by the capsule polysaccharide (cps) locus, which harbors several genes. *K. pneumoniae* is known to produce at least 79 types of capsules, which differ from one another by the structure and components of the repeating polysaccharide unit in the capsular polysaccharide[156,160,161]. Some strains of *K. pneumoniae* are capable of producing hypercapsules through specific virulence genes, such as *c-rmpA*, *c-rmpA2*, *p-rmpA*, *p-rmpA2*, and *wzy-K1*. This phenotype is commonly found in K1 and K2 serotypes of the capsule and is associated with hypervirulence[162,163].

As a Gram-negative bacterium, *K. pneumoniae* has also lipopolysaccharides (LPS) in its outer membrane, also known as endotoxin. The LPS is made up of lipid A, a core oligosaccharide, and O-antigens, which act as a protective layer against complement-mediated killing. *K. pneumoniae* has at least 8 O-antigen serotypes, of which O1 antigen is the most prevalent among clinical strains[164]. Additionally, two types of fimbriae are widely distributed in *K. pneumoniae*: Type 1 and 3 fimbriae, which are encoded by the *fim* and *mrk*ABCD operons, respectively. These fimbriae play a role in bacterial adhesion, invasion of host cells, and biofilm formation[165].

1.1.7 Colonization and dissemination and/or infection of *K. pneumoniae*

The relationship between *K. pneumoniae* and hosts is complex and variable, where *K. pneumoniae* can exist as either a harmless commensal, an opportunistic pathogen, or a direct pathogen. *K. pneumoniae* is commonly found colonizing the gut as a commensal organism, though the frequency of *K. pneumoniae* carriage differs based on variables like age, geographic location, and recent interactions with healthcare settings (reviewed in [166]).

Studies from the United States and Australia report a community prevalence of gut colonization by *K. pneumoniae* at approximately 4–6%[167,168]. However, this prevalence rises to around 25% among individuals who have recently been in contact with healthcare services in these countries

and England[169]. Notably, countries like Korea, Japan, Singapore, Taiwan, and Malaysia report much higher rates of healthy adult carriage, ranging from 18% to 87%[170,171]. The duration of colonization in the gut is poorly understood but can last over a year[172,173]. The significance of *K. pneumoniae* extends beyond mere colonization in the gut; it has been linked to chronic gastrointestinal diseases, including inflammatory bowel disease and colorectal cancer[174].

Globally, the majority of *K. pneumoniae* infections are opportunistic, linked to healthcare settings, and can lead to extraintestinal infections like pneumonia, urinary tract infections, sepsis, and wound infections, which may progress to bloodstream infections[155] **(Figure 3)**. The most vulnerable groups include neonates, the elderly, immunocompromised, and hospitalized patients. Intestinal carriage of *K. pneumoniae* significantly increases the risk of healthcare-associated infections, especially among intensive care and oncology patients, with a fourfold increased risk of infection[167,175].

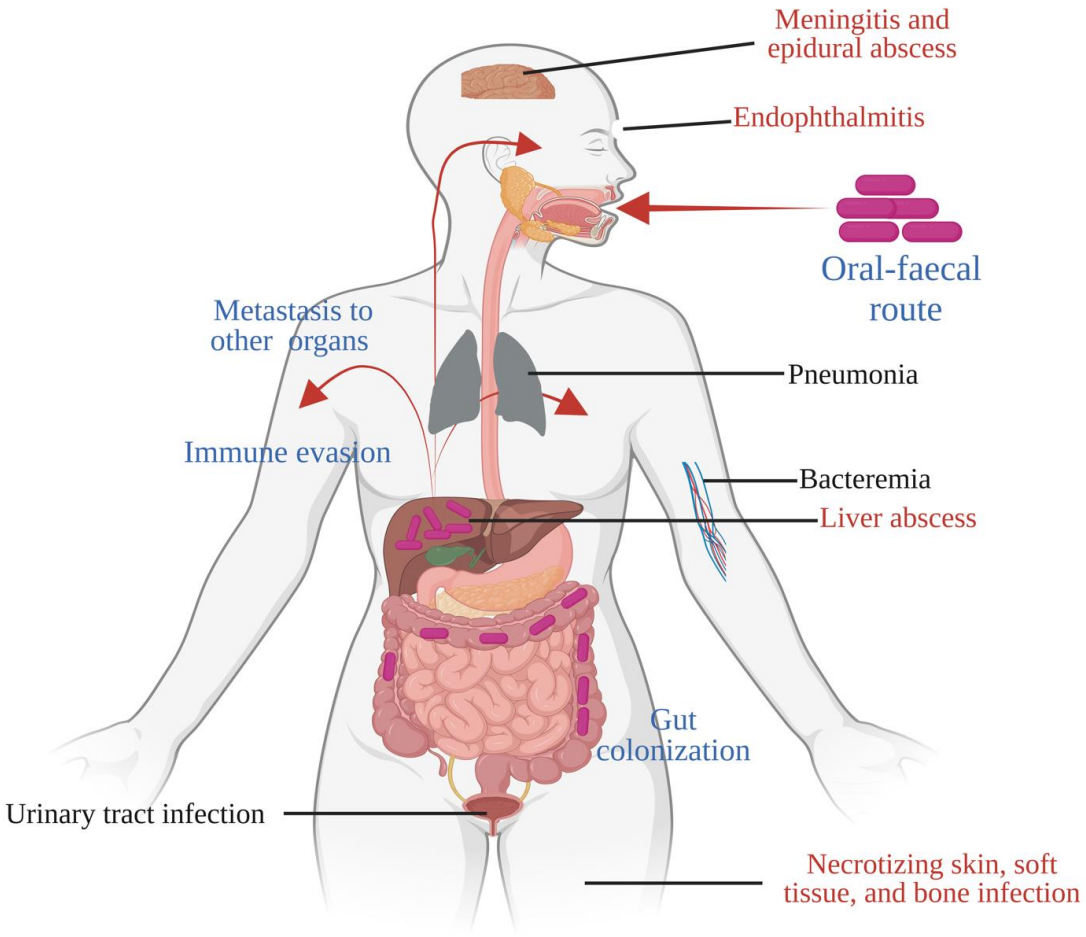

Figure 3. Common sites of *K. pneumoniae* colonization and the associated diseases. *K. pneumoniae* primarily enters the body through the oral- faecal route and can reside mainly in the gastrointestinal (GI) tract. The colonization of the gut increases the likelihood of dissemination to other parts of the body, evading the immune system and causing various extraintestinal diseases. Infections caused by hypervirulent *K. pneumoniae* (indicated in red) typically occur outside of hospital settings and can affect the central nervous system, liver, eyes, and soft tissue. Classical *K. pneumoniae* infections, which are known for rapidly developing resistance to multiple antibiotics, are more likely to arise within hospitals. Both variants of *K. pneumoniae* (highlighted in black) can lead to bloodstream infections, pneumonia, and urinary tract infections. The figure was created with biorender.com. and adapted from [166,176,177].

The treatment of healthcare-associated *K. pneumoniae* infections faces significant challenges due to the emergence of multidrug-resistant (MDR) and carbapenem-resistant *K. pneumoniae* strains. A meta-analysis has shown the mortality rate of carbapenem-resistant strains-associated healthcare infections to be twice as high as that for infections caused by carbapenem-susceptible strains[178]. This increasing resistance crisis has led to a renewed focus on limited treatment options, including the use of colistin and β-lactam/β-lactamase inhibitor combinations, despite

increasing resistance, and an emphasis on developing vaccines and other preventive measures against *K. pneumoniae*[179,180].

Outside healthcare environments, *K. pneumoniae* can be a true pathogen causing severe community-acquired infections in healthy individuals without typical healthcare-associated risk factors[181]. These community-acquired infections include a range of conditions such as endophthalmitis, pneumonia, necrotizing fasciitis, non-hepatic abscesses, meningitis, and pyogenic liver abscesses, even without underlying biliary disease[182]. Such infections, often involving hypervirulent *K. pneumoniae* strains, are known for their potential to infect unusual or multiple sites, which can lead to bacteremia and metastatic spread[182] **(Figure 3)**. Specific host risk factors, such as alcoholism (for pneumonia)[183] and diabetes (for pyogenic liver abscess)[184], have been identified alongside numerous pathogen-related risk factors.

Despite hypervirulent *K. pneumoniae* strains rarely being multidrug-resistant, there are increasing reports of these strains carrying AMR plasmids, highlighting the convergence of AMR and virulence[185,186]. This convergence poses a significant challenge, leading to invasive and difficult-to-treat infections, with at least one fatal outbreak reported in China, where carbapenemase-producing hypervirulent strains are becoming increasingly common[187-190]. The global healthcare community faces a dual challenge: managing the spread of *K. pneumoniae* in healthcare settings, where it acts as an opportunistic pathogen, and addressing the threat of hypervirulent strains that cause severe community-acquired infections. This situation underscores the need for continued vigilance, research into new treatments and preventive measures, and a comprehensive approach to managing both colonization and infection by *K. pneumoniae*.

1.1.8 Virulence of *K. pneumoniae*

Multiple virulence factors are described in *K. pneumoniae* that enhance the severity of infections and/or the propensity to cause disease, including capsular polysaccharides (CPSs), lipopolysaccharides (LPSs), fimbriae, pili, outer membrane proteins (OMPs), and siderophores[191], with more recently identified factors like other iron uptake systems, efflux pumps, and a type VI secretion system (**Figure 4**).

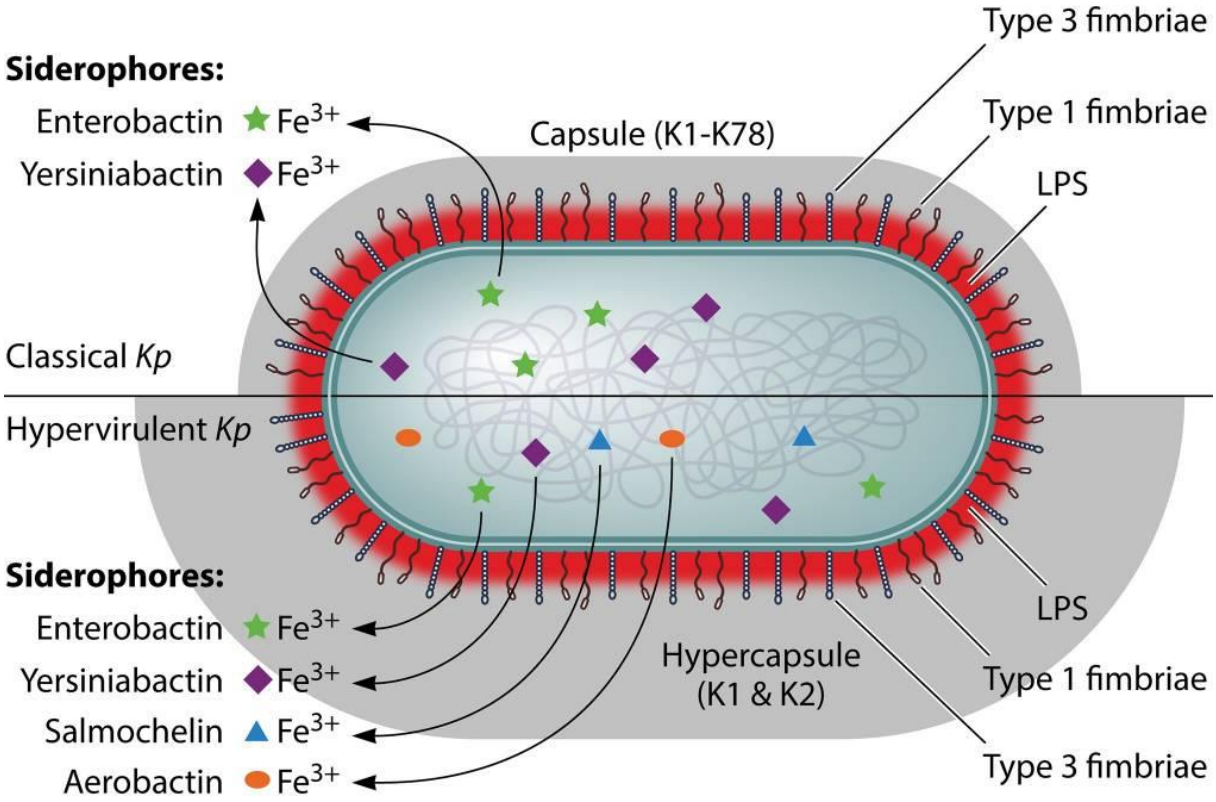

Figure 4. Key virulence factors in both classical and hypervirulent strains of *K. pneumoniae* play a crucial role in initiating infections and ensuring survival within the host. *The figure was reprinted with permission from Microbiology and molecular biology reviews (MMBR):Paczosa et al. (2016)*[191].

Among these, CPS is a key virulence factor for *K. pneumoniae* **(Figure 5)**. It consists of an acid polysaccharide with three to six repeating sugar units. It is synthesized through a Wzy-dependent polymerization pathway under the regulation of the cps gene cluster[192,193]. The process initiates with enzymes called glycosyltransferases assembling sugar units, followed by their transportation to the inner cell membrane, ultimately leading to their export to the cell surface[194]. The thick capsule on the surface of *K. pneumoniae* hinders phagocytosis by blocking its interaction with immune cells. Notably, the K1-CPS variant, found in hypervirulent *K. pneumoniae* strains, significantly reduces macrophage interactions with bacteria compared to less virulent types[195]. Additionally, CPS can diminish inflammatory responses by blocking IL-8 secretion from respiratory epithelial cells and interfering with Toll-like receptor signaling, thus preventing the immune system from responding effectively. CPS also protects the bacteria against antimicrobial peptides released by epithelial cells and inhibits the secretion of these antimicrobial substances by interfering with TLR-mediated responses. Moreover, it can prevent the maturation of dendritic cells and the activation of the complement system, crucial components of the host immune defense[196].

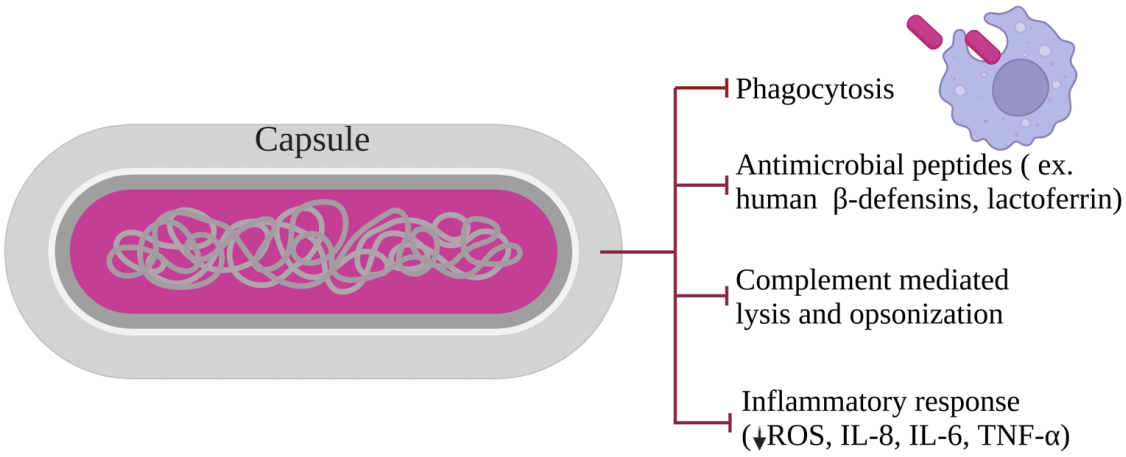

Figure 5. The capsule plays multiple roles in enhancing the virulence of *K. pneumoniae*. It serves several key functions. Firstly, it protects the bacteria from being engulfed and destroyed by immune cells by preventing phagocytosis and opsonophagocytosis. Secondly, the capsule acts as a barrier to the bactericidal effects of antimicrobial peptides, including human beta-defensins 1 to 3 and lactoferrin, by binding these molecules away from the bacterial outer membrane. Thirdly, it prevents complement components, such as C3, from attaching to the bacterial membrane, thereby inhibiting complement-mediated destruction and opsonization. Lastly, the capsule helps avoid the full activation of the immune system. This is evident from the reduced production of reactive oxygen species (ROS), IL-8, IL-6, and TNF-α, by facilitating the activation of a NOD-dependent pathway and preventing LPS from being recognized by immune cell receptors. The figure was created with biorender.com. and modified based on [191].

Another important virulence factor, LPS, especially its O-antigen, blocks the complement system from attacking the bacteria, thus protecting it from immune complement-mediated killing[197]. It also influences the bacterium's resistance to antimicrobial peptides, including those used in treatments. On the other hand, lipid A and core polysaccharides of LPS confer resistance to host-derived antibacterial agents and prevent phagocytosis[198,199]. Moreover, the lipid A part of LPS can trigger a strong immune reaction by activating TLR4, which in turn stimulates cytokine production and recruits immune cells.

Fimbriae (or pili), thin filamentous structures on the bacterial surface, promote attachment to host cells and biofilm formation, enabling infection spread within tissue[194]. Type 1 fimbriae in *K. pneumoniae* are known for their roles in urinary tract infections[200], whereas type 3 fimbriae mediate adhesion to epithelial cells in kidney and lung tissues[201]. Conversely, type 3 and kpc fimbriae mainly contribute to biofilm formation[202,203]. Additionally, the study showed that KPF-28 fimbriae facilitate the adherence of *K. pneumoniae* to human colon carcinoma cell lines, implying their participation in bacterial colonization of intestinal tissue[204].

Siderophores are iron-chelating molecules secreted by bacteria for iron acquisition, essential for bacterial growth and virulence[205]. *K. pneumoniae* produces multiple siderophores, including enterobactin from its core genome and others like salmochelin, yersiniabactin, and aerobactin from its accessory genome[191,206-208]. Each contributes differently to infection severity and immune evasion. Notably, yersiniabactin, is often associated with respiratory infections[209], while aerobactin provides iron for *K. pneumoniae* replication and contributes to inducing inflammation and bacterial dissemination[210].

Outer membrane proteins (OMPs), like OmpA, can suppress inflammatory responses in airway epithelial cells, prevent phagocytosis, and resist host antimicrobial molecules[199,211]. Additionally, other essential parts of OMPs, like porins, play an important role in the uptake of nutrients and expelling harmful substances, including antibiotics, from the bacteria[212]. Furthermore, efflux pumps, particularly AcrAB, are recognized for their role in antibiotic resistance and virulence by pumping out antibiotics, antimicrobial peptides, and other harmful substances to the outside of the bacteria[213,214].

The type VI secretion system (T6SS), a syringe-like structure for delivering effector molecules and toxins into cells, is found in various Gram-negative bacteria, including *K. pneumoniae*[215]. Recent studies have started to characterize the effectors of the Type VI secretion system (T6SS) in *K. pneumoniae*. The necessity of phospholipase D family protein (PLD1) for virulence has been demonstrated in the hypervirulent strain Kp52.145 in a pneumonia model[216]. Likewise, in the carbapenemase-producing strain HS11286, the phospholipase Tle1KP has been shown to facilitate both inter- and intra-species killing, and its secretion is increased by antibiotics[217]. The T6SS, found in both the core and accessory genomes, enhances competitiveness against other bacteria in colonization sites and increases survival in infection sites[218].

In summary, these virulence factors of *K. pneumoniae* act as a complex arsenal that enhances the bacterium's pathogenicity, enabling the bacterium to invade host tissues, evade the immune response, and establish infections.

1.1.9 Antibiotic resistance

The emergence of antibiotic resistance is a major problem in treating bacterial infections. Numerous public health institutions have described the rapid increase of antibiotic-resistant bacteria as a “crisis” or a “nightmare scenario”, warning of “catastrophic outcomes”[219]. In 2013, the Centers for Disease Control and Prevention (CDC) declared that humankind has entered a period known as the “post-antibiotic era,”[220] and by 2014, the World Health Organization

(WHO) warned that the situation regarding antibiotic resistance is reaching critical levels [221](reviewed in [222]).

Since Alexander Fleming discovered penicillin in 1928, antibiotics have dramatically changed the era of modern medicine, offering hope against bacterial infections[223]. However, our reliance on antibiotics has come at a significant cost, a concern Fleming himself highlighted in his 1945 Nobel Prize acceptance speech[224]. He warned about the risks of antibiotic misuse and the ease with which bacteria could develop resistance if not treated with adequate doses. Despite his warnings, these concerns were overlooked, leading to the current crisis of antibiotic resistance (**Figure 6**) (reviewed in [225]).

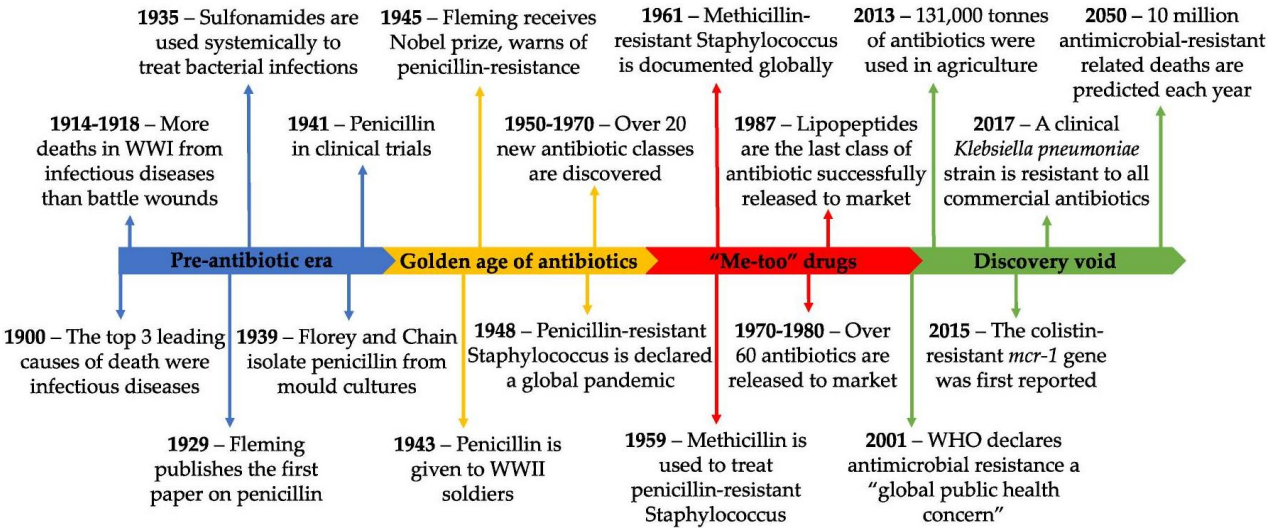

Figure 6. An overview of key milestones in the timeline of antibiotic resistance. WHO stands for the World Health Organization; WWI/II refers to World War I and World War II. *Browne et al. (2020)*[225].

The primary concern lies in the increasing frequency of treatment failures. Infections that were once easily treatable with standard antibiotic therapy are now becoming difficult, if not impossible, to cure. This situation is further exacerbated by the slow pace of new antibiotic development. Pharmaceutical research and development have not kept pace with the rate of resistance development. The discovery and approval of new antibiotics are complex, time-consuming, and costly processes, resulting in fewer new drugs reaching the market[226-228]. The WHO now recognizes antimicrobial resistance as one of the top ten global public health challenges facing humanity[229]. It is predicted that by 2050, antibiotic-resistant infections could result in up to 10 million deaths annually and lead to a loss of productivity that could cost the global economy up to $100 trillion[230,231].

Among the most concerning gram-positive pathogens is methicillin-resistant *Staphylococcus aureus* (MRSA). MRSA strains emerged just two years after methicillin was introduced into clinical practice to fight *S. aureu*s infections[232]. MRSA now represents a significant threat to global health, leading to complications in both community and healthcare settings. The rise of MRSA has necessitated the use of second-line antibiotics, which are often associated with less favorable outcomes and an increased risk of severe, life-threatening infections[233]. MRSA claims more American lives annually than HIV/AIDS, Parkinson's disease, emphysema, and homicide combined[234,235]. In 2019, MRSA was responsible for over 100,000 deaths worldwide[236].

On the other hand, the Gram-negative carbapenemase-prodcucing *K. pneumoniae* is becoming increasingly concerning due to its resistance to nearly all available antibiotic drugs, leading to scenarios reminiscent of the pre-antibiotic era[237]. The emergence of multidrug-resistant (MDR) and, more alarmingly, pandrug-resistant strains of *K. pneumoniae* has significantly affected medical practices in all fields[238]. As a result, in 2017, the WHO declared *K. pneumoniae* a critical pathogen that urgently requires new treatment options[9]. Furthermore, in 2019, the CDC identified carbapenem-resistant *K. pneumoniae* as an urgent threat to human health. In 2020, the European Antimicrobial Resistance Surveillance Network, along with the Central Asian and European Surveillance of Antimicrobial Resistance, reported that 38% of invasive *K. pneumoniae* were resistant to at least one category of antibiotic, with resistance to third generation cephalosporins being the most common[239]. In Europe, it is reported that infections caused by MDR *K. pneumoniae* exceed 90,000 cases annually, leading to more than 7,000 deaths, and accounting for 25% of the total disability-adjusted life years lost[240].

Bacteria have a remarkable ability to rapidly develop resistance to new antibiotics through various mechanisms (reviewed in[241-243]) (**Figure** 7). This includes spontaneous resistance that arises due to the mutations, as well as horizontal gene transfer. The key strategies bacteria use to resist antibiotics include the inactivation of drugs, modification of drug targets, the use of efflux pumps to remove drugs from the cell, decreased cell membrane permeability to prevent drug entry, and increased production of target molecules to counteract the drug's effect.

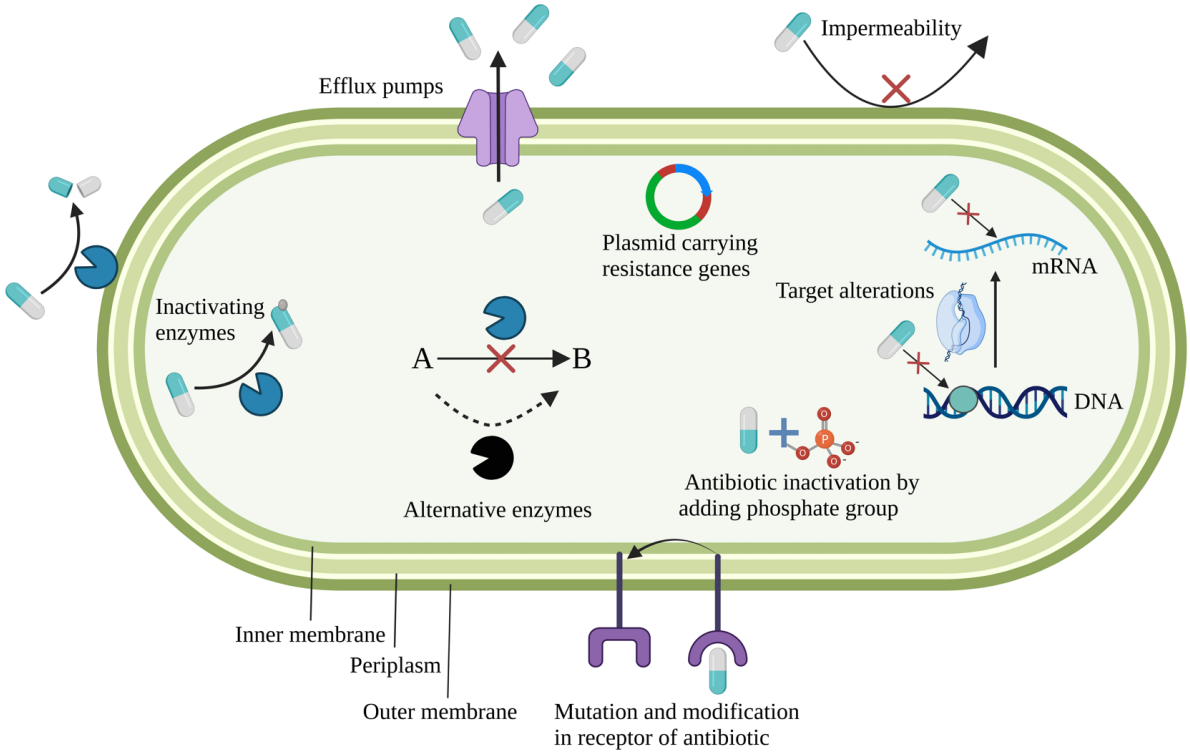

Figure 7. Strategies for different antibiotic resistance mechanisms are illustrated here, using gram-negative bacteria as an example. The figure was created with biorender.com. and adapted from [241-243].

To address the growing antibiotic resistance crisis, novel therapeutic strategies are urgently needed. These should focus not only on the development of new drugs but also on ensuring no resistance development and helping immune systems to effectively combat pathogens.

1.1.10 Targeting bacterial virulence as a new strategy to combat antibiotic-resistant pathogens

Targeting bacterial virulence offers a novel approach to treating bacterial infection, particularly antibiotic-resistant pathogens, focusing on neutralizing the mechanisms bacteria use to infect and damage their hosts rather than killing them completely (reviewed in[244-248]). This approach involves inhibiting virulence factors - molecules like toxins and enzymes that enable bacteria to invade host tissues and evade the immune system. By disarming bacteria, the strategy aims to reduce their infectivity, allowing the immune system to clear the infection more easily. Unlike conventional antibiotics that aim to eliminate bacteria, which often lead to resistance development, targeting bacterial virulence factors provides a less confrontational approach, potentially minimizing or reducing the likelihood of resistance development. In addition, this approach focuses on targeting not just bacterial viability but also functions essential for infection, such as those virulence factors necessary for causing host damage and disease. The

major advantages of this strategy are that it expands the range of bacterial targets, helps in preserving the host's natural microbiome, and exerts less selective pressure, which could result in decreased resistance. However, it poses challenges due to the complexity of bacterial virulence mechanisms and variability in human immune responses. Although it is currently in the early stages of research, this strategy holds promise as a complementary or alternative solution to traditional antibiotics in the fight against multidrug-resistant bacterial infections[247,249].

Since most virulence factors are secreted enzymes and proteins that remain functionally active during pathogenesis and play pivotal roles in a pathogen's ability to cause disease, robust tools for their precise identification and characterization are essential. Additionally, understanding the mechanisms of action of antivirulence agents and the ability to monitor the pathogen's response and resistance to these interventions is crucial.

2.1. Activity-Based Protein Profiling (ABPP)

Recent developments in 'omics'-based approaches have significantly advanced our understanding of the genetic, transcriptomic, and proteomic aspects of bacterial cells[250]. Despite this progress, these techniques are often inadequate in accurately identifying specific functional key regulators of a given cellular state at the protein level. This is particularly because of catalytic active enzymes are typically regulated by post-translational modifications and protein complex formation [251,252]. This means that changes in their activity may not always correlate with their expression levels as determined by conventional genomic or proteomic methods. To overcome this challenge, a chemoproteomic approach called activity-based protein profiling (ABPP) has been developed. ABPP uses active-site directed small-molecule probes called activity-based probes (ABPs) for directly capturing enzyme activity changes within their native biological systems, thus offering a more precise insight into enzyme function and regulation than traditional 'omics' methods alone. ABPs rapidly and irreversibly bind with their target enzymes by covalently modifying the active site of catalytically active enzymes via a specific chemical reaction (reviewed in[253-257]).

ABPs typically consist of three components (**Figure 8A**): 1) a reactive group (also referred to as a 'warhead'), often an electrophilic group that covalently binds with a conserved active site nucleophile; 2) a linker region or binding group that can modulate the reactivity and specificity of the probe; 3) a reporter tag that enables the identification, enrichment, and/or visualization of labeled enzymes (reviewed in[253-257]). The reporter tags can be either a reporter group that is

directly connected to the ABPs in a one-step (direct) labeling process (**Figure 8B, C**) or can be attached in a later stage via bioorthogonal ligation chemistry in a two-step labeling approach (**Figure 8D**)[258].

ABP probe scaffold can be used for dual purposes-visualization and the pull-down and enrichment of targets, depending on the specific functional handle integrated into it. As a result, the applications of ABPs are diverse, ranging from identifying enzyme activities and drug targets in chemical proteomics to the non-invasive *in vivo* imaging of enzymatic functions[257,259].

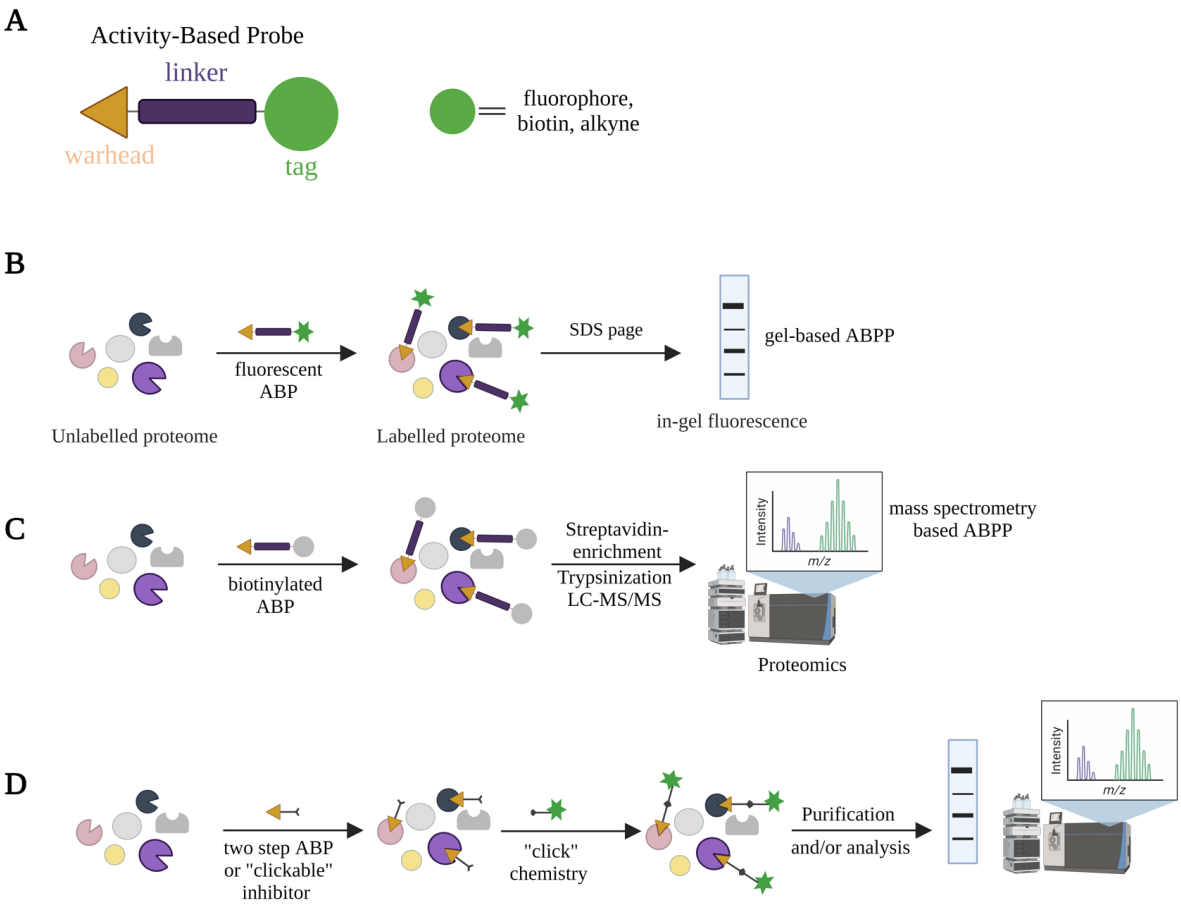

Figure 8. A general workflow for activity-based protein profiling (ABPP). **A**) Schematic structure of activity-based probes (ABPs) consists of an electrophile (often referred to as a "warhead"), a specific linker, and a reporter tag. ABPs selectively bind to active enzymes based on their activity levels. (**B**, **C**) Schematic representation of the direct ABPP method involves incubating a complex proteome with a probe containing a reporter tag. The enzymes that bind to the probe can then be visualized using a fluorescent tag through SDS-PAGE and in-gel fluorescence analysis (known as 'gel-based ABPP'). Alternatively, they can be enriched using a biotin tag for analysis via LC-MS/MS (termed 'mass spectrometry-based ABPP'). **D**) Schematic outline of the two-step ABPP method that requires bio-orthogonal chemistry ("click" chemistry) to introduce a reporter tag to a two-step process. Subsequently, labeled proteins can either be visualized or enriched. The figure was created with biorender.com.

ABPs can be used to label complex protein samples under different experimental conditions, including cell or tissue lysates (*in vitro*), within live cells (*in situ*), or even in living organisms (*in vivo*). The ABP-labeled proteins can be detected by using various analytical methods depending on the type of reporter tags used. For example, fluorescent reporter tags allow for quick analysis through a gel-based assay, where the labeled proteins are separated using sodium dodecyl sulfate polyacrylamide gel electrophoresis (SDS-PAGE) (**Figure 8B**). In-gel fluorescence scanning using fluorescent ABPs, while informative, comes with its limitations. It primarily detects the most abundant targets while their identity remains undefined. On the other hand, affinity tags such as biotin allow for the enrichment of target proteins using a streptavidin resin. Subsequent tryptic-digested peptides are analyzed by liquid chromatography-mass spectrometry (LC-MS) (**Figure 8C**). This mass spectrometry-based ABPP method, might be lower in throughput, but its higher sensitivity can identify low-abundance proteins and the depth of information makes it an extremely attractive technique[260,261].

2.1.1 Comparative and competitive ABPP

ABPP typically uses two common experimental setups: comparative ABPP and competitive ABPP (**Figure 9**). Comparative ABPP is highly useful for studying the activities of a particular (or enzyme family) across two or more proteomes, such as those from healthy versus diseased samples, or comparing pathogens versus commensal bacteria. This approach enables the identification of previously uncharacterized enzymatic activities involved in specific biological processes[260,262] (**Figure 9A**). Insights into variations in enzyme activity enhance our understanding of biological pathways and can assist in identifying new therapeutic targets. A significant advantage of ABPP over gene expression analysis is its ability to measure the enzyme activity directly, including changes due to post-translational modifications.

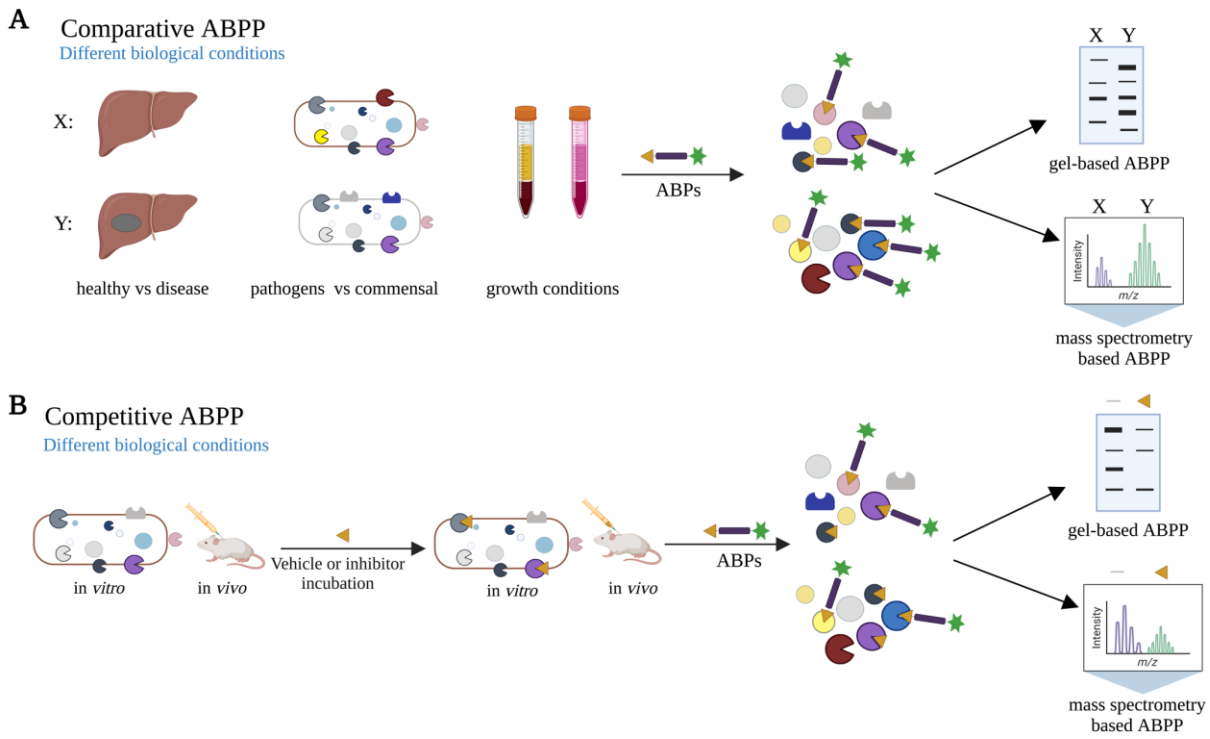

Figure 9. General workflow of comparative and competitive ABPP. **A**) Comparative ABPP involves analyzing proteomes from different biological samples, such as healthy versus diseased conditions, pathogens versus commensal bacteria, or varying growth conditions, by comparing them through gel- or mass spectrometry (MS)-based ABPP analysis of samples treated with activity-based probes (ABPs). **B**) Competitive ABPP is used for assessing target engagement and profiling off-target effects, followed by incubation with an ABP and subsequent analysis via gel or MS-based ABPP. The figure was created with biorender.com.

ABPP not only identifies relevant and druggable enzymes in a context of human disease, but it also enables the direct development of selective inhibitors for enzymes of interest. Competitive ABPP is a powerful technique that allows the testing of inhibitors against targets in their native environment without the need to express recombinant protein or even knowing the enzyme's native substrates[263]. Competitive ABPP also helps to guide lead identification, optimization, and pre-clinical trials in the drug development process. This technique involves pre-incubating a native proteome with a small molecule inhibitor, allowing for the identification of target enzymes by their reduced probe labeling post-incubation (**Figure 9B**)[255,264].

For example, in the profiling of ABPP in *S. aureus*, which is known for causing hospital-acquired infections and forming biofilms resistant to antibiotics[265], Lentz et al. discovered 12 fluorophosphonate binding hydrolases (Fphs), most of which were previously uncharacterized[266]. By screening a library of serine-reactive electrophiles against these hydrolases, they found selective inhibitors, such as Chloroisocoumarin **12**. This compound effectively inhibited one of these enzymes, FphB, reducing the virulence of *S. aureus* in a

mouse model, indicating its potential role in the initial stages of tissue colonization[266]. In a subsequent study, competitive ABPP was applied to screen a library of 1,2,3-triazole ureas, which resulted in identifying additional specific inhibitors for the Fphs enzymes[267]. One such promising inhibitor was later developed into a fluorescent ABP **13**, enabling selective imaging of heterogeneity of FphE enzyme activity within a population of genetically identical bacteria and uncovering compensatory functions within the Fphs enzyme network[267].

Another approach, inspired by natural products, involved the use of β-lactone-containing molecules by the Sieber lab and others to design a series of inhibitors[268,269]. Among these, the compound **14** was notably effective in suppressing the growth of *M. tuberculosis* at low concentrations[270]. By using an analog of this compound with an alkyne handle, Lehmann and colleagues identified two target enzymes, antigen 85 and polyketide synthase 13, both involved in mycolic acid biosynthesis. This compound not only inhibited these targets in vitro but also showed synergistic effects with other antibiotics, highlighting the potential of mimicking critical bacterial metabolites for developing novel antibiotics[270].

Recently, two research teams independently identified new chemical classes, 1,2,3-triazole urea and 7-urea chloroisocoumarin, which inhibit the growth of *M. tuberculosis* by interfering with cell wall biosynthesis[271,272]. Using competitive ABPP, both teams identified certain serine hydrolases as potential targets. Li et al. used 1,2,3-triazole urea derivatives, employing active (AA692) and inactive (AA702) isomers from a series of hits to narrow their focus to five serine hydrolases[271]. On the other hand, Babin et al. focused on 7-urea chloroisocoumarin chemical class, specifically JCP276, to identify nine hydrolase targets. Notably, inhibiting these hydrolases individually led to growth defects in *M. tuberculosis*, indicating that JCP276 may exhibit beneficial polypharmacological effects[272].

These instances underscore the versatility and effectiveness of ABPP in drug discovery, particularly in identifying and developing selective inhibitors for specific enzymes within complex biological systems.

In recent decades, a wide range of probes has been developed to target various enzyme families, including serine hydrolases[273,274], cysteine and threonine proteases[275,276], kinases[277], cytochrome P450s[278], and glycosidases[279]. The work in this thesis mainly focuses on activity-based protein profiling of the serine hydrolase and glycosidases.

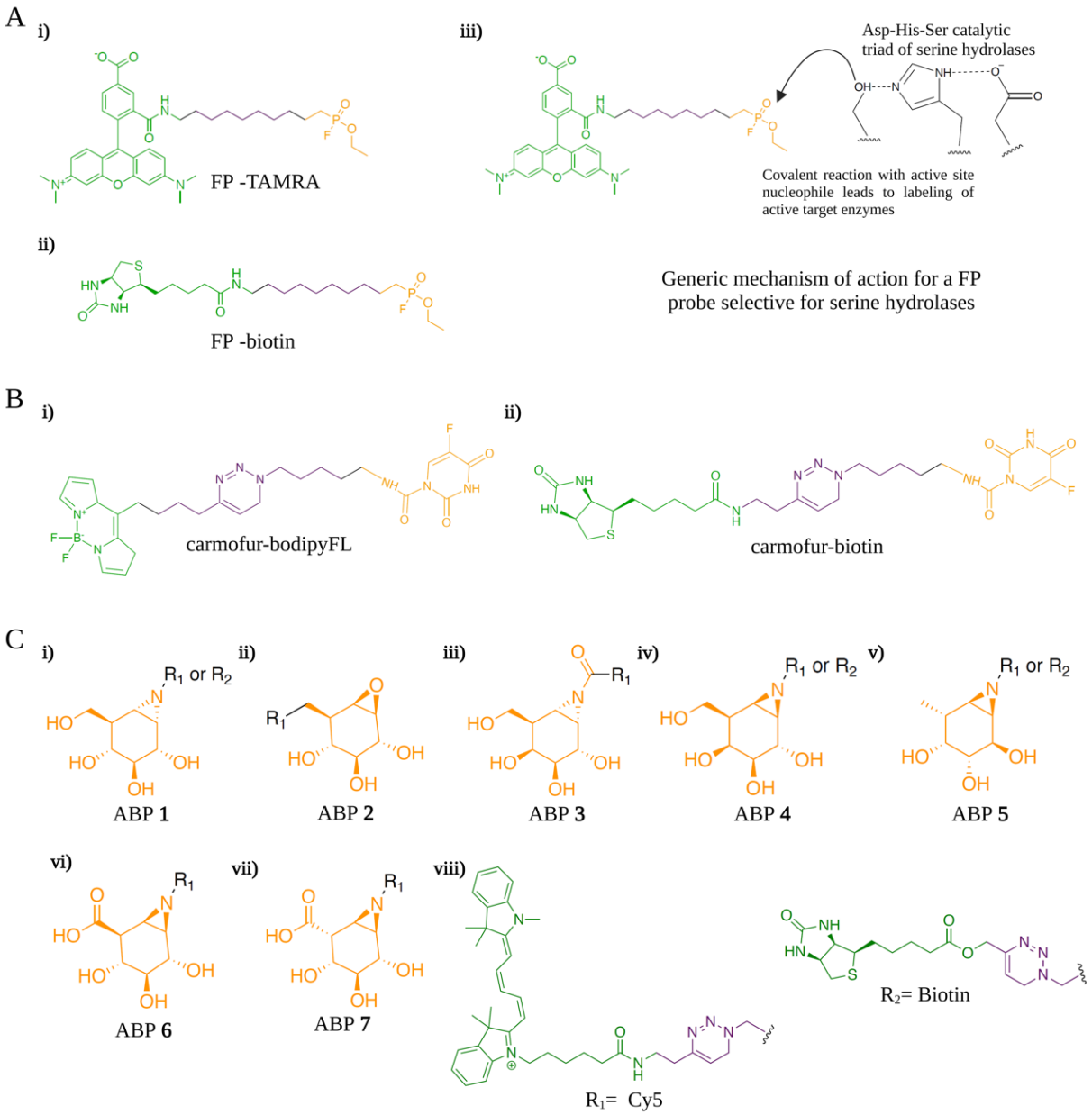

Figure 10. Activity-based probes (ABPs) used in this study. **A**) Structures of broad-spectrum serine hydrolase probes, including fluorophosphonate (FP)-TAMRA (i) and FP-biotin (ii), and the labeling mechanism of FP-TAMRA on the catalytic serine residue within the active sites of serine hydrolases (iii). **B**) Carmofur-derived probes, such as carmofur-bodipyFL (i) and carmofur-biotin (ii). **C**) Structures of glycosidases ABPs (**1-7**) equipped with Cy3 (R1) or biotin (R2) moieties.

2.1.2 Serine hydrolases and serine-reactive probes

Serine hydrolases (SHs) represent one of the largest and functionally diverse enzyme families found widely across all domains of life, including humans, plants, and microorganisms[280]. SHs are critical for various biological functions in mammals, playing central roles in numerous processes[281,282]. They also play an essential role in pathogens like bacteria and viruses, where

they contribute to infection-related pathways, including virulence[266,283] and antibiotic resistance[284,285]. Because of their critical functions in both normal cellular processes and disease mechanisms, serine hydrolases are considered promising targets for therapeutic interventions against various diseases[282], including bacterial infections[266,286], cancer[287], and neurological disorders[288]. Structurally, serine hydrolases are categorized into two main groups based on their functional roles. The first group consists of proteases, enzymes that specialize in breaking down peptide bonds in proteins. The second group comprises metabolic hydrolases, which include a diverse range of enzymes such as peptidases, amidases, lipases, esterases, and thioesterases. These enzymes are primarily involved in the processing of amide, ester, or thioester bonds found in small molecular metabolites, peptides, or in the post-translational modifications of proteins[280,281].

More than 60% of metabolic serine hydrolases (mSHs) are characterized by adopting an α,β-hydrolase structure and utilizing a catalytic trio of Ser-His-Asp[289,290]. However, a variety of distinct, evolutionarily unrelated subclasses of mSHs exist that employ different structural folds and catalytic mechanisms. Among these are the amidase signature enzymes, which use a Ser-Ser-Lys trio[291,292], and the patatin domain-containing lipases, which use a Ser-Asp dyad[293].

Lipases (lipid hydrolases) are the major catalytic members of the mSH family and the main driver of lipid catabolism[294,295]. Lipid hydrolases are part of the broad family of carboxylic ester hydrolases (EC 3.1.1). This group includes several subclasses: carboxylesterases (EC 3.1.1.1), arylesterases (EC 3.1.1.2), triacylglycerol lipases (EC 3.1.1.3), phospholipases A2 (EC 3.1.1.4), lysophospholipases (EC 3.1.1.5), acetyl esterases (EC 3.1.1.6), acetylcholinesterases (EC 3.1.1.7), and cholinesterases (EC 3.1.1.8)[296]. Each subclass plays a distinct role in lipid metabolism, breaking down various lipid components into simpler molecules.

Bacterial phospholipases can play multiple roles in the infection process across various hosts. By hydrolyzing structural membrane lipids, some of these enzymes lead to the lysis of host cells. This action aids in bacterial colonization and/or dissemination and supplies essential nutrients for the pathogens survival and replication[297-299]. Phospholipases are also categorized based on their cleavage site into 1) carboxyl ester acyl hydrolases, 2) phospholipase Cs (PLCs), and 3) phospholipase Ds (PLDs)[300]. The group of carboxyl ester acyl hydrolases includes phospholipase As (PLAs), phospholipase Bs (PLBs), and lysophospholipase As (LPLAs). Based on where they cleave the ester bond, PLAs are classified into PLA_1 (EC 3.1.1.32), which hydrolyzes the fatty acid at the glycerols sn-1 position, and PLA_2 (EC 3.1.1.4), which

hydrolyzes the sn-2 position. PLBs (EC 3.1.1.5) can cleave acyl groups at both the sn-1 and sn-2 positions of glycerophospholipids and possess lysophospholipase activity. Phosphoric diester hydrolases, PLCs (EC 3.1.4.3) and PLDs (EC 3.1.4.4) cleave glycerol-oriented or alcohol-oriented phosphodiester bonds, respectively. PLCs produce a phosphorylated head group (such as inositol triphosphate [IP3]) and diacylglycerol (DAG), while PLDs release a head group (like choline) and phosphatidic acid (PA)[300].

Since the common catalytic mechanism of serine hydrolases (SHs) involves the formation of an acyl-enzyme intermediate during substrate processing, it has enabled the design and development of ABPs that target the active serine as a reactive nucleophile (as reviewed in [301]). Over the last decades, a variety of covalent electrophiles have been described and utilized in probe scaffolds for serine hydrolases[301]. These include fluorophosphonates (FPs)[273], diphenyl phosphonates[302], sulfonyl fluorides[303], β-lactams[304], carbamates[305], triazole ureas[306], and isocoumarins[307].

Among these, fluorophosphonate (FP) electrophiles have emerged as particularly attractive for designing ABPs targeting serine hydrolases due to their broad reactivity towards serine hydrolases (SHs), enabling the simultaneous study of numerous enzymes. For instance, examining SH activity in cancer cells through comparative analysis has provided valuable information on enzymes that are dysregulated in eukaryotic systems[308]. FP probes have also been pivotal in studying bacterial SHs that play vital roles in bacterial physiology and virulence. For example, Ortega et al. explored the activity of SHs in *Mycobacterium tuberculosis* (Mtb), a clinically significant pathogen causing tuberculosis (TB), under both active and dormant conditions[309]. The persistent nature of TB poses considerable treatment challenges, highlighting the need for innovative approaches. The identification of enzymes that stay active in the Mtb dormant state presents an opportunity to develop new diagnostic markers and anti-TB drugs. SHs are vital at every phase of Mtbs lifecycle, affecting its growth, metabolism, and survival in dormant states. Using FP-based probes to measure SH activity in both replicating and non-replicating forms of Mtb revealed marked activity differences. Notably, certain SHs, such as the essential protease ClpP, were found to be active during dormancy, suggesting they could be valuable targets for developing treatments against dormant Mtb[309]. In another study, the activity of Mtb esterases was investigated using using FP ABPs together with substrate-based probes across active, dormant, and reactivating culture conditions[310]. This research led to the first-time identification of three esterase enzymes that become functional during the early reactivation phase from dormancy, which could play a critical role in pathophysiological phenomena[310]. To

elucidate host-pathogen interactions, FP-based probes (FP-TAMRA and FP-Biotin) were utilized in animal models infected with *Vibrio cholerae*[311]. This method enabled the detection of secreted bacterial and active host serine hydrolases (SHs). The study identified four *V. cholerae* proteases active in infected rabbits, and one was active in human cholera stool samples. Lentz et al. investigated serine hydrolase activities within *S. aureus* biofilms utilizing FP-TMR and FP-biotin probes[266]. Their research led to identifying 12 active serine hydrolase targets, including lipase 1 and 2 (SAL1, SAL2). Remarkably, 10 of these identified targets were previously uncharacterized, with functional studies revealing their potentially significant roles in bacterial virulence[266] and stress response[312].

2.1.3 Glycosidases and carbohydrate-based probes

Glycans, which are covalently attached carbohydrate chains, are essential components in all life forms, playing critical roles from energy storage to facilitating crucial cellular processes such as recognition, communication, and signaling[313,314]. They are pivotal in structural support within the extracellular matrix, protection in secreted mucus, and in the correct sorting and transport of glycoproteins, thereby ensuring proper cellular function[315]. Glycosylation, the process of attaching glycans to proteins, must be precisely regulated, as alterations in glycosylation patterns can lead to serious health issues, including autoimmune diseases and cancer[316-319].

The importance of glycans extends beyond human physiology; they are also involved in microbial interactions with the host[320]. Pathogens frequently target glycans to attach to and invade host cells, with examples including the role of glycans in the adhesion of *Helicobacter pylori* to gastric cells[321] and influenza A virus to sialic acid-containing glycans[322].

Glycosidases, or glycoside hydrolases (GHs), are a major class of enzymes that cleave the glycosidic bonds in a variety of substrates, including di-, oligo-, and polysaccharides, as well as glycoconjugates such as glycoproteins, glycolipids, and proteoglycans[323]. These enzymes are divided into two main groups based on the site of sugar cleavage. Exoglycosidases are responsible for the hydrolytic cleavage of specifically terminal, non-reducing sugar residues in glycan substrates, while endoglycosidases target the internal glycosidic bonds within the sugar chains[324].

Bacterial glycosidases, on the other hand, play a significant role in the mechanisms of bacterial pathogenesis. They are involved in immune modulation, adherence to host cells, colonization, and nutrient production[325]. Many pathogens often secrete glycosidase enzymes that break down

glycans to evade the immune response, aiding their survival and proliferation within the host[326,327]. Moreover, glycans serve as vital nutrients for pathogens, especially those in the gastrointestinal tract, where bacteria express glycosidases to metabolize glycans from host glycoproteins like mucins[328,329]. This nutrient acquisition is crucial for maintaining pathogens survival and continued colonization in various host niches[330,331].

Glycoside hydrolases (GHs) are categorized into two main types based on the stereochemical outcome of their enzymatic action: inverting or retaining[332]. Inverting glycosidases typically carry out hydrolysis through a direct, single-step nucleophilic attack at the anomeric center of the substrate, resulting in the inversion of stereochemistry. On the other hand, retaining glycosidases work via a more complex two-step mechanism. This mechanism is facilitated by two essential catalytic residues: a nucleophile and a general acid/base, facilitate the formation of a covalent glycosyl-enzyme intermediate[332]. The strategy of capturing this intermediate is fundamental to the design of most mechanism-based inhibitors and activity-based probes (ABPs) that specifically target retaining glycosidases[279,333].

Unlike retaining glycosidases, inverting glycosidases do not form covalent glycosyl-enzyme intermediate during the hydrolysis of their substrate. Instead, these enzymes directly utilize an activated water molecule to break the glycosidic bond in a single step[334]. As a result, designing ABPs that directly alter a catalytically active amino acid residue becomes challenging for inverting glycosidases. Conversely, two major classes of irreversible inhibitors that directly target the enzyme's active site nucleophile have been developed to retain glycosidases: cyclitol epoxides and fluorinated glycosides[335].

These inhibitors have been used to analyze various retaining glycosidases, especially in identifying catalytically active carboxylic acid residues. Cyclitol epoxides, such as cyclophellitol, use an epoxide warhead that is activated upon protonation by the enzyme's active site, leading to a fast and specific reaction with the target glycosidase, minimizing off-target interactions. In contrast, fluorinated glycosides, particularly 2-deoxy-2-fluoroglycosides, show lower intrinsic reactivity, as the fluorine substituent destabilizes the transition state. They rely on the presence of a strong anomeric leaving group for activation, ensuring specificity by reacting only within the enzyme's active site. Therefore, both cyclitol and fluorinated glycoside structures are effectively adaptable for creating selective ABPs targeting various retaining β-glucosidases, such as α-glucosidases[336], β-glucosidase[337], α-galactosidase[338], β-galactosidase[339], α-fucosidases[340,341], β-glucuronidase[342], and α-iduronidases[343], each with its unique mechanism of enzyme interaction.

Most glucosidase ABPs have been developed to study human diseases[344,345], including lysosomal storage disorders, Gaucher disease, plant enzymes[346] , and certain microbial metabolic pathways[347,348]. However, relatively few glycosidase ABPs have been developed to date to investigate bacterial enzymes that could potentially serve as virulence factors. Due to their conserved mechanism of action, these glycosidase probes are also well-suited for detecting bacterial enzymes.

3. Objectives of the study

The underlying hypothesis of this work was that certain enzymes with their putative roles in bacterial physiology and virulence remain unidentified and/or uncharacterized. The aim of this thesis was to identify and functionally characterize such enzymes in the bacterial pathogens *S. aureus* and *K. pneumoniae*, which may represent potential therapeutic targets.

Specifically, the objectives of this work were:

1. Identify active enzymes in *S. aureus* targeted by the antimicrobial agent carmofur
2. Identify active glycosidases in *S. aureus*
3. Identify active serine hydrolases in *K. pneumoniae*
4. Validate the enzyme function(s) in bacterial physiology and host-pathogen interactions

4. Methodological considerations

In order to achieve the objectives, ABPP was utilized throughout this thesis to identify different classes of active enzymes using a variety of ABPs. The materials and methods used in this work have already been outlined in Papers I, II, and III. Instead of repeating this content, this section will focus on providing a clear and brief overview of the methods used in this work and the rationale behind their selection.

4.1. *S. aureus* and *K. pneumoniae* as model organisms

The choice of *S. aureus*, a Gram-positive bacterium, and *K. pneumoniae*, a Gram-negative bacterium, as model organisms for this study is due to their significant clinical relevance and distinctive characteristics that make them ideal for investigating the mechanisms of bacterial pathogenesis and the development of innovative antibacterial approaches[27,166]. *S. aureus* is a versatile pathogen known for its capability to cause a wide spectrum of infections, from mild skin infections to life-threatening systemic diseases. Its adaptability and the emergence of MRSA strains underscore the critical need for novel therapeutic strategies. The well-characterized genome of *S. aureus* facilitates genetic modifications, such as gene knockouts, enabling in-depth investigation into gene/protein functions, and insights into virulence factors and resistance mechanisms[349].

K. pneumoniae, with its protective outer membrane that poses additional obstacles to antibacterial drug penetration, represents the challenges associated with treating gram-negative bacterial infections. It is particularly known for its role in hospital-acquired infections and its rapid acquisition of resistance to multiple antibiotics, including carbapenems[191]. Both organisms are pivotal in the study of bacterial virulence and resistance mechanisms. Their extensive use in research is attributed to their relevance in global health, the availability of genetic tools for manipulation, and the transposon mutant libraries[350,351] which facilitates the follow-up study. In addition, their role in testing the effectiveness of novel antimicrobial agents, makes them exemplary models for advancing the field of infectious disease and therapeutics.

4.2. Profiling of active enzymes by ABPP

Activity-based protein profiling (ABPP) advances beyond the scope of 'omics'-based techniques by focusing on the functional state of enzymes rather than their mere presence. By targeting enzymes in their active states with chemical probes, ABPP offers a precise measure

of enzymatic function, identifying key regulators and druggable targets. This method provides a higher level of validation for protein functionality, surpassing the limitations of transcriptomics and conventional proteomics (reviewed in[251,253-257]). Serine hydrolases have previously been identified in *S. aureus* using ABPP. This work has been extended to explore other enzyme families in *S. aureus* in Papers I and II. Additionally, serine hydrolases have been explored in *K. pneumoniae* in Paper III using FP probes that were also successfully employed in other organisms[272,311,352-354]. In general, after the bacterial strains were cultivated under specified conditions, they were exposed to fluorescent-tagged ABPs. Subsequently, the cells were lysed, and fractions were analyzed by SDS-PAGE, which allowed for the identification of labeled targets via fluorescence scanning **(Figure 11).**

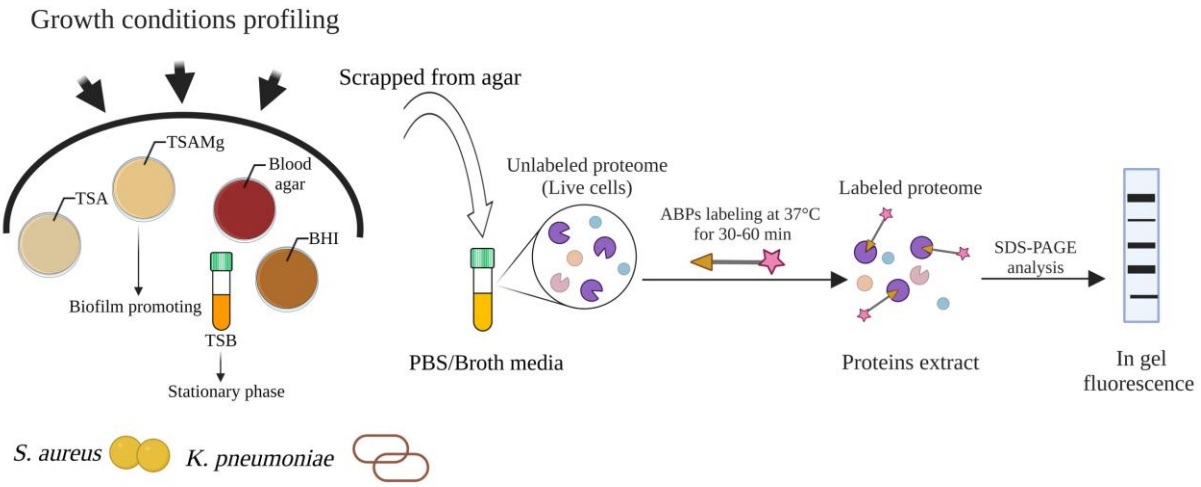

Figure 11. Profiling of active enzymes by ABPP. Bacteria are grown overnight either on agar plates such as Tryptic Soy Agar (TSA), TSA with magnesium chloride (TSAMg), Blood Agar, and Brain Heart Infusion (BHI) or in liquid culture. The bacteria are then scraped into PBS/broth to achieve the desired density before the addition of the ABP. After labeling, the cells are lysed, and labeled proteins are resolved by SDS-PAGE analysis and visualized by in-gel fluorescence scanning.

In Paper I, a carmofur-derived ABP, which acts as both an antineoplastic and antimicrobial agent, was utilized to detect active enzymes, including serine hydrolases, in *S. aureus*. The bacteria were cultivated on tryptic soy agar supplemented with $MgCl_2$ (TSAMg), a condition known to promote biofilm formation in *S. aureus*[355]. In Paper II, a panel of glycosidase ABPs was used to identify retaining glycosidases in MRSA strain. The bacteria were cultivated on various rich media, including TSA, TSAMg, BHI, and blood agar, and in stationary phase culture in TSB to check whether different growth conditions influence the activity of different retaining glycosidases. Since neither carmofur-derived ABP nor glycosidase ABPs had not

previously been used to detect active enzymes in bacterial pathogens, and their potency for detecting bacterial enzymes was unknown, dose-dependency labeling of these probes was also used to find the optimal labeling concentrations in Papers I and II. Since competitive ABPP is a suitable method for assessing the selectivity of probe labeling, it was employed in Papers I and II. In Paper I, unlabeled parent inhibitors of carmofur ABP, such as carmofur and 5-fluorouracil, were used, while in Paper II, cyclophellitol-based inhibitors were used to profile the specific labeling of the probes. In Paper III, the global serine-reactive electrophilic probe FP-TMR was utilized to label serine hydrolases in *K. pneumoniae* after growth on blood agar, which served as the standard culture medium.

4.2.1 Chemoproteomics method optimization to detect active enzymes by biotinylated probes

The gel-based method employing fluorescent ABPs provides valuable information but is limited to identifying only the most abundant targets, without revealing their specific identities. Additionally, the method of fluorescence-guided gel band extraction is not precise enough to isolate labeled enzyme(s), especially in highly complex samples or those that contain enzyme(s) migrating together with different specificities[356]. To overcome these limitations, a strategy involving a biotin-tagged probe combined with a chemoproteomic workflow was adopted. This approach, focusing on affinity-based enrichment, has proven highly effective in selectively identifying ABP targets.

The general workflow for this process includes several key steps: (1) labeling the bacteria with a biotinylated activity-based probe, (2) lysing the bacteria, (3) removing excess probes, (4) enriching for labeled enzymes by capturing them on streptavidin resin, (5) performing on-bead digest of enriched proteins, (6) desalting and concentrating, (7) conducting liquid chromatography-tandem mass spectrometry (LC-MS/MS) analysis, and (8) data analysis [357-360]. (**Figure 12A**).

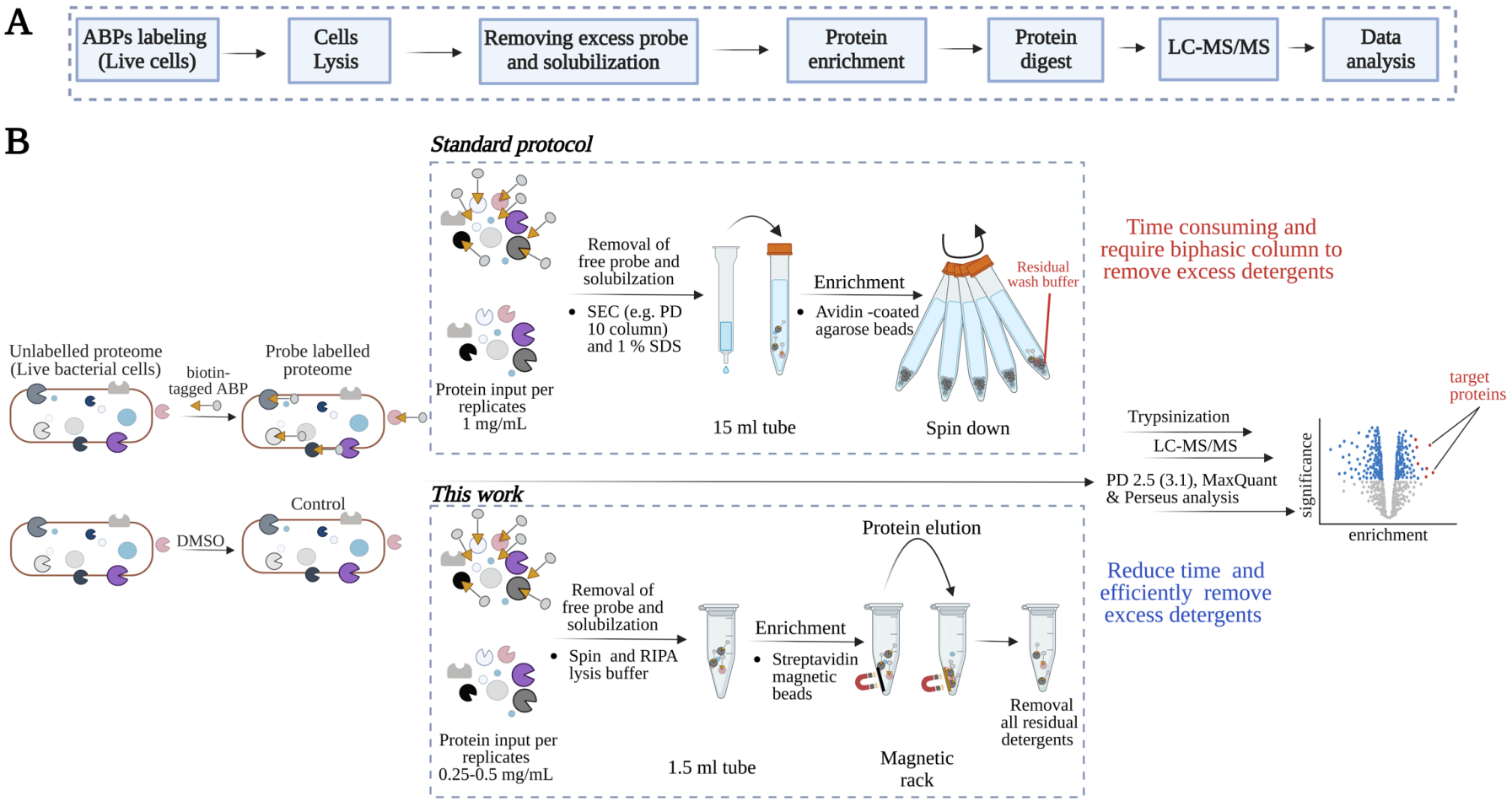

Figure 12. Schematic overview of the chemical proteomic workflow. (**A**) Essential steps in the standard chemical proteomics protocol and (**B**) a schematic outline of the workflow used in this thesis, including basic procedural parameters, compared to the traditional method involving avidin-coated agarose beads. PD 2.5 (3.1) stands for Proteome Discoverer 2.5 or 3.1 software. The figure was created with biorender.com.

Following probe labeling, proteins are subjected to size exclusion chromatography (SEC) to remove free probe and non-protein components from the cell lysate. The critical aspect of the full process is to increase the washing steps to remove nonspecifically bound proteins, thereby reducing the complexity of the final MS sample and improving the comparison between control and probe-treated samples[359,361-363]. In standard chemoproteomic workflows, sodium dodecyl sulfate (SDS) and other detergents are commonly used to solubilize proteins and minimize non-specific binding. However, even at low concentrations, detergents can impede enzymatic digestion and dominate mass spectra due to their high ionization efficiency and high relative abundance compared to peptides[364,365]. Therefore, the removal of detergent, like SDS is important for effective mass spectrometric analysis in proteomics[365]. Because the removal of SDS is traditionally thought to be impossible with in-solution digestion, various methods have been developed to eliminate detergents, including the use of protein precipitation in acetone or with trichloroacetic acid (TCA), the use of an S-trap, Oasis columns[366-370]. Alternatively, a biphasic column coupled with strong cation exchange can be integrated into the LC-MS/MS workflow for detergent removal before mass spectrometry analysis[12,13]. However, these methods require extensive washing steps, including methanol washes, which can lead to significant sample loss[370]. Unfortunately, the Proteomics and Metabolomics Core Facility (PRiME) lacks the necessary mass spectrometer set up to incorporate a combination of a biphasic column coupled with strong cation exchange resin (SCX) for detergent removal[367,368,371].

To address these challenges and minimize sample loss, sample preparation has been optimized by adopting strategies from the single-pot solid-phase-enhanced sample preparation (SP3)[372-375] and proximal labeling[376,377] using magnetic bead-based sample preparation. A detailed comparison is illustrated in **figure 12B**. This optimized protocol uses lower concentrations of biotin probe compared to previous studies, reducing the amount of free probe that can be easily removed through simple centrifugation, thus eliminating the need for desalting columns and common rotary evaporation steps, particularly for live cell labeling. However, for the labeling of protein extracts, the use of a desalting column is required to remove excess probes. RIPA lysis buffer (50 mM Tris-HCl, 150 mM NaCl, 0.1% (wt/vol) SDS, 0.5% (wt/vol) sodium deoxycholate, 1% (vol/vol) Triton X-100) is also used in sample preparation for its effectiveness in cell lysis and membrane protein solubilization. Importantly, the use of magnetic beads instead of avidin agarose beads offers advantages in sample preparation, such as protein

cleanup or enrichment. Utilizing a magnetic rack simplifies the removal of nonspecific proteins and excess detergents and enhances sample handling.

The MS raw data were analyzed using either Proteome Discoverer 2.5 or 3.1 software, or MaxQuant for protein label-free quantification (LFQ). LFQ was chosen for its simpler experimental setup, which avoids expensive and time-consuming labeling steps, does not require analysis of complex mass spectra, and allows for the addition of more samples to the data set later on[378,379]. The limitations of label-free quantification are that it heavily depends on very stable liquid chromatography (LC) separation and spray conditions and requires more replicates[380]. However, it is widely used in shotgun proteomics, and there are many instances of its successful application in conjunction with ABPP or affinity-based chemoproteomics[381-384]. While this work protocol only focused on label-free quantification for protein analysis, alternatives such as TMT or SILAC labeling are also possible. The choice of data analysis and the determination of cutoff criteria for enrichment proteins may vary depending on the mass spectrometry instruments and software utilized.

One limitation of this protocol, like other probe-labeled proteomics, is the proper solubilization of membrane proteins, which can be achieved to some degree by boiling the samples in 1% SDS[381,385]. Another potential shortcoming, as described by others[367], is that probe-labeled peptides are either too long or too short for accurate MS characterization. To overcome this limitation, an initial digestion with protease alternative to trypsin needs to be performed to generate peptides of suitable length and properties for MS analysis[367]. Although this protocol is described for biotinylated-tagged ABP enrichment, the customized protocols can also be used for click chemistry-based ABPP sample preparation, as the immobilized magnetic beads facilitate the removal of excess click chemistry reagents through acetone or methanol precipitation[361,367].

4.3. Functional validation of molecular targets

Studying enzymes targeted by ABPs often requires the deletion or heterologous expression of genes encoding these enzymes. Initially, mutants were obtained from the Nebraska Transposon Mutant Library[350] for *S. aureus* and the Manoil Lab Transposon Mutant Library[351] for *K. pneumoniae*. First, SDS-PAGE-based ABPP was performed on both mutant and wild-type strains to confirm the identity of the fluorescent ABP targets using gel-based ABPP. These experiments also revealed any potential compensatory upregulation of other enzymes within

the same family in knockout strains, which could suggest a functional connection between these genes.

Considering the possibility of non-specific effects arising from secondary mutations or polar effects within the transposon mutants, alternative mutant types were adopted in subsequent experiments. Specifically, phage-transduced mutants in the well-characterized *S. aureus* LAC strain were used for the experiments described in Paper I. In Paper II, CRISPR interference (CRISPRi)-based mutant constructs for the selected ABP targets were employed. Additionally, to eliminate concerns about polar effects caused by transposon insertion, other allele-specific mutants for *K. pneumoniae* were used in Paper III.

For further biological validation, the growth fitness of the transposon mutant strains of targeted enzymes was also monitored during *in vitro* growth conditions to determine whether they exhibit any growth defects in regular media.

4.4. Host model systems to study colonization and infection

In Paper III, seven previously uncharacterized or poorly annotated serine hydrolases (SHs) in *K. pneumoniae* were identified using a chemoproteomics strategy. This finding underscored the need for a robust model to study these enzymes roles at the host-pathogen interface. Ideally, the selected model system should replicate the environmental conditions that the bacteria (*K. pneumoniae*) encounter during colonization or infection. However, one challenge with using host model systems is their inability to incorporate every human component and condition that fully mimics bacterial colonization or infection. Since the primary niche of *K. pneumoniae* as a commensal bacterium is the human gut, the growth fitness of the SHs was initially monitored using *in vitro* models that mimic the gut-host interface. Consequently, a co-culture model with HT29-MTX cells, which are rich in mucus and goblet cells, was utilized. Following the identification of phenotypes for three hydrolases, the aim was to further validate these enzymes in models that more accurately reflect the complexity of the human gut. Hence, intestinal organoids, more specifically colon organoids, derived from adult human tissue stem cells, were employed. Besides tissue-derived organoids, intestinal organoids can also be created from human pluripotent stem cells[386,387]. However, this process takes up to four weeks and does not fully mimic the characteristics of adult tissue[386,387].

Colon organoids are three-dimensional, stem cell-derived structures that closely resemble the colonic epithelium architecture and functionality (reviewed in [388]). Human-derived organoid models offer several advantages including easy accessibility, higher reliability and relevance

than other models, e.g. immortalized human cell lines and animal models (reviewed in[389]). Moreover, they provide ample material for study. Animal models, in contrast, often fall short of offering the necessary experimental accessibility to study infection processes with the desired detail and their effectiveness in predicting disease phenotypes is debatable[390]. The emergence of organoids, self-organizing 3D structures from stem cells that reproduce key features of organ structure and function, presents robust models for studying infections in differentiated human tissues[391-393]. Their value in research, especially in mimicking human conditions for studying diseases, pathogenesis, and host-pathogen dynamics, is increasingly recognized[391,394,395]. For instance, researchers have used the 3D intestinal organoid model to investigate the mutational patterns of colorectal cancer caused by genotoxic *pks+ Escherichia coli* [396]. This model has also been key in studying the effects of *Clostridium difficile* [397]toxins and *Salmonella* spp. invasion on the intestinal epithelium[398].

However, accessing the luminal side presents challenges in 3D organoids. Intestinal organoids are made up of a single layer of epithelial cells forming a hollow central lumen (the apical side) and introducing microbes into this lumen requires microinjection techniques[399,400]. While microinjection provides precision, it is labor-intensive, challenging to standardize, and requires a high level of technical skill, resulting in relatively low throughput[399]. Additionally, the type of analysis being conducted, such as fluorescence, transcriptomic, proteomic, or metabolomic, often requires using multiple organoids to gather enough sample material for testing. Moreover, antibiotics are added to the culture medium of organoid cultures to prevent bacterial growth on the basolateral side, which can alter intestinal function in ways that are independent of the antimicrobial activity[399,401]. Another approach involves breaking the organoids to facilitate infection, but this exposes both apical and basolateral sides to pathogens[395,402].

Considering these challenges and to overcome some of the limitations mentioned above, 2D organoid monolayers have been adopted for studying bacterial pathogens[403-408]. This format allows for the direct introduction of pathogens to the apical side of the intestinal epithelium by adding them to the culture medium, facilitating a detailed examination of host-pathogen interactions at the intestinal barrier. Furthermore, 2D organoid monolayers support advanced microscopy techniques and provide a comprehensive model of the *in vivo* intestinal epithelium, including essential intestinal cell types like Paneth cells and stem cells. A limitation of static 2D monolayer models is their failure to sustain the strict anaerobic environment found in the intestine or a consistent nutrient supply. This makes it challenging to maintain long-term stable co-cultures due to the short lifespan of host cells and bacterial overgrowth[408,409].

Although air-liquid interface (ALI) cultures of 2D monolayers enhance oxygen supply and promote a more differentiated phenotype of epithelial cells[410], thus favoring bacterial growth, this method was not chosen for use. This decision was based on several factors, such as *K. pneumoniae* being a facultative anaerobe that can grow in low oxygen conditions. Additionally, maintaining monolayer cultures at the ALI requires up to four weeks[411], and bacterial overgrowth can occur within a few hours. To facilitate longer testing periods and more detailed observations of phenotypes, the protocol was modified by reducing the use of non-diffusible antibiotics compared to the original protocol[412], aiming to develop a better model for studying targeted enzymes. Despite these efforts, challenges were faced in sustaining co-culturing for longer periods (up to 16 hours) in order to observe pronounced phenotypes between wild-type and mutant strains, due to an insufficient continuous flow of nutrients, which longer cultures require. This limitation could be overcome by integrating a transwell monolayer into a microphysiological system that ensures a steady supply of nutrients to the bacterial compartment[413]. The development of the 2D monolayer system is still ongoing and shows promise for improving the study of bacterial pathogens[409,414,415].

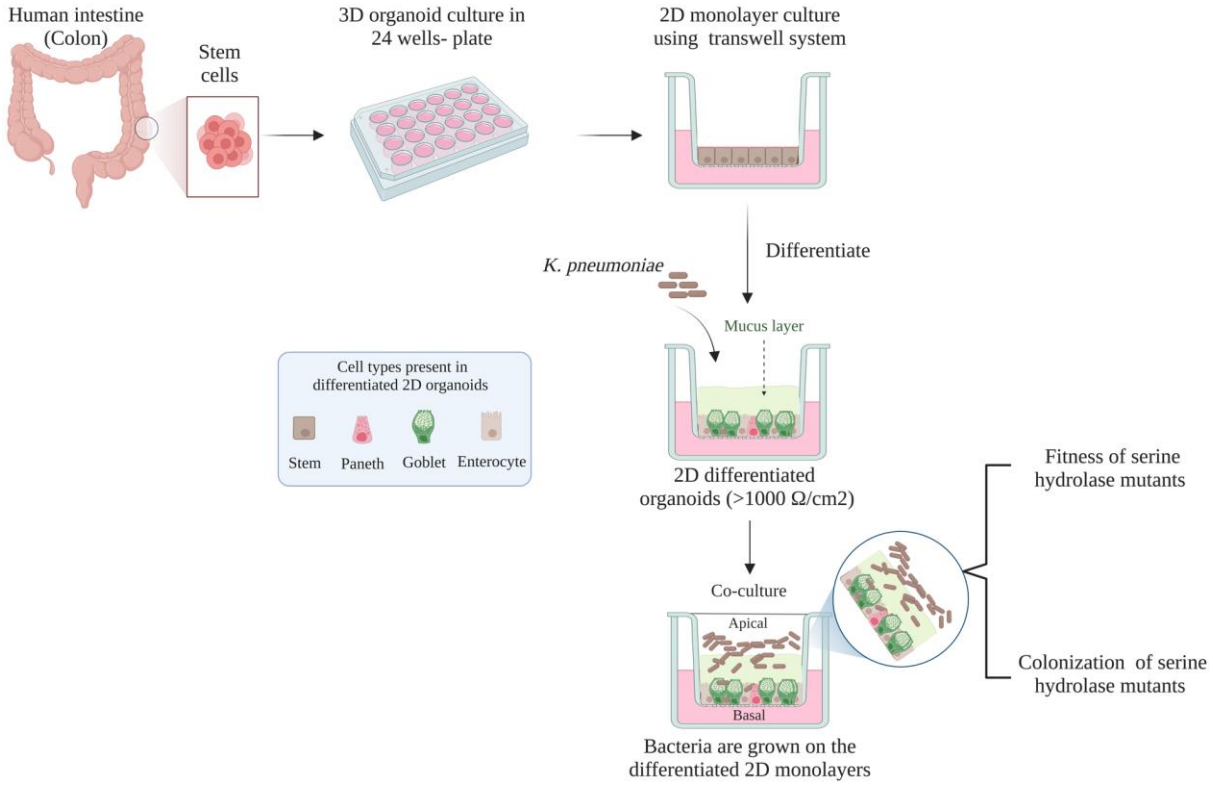

Figure 13. Schematic overview of the co-culture model of *K. pneumoniae* with colonic organoid monolayer. Human colon organoids, derived from stem cells isolated from intestinal biopsies or tissues, are initially cultured as 3D structures in extracellular matrices such as Cultrex Basement Membrane Extracts (BME) in 24-well plates. These 3D organoids are subsequently transferred as single organoid cells to a 2D monolayer format in Transwell systems, allowing them to differentiate into mature intestinal cells. The integrity of the differentiated monolayer barrier is determined by quantifying the transepithelial electrical resistance (TEER). *K. pneumoniae* wild-type and serine hydrolase mutants are then introduced to the apical side of the differentiated 2D organoid monolayers. Bacterial fitness and/or colonization efficacy are monitored by determining colony-forming unit (CFU) over time. The figure was created with biorender.com.

Serine hydrolase mutants exhibited reduced fitness compared to wildtype in organoid co-culture models (paper III), and it was therefore desired to determine their virulence properties in scenarios more similar to *in vivo* infections. In addition, this study identified two previously uncharacterized glycosidases in *S. aureus* that warrant further functional study in relation to host-pathogen interactions. Consequently, wax moth *Galleria mellonella* larvae were utilized as an infection model to study bacterial virulence.

The use of insect larvae, such as *G. mellonella*, for testing pathogen virulence offers a viable alternative to experimental infections in rodents or pigs and is not regulated by legislation[416]. This approach is crucial to comply with the 3Rs efforts that aim to reduce, refine, and replace

animal experiments[417]. *G. mellonella* larvae, in particular, have been employed as models for studying various significant pathogens[418] and evaluating the effectiveness of antibacterial and antifungal treatments[419,420]. This is because the innate immune system of the wax moth and higher organisms share general similarities (reviewed in[421]). *G. mellonella* larvae offer several technical advantages over mammalian infection models, such as high throughput, ease of handling, simple housing requirements, and the possibility to purchase large quantities of larvae at a relatively low price, with no legal or ethical issues. Unlike other non-mammalian models such as zebrafish larvae, *C. elegans*, or *Drosophila melanogaster*, experiments with *G. mellonella* can be conducted at the mammalian host's body temperature of 37°C. Thus, findings from insect-based studies can provide foundational insights into disease mechanisms and help formulate hypotheses that can be further explored in vertebrate models.

The organoids used in this study were obtained from the Foundation Hubrecht Organoid Biobank (Utrecht, The Netherlands) under TC-Bio protocol number 14-008 and were used in accordance with informed consent. Human blood was isolated after informed consent was obtained from all subjects in accordance with the Declaration of Helsinki. Approval was obtained from the Medical Ethics Committee of UMC Utrecht, The Netherlands. The human derived organoids and the complement assay using human serum were used during my research stay at UMC Utrecht, Netherlands.

5. Summary of main results

Paper I: Activity-Based Protein Profiling in Methicillin-Resistant *Staphylococcus aureus* Reveals the Broad Reactivity of a Carmofur-Derived Probe

In this paper, carmofur-derived probe, originally developed to target human acid ceramidase (ACase) after recognizing carmofur as a potent ACase inhibitor, was used for activity-based protein profiling in MRSA to identify active enzymes and potential targets of this drug. Carmofur, which is a prodrug of 5-Fluorouracil (5-FU), is a registered anti-neoplastic agent for colorectal cancer treatment in multiple countries and is being explored for various other therapeutic applications. Both carmofur and its parent compound, 5-FU, exhibit broad-spectrum antimicrobial and antibiofilm activity against various bacteria, including MRSA.

- Gel-based ABPP with a fluorescent carmofur probe showed dose-dependent labeling of specific *S. aureus* proteins, with multiple bands labeled at different concentrations.
- Pre-incubation with carmofur led to reduced labeling of specific bands by the fluorescent probe, suggesting specific interactions between the probe and its targets, while pre-incubation with 5-FU did not alter the labeling patterns significantly.
- Treatment with a carmofur-biotin probe resulted in the enrichment of 20 enzymes from diverse families in *S. aureus*, including the NTN hydrolase-related IMP cyclohydrolase PurH and previously uncharacterized fluorophosphonate-binding serine hydrolases (SHs). The enrichment of so many SHs was surprising since carmofur had previously been described to target enzymes with an active-site cysteine.
- This study did not observe the direct link between the enzyme targets of carmofur and the susceptibility of *S. aureus* to the antimicrobial effects of the drug, suggesting that the mechanism of action of carmofur may involve more complex interactions or the cumulative effect of multiple non-essential targets, which might alter cellular processes or metabolic pathways in a manner that contributes to the overall antimicrobial effect.

In conclusion, this paper highlighted the concern regarding the clinical use of carmofur, noting that the drug's broad and somewhat promiscuous reactivity with both human and microbial enzymes could influence its therapeutic effects and potential side effects.

Paper II: Activity-Based Protein Profiling Identifies an Alpha-amylase Family Protein Contributing to the Virulence of Methicillin-Resistant *Staphylococcus aureus*

In this paper, a panel of glycosidase ABPs was utilized to identify and characterize active retaining glycosidase activities in MRSA.

- Gel-based ABPP using fluorescent glycosidase ABPs (**1-7**) in *S. aureus* revealed specific labeling patterns identifying active enzymes. The ABP **1**, which primarily targets alpha glucosidases, labeled a band at 60-70 kDa in both culture supernatants and cell pellets. This band was consistently the most prominent under various liquid and agar-based growth media. Other probes such as ABP**2**, ABP**4**, and ABP**5** also identified specific bands in different growth conditions.

- Tests for dose-dependency revealed that a concentration of 1 μM was necessary for effective labeling by ABPs **1**, **4**, and **5**. Competitive ABPP with unlabeled inhibitors suggested specific interactions for ABP**1**, while others did not show changes in labeling patterns, indicating potential non-specific interactions or limitations in inhibitor potency.

- The study identified the two previously uncharacterized glycosidase family proteins: the putative 6-phospho-β-glucosidase (BglA) and the α-amylase family protein trehalase C (TreC), using biotinylated analogs of three probe cocktails, through mass spectrometry-based ABPP.

- Gel based validation using transposon mutants and CRISPRi-based mutants indicated that TreC is a target of ABP**1**, and possibly BglA and Atl as well.

- Further functional validation of the newly identified enzymes using CRISPRi gene silencing revealed that *tre*C-silenced, but not *bgl*A-silenced, led to reduced *S. aureus* virulence, as evident by a significantly higher larval survival rate in a *Galleria mellonella* infection model. However, silencing either gene did not affect bacterial growth in TSB.

In conclusion, this study supported the putative role of the α-amylase family protein, TreC, in bacterial virulence during *G. mellonella* infection.

Paper III: Activity-Based Protein Profiling Identifies *Klebsiella pneumoniae* Serine Hydrolases with Potential Roles in Host-Pathogen Interactions

In this paper, ABPP was used in *K. pneumoniae* to identify and characterize serine hydrolases (SHs), a highly druggable and functionally diverse enzyme family in nature.

- Fluorophosphonate probes were used to identify 10 SHs in *K. pneumoniae* by ABPP. Out of these 10 SHs, 8 were found to possess α,β-hydrolase domains, while the remaining two were linked to serine proteases with trypsin-like peptidase domains. Interestingly, 7 of these SHs were poorly annotated, and their definitive cellular functions are not yet known. Additionally, the majority of the identified SHs displayed limited or no homology with serine hydrolases from other gut commensal bacteria and humans.

- SH-deficient transposon mutants exhibited growth patterns similar to the wild-type strain when cultured in LB liquid media. However, interestingly, three of them demonstrated reduced fitness in an HT 29-MTX cell-based co-culture model.

- Further functional validation using transposon mutants deficient in the serine hydrolases PldB, YjfP, and YchK indicated reduced fitness in co-culture models with human-derived colonic organoids. Notably, the translocation efficacy of PldB and YchK was also low.

- Mechanistically, the transposon mutants of *pldB* and *yjfP* had increased susceptibility to complement and polymyxin B, suggesting that these enzymes have a role in shaping envelope integrity, whereas the putative secreted patatin-like phospholipase YchK had not.

- Additionally, transposon mutants of *yjfP*, *pldB*, and *ychK* were less virulent than the wild-type strain in the *G mellonella* infection model. Moreover, the assessment of virulence among different allele transposon mutants from the Manoil library with insertions in *pldB* (n=3 available strains), *yjfP* (n=3), and *ychK* (n=2) all showed similar phenotypes.

- Biochemical and substrate profiling revealed that both YjfP and PldB possess esterase activity. Structural and biochemical assays suggested that YjfP potentially has deacetylase activity.

In conclusion, this study provides important insights into the molecular mechanisms that govern the virulence and cell physiology of *K. pneumoniae* at the host-pathogen interface. It highlights PldB, YjfP, and YchK as potential targets for antimicrobial or anti-virulence therapies, the inhibition of which could complement existing antibiotics and human immune defense.

6. General discussion

The increasing prevalence of resistant and multi-resistant bacterial pathogens represents a considerable threat to human health. In light of the increasing antibiotic resistance crisis, there is an urgent need to discover new classes of putative antibacterial targets. A major obstacle in this endeavor is that large portions of many bacterial genomes remain functionally uncharacterized. This gap underscores the necessity for unbiased screening methods to identify promising new drug targets that can be pharmacologically modulated. ABPP offers a robust method by enabling the rapid, direct identification and quantification of enzyme activities within complex biological samples. This technique holds the potential to accelerate the discovery of viable new targets for antibacterial therapy.

The main focus of this study was to use ABPs to identify new enzymatic activities in bacterial pathogens, particularly *S. aureus* and *K. pneumoniae*. This follows a previous study where fluorophosphonate (FP) probe was used to identify previously uncharacterized enzymes in *S. aureus* that have emerging roles in pathogenesis and as potential anti-virulence targets[106]. In this work, additional enzyme families that remain underexplored in *S. aureus* were aimed to be identified (Papers I and II) under similar growth conditions that promote biofilm formation. Moreover, general serine-reactive FP probe was used to identify serine hydrolases in *K. pneumoniae* that had also been successfully used previously in other organisms[272,311,352-354].

6.1 ABPP in *S. aureus* and *K. pneumoniae*

ABPP is a powerful chemo-proteomics technique that identifies the on-target and off-target of a drug[422]. Initial efforts were undertaken to profile active target enzymes in *S. aureus* using carmofur-derived ABP (Paper I). Carmofur and its parent compound, 5-FU, are recognized for their broad-spectrum antimicrobial and antibiofilm activity against various bacteria[423]. However, the exact mechanism behind the antimicrobial effects of carmofur remains unknown. It is plausible that microbial enzymes targeted by carmofur may directly contribute to its antimicrobial and antibiofilm activities analogous to the role of human acid ceramidase (ACase) inhibition in the therapeutic efficacy of carmofur in humans. Interestingly, multiple enzyme families were identified using carmofur-derived biotin analog coupled with LC-MS/MS including NTN hydrolases, which are targeted by carmofur in humans as well as previously uncharacterized serine hydrolases (Paper I). Due to the promiscuous nature and broad reactivity of the carmofur probe, which may lead to the identification of a broad range of enzyme families,

understanding the functional characteristics of these enzymes can be challenging. Since carmofur is used as a colorectal cancer drug in the clinic, the same reactivity of carmofur with other gut microbiota enzymes and human enzymes, which might potentially relate to the therapeutic and side effects of carmofur, cannot be ruled out. The report has also shown that non-antibiotic drugs including 5FU, a prodrug of carmofur, can inhibit at least the growth of one commensal bacteria by 25%[424] (Paper I).

Glycosidases play crucial roles in bacterial pathogenesis, including immune modulation, adherence to host cells, colonization, and biofilm formation [325]. Given the high substrate specificity of glycosidases and the absence of a broad-spectrum probe, a panel of glycosidases ABPs has been applied to identify three glycosidase hydrolase family proteins: the alpha-amylase family protein phosphotrehalase (TreC), 6-phospho-β-glucosidase (BglA), and autolysin (Atl), two (TreC and BglA) of which were previously uncharacterized (Paper II). Since serine hydrolases play important roles in bacterial homeostasis, metabolism, and virulence, a broad-spectrum FP probe was used to identify 10 *K. pneumoniae* serine hydrolases, seven of which are poorly annotated and previously uncharacterized (Paper III).

However, in this current study, only simplistic *in vitro* growth conditions were used to profile the active enzymes. Bacteria may express alternative enzymes under other conditions. Future efforts will involve using more complex infection models to identify additional enzymatic activities. Moreover, cell-based ABPP strategies have already been successfully employed to identify active enzymes at the host-pathogen interface and in other physiological environments[311,425].

ABPP can identify enzymes that are already known for their potential to contribute to biofilm formation and bacterial pathogenesis. Several enzymes identified in this thesis through ABPP studies had already been recognized previously for their important roles in biofilm formation and bacterial pathogenesis and could serve as potential targets for anti-virulence and putative drug therapies. For instance, the NTN hydrolase family member, IMP cyclohydrolase, PurH have been recognized for their roles in biofilm formation[426] and the FphB has recently been characterized as a virulence factor in *S. aureus*[106] (Paper I). In addition, the O-acetyltransferase Oat that features a SGNH-hydrolase-type esterase domain[427], is common across a wide variety of bacteria and serves various functions[428] (Paper I). The teichoic acid d-Ala esterase FmtA is responsible for the hydrolytic removal of d-alanine esters from wall teichoic acid (WTA), a crucial process that helps regulate the charge and integrity of the bacterial cell wall[429,430] (Paper I). In Paper II, Autolysin (Atl), also known as peptidoglycan hydrolase, was identified, which

plays crucial roles in cell envelope remodeling, virulence, and biofilm formation[431,432]. This broad functional spectrum underscores the critical nature of autolysin in bacterial pathophysiology and its potential as a therapeutic target. The HtrA-like serine proteases DegP and DegQ were identified, which demonstrated increased susceptibility to complement-mediated killing and exhibited reduced levels of capsule polysaccharide[433](Paper III). However, the mechanisms through which these proteases exert their effects are not yet fully understood. Additionally, the carboxylesterase BioH, which plays a role in the biosynthesis of biotin[434] was enriched (Paper III). In *Mycobacterium tuberculosis*, biotin metabolism is recognized as a viable target pathway for antibacterial drugs[435 436]. Since ABPP identifies enzyme targets through covalent interactions with a small molecule probe, it confirms that all identified targets are druggable and facilitates the identification of target-specific inhibitors.

Besides glycosidases and serine hydrolases, the MS-based ABPP also detected other hydrolytic enzymes (papers II and III). This is a known limitation of affinity-based pulldown experiments, as they can enrich ribosomal proteins, and endogenously biotinylated proteins and sometimes targets are even enriched due to less stable, non-covalent, reversible interactions with the probe[437,438]. However, this study excluded those hydrolytic enzymes and specifically focused on glycosidase in *S. aureus* and serine hydrolases in *K. pneumoniae* (Paper II and III).

6.2 Functional validation of uncharacterized enzymes in host-pathogen interactions

Enzymes that are active can be crucial for bacterial virulence or the hosts immune response to infection, thus constituting potential therapeutic targets. Retaining glycosidases and serine hydrolases play crucial roles in numerous biological processes in both bacteria and their hosts and can be selectively targeted by cyclophellitol-aziridine and well-characterized fluorophosphonate (FP)-containing ABPs. However, the understanding of these enzymes in the bacterial pathogens *S. aureus* and *K. pneumoniae* remains limited. Since this study identified two previously uncharacterized glycosidases in *S. aureus* and seven uncharacterized serine hydrolases (SHs) in *K. pneumoniae*, this study aimed to further assess cellular functions in relation to host-pathogen interactions and bacterial physiology. Although the Nebraska Transposon Mutant Library for *S. aureus* JE2 strains is available in the lab, due to the non-specific effects from secondary mutations or polar effects within the transposon mutants, alternative IPTG-induced CRISPRi mutants were used for the functional validation of

glycosidase targets (Paper II). Despite the challenges of IPTG induction *in vivo*, like in the wax moth larvae model, CRISPRi constructs were chosen. CRISPRi constructs specifically block the transcription of genes, thus reducing secondary mutational effects. In addition, they were constructed in the well-characterized *S. aureus* LAC strain. On the other hand, due to the absence of alternative mutants, transposon mutants were utilized in Paper III. Given the critical role of glycosidases in degrading host glycans, which may assist in extracting nutrients for bacteria and facilitate colonization[439], CRISPRi gene silencing was employed to investigate the roles of BglA and TreC in wax moth *Galleria mellonella* larvae, as an infection model (Paper II). Interestingly, the results indicated that TreC might contribute to virulence in the *G. mellonella* infection model. The mechanisms by which TreC acts as a virulence factor remain unknown. However, TreC is part of the alpha-amylase family within GH13, one of the largest families of glycoside hydrolases[440]. Additionally, an alpha-amylase family protein has previously been identified as a putative virulence factor in *Streptococcus pneumoniae* through a single signature-tagged mutagenesis (STM) screen[441]. Future studies, including biochemical characterization, identification of physiological substrates, and other infection models, including *in vivo* animal studies, are necessary to substantiate the role of this enzyme as a virulence factor.

Since 7 of the identified serine hydrolases (SHs) in *K. pneumoniae* (Paper III) are previously uncharacterized and their cellular functions are poorly defined, their roles at the host-pathogen interface for this critical priority pathogen were also addressed. This thesis also focused on SHs due to their significant impact on microbial pathogenicity[442]; their frequent activation at the post-translational stage[443] makes them ideal candidates for activity-based studies[444,445]. Additionally, since these enzymes can be targeted through covalent interactions with small molecule probes, they represent promising lead molecules for validating targets for anti-virulence therapy and as potential antibiotic sensitizers.

However, to replicate the environmental conditions bacteria encounter during colonization and infection, several model systems are necessary. Since the primary niche of *K. pneumoniae* is as a commensal in the gut, the HT29-MTX cells, which is rich in goblet cells and mucus, were utilized as an *in vitro* model to mimic the gut environment. Interestingly, pronounced growth defects were exhibited by three SH-deficient transposon mutants, *pldB*, *ychK*, and *yjfP*, in this co-culture model (Paper III). To further validate these mutants, a human-derived colonic organoid model was used (Paper III). The advantage of using organoid models lies in their accessibility, providing faster and more reliable results than animal models and offering a more

accurate representation of human tissue along with greater material availability[389]. The SH-deficient transposon mutants *pldB*, *ychK*, and *yjfP* also showed a pronounced fitness loss upon co-culturing with a colonic organoid monolayer. Since these mutants were unable to grow in organoid growth media alone, it was assumed that interactions with host cells are crucial for sustaining the growth of these mutants in the co-culture model. Interestingly, the translocation efficacy was relatively low for PldB and YchK, suggesting these enzymes might be important in hampering the epithelial cell barrier. The mucus layer, primarily composed of glycoproteins, acts as a defense against the bacteria residing in the colon[446-448] but also contains phosphatidylcholine (PC), an essential component of the intestinal mucus layer's structure[449]. Bacterial phospholipases in this layer can convert PC to lyso-PC, disrupting the mucus structure and damaging epithelial cells[449-451]. For example, *H. pylori*, secreted lipases can breach mucus-associated phospholipids, aiding this pathogen to invade gastric mucus[452,453]. A similar mechanism could be plausible for putative secreted patatin-like phospholipases YchK, either accessing nutrients through it is hydrolytic activity directly from mucus-associated phospholipids or breaking the defensive barrier for cell invasion and nutrient extraction.

While the specific mechanisms by which the other two enzymes, PldB and YjfP, act on the gut are speculative, maintaining cell envelope integrity might be involved. However, mutants deficient in proteins PldB and YjfP, but not the secreted lipase YchK, showed increased susceptibility to antimicrobial peptide (AMP) antibiotics such as polymyxin B, and to complement-induced killing. Polymyxin B is a membrane-destabilizing AMP that interacts with lipopolysaccharide (LPS) of the outer membrane in gram-negative bacteria and disrupts the bacterial membrane[454]. Complement also targets the outer membrane of Gram-negative bacteria, disrupting it by forming pores[455]. The presence of lysozyme C in colonic organoids model indirectly indicated the presence of Paneth cells, which are typically found in the small intestine[456] and known for producing antimicrobial peptides and defensins[457]. The initial drop in *K. pneumoniae* growth in organoid models was likely due to the bactericidal effects of AMPs produced by the organoids. Reduced virulence was also observed for these three SH-deficient mutants in *Galleria mellonella* infection models. Given that AMPs are important effectors of innate immunity in larvae, it is possible that *G. mellonella* also produces AMPs[458].

Biochemical and structural characterization of YjfP indicates that it is a deacetylase, acting on small molecules of peptides and proteins. On the other hand, PldB cleaves a range of saturated lipid esters fluorogenic substrates up to C8 fatty acid chain length. The interesting phenotypes of these SH mutants demand further investigation of their physiological substrates. In addition,

protein BLAST searches with non-redundant protein sequences indicate that these serine hydrolases exhibited little or no homology with those of other gut commensal bacteria or humans. This result suggests that these three serine hydrolases could be important targets for small-molecule drugs, potentially minimizing off-target effects and reducing the inhibition of enzymes in other microbes. This notion also supports the integration of bioinformatics with ABPP to enhance drug development, providing additional insights into their potential as drug targets[459].

Since transposon mutants might carry secondary mutations affecting these phenotypes, other allelic transposon mutants were also tested in the *G. mellonella* infection model, and similar phenotypes were observed. However, future studies involving gene complementation and gene knockouts through allelic exchange are necessary to fully determine their roles.

7. Concluding remarks and future aspects

Bacterial infections have always posed a significant threat to human health. However, improvements in hygiene practices and the development and use of antibiotics over the past century have significantly reduced the burden and mortality rates associated with these infections. Despite these advances, the extensive use and misuse of antibiotics have led to increased resistance, raising concerns that we are approaching a post-antibiotic era marked by untreatable bacterial infections. This emerging crisis underscores the urgent need for a novel approach to combat antibiotic-resistant bacteria. One promising strategy could involve exploring virulence factors that disarm or neutralize the mechanisms bacteria use to infect and damage their hosts, rather than fully killing the bacteria, which could likely prevent the development of resistance. This thesis has focused on using ABPP to identify previously uncharacterized druggable enzymes and functionally validate them within the context of bacterial physiology and the host-pathogen interface.

Overall, this study identified and functionally validated previously uncharacterized enzyme targets: one glycosidase, TreC, in *S. aureus*, and three serine hydrolases, PldB, YjfP, and YchK, in *K. pneumoniae*. These targets have shown potential as anti-virulence targets. ABPP, which identifies enzyme targets through covalent interaction with small molecule probes, confirms the druggability of the targets and facilitates the development of target-specific inhibitors. Competitive ABPP, in particular, allows for the identification of selective cell-permeable inhibitors. In contrast, traditional target-based antibiotic drug design projects often fail due to the drug's lack of cellular permeability. If performed on live cells, as in this study, cell-based competitive ABPP also pre-validates the accessibility of the targets to the inhibitors. This study provides the groundwork for future investigations into the biological functions of these enzymes, highlighting their potential as promising targets for the development of selective inhibitors and activity-based probes, which will be crucial in characterizing their activities within physiological environments. The initial functional studies of these enzymes suggest that inhibiting these targets, having role in virulence, could potentiate with existing antibiotics and human immune defense to prevent bacterial infection and/or colonization. However, further functional validation of these enzymes in more complex models of infection and host-pathogen interactions is necessary to better understand these newly identified enzymes. This deeper exploration is essential to fully assess their potential as putative antibacterial drugs.

8. References

1. van der Meer, J.W. The infectious disease challenges of our time. *Front Public Health* **1**, 7 (2013).
2. Morens, D.M., Folkers, G.K. & Fauci, A.S. The challenge of emerging and re-emerging infectious diseases. *Nature* **430**, 242-249 (2004).
3. Binder, S., Levitt, A.M., Sacks, J.J. & Hughes, J.M. Emerging infectious diseases: public health issues for the 21st century. *Science* **284**, 1311-1313 (1999).
4. Alirol, E., Getaz, L., Stoll, B., Chappuis, F. & Loutan, L. Urbanisation and infectious diseases in a globalised world. *Lancet Infect Dis* **11**, 131-41 (2011).
5. Hierink, F., Okiro, E.A., Flahault, A. & Ray, N. The winding road to health: A systematic scoping review on the effect of geographical accessibility to health care on infectious diseases in low- and middle-income countries. *PLoS One* **16**, e0244921 (2021).
6. Jones, K.E. et al. Global trends in emerging infectious diseases. *Nature* **451**, 990-3 (2008).
7. Pendleton, J.N., Gorman, S.P. & Gilmore, B.F. Clinical relevance of the ESKAPE pathogens. *Expert Review of Anti-infective Therapy* **11**, 297-308 (2013).
8. Mancuso, G., Midiri, A., Gerace, E. & Biondo, C. Bacterial Antibiotic Resistance: The Most Critical Pathogens. *Pathogens* **10**(2021).
9. WHO (2017). Fact Sheet on Antimicrobial Resistance. https://www.who.int/news-room/detail/27-02-2017-who-publishes-list-of-bacteria-for-which-new-antibiotics-are-urgently-needed.
10. Lee, H.A. et al. Global Infectious Disease Surveillance and Case Tracking System for COVID-19: Development Study. *JMIR Med Inform* **8**, e20567 (2020).
11. Cui, F., Zhou, Z. & Zhou, H.S. Molecularly Imprinted Polymers and Surface Imprinted Polymers Based Electrochemical Biosensor for Infectious Diseases. *Sensors (Basel)* **20**(2020).
12. Smith, K.F. et al. Global rise in human infectious disease outbreaks. *J R Soc Interface* **11**, 20140950 (2014).
13. Baker, R.E. et al. Infectious disease in an era of global change. *Nat Rev Microbiol* **20**, 193-205 (2022).
14. Ogston, A. Report upon Micro-Organisms in Surgical Diseases. *Br Med J* **1**, 369.b2-375 (1881).
15. Ogston, A. Micrococcus poisoning. *Journal of anatomy and physiology* **16**, 526 (1882).
16. Licitra, G. Etymologia: staphylococcus. *Emerging Infectious Diseases* **19**, 1553 (2013).
17. Rosenbach, A.J.F. *Mikro-organismen bei den Wund-infections-krankheiten des Menschen*, (JF Bergmann, 1884).
18. Marshall, J.H. & Wilmoth, G.J. Pigments of *Staphylococcus aureus*, a series of triterpenoid carotenoids. *Journal of bacteriology* **147**, 900-913 (1981).

19. Gnanamani, A., Hariharan, P. & Paul-Satyaseela, M. *Staphylococcus aureus*: Overview of bacteriology, clinical diseases, epidemiology, antibiotic resistance and therapeutic approach. *Frontiers in Staphylococcus aureus* **4**, 10-5772 (2017).

20. Foster, T. Staphylococcus. *Medical Microbiology. 4th edition* (1996).

21. O'Riordan, K. & Lee, J.C. *Staphylococcus aureus* capsular polysaccharides. *Clinical microbiology reviews* **17**, 218-234 (2004).

22. Pasquina-Lemonche, L. et al. The architecture of the Gram-positive bacterial cell wall. *Nature* **582**, 294-297 (2020).

23. Rajagopal, M. & Walker, S. Envelope structures of Gram-positive bacteria. *Protein and sugar export and assembly in Gram-positive bacteria*, 1-44 (2017).

24. Parfentjev, I. & Catelli, A.R. Tolerance of *Staphylococcus aureus* to sodium chloride. *Journal of bacteriology* **88**, 1-3 (1964).

25. Dinges, M.M., Orwin, P.M. & Schlievert, P.M. Exotoxins of *Staphylococcus aureus*. *Clinical microbiology reviews* **13**, 16-34 (2000).

26. Otto, M. *Staphylococcus aureus* toxins. *Current opinion in microbiology* **17**, 32-37 (2014).

27. Tong, S.Y., Davis, J.S., Eichenberger, E., Holland, T.L. & Fowler, V.G., Jr. *Staphylococcus aureus* infections: epidemiology, pathophysiology, clinical manifestations, and management. *Clin Microbiol Rev* **28**, 603-61 (2015).

28. van Belkum, A. et al. Co-evolutionary aspects of human colonisation and infection by *Staphylococcus aureus*. *Infect Genet Evol* **9**, 32-47 (2009).

29. Sakr, A., Brégeon, F., Mège, J.L., Rolain, J.M. & Blin, O. *Staphylococcus aureus* Nasal Colonization: An Update on Mechanisms, Epidemiology, Risk Factors, and Subsequent Infections. *Front Microbiol* **9**, 2419 (2018).

30. Weidenmaier, C., Goerke, C. & Wolz, C. *Staphylococcus aureus* determinants for nasal colonization. *Trends in Microbiology* **20**, 243-250 (2012).

31. Mertz, D. et al. Throat Swabs Are Necessary to Reliably Detect Carriers of *Staphylococcus aureus*. *Clinical Infectious Diseases* **45**, 475-477 (2007).

32. Acton, D.S., Tempelmans Plat-Sinnige, M.J., van Wamel, W., de Groot, N. & van Belkum, A. Intestinal carriage of *Staphylococcus aureus*: how does its frequency compare with that of nasal carriage and what is its clinical impact? *European Journal of Clinical Microbiology & Infectious Diseases* **28**, 115-127 (2009).

33. Bourgeois-Nicolaos, N. et al. Maternal vaginal colonisation by *Staphylococcus aureus* and newborn acquisition at delivery. *Paediatric and Perinatal Epidemiology* **24**, 488-491 (2010).

34. Berry, K.A., Verhoef, M.T.A., Leonard, A.C. & Cox, G. *Staphylococcus aureus* adhesion to the host. *Annals of the New York Academy of Sciences* **1515**, 75-96 (2022).

35. Brown, A.F., Leech, J.M., Rogers, T.R. & McLoughlin, R.M. *Staphylococcus aureus* Colonization: Modulation of Host Immune Response and Impact on Human Vaccine Design. *Front Immunol* **4**, 507 (2014).

36. Kang, J., Dietz, M.J. & Li, B. Antimicrobial peptide LL-37 is bactericidal against *Staphylococcus aureus* biofilms. *PLOS ONE* **14**, e0216676 (2019).

37. Thomer, L., Schneewind, O. & Missiakas, D. Pathogenesis of *Staphylococcus aureus* Bloodstream Infections. *Annu Rev Pathol* **11**, 343-64 (2016).

38. Casadevall, A. & Pirofski, L. Host-pathogen interactions: the attributes of virulence. *J Infect Dis* **184**, 337-44 (2001).

39. Bishop, W.J. The Story Behind the Word: Some Interesting Origins of Medical Terms. Harry WainM.D. Springfield, Illinois: C. C. Thomas; Oxford: Blackwell Scientific Publications, 1958; PP. Viii, 342. 63s. *Medical History* **2**, 321-322 (1958).

40. Powers, M.E. & Wardenburg, J.B. Igniting the Fire: *Staphylococcus aureus* Virulence Factors in the Pathogenesis of Sepsis. *PLOS Pathogens* **10**, e1003871 (2014).

41. Zhu, J., Wang, T., Chen, L. & Du, H. Virulence Factors in Hypervirulent *Klebsiella pneumoniae*. *Frontiers in Microbiology* **12**(2021).

42. Weiss, R.A. Virulence and pathogenesis. *Trends Microbiol* **10**, 314-7 (2002).

43. Ribet, D. & Cossart, P. How bacterial pathogens colonize their hosts and invade deeper tissues. *Microbes and Infection* **17**, 173-183 (2015).

44. Tuchscherr, L. et al. *Staphylococcus aureus* phenotype switching: an effective bacterial strategy to escape host immune response and establish a chronic infection. *EMBO Mol Med* **3**, 129-41 (2011).

45. Lindsay, J.A. Staphylococci: Evolving Genomes. *Microbiology Spectrum* **7**, 10.1128/microbiolspec.gpp3-0071-2019 (2019).

46. Malachowa, N. & DeLeo, F.R. Mobile genetic elements of *Staphylococcus aureus*. *Cellular and Molecular Life Sciences* **67**, 3057-3071 (2010).

47. Foster, T.J., Geoghegan, J.A., Ganesh, V.K. & Höök, M. Adhesion, invasion and evasion: the many functions of the surface proteins of Staphylococcus aureus. *Nat Rev Microbiol* **12**, 49-62 (2014).

48. Tam, K. & Torres, V.J. *Staphylococcus aureus* Secreted Toxins and Extracellular Enzymes. *Microbiology Spectrum* **7**, 10.1128/microbiolspec.gpp3-0039-2018 (2019).

49. Cheung, G.Y.C., Bae, J.S. & Otto, M. Pathogenicity and virulence of *Staphylococcus aureus*. *Virulence* **12**, 547-569 (2021).

50. Keane, F.M. et al. Fibrinogen and elastin bind to the same region within the A domain of fibronectin binding protein A, an MSCRAMM of *Staphylococcus aureus*. *Molecular Microbiology* **63**, 711-723 (2007).

51. Fowler, T. et al. Cellular invasion by *Staphylococcus aureus* involves a fibronectin bridge between the bacterial fibronectin-binding MSCRAMMs and host cell β1 integrins. *European journal of cell biology* **79**, 672-679 (2000).

52. Ganesh, V.K. et al. A structural model of the Staphylococcus aureus ClfA–fibrinogen interaction opens new avenues for the design of anti-staphylococcal therapeutics. *PLoS pathogens* **4**, e1000226 (2008).

53. Mulcahy, M.E. et al. Nasal colonisation by *Staphylococcus aureus* depends upon clumping factor B binding to the squamous epithelial cell envelope protein loricrin. *PLoS pathogens* **8**, e1003092 (2012).

54. Corrigan, R.M., Miajlovic, H. & Foster, T.J. Surface proteins that promote adherence of *Staphylococcus aureus* to human desquamated nasal epithelial cells. *BMC microbiology* **9**, 1-10 (2009).

55. Sharp, J.A. et al. *Staphylococcus aureus* surface protein SdrE binds complement regulator factor H as an immune evasion tactic. *PloS one* **7**, e38407 (2012).

56. Vazquez, V. et al. Fibrinogen is a ligand for the *Staphylococcus aureus* microbial surface components recognizing adhesive matrix molecules (MSCRAMM) bone sialoprotein-binding protein (Bbp). *Journal of Biological Chemistry* **286**, 29797-29805 (2011).

57. Zong, Y. et al. A 'Collagen Hug'model for *Staphylococcus aureus* CNA binding to collagen. *The EMBO journal* **24**, 4224-4236 (2005).

58. Kang, M. et al. Collagen-binding microbial surface components recognizing adhesive matrix molecule (MSCRAMM) of Gram-positive bacteria inhibit complement activation via the classical pathway. *Journal of biological chemistry* **288**, 20520-20531 (2013).

59. Grigg, J.C., Ukpabi, G., Gaudin, C.F. & Murphy, M.E. Structural biology of heme binding in the *Staphylococcus aureus* Isd system. *Journal of inorganic biochemistry* **104**, 341-348 (2010).

60. Clarke, S.R., Wiltshire, M.D. & Foster, S.J. IsdA of *Staphylococcus aureus* is a broad spectrum, iron-regulated adhesin. *Molecular microbiology* **51**, 1509-1519 (2004).

61. Zapotoczna, M., Jevnikar, Z., Miajlovic, H., Kos, J. & Foster, T.J. Iron-regulated surface determinant B (IsdB) promotes *Staphylococcus aureus* adherence to and internalization by non-phagocytic human cells. *Cellular microbiology* **15**, 1026-1041 (2013).

62. Visai, L. et al. Immune evasion by *Staphylococcus aureus* conferred by iron-regulated surface determinant protein IsdH. *Microbiology* **155**, 667-679 (2009).

63. Roche, F.M., Meehan, M. & Foster, T.J. The *Staphylococcus aureus* surface protein SasG and its homologues promote bacterial adherence to human desquamated nasal epithelial cells. *Microbiology* **149**, 2759-2767 (2003).

64. Geoghegan, J.A. et al. Role of surface protein SasG in biofilm formation by *Staphylococcus aureus*. *Journal of bacteriology* **192**, 5663-5673 (2010).

65. Li, M. et al. MRSA epidemic linked to a quickly spreading colonization and virulence determinant. *Nature medicine* **18**, 816-819 (2012).

66. Graille, M. et al. Crystal structure of a *Staphylococcus aureus* protein A domain complexed with the Fab fragment of a human IgM antibody: structural basis for recognition of B-cell receptors and superantigen activity. *Proceedings of the National Academy of Sciences* **97**, 5399-5404 (2000).

67. Gómez, M.I. et al. *Staphylococcus aureus* protein A induces airway epithelial inflammatory responses by activating TNFR1. *Nature medicine* **10**, 842-848 (2004).

68. Chavakis, T. et al. Staphylococcus aureus extracellular adherence protein serves as anti-inflammatory factor by inhibiting the recruitment of host leukocytes. *Nature medicine* **8**, 687-693 (2002).

69. Woehl, J.L. et al. The extracellular adherence protein from *Staphylococcus aureus* inhibits the classical and lectin pathways of complement by blocking formation of the C3 proconvertase. *The journal of immunology* **193**, 6161-6171 (2014).

70. Thomas, S. et al. The complex fibrinogen interactions of the *Staphylococcus aureus* coagulases. *Frontiers in Cellular and Infection Microbiology* **9**, 106 (2019).

71. Cheng, A.G. et al. Contribution of coagulases towards *Staphylococcus aureus* disease and protective immunity. *PLoS pathogens* **6**, e1001036 (2010).

72. Guggenberger, C., Wolz, C., Morrissey, J.A. & Heesemann, J. Two distinct coagulase-dependent barriers protect *Staphylococcus aureus* from neutrophils in a three dimensional in vitro infection model. *PLoS pathogens* **8**, e1002434 (2012).

73. van Dalen, R., Peschel, A. & van Sorge, N.M. Wall teichoic acid in *Staphylococcus aureus* host interaction. *Trends in microbiology* **28**, 985-998 (2020).

74. Baur, S. et al. A nasal epithelial receptor for *Staphylococcus aureus* WTA governs adhesion to epithelial cells and modulates nasal colonization. *Plos pathogens* **10**, e1004089 (2014).

75. Biswas, R. et al. Activity of the major staphylococcal autolysin Atl. *FEMS Microbiology Letters* **259**, 260-268 (2006).

76. Schlesier, T., Siegmund, A., Rescher, U. & Heilmann, C. Characterization of the Atl-mediated staphylococcal internalization mechanism. *International Journal of Medical Microbiology* **310**, 151463 (2020).

77. Wilke, G.A. & Bubeck Wardenburg, J. Role of a disintegrin and metalloprotease 10 in *Staphylococcus aureus* alpha-hemolysin-mediated cellular injury. *Proc Natl Acad Sci U S A* **107**, 13473-8 (2010).

78. Inoshima, I. et al. A *Staphylococcus aureus* pore-forming toxin subverts the activity of ADAM10 to cause lethal infection in mice. *Nature Medicine* **17**, 1310-1314 (2011).

79. Nygaard, T.K. et al. Alpha-Toxin Induces Programmed Cell Death of Human T cells, B cells, and Monocytes during USA300 Infection. *PLOS ONE* **7**, e36532 (2012).

80. Lina, G. et al. Standard nomenclature for the superantigens expressed by Staphylococcus. *J Infect Dis* **189**, 2334-6 (2004).

81. Balaban, N. & Rasooly, A. Staphylococcal enterotoxins. *Int J Food Microbiol* **61**, 1-10 (2000).

82. Pinchuk, I.V., Beswick, E.J. & Reyes, V.E. Staphylococcal enterotoxins. *Toxins (Basel)* **2**, 2177-97 (2010).

83. Kim, J., Urban, R.G., Strominger, J.L. & Wiley, D.C. Toxic shock syndrome toxin-1 complexed with a class II major histocompatibility molecule HLA-DR1. *Science* **266**, 1870-4 (1994).

84. Dinges, M.M., Orwin, P.M. & Schlievert, P.M. Exotoxins of *Staphylococcus aureus*. *Clin Microbiol Rev* **13**, 16-34, table of contents (2000).

85. Novick, R.P. Mobile genetic elements and bacterial toxinoses: the superantigen-encoding pathogenicity islands of *Staphylococcus aureus*. *Plasmid* **49**, 93-105 (2003).

86. Hart, M.E., Hart, M.J. & Roop, A.J. Genotypic and Phenotypic Assessment of Hyaluronidase among Type Strains of a Select Group of Staphylococcal Species. *International Journal of Microbiology* **2009**, 614371 (2009).

87. Makris, G., Wright, J.D., Ingham, E. & Holland, K.T. The hyaluronate lyase of *Staphylococcus aureus* – a virulence factor? *Microbiology* **150**, 2005-2013 (2004).

88. Wang, Z. et al. Two Novel Functions of Hyaluronidase from Streptococcus agalactiae Are Enhanced Intracellular Survival and Inhibition of Proinflammatory Cytokine Expression. *Infection and Immunity* **82**, 2615-2625 (2014).

89. Sako, T. et al. Cloning and expression of the staphylokinase gene of *Staphylococcus aureus* in *Escherichia coli*. *Mol Gen Genet* **190**, 271-7 (1983).

90. de Haas, C.J. et al. Chemotaxis inhibitory protein of *Staphylococcus aureus*, a bacterial antiinflammatory agent. *J Exp Med* **199**, 687-95 (2004).

91. Murphy, J. et al. *Staphylococcus Aureus* V8 protease disrupts the integrity of the airway epithelial barrier and impairs IL-6 production in vitro. *The Laryngoscope* **128**, E8-E15 (2018).

92. Rice, K., Peralta, R., Bast, D., de Azavedo, J. & McGavin, M.J. Description of staphylococcus serine protease (ssp) operon in Staphylococcus aureus and nonpolar inactivation of sspA-encoded serine protease. *Infection and immunity* **69**, 159-169 (2001).

93. Arvidson, S. Studies on extracellular proteolytic enzymes from *Staphylococcus aureus*: II. Isolation and characterization of an EDTA-sensitive protease. *Biochimica et Biophysica Acta (BBA) - Enzymology* **302**, 149-157 (1973).

94. Sieprawska-Lupa, M. et al. Degradation of Human Antimicrobial Peptide LL-37 by *Staphylococcus aureus*-Derived Proteinases. *Antimicrobial Agents and Chemotherapy* **48**, 4673-4679 (2004).

95. Laarman, A.J. et al. *Staphylococcus aureus* metalloprotease aureolysin cleaves complement C3 to mediate immune evasion. *Journal of immunology (Baltimore, Md.: 1950)* **186**, 6445-6453 (2011).

96. Kalińska, M. et al. Substrate specificity of *Staphylococcus aureus* cysteine proteases–Staphopains A, B and C. *Biochimie* **94**, 318-327 (2012).

97. Kubica, M. et al. A potential new pathway for *Staphylococcus aureus* dissemination: the silent survival of S. aureus phagocytosed by human monocyte-derived macrophages. *PloS one* **3**, e1409 (2008).

98. Schindler, D. et al. Dendritic cells are central coordinators of the host immune response to *Staphylococcus aureus* bloodstream infection. *The American journal of pathology* **181**, 1327-1337 (2012).

99. Paharik, A.E. et al. The Spl serine proteases modulate *Staphylococcus aureus* protein production and virulence in a rabbit model of pneumonia. *Msphere* **1**, 10.1128/msphere.00208-16 (2016).

100. Reed, S.B. et al. Molecular characterization of a novel *Staphylococcus aureus* serine protease operon. *Infection and immunity* **69**, 1521-1527 (2001).

101. Doery, H.M., Magnusson, B., Gulasekharam, J. & PEARSON, J.E. The properties of phospholipase enzymes in staphylococcal toxins. *Microbiology* **40**, 283-296 (1965).

102. Daugherty, S. & Low, M.G. Cloning, expression, and mutagenesis of phosphatidylinositol-specific phospholipase C from *Staphylococcus aureus*: a potential staphylococcal virulence factor. *Infection and immunity* **61**, 5078-5089 (1993).

103. White, M.J., Boyd, J.M., Horswill, A.R. & Nauseef, W.M. Phosphatidylinositol-specific phospholipase C contributes to survival of *Staphylococcus aureus* USA300 in human blood and neutrophils. *Infection and immunity* **82**, 1559-1571 (2014).

104. Cadieux, B., Vijayakumaran, V., Bernards, M.A., McGavin, M.J. & Heinrichs, D.E. Role of lipase from community-associated methicillin-resistant *Staphylococcus aureus* strain USA300 in hydrolyzing triglycerides into growth-inhibitory free fatty acids. *Journal of bacteriology* **196**, 4044-4056 (2014).

105. Shryock, T., Dye, E. & Kapral, F. The accumulation of bactericidal lipids in staphylococcal abscesses. *Journal of medical microbiology* **36**, 332-336 (1992).

106. Lentz, C.S. et al. Identification of a S. aureus virulence factor by activity-based protein profiling (ABPP). *Nat Chem Biol* **14**, 609-617 (2018).

107. Cheung, A.L., Bayer, A.S., Zhang, G., Gresham, H. & Xiong, Y.-Q. Regulation of virulence determinants in vitro and in vivo in *Staphylococcus aureus*. *FEMS Immunology & Medical Microbiology* **40**, 1-9 (2004).

108. Donlan, R.M. & Costerton, J.W. Biofilms: survival mechanisms of clinically relevant microorganisms. *Clinical microbiology reviews* **15**, 167-193 (2002).

109. Flemming, H.-C. et al. Biofilms: an emergent form of bacterial life. *Nature Reviews Microbiology* **14**, 563-575 (2016).

110. Archer, N.K. et al. *Staphylococcus aureus* biofilms. *Virulence* **2**, 445-459 (2011).

111. Abraham, N.M. & Jefferson, K.K. *Staphylococcus aureus* clumping factor B mediates biofilm formation in the absence of calcium. *Microbiology* **158**, 1504-1512 (2012).

112. Flemming, H.-C. & Wingender, J. The biofilm matrix. *Nature Reviews Microbiology* **8**, 623-633 (2010).

113. Fitzpatrick, F., Humphreys, H. & O'Gara, J.P. Evidence for icaADBC-independent biofilm development mechanism in methicillin-resistant *Staphylococcus aureus* clinical isolates. *Journal of clinical microbiology* **43**, 1973-1976 (2005).

114. Sauer, K. et al. The biofilm life cycle: expanding the conceptual model of biofilm formation. *Nat Rev Microbiol* **20**, 608-620 (2022).

115. Sutherland, I.W. Biofilm exopolysaccharides: a strong and sticky framework. *Microbiology* **147**, 3-9 (2001).

116. Donlan, R.M. Biofilms: microbial life on surfaces. *Emerg Infect Dis* **8**, 881-90 (2002).

117. Scherr, T.D., Heim, C.E., Morrison, J.M. & Kielian, T. Hiding in plain sight: interplay between staphylococcal biofilms and host immunity. *Frontiers in immunology* **5**, 74123 (2014).

118. De la Fuente-Núñez, C., Reffuveille, F., Fernández, L. & Hancock, R.E. Bacterial biofilm development as a multicellular adaptation: antibiotic resistance and new therapeutic strategies. *Current opinion in microbiology* **16**, 580-589 (2013).

119. Singh, R., Ray, P., Das, A. & Sharma, M. Role of persisters and small-colony variants in antibiotic resistance of planktonic and biofilm-associated *Staphylococcus aureus*: an in vitro study. *Journal of medical microbiology* **58**, 1067-1073 (2009).

120. Lewis, K. Persister cells. *Annual review of microbiology* **64**, 357-372 (2010).

121. Bhattacharya, M., Wozniak, D.J., Stoodley, P. & Hall-Stoodley, L. Prevention and treatment of *Staphylococcus aureus* biofilms. *Expert Rev Anti Infect Ther* **13**, 1499-516 (2015).

122. Lister, J.L. & Horswill, A.R. *Staphylococcus aureus* biofilms: recent developments in biofilm dispersal. *Frontiers in Cellular and Infection Microbiology* **4**(2014).

123. Kostakioti, M., Hadjifrangiskou, M. & Hultgren, S.J. Bacterial biofilms: development, dispersal, and therapeutic strategies in the dawn of the postantibiotic era. *Cold Spring Harbor perspectives in medicine* **3**, a010306 (2013).

124. Moormeier, D.E. & Bayles, K.W. *Staphylococcus aureus* biofilm: a complex developmental organism. *Mol Microbiol* **104**, 365-376 (2017).

125. Moormeier, D., Bose, J., Horswill, A. & Bayles, K. Temporal and stochastic control of *Staphylococcus aureus* biofilm development. MBio 5 (5): e01341-01314. (2014).

126. Kennedy, C.A. & O'Gara, J.P. Contribution of culture media and chemical properties of polystyrene tissue culture plates to biofilm development by *Staphylococcus aureus*. *Journal of medical microbiology* **53**, 1171-1173 (2004).

127. Gross, M., Cramton, S.E., Götz, F. & Peschel, A. Key role of teichoic acid net charge in *Staphylococcus aureus* colonization of artificial surfaces. *Infection and immunity* **69**, 3423-3426 (2001).

128. Houston, P., Rowe, S.E., Pozzi, C., Waters, E.M. & O'Gara, J.P. Essential role for the major autolysin in the fibronectin-binding protein-mediated *Staphylococcus aureus* biofilm phenotype. *Infection and immunity* **79**, 1153-1165 (2011).

129. Foster, T.J., Geoghegan, J.A., Ganesh, V.K. & Höök, M. Adhesion, invasion and evasion: the many functions of the surface proteins of *Staphylococcus aureus*. *Nature Reviews Microbiology* **12**, 49-62 (2014).

130. O'Neill, E. et al. A novel *Staphylococcus aureus* biofilm phenotype mediated by the fibronectin-binding proteins, FnBPA and FnBPB. *Journal of bacteriology* **190**, 3835-3850 (2008).

131. McDevitt, D., Francois, P., Vaudaux, P. & Foster, T. Molecular characterization of the clumping factor (fibrinogen receptor) of *Staphylococcus aureus*. *Molecular microbiology* **11**, 237-248 (1994).

132. Speziale, P., Pietrocola, G., Foster, T.J. & Geoghegan, J.A. Protein-based biofilm matrices in Staphylococci. *Frontiers in cellular and infection microbiology* **4**, 171 (2014).

133. Merino, N. et al. Protein A-mediated multicellular behavior in *Staphylococcus aureus*. *Journal of bacteriology* **191**, 832-843 (2009).

134. Schroeder, K. et al. Molecular characterization of a novel *Staphylococcus aureus* surface protein (SasC) involved in cell aggregation and biofilm accumulation. *PloS one* **4**, e7567 (2009).

135. Cucarella, C. et al. Bap, a *Staphylococcus aureus* surface protein involved in biofilm formation. *Journal of bacteriology* **183**, 2888-2896 (2001).

136. Hall-Stoodley, L., Costerton, J.W. & Stoodley, P. Bacterial biofilms: from the natural environment to infectious diseases. *Nature reviews microbiology* **2**, 95-108 (2004).

137. Stewart, P.S. & Franklin, M.J. Physiological heterogeneity in biofilms. *Nature Reviews Microbiology* **6**, 199-210 (2008).

138. Mann, E.E. et al. Modulation of eDNA release and degradation affects *Staphylococcus aureus* biofilm maturation. *PloS one* **4**, e5822 (2009).

139. Moormeier, D.E. et al. Use of microfluidic technology to analyze gene expression during *Staphylococcus aureus* biofilm formation reveals distinct physiological niches. *Applied and environmental microbiology* **79**, 3413-3424 (2013).

140. Periasamy, S. et al. How *Staphylococcus aureus* biofilms develop their characteristic structure. *Proceedings of the National Academy of Sciences* **109**, 1281-1286 (2012).

141. Toledo-Arana, A. et al. *Staphylococcus aureus* develops an alternative, ica-independent biofilm in the absence of the arlRS two-component system. *Journal of bacteriology* **187**, 5318-5329 (2005).

142. Jefferson, K.K., Cramton, S.E., Götz, F. & Pier, G.B. Identification of a 5-nucleotide sequence that controls expression of the ica locus in *Staphylococcus aureus* and characterization of the DNA-binding properties of IcaR. *Mol Microbiol* **48**, 889-99 (2003).

143. Fitzpatrick, F., Humphreys, H. & O'Gara, J.P. Evidence for icaADBC-independent biofilm development mechanism in methicillin-resistant *Staphylococcus aureus* clinical isolates. *J Clin Microbiol* **43**, 1973-6 (2005).

144. Houston, P., Rowe, S.E., Pozzi, C., Waters, E.M. & O'Gara, J.P. Essential role for the major autolysin in the fibronectin-binding protein-mediated *Staphylococcus aureus* biofilm phenotype. *Infect Immun* **79**, 1153-65 (2011).

145. Boles, B.R. & Horswill, A.R. Staphylococcal biofilm disassembly. *Trends Microbiol* **19**, 449-55 (2011).

146. Otto, M. Staphylococcal infections: mechanisms of biofilm maturation and detachment as critical determinants of pathogenicity. *Annu Rev Med* **64**, 175-88 (2013).

147. Vuong, C., Saenz, H.L., Götz, F. & Otto, M. Impact of the agr quorum-sensing system on adherence to polystyrene in *Staphylococcus aureus*. *The Journal of infectious diseases* **182**, 1688-1693 (2000).

148. Yarwood, J.M., Bartels, D.J., Volper, E.M. & Greenberg, E.P. Quorum sensing in *Staphylococcus aureus* biofilms. *Journal of bacteriology* **186**, 1838-1850 (2004).

149. Boles, B.R. & Horswill, A.R. Agr-mediated dispersal of *Staphylococcus aureus* biofilms. *PLoS pathogens* **4**, e1000052 (2008).

150. Friedländer, C. Ueber die Schizomyceten bei der acuten fibrösen Pneumonie. *Archiv für pathologische Anatomie und Physiologie und für klinische Medicin* **87**, 319-324 (1882).

151. Adeolu, M., Alnajar, S., Naushad, S. & S. Gupta, R. Genome-based phylogeny and taxonomy of the 'Enterobacteriales': proposal for Enterobacterales ord. nov. divided into the families Enterobacteriaceae, Erwiniaceae fam. nov., Pectobacteriaceae fam. nov., Yersiniaceae fam. nov., Hafniaceae fam. nov., Morganellaceae fam. nov., and Budviciaceae fam. nov. *International journal of systematic and evolutionary microbiology* **66**, 5575-5599 (2016).

152. Garrity, G. Bergey's manual® of systematic bacteriology: volume 2: the Proteobacteria, part B: the Gammaproteobacteria. Vol. 2 (Springer Science & Business Media, 2007).

153. Abbas, R. et al. General Overview of *Klebsiella pneumonia*: Epidemiology and the Role of Siderophores in Its Pathogenicity. *Biology (Basel)* **13**(2024).

154. Bagley, S.T. Habitat association of Klebsiella species. *Infection Control & Hospital Epidemiology* **6**, 52-58 (1985).

155. Podschun, R. & Ullmann, U. *Klebsiella* spp. as nosocomial pathogens: epidemiology, taxonomy, typing methods, and pathogenicity factors. *Clinical microbiology reviews* **11**, 589-603 (1998).

156. Wen, Z. & Zhang, J.-R. Bacterial capsules. in *Molecular medical microbiology* 33-53 (Elsevier, 2015).

157. Rendueles, O., Garcia-Garcerà, M., Néron, B., Touchon, M. & Rocha, E.P. Abundance and co-occurrence of extracellular capsules increase environmental breadth: Implications for the emergence of pathogens. *PLoS pathogens* **13**, e1006525 (2017).

158. Domenico, P., Salo, R.J., Cross, A.S. & Cunha, B.A. Polysaccharide capsule-mediated resistance to opsonophagocytosis in *Klebsiella pneumoniae*. *Infection and immunity* **62**, 4495-4499 (1994).

159. Lawlor, M.S., Handley, S.A. & Miller, V.L. Comparison of the host responses to wild-type and cpsB mutant *Klebsiella pneumoniae* infections. *Infection and immunity* **74**, 5402-5407 (2006).

160. Pan, Y.-J. et al. Genetic analysis of capsular polysaccharide synthesis gene clusters in 79 capsular types of *Klebsiella* spp. *Scientific reports* **5**, 15573 (2015).

161. Walker, K.A. & Miller, V.L. The intersection of capsule gene expression, hypermucoviscosity and hypervirulence in *Klebsiella pneumoniae*. *Current opinion in microbiology* **54**, 95-102 (2020).

162. Russo, T. et al. for the Hypervirulent Klebsiella pneumoniae Investigator Group (HVKPIG). Identification of biomarkers for differentiation of hypervirulent Klebsiella pneumoniae from classical K. pneumoniae. *J. Clin. Microbiol* **56**, 00776-18 (2018).

163. Dai, P. & Hu, D. The making of hypervirulent *Klebsiella pneumoniae*. *J Clin Lab Anal* **36**, e24743 (2022).

164. Shankar-Sinha, S. et al. The *Klebsiella pneumoniae* O antigen contributes to bacteremia and lethality during murine pneumonia. *Infection and immunity* **72**, 1423-1430 (2004).

165. Schroll, C., Barken, K.B., Krogfelt, K.A. & Struve, C. Role of type 1 and type 3 fimbriae in *Klebsiella pneumoniae* biofilm formation. *BMC Microbiology* **10**, 179 (2010).

166. Wyres, K.L., Lam, M.M.C. & Holt, K.E. Population genomics of *Klebsiella pneumoniae*. *Nature Reviews Microbiology* **18**, 344-359 (2020).

167. Gorrie, C.L. et al. Gastrointestinal carriage is a major reservoir of *Klebsiella pneumoniae* infection in intensive care patients. *Clinical infectious diseases* **65**, 208-215 (2017).

168. Conlan, S., Kong, H.H. & Segre, J.A. Species-level analysis of DNA sequence data from the NIH Human Microbiome Project. (2012).

169. Ludden, C. et al. A One Health study of the genetic relatedness of *Klebsiella pneumoniae* and their mobile elements in the East of England. *Clinical Infectious Diseases* **70**, 219-226 (2020).

170. Chung, D. et al. Fecal carriage of serotype K1 *Klebsiella pneumoniae* ST23 strains closely related to liver abscess isolates in Koreans living in Korea. *European journal of clinical microbiology & infectious diseases* **31**, 481-486 (2012).

171. Lin, Y.-T. et al. Seroepidemiology of *Klebsiella pneumoniae* colonizing the intestinal tract of healthy Chinese and overseas Chinese adults in Asian countries. *BMC microbiology* **12**, 1-7 (2012).

172. Löhr, I.H. et al. Long-term faecal carriage in infants and intra-household transmission of CTX-M-15-producing *Klebsiella pneumoniae* following a nosocomial outbreak. *Journal of Antimicrobial Chemotherapy* **68**, 1043-1048 (2013).

173. Mo, Y. et al. Carriage duration of carbapenemase-producing *Enterobacteriaceae* in a hospital cohort-implications for infection control measures. *medRxiv*, 19001479 (2019).

174. Kaur, C.P., Vadivelu, J. & Chandramathi, S. Impact of *Klebsiella pneumoniae* in lower gastrointestinal tract diseases. *Journal of digestive diseases* **19**, 262-271 (2018).

175. Martin, R. et al. Molecular epidemiology of colonizing and infecting isolates of *Klebsiella pneumoniae*. mSphere 1. (2016).

176. Gonzalez-Ferrer, S. et al. Finding Order in the Chaos: Outstanding Questions in *Klebsiella pneumoniae* Pathogenesis. *Infection and Immunity* **89**, 10.1128/iai.00693-20 (2021).

177. Choby, J.E., Howard-Anderson, J. & Weiss, D.S. Hypervirulent *Klebsiella pneumoniae* - clinical and molecular perspectives. *J Intern Med* **287**, 283-300 (2020).

178. Xu, L., Sun, X. & Ma, X. Systematic review and meta-analysis of mortality of patients infected with carbapenem-resistant *Klebsiella pneumoniae*. *Annals of clinical microbiology and antimicrobials* **16**, 1-12 (2017).

179. Bassetti, M., Peghin, M., Vena, A. & Giacobbe, D.R. Treatment of infections due to MDR Gram-negative bacteria. *Frontiers in medicine* **6**, 74 (2019).

180. Manohar, P., Tamhankar, A.J. & Nachimuthu, R. Therapeutic characterization and efficacy of bacteriophage cocktails infecting *Escherichia coli*, *Klebsiella pneumoniae*, and *Enterobacter* species. *Frontiers in microbiology* **10**, 431926 (2019).

181. Meatherall, B.L., Gregson, D., Ross, T., Pitout, J.D. & Laupland, K.B. Incidence, risk factors, and outcomes of *Klebsiella pneumoniae* bacteremia. *The American journal of medicine* **122**, 866-873 (2009).

182. Russo, T.A. & Marr, C.M. Hypervirulent *klebsiella pneumoniae*. *Clinical microbiology reviews* **32**, 10.1128/cmr. 00001-19 (2019).

183. Ko, W.-C. et al. Community-acquired *Klebsiella pneumoniae* bacteremia: global differences in clinical patterns. *Emerging infectious diseases* **8**, 160 (2002).

184. Kim, J.-K. et al. Risk factor analysis of invasive liver abscess caused by the K1 serotype *Klebsiella pneumoniae*. *European journal of clinical microbiology & infectious diseases* **28**, 109-111 (2009).

185. Chen, L. & Kreiswirth, B.N. Convergence of carbapenem-resistance and hypervirulence in *Klebsiella pneumoniae*. *The Lancet infectious diseases* **18**, 2-3 (2018).

186. Zhan, L. et al. Outbreak by hypermucoviscous *Klebsiella pneumoniae* ST11 isolates with carbapenem resistance in a tertiary hospital in China. *Frontiers in cellular and infection microbiology* **7**, 182 (2017).

187. Gu, D. et al. A fatal outbreak of ST11 carbapenem-resistant hypervirulent *Klebsiella pneumoniae* in a Chinese hospital: a molecular epidemiological study. *The Lancet infectious diseases* **18**, 37-46 (2018).

188. Xu, M. et al. High prevalence of KPC-2-producing hypervirulent *Klebsiella pneumoniae* causing meningitis in Eastern China. *Infection and drug resistance*, 641-653 (2019).

189. Dong, N. et al. Genome analysis of clinical multilocus sequence Type 11 *Klebsiella pneumoniae* from China. *Microbial genomics* **4**, e000149 (2018).

190. Yao, H., Qin, S., Chen, S., Shen, J. & Du, X.D. Emergence of carbapenem-resistant hypervirulent *Klebsiella pneumoniae*. *Lancet Infect Dis* **18**, 25 (2018).

191. Paczosa, M.K. & Mecsas, J. *Klebsiella pneumoniae*: going on the offense with a strong defense. *Microbiology and molecular biology reviews* **80**, 629-661 (2016).

192. Hsu, C.-R., Lin, T.-L., Pan, Y.-J., Hsieh, P.-F. & Wang, J.-T. Isolation of a Bacteriophage Specific for a New Capsular Type of *Klebsiella pneumoniae* and Characterization of Its Polysaccharide Depolymerase. *PLOS ONE* **8**, e70092 (2013).

193. Ramos, P.I.P. et al. Pyrosequencing-based analysis reveals a novel capsular gene cluster in a KPC-producing *Klebsiella pneumoniae* clinical isolate identified in Brazil. *BMC Microbiology* **12**, 173 (2012).

194. Li, B., Zhao, Y., Liu, C., Chen, Z. & Zhou, D. Molecular pathogenesis of *Klebsiella pneumoniae*. *Future microbiology* **9**, 1071-1081 (2014).

195. Yang, F.-L. et al. Structure and immunological characterization of the capsular polysaccharide of a pyrogenic liver abscess caused by *Klebsiella pneumoniae*:

activation of macrophages through Toll-like receptor 4. *Journal of Biological Chemistry* **286**, 21041-21051 (2011).

196. Gonzalez-Ferrer, S. et al. Finding order in the chaos: Outstanding questions in *Klebsiella pneumoniae* pathogenesis. *Infection and immunity* **89**, 10.1128/iai. 00693-20 (2021).

197. Merino, S. et al. Cloning and sequencing of the *Klebsiella pneumoniae* O5 wb gene cluster and its role in pathogenesis. *Infection and immunity* **68**, 2435-2440 (2000).

198. Clements, A. et al. Secondary acylation of *Klebsiella pneumoniae* lipopolysaccharide contributes to sensitivity to antibacterial peptides. *Journal of Biological Chemistry* **282**, 15569-15577 (2007).

199. March, C. et al. Role of bacterial surface structures on the interaction of *Klebsiella pneumoniae* with phagocytes. *PloS one* **8**, e56847 (2013).

200. Struve, C., Bojer, M. & Krogfelt, K.A. Characterization of *Klebsiella pneumoniae* type 1 fimbriae by detection of phase variation during colonization and infection and impact on virulence. *Infection and immunity* **76**, 4055-4065 (2008).

201. Stahlhut, S.G., Struve, C. & Krogfelt, K.A. *Klebsiella pneumoniae* type 3 fimbriae agglutinate yeast in a mannose-resistant manner. *Journal of medical microbiology* **61**, 317-322 (2012).

202. Struve, C., Bojer, M. & Krogfelt, K.A. Identification of a conserved chromosomal region encoding *Klebsiella pneumoniae* type 1 and type 3 fimbriae and assessment of the role of fimbriae in pathogenicity. *Infection and immunity* **77**, 5016-5024 (2009).

203. Wu, C.-C., Huang, Y.-J., Fung, C.-P. & Peng, H.-L. Regulation of the *Klebsiella pneumoniae* Kpc fimbriae by the site-specific recombinase KpcI. *Microbiology* **156**, 1983-1992 (2010).

204. Di Martino, P., Livrelli, V., Sirot, D., Joly, B. & Darfeuille-Michaud, A. A new fimbrial antigen harbored by CAZ-5/SHV-4-producing *Klebsiella pneumoniae* strains involved in nosocomial infections. *Infection and immunity* **64**, 2266-2273 (1996).

205. Griffiths, E. High-affinity iron uptake system and bacterial virulence. *Virulence mechanisms of bacterial pathogens*, 121-137 (1988).

206. Holden, V.I. & Bachman, M.A. Diverging roles of bacterial siderophores during infection. *Metallomics* **7**, 986-995 (2015).

207. Pollack, J.R. & Neilands, J. Enterobactin, an iron transport compound from S*almonella typhimurium*. *Biochemical and biophysical research communications* **38**, 989-992 (1970).

208. Abbas, R. et al. General Overview of *Klebsiella pneumonia*: Epidemiology and the Role of Siderophores in Its Pathogenicity. *Biology* **13**, 78 (2024).

209. Bachman, M.A. et al. *Klebsiella pneumoniae* yersiniabactin promotes respiratory tract infection through evasion of lipocalin 2. *Infection and immunity* **79**, 3309-3316 (2011).

210. Russo, T.A. et al. Aerobactin mediates virulence and accounts for increased siderophore production under iron-limiting conditions by hypervirulent (hypermucoviscous) *Klebsiella pneumoniae*. *Infect Immun* **82**, 2356-67 (2014).

211. Llobet, E., March, C., Giménez, P. & Bengoechea, J.A. *Klebsiella pneumoniae* OmpA confers resistance to antimicrobial peptides. *Antimicrobial agents and chemotherapy* **53**, 298-302 (2009).

212. Tsai, Y.-K. et al. *Klebsiella pneumoniae* outer membrane porins OmpK35 and OmpK36 play roles in both antimicrobial resistance and virulence. *Antimicrobial agents and chemotherapy* **55**, 1485-1493 (2011).

213. Filgona, J., Banerjee, T. & Anupurba, S. Role of efflux pumps inhibitor in decreasing antibiotic resistance of *Klebsiella pneumoniae* in a tertiary hospital in North India. *The Journal of Infection in Developing Countries* **9**, 815-820 (2015).

214. Padilla, E. et al. *Klebsiella pneumoniae* AcrAB efflux pump contributes to antimicrobial resistance and virulence. *Antimicrobial agents and chemotherapy* **54**, 177-183 (2010).

215. Journet, L. & Cascales, E. The Type VI Secretion System in *Escherichia coli* and Related Species. *EcoSal Plus* **7**, 10.1128/ecosalplus.ESP-0009-2015 (2016).

216. Lery, L.M. et al. Comparative analysis of *Klebsiella pneumoniae* genomes identifies a phospholipase D family protein as a novel virulence factor. *BMC biology* **12**, 1-15 (2014).

217. Liu, L. et al. Identification and characterization of an antibacterial type VI secretion system in the carbapenem-resistant strain *Klebsiella pneumoniae* HS11286. *Frontiers in cellular and infection microbiology* **7**, 442 (2017).

218. Sarris, P.F., Zoumadakis, C., Panopoulos, N.J. & Scoulica, E.V. Distribution of the putative type VI secretion system core genes in *Klebsiella* spp. *Infection, Genetics and Evolution* **11**, 157-166 (2011).

219. Viswanathan, V.K. Off-label abuse of antibiotics by bacteria. *Gut Microbes* **5**, 3-4 (2014).

220. Antibiotic resistance threats in the United States, 2013. (2013).

221. Organization, W.H. *Antimicrobial resistance: global report on surveillance*, (World Health Organization, 2014).

222. Michael, C.A., Dominey-Howes, D. & Labbate, M. The Antimicrobial Resistance Crisis: Causes, Consequences, and Management. *Frontiers in Public Health* **2**(2014).

223. Fleming, A. On the antibacterial action of cultures of a penicillium, with special reference to their use in the isolation of B. influenzae. *British journal of experimental pathology* **10**, 226 (1929).

224. Fleming, S.A. *Nobel lecture on penicillin*, (PA Norstedt & Söner, 1947).

225. Browne, K. et al. A New Era of Antibiotics: The Clinical Potential of Antimicrobial Peptides. *Int J Mol Sci* **21**(2020).

226. Salam, M.A. et al. Antimicrobial Resistance: A Growing Serious Threat for Global Public Health. *Healthcare* **11**, 1946 (2023).

227. Ventola, C.L. The antibiotic resistance crisis: part 1: causes and threats. *P t* **40**, 277-83 (2015).

228. Muteeb, G., Rehman, M.T., Shahwan, M. & Aatif, M. Origin of Antibiotics and Antibiotic Resistance, and Their Impacts on Drug Development: A Narrative Review. *Pharmaceuticals (Basel)* **16**(2023).

229. Organization, W.H. Antimicrobial resistance fact sheet. *Quality indicators of all prescriptions and prescriptions for lower respiratory tract infections only All prescriptions* (2018).

230. O'neill, J. Antimicrobial resistance: tackling a crisis for the health and wealth of nations. *Rev. Antimicrob. Resist.* (2014).

231. Strathdee, S.A., Davies, S.C. & Marcelin, J.R. Confronting antimicrobial resistance beyond the COVID-19 pandemic and the 2020 US election. *The Lancet* **396**, 1050-1053 (2020).

232. Jevons, M.P. "Celbenin"-resistant staphylococci. *British medical journal* **1**, 124 (1961).

233. Lee, A.S. et al. Methicillin-resistant *Staphylococcus aureus*. *Nature Reviews Disease Primers* **4**, 18033 (2018).

234. Klevens, R.M. et al. Invasive methicillin-resistant *Staphylococcus aureus* infections in the United States. *Jama* **298**, 1763-1771 (2007).

235. Spellberg, B. et al. Combating antimicrobial resistance: policy recommendations to save lives. *Clin Infect Dis* **52 Suppl 5**, S397-428 (2011).

236. Murray, C.J. et al. Global burden of bacterial antimicrobial resistance in 2019: a systematic analysis. *The lancet* **399**, 629-655 (2022).

237. Rossolini, G.M., Arena, F., Pecile, P. & Pollini, S. Update on the antibiotic resistance crisis. *Current Opinion in Pharmacology* **18**, 56-60 (2014).

238. Navon-Venezia, S., Kondratyeva, K. & Carattoli, A. *Klebsiella pneumoniae*: a major worldwide source and shuttle for antibiotic resistance. *FEMS Microbiology Reviews* **41**, 252-275 (2017).

239. Organization, W.H. *Antimicrobial resistance surveillance in Europe 2022–2020 data*, (World Health Organization. Regional Office for Europe, 2022).

240. Cassini, A. et al. Attributable deaths and disability-adjusted life-years caused by infections with antibiotic-resistant bacteria in the EU and the European Economic Area in 2015: a population-level modelling analysis. *The Lancet infectious diseases* **19**, 56-66 (2019).

241. Munita, J.M. & Arias, C.A. Mechanisms of Antibiotic Resistance. *Microbiol Spectr* **4**(2016).

242. Blair, J.M., Webber, M.A., Baylay, A.J., Ogbolu, D.O. & Piddock, L.J. Molecular mechanisms of antibiotic resistance. *Nat Rev Microbiol* **13**, 42-51 (2015).

243. Peterson, E. & Kaur, P. Antibiotic Resistance Mechanisms in Bacteria: Relationships Between Resistance Determinants of Antibiotic Producers, Environmental Bacteria, and Clinical Pathogens. *Frontiers in Microbiology* **9**(2018).

244. Clatworthy, A.E., Pierson, E. & Hung, D.T. Targeting virulence: a new paradigm for antimicrobial therapy. *Nat Chem Biol* **3**, 541-8 (2007).

245. Cegelski, L., Marshall, G.R., Eldridge, G.R. & Hultgren, S.J. The biology and future prospects of antivirulence therapies. *Nat Rev Microbiol* **6**, 17-27 (2008).

246. Escaich, S. Antivirulence as a new antibacterial approach for chemotherapy. *Current Opinion in Chemical Biology* **12**, 400-408 (2008).

247. Dehbanipour, R. & Ghalavand, Z. Anti-virulence therapeutic strategies against bacterial infections: recent advances. *Germs* **12**, 262-275 (2022).

248. Dickey, S.W., Cheung, G.Y.C. & Otto, M. Different drugs for bad bugs: antivirulence strategies in the age of antibiotic resistance. *Nature Reviews Drug Discovery* **16**, 457-471 (2017).

249. Allen, R.C., Popat, R., Diggle, S.P. & Brown, S.P. Targeting virulence: can we make evolution-proof drugs? *Nature Reviews Microbiology* **12**, 300-308 (2014).

250. Bock, C., Farlik, M. & Sheffield, N.C. Multi-Omics of Single Cells: Strategies and Applications. *Trends Biotechnol* **34**, 605-608 (2016).

251. Vogel, C. & Marcotte, E.M. Insights into the regulation of protein abundance from proteomic and transcriptomic analyses. *Nature Reviews Genetics* **13**, 227-232 (2012).

252. Malinovska, L. et al. Proteome-wide structural changes measured with limited proteolysis-mass spectrometry: an advanced protocol for high-throughput applications. *Nature Protocols* **18**, 659-682 (2023).

253. Faucher, F., Bennett, J.M., Bogyo, M. & Lovell, S. Strategies for tuning the selectivity of chemical probes that target serine hydrolases. *Cell chemical biology* **27**, 937-952 (2020).

254. Deng, H., Lei, Q., Wu, Y., He, Y. & Li, W. Activity-based protein profiling: Recent advances in medicinal chemistry. *European journal of medicinal chemistry* **191**, 112151 (2020).

255. Niphakis, M.J. & Cravatt, B.F. Enzyme inhibitor discovery by activity-based protein profiling. *Annual review of biochemistry* **83**, 341-377 (2014).

256. van Kasteren, S.I., Florea, B.I. & Overkleeft, H.S. Activity-based protein profiling: From chemical novelty to biomedical stalwart. *Activity-Based Proteomics: Methods and Protocols*, 1-8 (2017).

257. Porta, E.O.J. & Steel, P.G. Activity-based protein profiling: A graphical review. *Curr Res Pharmacol Drug Discov* **5**, 100164 (2023).

258. Verhelst, S.H.L., Bonger, K.M. & Willems, L.I. Bioorthogonal Reactions in Activity-Based Protein Profiling. *Molecules* **25**(2020).

259. Paulick, M.G. & Bogyo, M. Application of activity-based probes to the study of enzymes involved in cancer progression. *Curr Opin Genet Dev* **18**, 97-106 (2008).

260. Cravatt, B.F., Wright, A.T. & Kozarich, J.W. Activity-based protein profiling: from enzyme chemistry to proteomic chemistry. *Annu Rev Biochem* **77**, 383-414 (2008).

261. van Rooden, E.J. et al. Mapping in vivo target interaction profiles of covalent inhibitors using chemical proteomics with label-free quantification. *Nat Protoc* **13**, 752-767 (2018).

262. Nomura, D.K., Dix, M.M. & Cravatt, B.F. Activity-based protein profiling for biochemical pathway discovery in cancer. *Nat Rev Cancer* **10**, 630-8 (2010).

263. Leung, D., Hardouin, C., Boger, D.L. & Cravatt, B.F. Discovering potent and selective reversible inhibitors of enzymes in complex proteomes. *Nature biotechnology* **21**, 687-691 (2003).

264. Zhu, H. et al. Strategies for Competitive Activity-Based Protein Profiling in Small Molecule Inhibitor Discovery and Characterization. *Israel Journal of Chemistry* **63**, e202200113 (2023).

265. McCarthy, H. et al. Methicillin resistance and the biofilm phenotype in *Staphylococcus aureus*. *Frontiers in cellular and infection microbiology* **5**, 1 (2015).

266. Lentz, C.S. et al. Identification of a *S. aureu*s virulence factor by activity-based protein profiling (ABPP). *Nature chemical biology* **14**, 609-617 (2018).

267. Chen, L., Keller, L.J., Cordasco, E., Bogyo, M. & Lentz, C.S. Fluorescent Triazole Urea Activity-Based Probes for the Single-Cell Phenotypic Characterization of *Staphylococcus aureus*. *Angewandte Chemie* **131**, 5699-5703 (2019).

268. Böttcher, T. & Sieber, S.A. β-lactones as specific inhibitors of ClpP attenuate the production of extracellular virulence factors of *Staphylococcus aureus*. *Journal of the American Chemical Society* **130**, 14400-14401 (2008).

269. Sharifzadeh, S. et al. Novel electrophilic scaffold for imaging of essential penicillin-binding proteins in *Streptococcus pneumoniae*. *ACS Chemical biology* **12**, 2849-2857 (2017).

270. Lehmann, J. et al. An antibacterial β-lactone kills *Mycobacterium tuberculosis* by disrupting mycolic acid biosynthesis. *Angewandte Chemie International Edition* **57**, 348-353 (2018).

271. Li, M. et al. Identification of cell wall synthesis inhibitors active against *Mycobacterium tuberculosis* by competitive activity-based protein profiling. *Cell chemical biology* **29**, 883-896. e5 (2022).

272. Babin, B.M. et al. Identification of covalent inhibitors that disrupt *M. tuberculosis* growth by targeting multiple serine hydrolases involved in lipid metabolism. *Cell Chem Biol* **29**, 897-909.e7 (2022).

273. Liu, Y., Patricelli, M.P. & Cravatt, B.F. Activity-based protein profiling: The serine hydrolases. *Proceedings of the National Academy of Sciences* **96**, 14694-14699 (1999).

274. Faucher, F., Bennett, J.M., Bogyo, M. & Lovell, S. Strategies for Tuning the Selectivity of Chemical Probes that Target Serine Hydrolases. *Cell Chemical Biology* (2020).

275. Kato, D. et al. Activity-based probes that target diverse cysteine protease families. *Nat Chem Biol* **1**, 33-8 (2005).

276. Serim, S., Haedke, U. & Verhelst, S.H. Activity-based probes for the study of proteases: recent advances and developments. *ChemMedChem* **7**, 1146-59 (2012).

277. Patricelli, M.P. et al. Functional interrogation of the kinome using nucleotide acyl phosphates. *Biochemistry* **46**, 350-8 (2007).

278. Wright, A.T. & Cravatt, B.F. Chemical proteomic probes for profiling cytochrome p450 activities and drug interactions in vivo. *Chem Biol* **14**, 1043-51 (2007).

279. Wu, L. et al. An overview of activity-based probes for glycosidases. *Current Opinion in Chemical Biology* **53**, 25-36 (2019).

280. Simon, G.M. & Cravatt, B.F. Activity-based proteomics of enzyme superfamilies: serine hydrolases as a case study. *Journal of Biological Chemistry* **285**, 11051-11055 (2010).

281. Long, J.Z. & Cravatt, B.F. The Metabolic Serine Hydrolases and Their Functions in Mammalian Physiology and Disease. *Chemical Reviews* **111**, 6022-6063 (2011).

282. Bachovchin, D.A. & Cravatt, B.F. The pharmacological landscape and therapeutic potential of serine hydrolases. *Nature Reviews Drug Discovery* **11**, 52-68 (2012).

283. White, M.J. et al. The HtrA-like serine protease PepD interacts with and modulates the *Mycobacterium tuberculosis* 35-kDa antigen outer envelope protein. *PLoS One* **6**, e18175 (2011).

284. Brandt, C. et al. In silico serine β-lactamases analysis reveals a huge potential resistome in environmental and pathogenic species. *Sci Rep* **7**, 43232 (2017).

285. Damblon, C. et al. The catalytic mechanism of beta-lactamases: NMR titration of an active-site lysine residue of the TEM-1 enzyme. *Proceedings of the National Academy of Sciences* **93**, 1747-1752 (1996).

286. Lentz, C.S. et al. Design of Selective Substrates and Activity-Based Probes for Hydrolase Important for Pathogenesis 1 (HIP1) from *Mycobacterium tuberculosis*. *ACS Infectious Diseases* **2**, 807-815 (2016).

287. Mehner, C. et al. Activity-based protein profiling reveals active serine proteases that drive malignancy of human ovarian clear cell carcinoma. *Journal of Biological Chemistry* **298**(2022).

288. Bajda, M., Łątka, K., Hebda, M., Jończyk, J. & Malawska, B. Novel carbamate derivatives as selective butyrylcholinesterase inhibitors. *Bioorganic Chemistry* **78**, 29-38 (2018).

289. Holmquist, M. Alpha beta-hydrolase fold enzymes structures, functions and mechanisms. *Current Protein and Peptide Science* **1**, 209-235 (2000).

290. Ollis, D.L. et al. The α/β hydrolase fold. *Protein Engineering, Design and Selection* **5**, 197-211 (1992).

291. Shin, S. et al. Structure of malonamidase E2 reveals a novel Ser-cisSer-Lys catalytic triad in a new serine hydrolase fold that is prevalent in nature. *The EMBO journal* (2002).

292. Bracey, M.H., Hanson, M.A., Masuda, K.R., Stevens, R.C. & Cravatt, B.F. Structural adaptations in a membrane enzyme that terminates endocannabinoid signaling. *Science* **298**, 1793-1796 (2002).

293. Kienesberger, P.C., Oberer, M., Lass, A. & Zechner, R. Mammalian patatin domain containing proteins: a family with diverse lipolytic activities involved in multiple biological functions. *Journal of lipid research* **50**, S63-S68 (2009).

294. Honeder, S.E. et al. Research Advances Through Activity-Based Lipid Hydrolase Profiling. *Israel Journal of Chemistry* **63**, e202200078 (2023).

295. Dolui, A.K. et al. Chemoproteomic profiling of serine hydrolases reveals the dynamic role of lipases in *Phaeodactylum tricornutum*. *bioRxiv*, 2024.03.12.582592 (2024).

296. McDonald, A.G., Boyce, S. & Tipton, K.F. ExplorEnz: the primary source of the IUBMB enzyme list. *Nucleic acids research* **37**, D593-D597 (2009).

297. Schmiel, D.H. & Miller, V.L. Bacterial phospholipases and pathogenesis. *Microbes and infection* **1**, 1103-1112 (1999).

298. van der Meer-Janssen, Y.P., van Galen, J., Batenburg, J.J. & Helms, J.B. Lipids in host–pathogen interactions: pathogens exploit the complexity of the host cell lipidome. *Progress in lipid research* **49**, 1-26 (2010).

299. Songer, J.G. Bacterial phospholipases and their role in virulence. *Trends in microbiology* **5**, 156-161 (1997).

300. Flores-Díaz, M., Monturiol-Gross, L., Naylor, C., Alape-Girón, A. & Flieger, A. Bacterial Sphingomyelinases and Phospholipases as Virulence Factors. *Microbiol Mol Biol Rev* **80**, 597-628 (2016).

301. Faucher, F., Bennett, J.M., Bogyo, M. & Lovell, S. Strategies for Tuning the Selectivity of Chemical Probes that Target Serine Hydrolases. *Cell Chem Biol* **27**, 937-952 (2020).

302. Jackson, D.S. et al. Synthesis and evaluation of diphenyl phosphonate esters as inhibitors of the trypsin-like granzymes A and K and mast cell tryptase. *Journal of medicinal chemistry* **41**, 2289-2301 (1998).

303. Narayanan, A. & Jones, L.H. Sulfonyl fluorides as privileged warheads in chemical biology. *Chemical science* **6**, 2650-2659 (2015).

304. Böttcher, T. & Sieber, S.A. β-Lactams and β-lactones as activity-based probes in chemical biology. *MedChemComm* **3**, 408-417 (2012).

305. Alexander, J.P. & Cravatt, B.F. Mechanism of carbamate inactivation of FAAH: implications for the design of covalent inhibitors and in vivo functional probes for enzymes. *Chemistry & biology* **12**, 1179-1187 (2005).

306. Adibekian, A. et al. Click-generated triazole ureas as ultrapotent in vivo–active serine hydrolase inhibitors. *Nature chemical biology* **7**, 469-478 (2011).

307. Harper, J.W., Hemmi, K. & Powers, J.C. Reaction of serine proteases with substituted isocoumarins: discovery of 3, 4-dichloroisocoumarin, a new general mechanism based serine protease inhibitor. *Biochemistry* **24**, 1831-1841 (1985).

308. Nomura, D.K., Dix, M.M. & Cravatt, B.F. Activity-based protein profiling for biochemical pathway discovery in cancer. *Nature Reviews Cancer* **10**, 630-638 (2010).

309. Ortega, C. et al. Systematic survey of serine hydrolase activity in *Mycobacterium tuberculosis* defines changes associated with persistence. *Cell chemical biology* **23**, 290-298 (2016).

310. Tallman, K.R., Levine, S.R. & Beatty, K.E. Small-Molecule Probes Reveal Esterases with Persistent Activity in Dormant and Reactivating *Mycobacterium tuberculosis*. *ACS Infectious Diseases* **2**, 936-944 (2016).

311. Hatzios, S.K. et al. Chemoproteomic profiling of host and pathogen enzymes active in cholera. *Nature chemical biology* **12**, 268-274 (2016).

312. Fellner, M. et al. Biochemical and Cellular Characterization of the Function of Fluorophosphonate-Binding Hydrolase H (FphH) in *Staphylococcus aureus* Support a Role in Bacterial Stress Response. *ACS Infect Dis* **9**, 2119-2132 (2023).

313. Varki, A. Biological roles of glycans. *Glycobiology* **27**, 3-49 (2017).

314. Kobata, A. Structures and functions of the sugar chains of glycoproteins. *European Journal of Biochemistry* **209**, 483-501 (1992).

315. Helenius, A., Aebi & Markus. Intracellular Functions of N-Linked Glycans. *Science* **291**, 2364-2369 (2001).

316. Kim, Y.J. & Varki, A. Perspectives on the significance of altered glycosylation of glycoproteins in cancer. *Glycoconjugate journal* **14**, 569-576 (1997).

317. Reily, C., Stewart, T.J., Renfrow, M.B. & Novak, J. Glycosylation in health and disease. *Nature Reviews Nephrology* **15**, 346-366 (2019).

318. Maverakis, E. et al. Glycans in the immune system and The Altered Glycan Theory of Autoimmunity: a critical review. *J Autoimmun* **57**, 1-13 (2015).

319. Varki, A., Kannagi, R. & Toole, B.P. Glycosylation changes in cancer. *Essentials of Glycobiology. 2nd edition* (2009).

320. Karlsson, K.-A. Microbial recognition of target-cell glycoconjugates. *Current opinion in structural biology* **5**, 622-635 (1995).

321. Magalhaes, A. et al. Fut2-null mice display an altered glycosylation profile and impaired BabA-mediated *Helicobacter pylori* adhesion to gastric mucosa. *Glycobiology* **19**, 1525-1536 (2009).

322. Weis, W. et al. Structure of the influenza virus haemagglutinin complexed with its receptor, sialic acid. *Nature* **333**, 426-431 (1988).

323. Wolfenden, R., Lu, X. & Young, G. Spontaneous Hydrolysis of Glycosides. *Journal of the American Chemical Society* **120**, 6814-6815 (1998).

324. Kobata, A. Exo- and endoglycosidases revisited. *Proc Jpn Acad Ser B Phys Biol Sci* **89**, 97-117 (2013).

325. Sjögren, J. & Collin, M. Bacterial glycosidases in pathogenesis and glycoengineering. *Future Microbiol* **9**, 1039-51 (2014).

326. Rudd, P.M., Elliott, T., Cresswell, P., Wilson, I.A. & Dwek, R.A. Glycosylation and the Immune System. *Science* **291**, 2370-2376 (2001).

327. Benz, I. & Schmidt, M.A. Never say never again: protein glycosylation in pathogenic bacteria. *Molecular Microbiology* **45**, 267-276 (2002).

328. Falk, P., Hoskins, L.C. & Larson, G. Bacteria of the human intestinal microbiota produce glycosidases specific for lacto-series glycosphingolipids. *The Journal of Biochemistry* **108**, 466-474 (1990).

329. Hooper, L.V. & Gordon, J.I. Commensal Host-Bacterial Relationships in the Gut. *Science* **292**, 1115-1118 (2001).

330. Burnaugh, A.M., Frantz, L.J. & King, S.J. Growth of *Streptococcus pneumoniae* on human glycoconjugates is dependent upon the sequential activity of bacterial exoglycosidases. *Journal of bacteriology* **190**, 221-230 (2008).

331. Roberts, G., Tarelli, E., Homer, K.A., Philpott-Howard, J. & Beighton, D. Production of an endo-β-N-acetylglucosaminidase activity mediates growth of *Enterococcus faecalis* on a high-mannose-type glycoprotein. *Journal of bacteriology* **182**, 882-890 (2000).

332. Davies, G. & Henrissat, B. Structures and mechanisms of glycosyl hydrolases. *Structure* **3**, 853-859 (1995).

333. Kallemeijn, W.W., Witte, M.D., Wennekes, T. & Aerts, J.M.F.G. Chapter 4 - Mechanism-Based Inhibitors of Glycosidases: Design and Applications. in *Advances in Carbohydrate Chemistry and Biochemistry*, Vol. 71 (ed. Horton, D.) 297-338 (Academic Press, 2014).

334. Zechel, D.L. & Withers, S.G. Glycosidase Mechanisms: Anatomy of a Finely Tuned Catalyst. *Accounts of Chemical Research* **33**, 11-18 (2000).

335. Witte, M.D. et al. Activity-Based Profiling of Retaining β-Glucosidases: A Comparative Study. *ChemBioChem* **12**, 1263-1269 (2011).

336. Jiang, J. et al. Detection of Active Mammalian GH31 α-Glucosidases in Health and Disease Using In-Class, Broad-Spectrum Activity-Based Probes. *ACS Central Science* **2**, 351-358 (2016).

337. Artola, M. et al. Functionalized Cyclophellitols Are Selective Glucocerebrosidase Inhibitors and Induce a Bona Fide Neuropathic Gaucher Model in Zebrafish. *J Am Chem Soc* **141**, 4214-4218 (2019).

338. Kytidou, K. et al. Nicotiana benthamiana α-galactosidase A1.1 can functionally complement human α-galactosidase A deficiency associated with Fabry disease. *J Biol Chem* **293**, 10042-10058 (2018).

339. Willems, L.I. et al. Synthesis of α- and β-Galactopyranose-Configured Isomers of Cyclophellitol and Cyclophellitol Aziridine. *European Journal of Organic Chemistry* **2014**, 6044-6056 (2014).

340. Jiang, J. et al. Comparing Cyclophellitol N-Alkyl and N-Acyl Cyclophellitol Aziridines as Activity-Based Glycosidase Probes. *Chemistry – A European Journal* **21**, 10861-10869 (2015).

341. Jiang, J. et al. In vitro and in vivo comparative and competitive activity-based protein profiling of GH29 α-l-fucosidases. *Chem Sci* **6**, 2782-false (2015).

342. Wu, L. et al. Activity-based probes for functional interrogation of retaining β-glucuronidases. *Nat Chem Biol* **13**, 867-873 (2017).

343. Artola, M. et al. New Irreversible α-l-Iduronidase Inhibitors and Activity-Based Probes. *Chemistry – A European Journal* **24**, 19081-19088 (2018).

344. Jiang, J. et al. Detection of Active Mammalian GH31 α-Glucosidases in Health and Disease Using In-Class, Broad-Spectrum Activity-Based Probes. *ACS Cent Sci* **2**, 351-8 (2016).

345. Aerts, J.M.F.G. et al. Glycosphingolipids and lysosomal storage disorders as illustrated by gaucher disease. *Current Opinion in Chemical Biology* **53**, 204-215 (2019).

346. Kytidou, K., Artola, M., Overkleeft, H.S. & Aerts, J. Plant Glycosides and Glycosidases: A Treasure-Trove for Therapeutics. *Front Plant Sci* **11**, 357 (2020).

347. Chauvigné-Hines, L.M. et al. Suite of activity-based probes for cellulose-degrading enzymes. *Journal of the American Chemical Society* **134**, 20521-20532 (2012).

348. Liu, Y. et al. Advancing understanding of microbial bioenergy conversion processes by activity-based protein profiling. *Biotechnology for biofuels* **8**, 1-15 (2015).

349. Turner, N.A. et al. Methicillin-resistant *Staphylococcus aureus*: an overview of basic and clinical research. *Nature Reviews Microbiology* **17**, 203-218 (2019).

350. Fey, P.D. et al. A genetic resource for rapid and comprehensive phenotype screening of nonessential *Staphylococcus aureus* genes. *mBio* **4**, e00537-12 (2013).

351. Ramage, B. et al. Comprehensive Arrayed Transposon Mutant Library of *Klebsiella pneumoniae* Outbreak Strain KPNIH1. *J Bacteriol* **199**(2017).

352. Keller, L.J. et al. Chemoproteomic identification of a DPP4 homolog in Bacteroides thetaiotaomicron. *Nat Chem Biol* **19**, 1469-1479 (2023).

353. Ortega, C. et al. Systematic Survey of Serine Hydrolase Activity in *Mycobacterium tuberculosis* Defines Changes Associated with Persistence. *Cell Chem Biol* **23**, 290-298 (2016).

354. Li, M. et al. Identification of cell wall synthesis inhibitors active against *Mycobacterium tuberculosis* by competitive activity-based protein profiling. *Cell Chem Biol* **29**, 883-896.e5 (2022).

355. Koch, G. et al. Evolution of resistance to a last-resort antibiotic in *Staphylococcus aureus* via bacterial competition. *Cell* **158**, 1060-1071 (2014).

356. McGregor, N.G.S., Overkleeft, H.S. & Davies, G.J. Detecting and identifying glycoside hydrolases using cyclophellitol-derived activity-based probes. *Methods Enzymol* **664**, 103-134 (2022).

357. Chen, X. et al. Target identification with quantitative activity based protein profiling (ABPP). *Proteomics* **17**, 1600212 (2017).

358. Galmozzi, A., Dominguez, E., Cravatt, B.F. & Saez, E. Chapter Nine - Application of Activity-Based Protein Profiling to Study Enzyme Function in Adipocytes. in *Methods in Enzymology*, Vol. 538 (ed. MacDougald, O.A.) 151-169 (Academic Press, 2014).

359. Speers, A.E. & Cravatt, B.F. Activity-Based Protein Profiling (ABPP) and Click Chemistry (CC)-ABPP by MudPIT Mass Spectrometry. *Curr Protoc Chem Biol* **1**, 29-41 (2009).

360. Hatzios, S.K. et al. Chemoproteomic profiling of host and pathogen enzymes active in cholera. *Nat Chem Biol* **12**, 268-274 (2016).

361. Kallemeijn, W.W. et al. Proteome-wide analysis of protein lipidation using chemical probes: in-gel fluorescence visualization, identification and quantification of N-myristoylation, N- and S-acylation, O-cholesterylation, S-farnesylation and S-geranylgeranylation. *Nature Protocols* **16**, 5083-5122 (2021).

362. Okerberg, E.S. et al. High-resolution functional proteomics by active-site peptide profiling. *Proceedings of the National Academy of Sciences* **102**, 4996-5001 (2005).

363. Adam, G.C., Burbaum, J., Kozarich, J.W., Patricelli, M.P. & Cravatt, B.F. Mapping enzyme active sites in complex proteomes. *Journal of the American Chemical Society* **126**, 1363-1368 (2004).

364. Botelho, D. et al. Top-Down and Bottom-Up Proteomics of SDS-Containing Solutions Following Mass-Based Separation. *Journal of Proteome Research* **9**, 2863-2870 (2010).

365. Wiśniewski, J.R., Zougman, A., Nagaraj, N. & Mann, M. Universal sample preparation method for proteome analysis. *Nature Methods* **6**, 359-362 (2009).

366. Thanou, E. et al. Suspension TRAPping Filter (sTRAP) Sample Preparation for Quantitative Proteomics in the Low µg Input Range Using a Plasmid DNA Micro-Spin Column: Analysis of the Hippocampus from the 5xFAD Alzheimer's Disease Mouse Model. *Cells* **12**, 1242 (2023).

367. Weerapana, E., Speers, A.E. & Cravatt, B.F. Tandem orthogonal proteolysis-activity-based protein profiling (TOP-ABPP)—a general method for mapping sites of probe modification in proteomes. *Nature Protocols* **2**, 1414-1425 (2007).

368. Speers, A.E. & Cravatt, B.F. A Tandem Orthogonal Proteolysis Strategy for High-Content Chemical Proteomics. *Journal of the American Chemical Society* **127**, 10018-10019 (2005).

369. Elinger, D., Gabashvili, A. & Levin, Y. Suspension trapping (S-Trap) is compatible with typical protein extraction buffers and detergents for bottom-up proteomics. *Journal of proteome research* **18**, 1441-1445 (2019).

370. Kachuk, C., Stephen, K. & Doucette, A. Comparison of sodium dodecyl sulfate depletion techniques for proteome analysis by mass spectrometry. *Journal of Chromatography A* **1418**, 158-166 (2015).

371. Duong, V.A., Park, J.M. & Lee, H. Review of Three-Dimensional Liquid Chromatography Platforms for Bottom-Up Proteomics. *Int J Mol Sci* **21**(2020).

372. Hughes, C.S. et al. Single-pot, solid-phase-enhanced sample preparation for proteomics experiments. *Nature Protocols* **14**, 68-85 (2019).

373. Becker, T. et al. Transforming Chemical Proteomics Enrichment into a High-Throughput Method Using an SP2E Workflow. *JACS Au* **2**, 1712-1723 (2022).

374. Yan, T. et al. SP3-FAIMS Chemoproteomics for High-Coverage Profiling of the Human Cysteinome*. *Chembiochem* **22**, 1841-1851 (2021).

375. Hughes, C.S. et al. Ultrasensitive proteome analysis using paramagnetic bead technology. *Mol Syst Biol* **10**, 757 (2014).

376. Cho, K.F. et al. Proximity labeling in mammalian cells with TurboID and split-TurboID. *Nature Protocols* **15**, 3971-3999 (2020).

377. Herfurth, M., Müller, F., Søgaard-Andersen, L. & Glatter, T. A miniTurbo-based proximity labeling protocol to identify conditional protein interactomes in vivo in Myxococcus xanthus. *STAR Protoc* **4**, 102657 (2023).

378. Cox, J. et al. Accurate proteome-wide label-free quantification by delayed normalization and maximal peptide ratio extraction, termed MaxLFQ. *Molecular & cellular proteomics* **13**, 2513-2526 (2014).

379. Neilson, K.A. et al. Less label, more free: approaches in label-free quantitative mass spectrometry. *Proteomics* **11**, 535-553 (2011).

380. Dowell, J.A., Wright, L.J., Armstrong, E.A. & Denu, J.M. Benchmarking Quantitative Performance in Label-Free Proteomics. *ACS Omega* **6**, 2494-2504 (2021).

381. van Rooden, E.J. et al. Mapping *in vivo* target interaction profiles of covalent inhibitors using chemical proteomics with label-free quantification. *Nature Protocols* **13**, 752-767 (2018).

382. Zhao, Q. et al. Broad-spectrum kinase profiling in live cells with lysine-targeted sulfonyl fluoride probes. *Journal of the American Chemical Society* **139**, 680-685 (2017).

383. Kleiner, P., Heydenreuter, W., Stahl, M., Korotkov, V.S. & Sieber, S.A. A whole proteome inventory of background photocrosslinker binding. *Angewandte Chemie International Edition* **56**, 1396-1401 (2017).

384. Yang, W.S. et al. Regulation of ferroptotic cancer cell death by GPX4. *Cell* **156**, 317-331 (2014).

385. Chandramouli, K. & Qian, P.Y. Proteomics: challenges, techniques and possibilities to overcome biological sample complexity. *Hum Genomics Proteomics* **2009**(2009).

386. Spence, J.R. et al. Directed differentiation of human pluripotent stem cells into intestinal tissue in vitro. *Nature* **470**, 105-109 (2011).

387. McCracken, K.W., Howell, J.C., Wells, J.M. & Spence, J.R. Generating human intestinal tissue from pluripotent stem cells in vitro. *Nature protocols* **6**, 1920-1928 (2011).

388. In, J.G. et al. Human mini-guts: new insights into intestinal physiology and host-pathogen interactions. *Nat Rev Gastroenterol Hepatol* **13**, 633-642 (2016).

389. Kim, J., Koo, B.K. & Knoblich, J.A. Human organoids: model systems for human biology and medicine. *Nat Rev Mol Cell Biol* **21**, 571-584 (2020).

390. Kostic, A.D., Howitt, M.R. & Garrett, W.S. Exploring host–microbiota interactions in animal models and humans. *Genes & development* **27**, 701-718 (2013).

391. Lancaster, M.A. & Huch, M. Disease modelling in human organoids. *Disease models & mechanisms* **12**, dmm039347 (2019).

392. Clevers, H. Modeling Development and Disease with Organoids. *Cell* **165**, 1586-1597 (2016).

393. Zhao, Z. et al. Organoids. *Nature Reviews Methods Primers* **2**, 94 (2022).

394. Tang, X.-Y. et al. Human organoids in basic research and clinical applications. *Signal Transduction and Targeted Therapy* **7**, 168 (2022).

395. Dutta, D. & Clevers, H. Organoid culture systems to study host-pathogen interactions. *Curr Opin Immunol* **48**, 15-22 (2017).

396. Pleguezuelos-Manzano, C. et al. Mutational signature in colorectal cancer caused by genotoxic pks(+) *E. coli*. *Nature* **580**, 269-273 (2020).

397. Leslie, J.L. et al. Persistence and toxin production by *Clostridium difficile* within human intestinal organoids result in disruption of epithelial paracellular barrier function. *Infection and immunity* **83**, 138-145 (2015).

398. Yin, Y. & Zhou, D. Organoid and Enteroid Modeling of *Salmonella* Infection. *Front Cell Infect Microbiol* **8**, 102 (2018).

399. Williamson, I.A. et al. A high-throughput organoid microinjection platform to study gastrointestinal microbiota and luminal physiology. *Cellular and molecular gastroenterology and hepatology* **6**, 301-319 (2018).

400. Hill, D.R. et al. Bacterial colonization stimulates a complex physiological response in the immature human intestinal epithelium. *Elife* **6**, e29132 (2017).

401. Kester, J.C. et al. *Clostridioides difficile*-associated antibiotics alter human mucosal barrier functions by microbiome-independent mechanisms. *Antimicrobial agents and chemotherapy* **64**, 10.1128/aac. 01404-19 (2020).

402. Saxena, K. et al. Human intestinal enteroids: a new model to study human rotavirus infection, host restriction, and pathophysiology. *Journal of virology* **90**, 43-56 (2016).

403. Roodsant, T. et al. A Human 2D Primary Organoid-Derived Epithelial Monolayer Model to Study Host-Pathogen Interaction in the Small Intestine. *Front Cell Infect Microbiol* **10**, 272 (2020).

404. Wilke, G. et al. In vitro culture of *Cryptosporidium parvum* using stem cell-derived intestinal epithelial monolayers. *Cryptosporidium: Methods and Protocols*, 351-372 (2020).

405. In, J. et al. Enterohemorrhagic *Escherichia coli* reduces mucus and intermicrovillar bridges in human stem cell-derived colonoids. *Cellular and molecular gastroenterology and hepatology* **2**, 48-62. e3 (2016).

406. Kozuka, K. et al. Development and characterization of a human and mouse intestinal epithelial cell monolayer platform. *Stem cell reports* **9**, 1976-1990 (2017).

407. In, J.G., Foulke-Abel, J., Clarke, E. & Kovbasnjuk, O. Human colonoid monolayers to study interactions between pathogens, commensals, and host intestinal epithelium. *JoVE (Journal of Visualized Experiments)*, e59357 (2019).

408. Zhang, J. et al. Coculture of primary human colon monolayer with human gut bacteria. *Nat Protoc* **16**, 3874-3900 (2021).

409. Fofanova, T. et al. A novel human enteroid-anaerobe co-culture system to study microbial-host interaction under physiological hypoxia. *BioRxiv*, 555755 (2019).

410. Nossol, C. et al. Air-liquid interface cultures enhance the oxygen supply and trigger the structural and functional differentiation of intestinal porcine epithelial cells (IPEC). *Histochem Cell Biol* **136**, 103-15 (2011).

411. Leach, T. et al. Development of a novel air–liquid interface airway tissue equivalent model for in vitro respiratory modeling studies. *Scientific Reports* **13**, 10137 (2023).

412. Vonk, A.M. et al. Protocol for Application, Standardization and Validation of the Forskolin-Induced Swelling Assay in Cystic Fibrosis Human Colon Organoids. *STAR Protoc* **1**, 100019 (2020).

413. Zhang, J. et al. Primary human colonic mucosal barrier crosstalk with super oxygen-sensitive Faecalibacterium prausnitzii in continuous culture. *Med* **2**, 74-98. e9 (2021).

414. Kim, R. et al. An in vitro intestinal platform with a self-sustaining oxygen gradient to study the human gut/microbiome interface. *Biofabrication* **12**, 015006 (2019).

415. Wang, Y. et al. Self-renewing monolayer of primary colonic or rectal epithelial cells. *Cellular and molecular gastroenterology and hepatology* **4**, 165-182. e7 (2017).

416. Cook, S.M. & McArthur, J.D. Developing *Galleria mellonella* as a model host for human pathogens. *Virulence* **4**, 350-353 (2013).

417. Graham, M.L. & Prescott, M.J. The multifactorial role of the 3Rs in shifting the harm-benefit analysis in animal models of disease. *European Journal of Pharmacology* **759**, 19-29 (2015).

418. Kavanagh, K. & Reeves, E.P. Exploiting the potential of insects for in vivo pathogenicity testing of microbial pathogens. *FEMS microbiology reviews* **28**, 101-112 (2004).

419. Desbois, A.P. & Coote, P.J. Wax moth larva (*Galleria mellonella*): an *in vivo* model for assessing the efficacy of antistaphylococcal agents. *Journal of Antimicrobial Chemotherapy* **66**, 1785-1790 (2011).

420. Desbois, A.P. & Coote, P.J. Utility of greater wax moth larva (*Galleria mellonella*) for evaluating the toxicity and efficacy of new antimicrobial agents. in *Advances in applied microbiology*, Vol. 78 25-53 (Elsevier, 2012).

421. Salzet, M. Vertebrate innate immunity resembles a mosaic of invertebrate immune responses. *Trends in immunology* **22**, 285-288 (2001).

422. Song, Y., Luo, L. & Wang, K. Off-target identification by chemical proteomics for the understanding of drug side effects. *Expert Review of Proteomics* **17**, 695-697 (2020).

423. Rangel-Vega, A., Bernstein, L.R., Mandujano-Tinoco, E.A., García-Contreras, S.J. & García-Contreras, R. Drug repurposing as an alternative for the treatment of recalcitrant bacterial infections. *Frontiers in microbiology* **6**, 282 (2015).

424. Maier, L. et al. Extensive impact of non-antibiotic drugs on human gut bacteria. *Nature* **555**, 623-628 (2018).

425. Shahiduzzaman, M. & Coombs, K.M. Activity based protein profiling to detect serine hydrolase alterations in virus infected cells. *Frontiers in Microbiology* **3**, 31046 (2012).

426. Gélinas, M., Museau, L., Milot, A. & Beauregard, P.B. The de novo purine biosynthesis pathway is the only commonly regulated cellular pathway during biofilm formation in

TSB-based medium in *Staphylococcus aureus* and *Enterococcus faecalis*. *Microbiology spectrum* **9**, e00804-21 (2021).

427. Jones, C.S., Anderson, A.C. & Clarke, A.J. Mechanism of *Staphylococcus aureus* peptidoglycan O-acetyltransferase A as an O-acyltransferase. *Proceedings of the National Academy of Sciences* **118**, e2103602118 (2021).

428. Anderson, A.C., Stangherlin, S., Pimentel, K.N., Weadge, J.T. & Clarke, A.J. The SGNH hydrolase family: a template for carbohydrate diversity. *Glycobiology* **32**, 826-848 (2022).

429. Dalal, V. et al. Repurposing an ancient protein core structure: Structural studies on FmtA, a novel esterase of *Staphylococcus aureus*. *Journal of molecular biology* **431**, 3107-3123 (2019).

430. Rahman, M.M. et al. The *Staphylococcus aureus* Methicillin Resistance Factor FmtA Is a d-Amino Esterase That Acts on Teichoic Acids. *mBio* **7**, e02070-15 (2016).

431. Ouairy, C.M. et al. Development of an acid ceramidase activity-based probe. *Chemical communications* **51**, 6161-6163 (2015).

432. Pizzirani, D. et al. Discovery of a new class of highly potent inhibitors of acid ceramidase: synthesis and structure–activity relationship (SAR). *Journal of medicinal chemistry* **56**, 3518-3530 (2013).

433. Cortés, G., de Astorza, B., Benedí, V.J. & Albertí, S. Role of the htrA gene in *Klebsiella pneumoniae* virulence. *Infect Immun* **70**, 4772-6 (2002).

434. Wang, L. et al. Structural insight into the carboxylesterase BioH from *Klebsiella pneumoniae*. *Biochem Biophys Res Commun* **520**, 538-543 (2019).

435. Park, S.W. et al. Target-based identification of whole-cell active inhibitors of biotin biosynthesis in *Mycobacterium tuberculosis*. *Chem Biol* **22**, 76-86 (2015).

436. Salaemae, W., Booker, G.W. & Polyak, S.W. The Role of Biotin in Bacterial Physiology and Virulence: a Novel Antibiotic Target for *Mycobacterium tuberculosis*. *Microbiol Spectr* **4**(2016).

437. Wang, S. et al. Advanced Activity-Based Protein Profiling Application Strategies for Drug Development. *Frontiers in Pharmacology* **9**(2018).

438. Tully, S.E. & Cravatt, B.F. Activity-Based Probes That Target Functional Subclasses of Phospholipases in Proteomes. *Journal of the American Chemical Society* **132**, 3264-3265 (2010).

439. Mathew, B.J. et al. Role of *Streptococcus pneumoniae* extracellular glycosidases in immune evasion. *Frontiers in Cellular and Infection Microbiology* **13**, 1109449 (2023).

440. Stam, M.R., Danchin, E.G.J., Rancurel, C., Coutinho, P.M. & Henrissat, B. Dividing the large glycoside hydrolase family 13 into subfamilies: towards improved functional annotations of α-amylase-related proteins. *Protein Engineering, Design and Selection* **19**, 555-562 (2006).

441. Hava, D.L. & Camilli, A. Large-scale identification of serotype 4 *Streptococcus pneumoniae* virulence factors. *Molecular Microbiology* **45**, 1389-1406 (2002).

442. Ruiz-Perez, F. & Nataro, J.P. Bacterial serine proteases secreted by the autotransporter pathway: classification, specificity, and role in virulence. *Cellular and molecular life sciences* **71**, 745-770 (2014).

443. Stroud, R.M., Kossiakoff, A.A. & Chambers, J.L. Mechanisms of zymogen activation. *Annual review of biophysics and bioengineering* **6**, 177-193 (1977).

444. Kidd, D., Liu, Y. & Cravatt, B.F. Profiling serine hydrolase activities in complex proteomes. *Biochemistry* **40**, 4005-4015 (2001).

445. Patricelli, M.P., Giang, D.K., Stamp, L.M. & Burbaum, J.J. Direct visualization of serine hydrolase activities in complex proteomes using fluorescent active site-directed probes. *PROTEOMICS: International Edition* **1**, 1067-1071 (2001).

446. Braun, A., Stremmel, W. & Ehehalt, R. The Role of Phospholipids Within the Intestinal Mucosal Barrier. *Z Gastroenterol* **49**, A11 (2011).

447. Swidsinski, A. et al. Mucosal flora in inflammatory bowel disease. *Gastroenterology* **122**, 44-54 (2002).

448. Stremmel, W. et al. Mucosal protection by phosphatidylcholine. *Dig Dis* **30 Suppl 3**, 85-91 (2012).

449. Ehehalt, R., Braun, A., Karner, M., Füllekrug, J. & Stremmel, W. Phosphatidylcholine as a constituent in the colonic mucosal barrier—Physiological and clinical relevance. *Biochimica et Biophysica Acta (BBA) - Molecular and Cell Biology of Lipids* **1801**, 983-993 (2010).

450. Stremmel, W. et al. Phosphatidylcholine passes through lateral tight junctions for paracellular transport to the apical side of the polarized intestinal tumor cell-line CaCo2. *Biochimica et Biophysica Acta (BBA) - Molecular and Cell Biology of Lipids* **1861**, 1161-1169 (2016).

451. Tannaes, T., Bukholm, I.K. & Bukholm, G. High relative content of lysophospholipids of *Helicobacter pylori* mediates increased risk for ulcer disease. *FEMS Immunology & Medical Microbiology* **44**, 17-23 (2005).

452. Goggin, P.M. et al. Surface hydrophobicity of gastric mucosa in Helicobacter pylori infection: effect of clearance and eradication. *Gastroenterology* **103**, 1486-90 (1992).

453. Mauch, F., Bode, G., Ditschuneit, H. & Malfertheiner, P. Demonstration of a phospholipid-rich zone in the human gastric epithelium damaged by *Helicobacter pylori*. *Gastroenterology* **105**, 1698-704 (1993).

454. Trimble, M.J., Mlynárčik, P., Kolář, M. & Hancock, R.E. Polymyxin: Alternative Mechanisms of Action and Resistance. *Cold Spring Harb Perspect Med* **6**(2016).

455. Doorduijn, D.J., Rooijakkers, S.H., van Schaik, W. & Bardoel, B.W. Complement resistance mechanisms of *Klebsiella pneumoniae*. *Immunobiology* **221**, 1102-9 (2016).

456. Yu, S. et al. Paneth Cell-Derived Lysozyme Defines the Composition of Mucolytic Microbiota and the Inflammatory Tone of the Intestine. *Immunity* **53**, 398-416.e8 (2020).

457. Bevins, C.L. & Salzman, N.H. Paneth cells, antimicrobial peptides and maintenance of intestinal homeostasis. *Nature Reviews Microbiology* **9**, 356-368 (2011).

458. Mak, P., Zdybicka-Barabas, A. & Cytryńska, M. A different repertoire of *Galleria mellonella* antimicrobial peptides in larvae challenged with bacteria and fungi. *Developmental & Comparative Immunology* **34**, 1129-1136 (2010).

459. Keller, L.J. et al. Chemoproteomic identification of a DPP4 homolog in Bacteroides thetaiotaomicron. *Nature Chemical Biology* **19**, 1469-1479 (2023).

Paper I

ChemBioChem

Research Article
doi.org/10.1002/cbic.202300473

Chemistry Europe
European Chemical Societies Publishing

www.chembiochem.org

Activity-Based Protein Profiling in Methicillin-Resistant *Staphylococcus aureus* Reveals the Broad Reactivity of a Carmofur-Derived Probe

Md Jalal Uddin,[a] Hermen S. Overkleeft,[b] and Christian S. Lentz*[a]

Activity-based protein profiling is a powerful chemoproteomic technique to detect active enzymes and identify targets and off-targets of drugs. Here, we report the use of carmofur- and activity-based probes to identify biologically relevant enzymes in the bacterial pathogen *Staphylococcus aureus*. Carmofur is an anti-neoplastic prodrug of 5-fluorouracil and also has antimicrobial and anti-biofilm activity. Carmofur probes were originally designed to target human acid ceramidase, a member of the NTN hydrolase family with an active-site cysteine nucleophile. Here, we first profiled the targets of a fluorescent carmofur probe in live *S. aureus* under biofilm-promoting conditions and in liquid culture, before proceeding to target identification by liquid chromatography/mass spectrometry. Treatment with a carmofur-biotin probe led to enrichment of 20 enzymes from diverse families awaiting further characterization, including the NTN hydrolase-related IMP cyclohydrolase PurH. However, the probe preferentially labeled serine hydrolases, thus displaying a reactivity profile similar to that of carbamates. Our results suggest that the electrophilic *N*-carbamoyl-5-fluorouracil scaffold could potentially be optimized to achieve selectivity towards diverse enzyme families. The observed promiscuous reactivity profile suggests that the clinical use of carmofur presumably leads to inactivation of a number human and microbial enzymes, which could lead to side effects and/or contribute to therapeutic efficacy.

Introduction

Activity-based protein profiling (ABPP) uses functionalized active-site directed small molecule probes known as activity-based probes (ABPs) to selectively label active enzymes, which can then be detected, identified and quantified through various analytical methods. A broad variety of probes has been designed to target diverse enzyme families and the application range spans from identification of drug targets and off-targets by chemical proteomics[1] to in vivo imaging or single-cell imaging studies in diverse organisms as extensively reviewed elsewhere.[2–6]

Some probes have been designed to target enzyme families in the broadest possible way[7] and have been applied for profiling studies in diverse organisms, whereas other probes have primarily been designed and validated for interaction with a particular target in a certain organism of interest. Repurposing these probes and validating their potential interactions with as of yet unidentified targets in other biological specimen may provide a short-cut for the discovery and functional validation of previously uncharacterized enzymes.

One focus of our research has been the characterization of new enzyme activities in bacterial pathogens. In a previous ABPP-study we have used fluorophosphonate probes to identify ten uncharacterized serine hydrolases in the bacterial pathogen *Staphylococcus aureus* that have emerging roles in pathogenesis and as potential anti-virulence targets.[8] In an ongoing effort to expand this work we seek to characterize the activity of additional enzyme families that are not well characterized. One interesting candidate for this approach are carmofur-derived probes (Scheme 1) that were generated to target human acid ceramidase (ACase)[9] after carmofur had been identified as a potent inhibitor of ACase.[10] Carmofur, or 1-hexylcarbamoyl-5-fluorouracil, is a registered anti-neoplastic drug for treatment for colorectal cancer in several countries[11,12] and a number of other potential therapeutic applications are under investigation as summarized in a recent review.[13] Carmofur is a prodrug of the antimetabolite 5-fluorouracil (5-FU) and its bioconversion pathways and known mechanism of action are illustrated in Scheme 1C. In human cells, 5-FU is converted to various bioactive metabolites that, in a complex mechanism, ultimately result in DNA damage and cell death.[14,15] The bioactive 5-FU-derived metabolites include, for example, fluorodeoxyuridine monophosphate, which inhibits thymidylate synthase, and fluorouridine triphosphate, which is irregularly incorporated into RNA.[12,15] Whereas carmofur had originally been designed as a prodrug, it has been shown that this compound retains activity against 5-FU-resistant cancers, suggesting involvement

[a] *M. J. Uddin, Prof. Dr. C. S. Lentz*
Department of Medical Biology
UiT- The Arctic University of Norway
9019 Tromsø (Norway)
E-mail: christian.s.lentz@uit.no

[b] *Prof. Dr. H. S. Overkleeft*
Department of Bioorganic Synthesis
Leiden Institute of Chemistry, Leiden University
Einsteinweg 55, 2333 CC Leiden (The Netherlands)

Supporting information for this article is available on the WWW under https://doi.org/10.1002/cbic.202300473

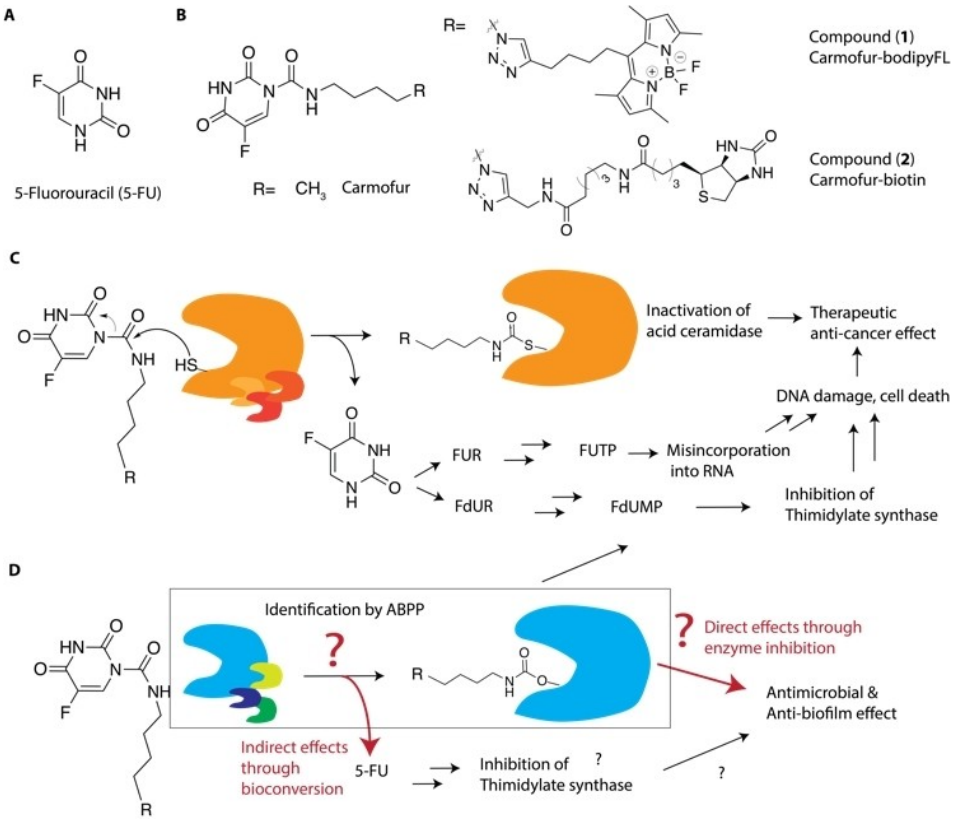

Scheme 1. Chemical structures of compounds used in this study. A) 5-FU. B) Carmofur and related probes carmofur-bodipyFL (**1**) and carmofur-biotin (**2**). C) Bioconversion of carmofur and 5-FU in humans and mechanism of action; FUR: fluorouridine, FdUR: fluorodeoxyuridine, FUTP: fluorouracil triphosphate, FdUMP: fluorodeoxyuridine monophosphate. D) Schematic illustration of the bioconversion pathway and mechanism of action underlying the antimicrobial and anti-biofilm effects of carmofur in *S. aureus.* Enzymes identified by ABPP could directly contribute to the biological effects and/or indirectly have relevance for the bioconversion to 5-FU as indicated by red font and arrows. Whereas (C) shows the presumed inactivation mechanism of carmofur through carbamoylation of the active-site Cys nucleophile of the cysteine amidase ACase, (D) illustrates the proposed carbamoylation of active-site Ser of serine hydrolases, which this study determined as the major target class of carmofur probes in *S. aureus.*

of additional targets not shared with 5-FU, such as ACase[16–18] (Scheme 1C).

ACase is a cysteine amidase belonging to the N-terminal nucleophile (NTN) hydrolase family and catalyzes the hydrolysis of ceramide to sphingosine and free fatty acids, which is the last step in the lysosomal degradation of (glycol)sphingolipids. Deficiency in ACase causes the lysosomal storage disorder Farber disease.[19] In another lysosomal storage disease, Gaucher Disease, a deficiency in glucocerebrosidase leads to an accumulation in glucosylceramide which is a potential substrate of ACase. Intriguingly, a fluorescent carmofur probe has been used to quantify ACase levels in human tissue extracts, thus revealing higher levels of ACase activity in splenic tissues from Gaucher disease patients compared to tissues from a healthy control group.[9]

Interestingly, carmofur and its parent drug 5-FU have been shown to exhibit general antimicrobial as well as antibiofilm activity against various bacteria including methicillin-resistant *S. aureus* (MRSA).[20,21] The mechanism behind the antimicrobial activity of 5-FU in bacteria is not well understood, but believed to be connected to inhibition of thymidylate synthase and a resulting blockade of DNA synthesis.[22] The anti-biofilm and virulence-attenuating activities in several species have been connected with competition with regulatory functions of uracil[23] and interference with quorum sensing.[24,25] The mechanism underlying the antimicrobial activity of carmofur has not been investigated. We hypothesized that, in analogy to the contribution of ACase inhibition to the therapeutic effect of carmofur in human, microbial enzymes targeted by carmofur might directly contribute to the antimicrobial and anti-biofilm effects of the drug and/or contribute to the bioconversion of carmofur to 5-FU.

In this study, we therefore applied carmofur-derived ABPs to profile enzymatic targets of this drug in MRSA. Because members of the NTN hydrolases family, which carmofur targets in human, are poorly characterized in bacteria, we hypothesized that this approach would be suitable to identify novel enzymes of this family with relevant biological functions. Our study revealed that, in addition to NTN hydrolases, carmofur interacts with a diversity of bacterial enzymes, particularly serine hydrolases. We demonstrate that lack of several individual target enzymes does not affect the susceptibility of *S. aureus* to carmofur and propose that these enzymes collectively contribute to the bioconversion of this drug to 5-FU and might also play a role for its anti-biofilm activity. Our study also has important implications regarding the use of carmofur in the

clinic, since it suggests that the drug might inactivate a similarly broad range of enzymes in humans as well as the human gut microbiome, which may affect the therapeutic outcome and cause side-effects.

Results and Discussion

Gel-based activity-based protein profiling by using a fluorescent carmofur probe

We conducted initial ABPP studies with the fluorescent carmofur-derived ABP (**1**) on live *S. aureus* cells (clinically relevant methicillin-resistant strain USA300 JE2) that were grown under biofilm-promoting growth conditions on tryptic soy agar supplemented with 100 mM $MgCl_2$ (TSAMg) in analogy to previous studies.[8] After labeling, cells were lysed and labeled proteins resolved by SDS-PAGE analysis and visualized by in-gel fluorescence scanning. We observed that the carmofur probe indeed led to dose-dependent labeling of certain *S. aureus* proteins (Figure 1). Two species corresponding to a molecular weight of >52 kD were most potently labeled (with bands apparent already at a probe concentration of 100 nM). Several additional bands with a molecular weight of around 31, 38, 54, 58, and 76 kDa, respectively, were labeled at 1 μM (Figure 1A). Since bacteria are expected to produce different enzymes depending on their growth environment, we compared the labeling profile of bacteria grown on TSAMg with that of bacteria grown to stationary phase in liquid culture using a standard rich cultivation medium (tryptic soy broth, TSB; Figure 1B). To differentiate secreted proteins that accumulate over the course of liquid cultivation from cell-associated proteins, we separated cells from the culture media that contains secreted proteins by centrifugation for differential analysis. We observed three dominant bands in the culture supernatant, whereas several proteins were detected in the cell pellet (Figure 1B).

To address whether the observed labeling profile achieved under biofilm-promoting conditions is the result of specific active-site directed interactions, we investigated if pre-incubation with the unlabeled parent inhibitor carmofur could block labeling of the fluorescent carmofur probe **1** in a competitive ABPP setup. Indeed, pre-incubation with carmofur (3–30 μM) led to reduced labeling of three of the most pronounced bands at 31, 38, and 54 kDa, suggesting that carmofur can compete with ABP (**1**). In contrast, pre-incubation with 5-FU, which is not expected to irreversibly interact with any of the targets, did not lead to alterations in the ABP-labeling patterns up to a concentration of 30 μM.

We suspected that the alterations in the labeling profile at high concentrations of 5-FU might be due to nonspecific effects related to its antimicrobial activity rather than competition labeling. We therefore determined the Minimum inhibitory concentrations (MICs) of the inhibitors carmofur and 5-FU against *S. aureus* USA300 JE2, which were both 5 μM. Thus, specific competition of carmofur with the targets of **1** becomes evident at sub-MIC concentrations, supporting the specific nature of these interactions. For 5-FU, in contrast, the changes in the labeling profile are seen at concentrations six times higher than its MIC (Figure 1C) and therefore most likely result nonspecifically from its antimicrobial activity rather than from specific competition with the probe.

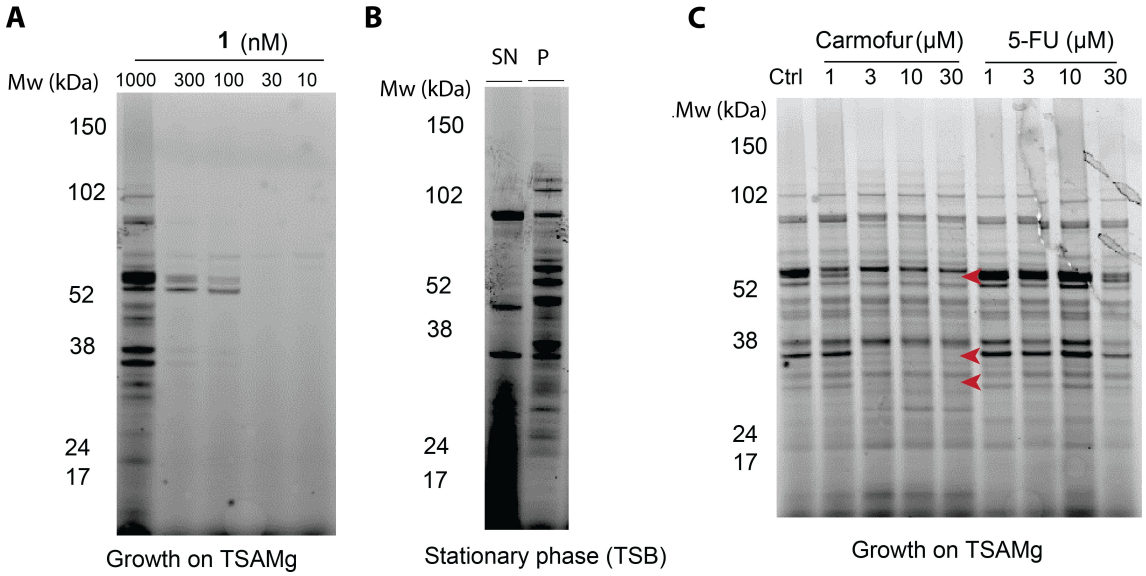

Figure 1. Fluorescent ABP-labeling profiles of *S. aureus* USA300 JE2 with carmofur probe **1**. Live bacteria were labeled with different concentrations of probe **1** for 60 min at 37 °C before cells were lysed, and samples were subjected to SDS-PAGE analysis. All graphs show fluorescent scans in the Cy2 (488 nm) channel on an Amersham™ Typhoon™ 5 (Cytiva). A) Dose-dependent labeling profile of *S. aureus* USA300 JE2 cells harvested from TSAMg with probe **1** and B) labeling profile of *S. aureus* USA300 JE2 cell fractions from the stationary phase in liquid culture with probe **1** (1 μM); SN: culture supernatant, P: cell pellet. C) Competitive ABPP. Cells were pre-incubated with carmofur or 5-FU at the indicated concentrations for 60 min before the addition of probe **1** (1 μM). Arrowheads indicate bands with consistently reduced labeling after pre-incubation with carmofur.

Target Identification

A limitation of the gel-based approach using fluorescent ABPs is that only the most abundant targets are detected and that their identity remains undefined. To overcome these shortcomings, we switched to using the biotin-tagged probe (**2**) in combination with a chemoproteomic workflow. It should be noted, however, that also this approach focuses on covalently bound targets and less stable, reversible interactions may be overlooked. In brief, live bacteria were grown under biofilm-promoting conditions on TSAMg before labeling with the biotin-tagged ABP (**2**) or carmofur as a control, lysed, and enriched for biotinylated proteins using a streptavidin resin. Samples were then analyzed by LC–MS/MS. Although the probe was used at 2 μM, which is lower than the MIC of carmofur (5 μM), we reasoned that its biological effects may still induce nonspecific changes to the general proteome that could translate to changes in the enrichment and detection of nonspecifically enriched "background" proteins in the probe-treated versus untreated chemoproteomic dataset. To account for such false positives, we decided to treat the unlabeled control sample with an equal concentration of carmofur. Treatment with carmofur-biotin (**2**) resulted in significant enrichment (p value < 0.05, enrichment > 1.5-fold) of 23 proteins compared to the carmofur-treated control dataset (Supporting Dataset 1, data are available from ProteomeXchange with identifier PXD043275). These 23 enriched proteins included 20 putative enzymes with diverse annotations (12 hydrolases or transferases, three oxidoreductases, three lyases, one isomerase, one putative chaperone-like protein; Table 1) as well as three non-enzymatic proteins that are likely false positives.

We identified one enzyme with structural similarity to the NTN hydrolase family,[29,30] the multifunctional PurH.[26] Featuring inosine 5'monophosphate (IMP) cyclohydrolase and 5-aminoimidazole-4-carboxamide ribonucleotide (AICAR) formyltransferase domains, this enzyme has a dual role in de novo purine synthesis.[26] Canonical members of the NTN hydrolase superfamily undergo self-processing to eliminate an N-terminal polypeptide, resulting in the active enzyme with a Ser, Thr or Cys nucleophile at the new N-terminus.[27,30] The bifunctional PurH however possesses an NTN-like fold, but the putative binding site with the corresponding nucleophile responsible for covalent binding to the carmofur probe remains to be identified.

The enzyme family for which the highest number of members were enriched by the carmofur probe **2** were serine hydrolases. This includes 3 α,β-hydrolases, the fluorophosphonate-binding hydrolases (FphB, FphC, and FphF) that we have described recently and which share a conserved Ser-His-Asp catalytic triad with serine as the active site nucleophile.[8,28] We also identified additional hydrolases/transferases that are annotated with a serine in the active site: the putative O-acetyltransferase Oat with an annotated SGNH-hydrolase-type esterase domain and the teichoid acid D-Ala esterase FmtA, which harbors a β-lactamase domain with a conserved catalytic triad of Ser-Lys-Asp. FmtA catalyzes the hydrolytic removal of D-alanine esters on wall teichoic acid (WTA),[29,30] thereby regulating charge and integrity of the bacterial cell wall.

Among these serine hydrolase targets of carmofur, the only enzyme for which a substrate-bound crystal structure is available that could give indications on the molecular basis of binding of carmofur, is FphF.[28] FphF is a serine carboxylesterase with a broad substrate-selectivity profile against synthetic fluorogenic substrates. The enzyme had peak activity against a heptanoate- based substrate and the crystal structure showed that the C7 acyl chain fully occupied the hydrophobic acyl binding pocket of FphF.[28] We propose that carmofur binding leads to carbamoylation of the active site serine and assume that the hexyl-carbamoyl group of carmofur, which has a similar chain length to the C7 acyl of the preferred substrate, fits well into the acyl binding pocket. Since the partially open architecture of the acyl binding pocket of FphF can also accommodate substrates with longer acyl chains (although with poorer fits in docking studies) with terminal atoms pointing out of the pocket,[28] this provides a molecular basis for binding of the longer carmofur-derived probes. The observed promiscuity and reactivity toward serine hydrolases concurs with a recent report identifying carmofur as an inhibitor of another N-terminal cysteine hydrolase (*N*-acylethanolamine acid hydrolase), as well as of a human serine hydrolase (fatty acid amide hydrolase).[31] We therefore conclude that the carbamoyl-5-flurouracil electrophile elicits a similar reactivity profile to carbamates, which are known inhibitors of serine hydrolases.[32]

The molecular basis and specificity of the interactions of the carmofur probes with the diverse other enriched enzymes such as lyases, oxidoreductases or metal-dependent hydrolases with in part unknown or even without predicted active site nucleophiles (as indicated in Table 1), remains to be determined.

Gel-based target validation

To validate the chemoproteomic results and to assign the bands identified in gel-based ABPP, we performed gel-based labeling studies using transposon mutants deficient in targets identified by MS, with a focus on the NTN and serine hydrolases. As we detected several Fph enzymes in the MS dataset, we first tested the entire panel of Fph A–H mutants and the secreted lipases SAL1 and −2 which was available from previous studies[8] in strain USA300 LAC. This allowed for a clear assignment of SAL2, FphB, FphE, FphF as labeled targets of the carmofur probe **1** (Figure 2A). Among the α,β-hydrolases some differences were apparent in the gel-based and MS-based studies: FphC was not detected by the gel-based approach, whereas SAL2 and FphE were detected on the gel, but not by MS. These differences could result from differences in permeability and activity of the fluorescent versus biotinylated probe. In the case of FphC this might also be due to limited resolution and lower sensitivity of gel-based ABPP. Interestingly, α,β-hydrolases also accounted for all fluorescently labeled bands that were detected after growth in liquid culture. SAL2 was found as the two dominant bands in the supernatant at around

Table 1. Target enzymes of carmofur probe (2) in *S. aureus* USA300 JE2.

Accession no.	Protein	Description	Active-site nucleophile/ putative site of attachment	Gene name	Unique peptides	Mol weight [kDa]	Abundance ratio: biotin/ctrl	Abundance ratio p value
QPB88705.1	FphF	carboxylesterase[28]	Ser	*est*A/*fph*F[8,28]	2	29.1	100.0	1×10^{-17}
WP_ 001146763.1	AhpD	alkyl hydroperoxide reductase	Cys	*ahp*D	5	16.5	10.0	7.34368×10^{-12}
QPB88396.1	YndB	SRPBCC domain-containing protein	unknown	*Ynd*B	2	20.1	5.8	0.0009
WP_ 001184005.1	AcuC	acetoin utilization protein	Lys	*acu*C	5	44.6	4.7	0.0036
WP_ 000379821.1	OatA	acetyltransferase	Ser	*oat*A	7	69.1	2.9	0.0008
QPB87247.1	PyrF	orotidine-5′-phosphate decarboxylase	Lys	*pyr*F	7	25.6	2.8	0.0257
WP_ 000058383.1	MaeB	NAD-dependent malic enzyme 4	Lys	*mae*B	3	44.2	2.6	0.0108
QPB88680.1	BetB	betaine-aldehyde dehydrogenase	Cys	*bet*B	3	54.6	2.2	0.0132
QPB86902.1	Eno	phosphopyruvate hydratase	Lys, Glu	*eno*	6	47.1	1.9	0.0243
QPB88514.1	ApbA	2-dehydropantoate 2-reductase	Lys, Glu	*apb*A	4	34.4	1.9	0.0322
WP_ 001178942.1	CshA	DEAD/DEAH box helicase	unknown	*csh*A	24	56.9	1.9	0.0099
QPB87344.1	FphC	hydrolase, α/β hydrolase fold family	Ser	SAUSA300_ 1194/ *fph*C[8]	9	35.2	1.7	0.0023
WP_ 001248939.1	YvcK	YvcK family protein	unknown	*yvc*K	5	36.2	1.7	0.0341
QPB87084.1	GNAT	GNAT family N-acetyltransferase	unknown	SAUSA300_ 0943	6	21.3	1.7	0.0294
QPB87049.1	YjbK	CYTH domain-containing protein	unknown (metal-dependent)	*yjb*K	2	23.4	1.7	0.0326
QPB86868.1	PepT	peptidase T	unknown (metal-dependent)	*pep*T	12	45.8	1.6	0.0224
WP_ 001281145.1	Alr	alanine racemase	Lys	*alr*	3	42.8	1.6	0.0105
QPB88602.1	FphB	Carboxylesterase[8]	Ser	SAUSA300_ 2473/*fph*B[8]	10	36.8	1.5	0.0388
QPB87101.1	FmtA	teichoic acid D-Ala esterase	Ser	*fmt*A	3	46	1.5	0.0390
QPB87118.1	PurH	IMP cyclohydrolase	Ser, Thr or Cys	*pur*H	26	54.3	1.5	0.0114

76 and >38 kDa (Figure 2B). SAL1 was associated to the cell pellet and appeared as diverse species of various molecular weight (Figure 2C). The only relevant remaining band in both fractions was assigned to the 31 kDa FphE (Figure 2B, C).

To account for the unidentified bands that can be detected in cells grown on TSAMg, we tested additional JE2-based mutants from the Nebraska Transposon Mutant Library (Figure 2D).[33] The *purH* transposon mutant, showed an altered labeling profile where several bands around and below the expected size of 54 kDa are missing (Figure 2D). It remains to be determined if the bands in question are all different fragments of PurH or if some of these changes may be attributed to secondary effects of the knock-out (Figure 2D). Certain ambiguity also remains regarding identification of the 46 kDa FmtA on the gel, as a band of this size was clearly reduced, but not absent (Figure 2D). In conclusion, these data confirm that the majority of the targets of the fluorescent carmofur probe in gel-based ABPP are indeed serine hydrolases.

Transposon mutations in abundant carmofur targets do not affect antimicrobial susceptibility to carmofur

Because the mechanism underlying the antimicrobial activities of carmofur is not properly documented, we aimed to determine if the enzymes enriched by the carmofur probe are relevant for the susceptibility to carmofur. Carmofur-binding to these targets could contribute to the antimicrobial effect

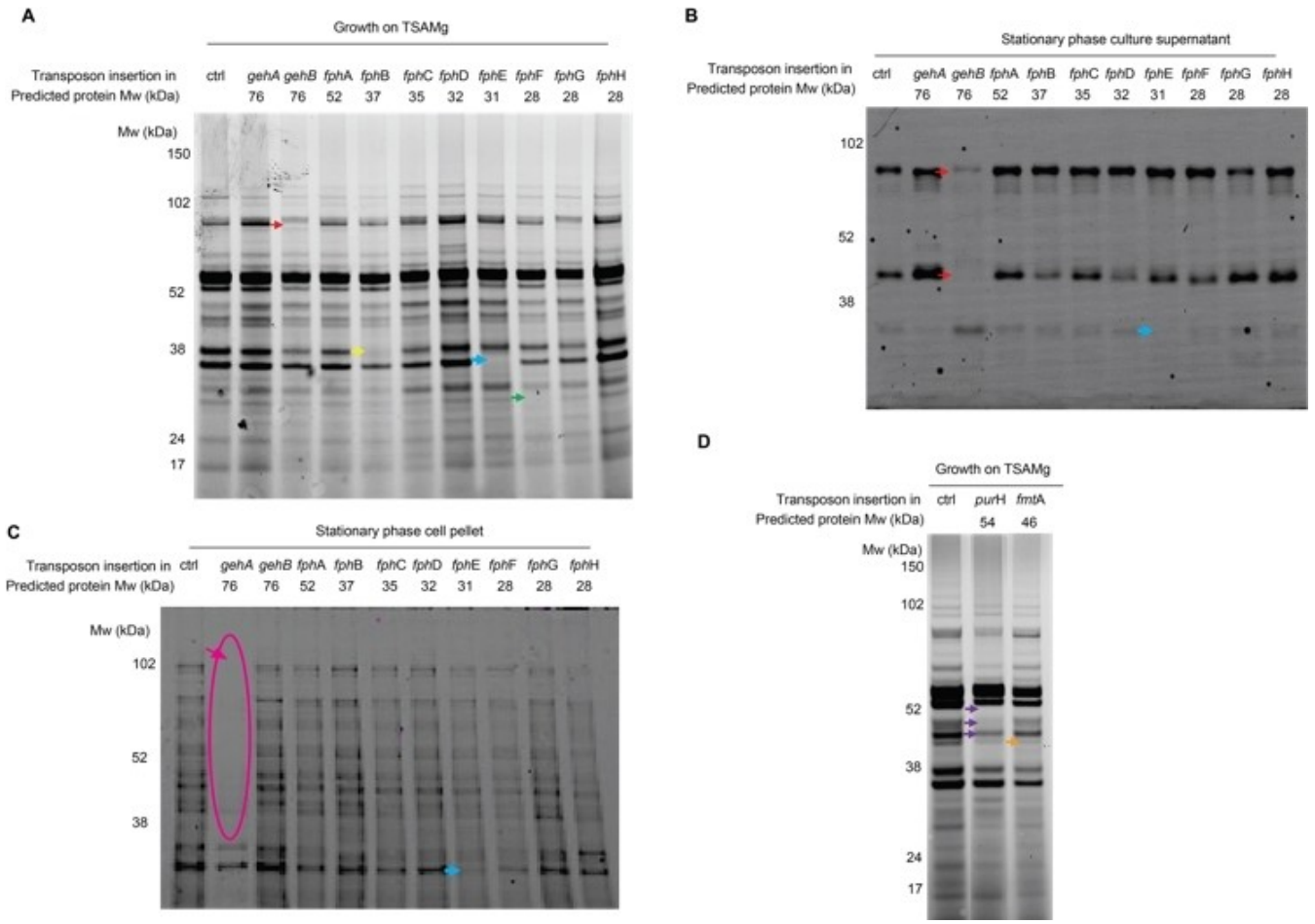

Figure 2. Fluorescent carmofur probe **1** labeling profiles of *S. aureus* USA 300 LAC transposon mutant strains with insertions of fluorophosphonate-binding hydrolases (Fphs) A–H and the secreted lipases SAL1 and −2 genes. The cells were labeled under two different conditions: A) cells grown in TSAMg and cells in stationary phase culture in TSB, fractionated into B) supernatant (SN) and C) cell pellet (P). D) Labeling profiles of *S. aureus* USA 300 JE2 transposon mutant strains with insertions of purine biosynthesis protein (*purH*) and teichoic acid D-Ala esterase (*FmtA*) genes. The cells were harvested in TSAMg. The labeled proteins disappearing in individual mutant strains are indicated by arrowheads.

directly (through target inhibition), but this is unlikely since none of the targets are essential. Alternatively, carmofur-binding can affect the antimicrobial activity indirectly by means of releasing 5-FU (Scheme 1D). Assuming that both the carmofur probes **1** and **2** and their parent drug lead to carbamoylation of the active site nucleophile (similar to ACase[9,18]) and the mode of action of carbamates on serine proteases,[32] these events will lead to release of 5-FU. We reasoned that, if activation of the prodrug was required, this could be reflected by slower bacterial killing by carmofur compared to 5-FU.

However, time-kill curve analysis revealed no differences in the kinetics of bactericidal effects elicited by 5-FU and carmofur (Figure 3). This suggests that either no conversion of carmofur to 5-FU is required, or more likely, that this conversion occurs very quickly. Unfortunately, there are – to the best of our knowledge–no available data on the biotransformation kinetics of carmofur to 5-FU in either bacteria, mammalian cells, humans, or animals that could help put these results into perspective.

We proceeded to determine the antimicrobial susceptibility of transposon mutant strains deficient in probe targets SAL1, SAL2, FphB, FphC, FphE, FphF, PurH, or FmtA and their corresponding WT strains LAC or JE2 by broth microdilution testing. All strains showed an identical MIC of 5 μM. Our data

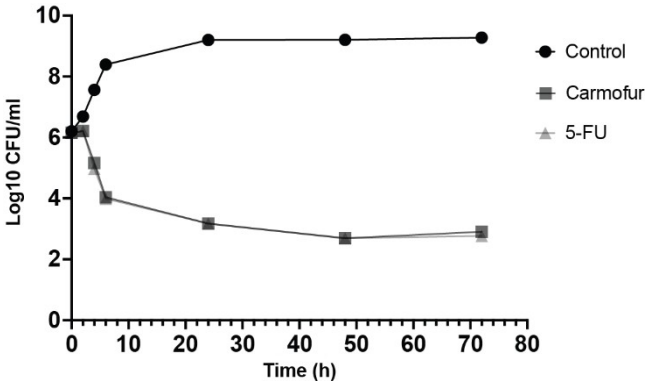

Figure 3. Time–kill curve analysis of carmofur and 5-FU. Stationary-phase *S. aureus* USA300 JE2 were treated with 4× the MIC of carmofur and 5-FU at 37 °C for 72 h. At various timepoints, aliquots were analyzed for CFU determination.

suggest that the activity of these enzymes individually does not affect the bactericidal activity of carmofur. Because the carmofur probe interacts promiscuously with a wealth of targets, it could be expected that they contribute collectively to the conversion of carmofur to 5-FU and that hence single knock-outs have only limited effects. It is also possible that other bacterial enzymes can hydrolyze carmofur to release 5-FU without being inactivated and labeled by the carmofur probes.

In contrast to the bactericidal activity, it seems plausible that inactivation of some of the identified enzymes may contribute to the anti-biofilm activities of carmofur.[21] PurH, for example, has already been attributed an important role in biofilm formation[34] and a putative involvement of other targets of the carmofur probe in biofilm formation merits further investigations.

Conclusions

This study has revealed the surprisingly broad reactivity profile of carmofur- and activity-based probes in the bacterial pathogen *S. aureus* and revealed the activity of a number of previously uncharacterized enzymes under biofilm-promoting conditions that merit further functional characterization. In addition to one expected member of the NTN hydrolase family, the IMP cyclohydrolase PurH, carmofur probes showed a similar reactivity to carbamates, in that they were able to interact with a number α,β-hydrolases and other serine hydrolases. Future studies might alter the electrophilic *N*-carbamoyl-5-fluorouracil scaffold in carmofur in order to generate more selective probes or inhibitors for some of the underexplored enzyme families targeted. In light of the clinical use of carmofur as a drug in colorectal cancer (as reviewed in ref. [13]) it must be considered that this drug might exhibit a similarly broad reactivity profile against human enzymes that could be potentially be related to both therapeutic and side effects. It is also plausible that carmofur reacts promiscuously with enzymes from human-associated microbiota. Considering the emerging knowledge of the impact gut microbiota have on human physiology, microbial (off−)targets could even be implicated in the mechanisms leading to its therapeutic effects. A prominent study has reported the impact of non-antibiotic drugs, including 5-FU, on human gut microbiota, even though the study concluded that the body concentration of 5-FU (in plasma) is lower than the concentration that reduces growth of at least one commensal bacteria by 25%.[35] However, in contrast to 5-FU, which is administered intravenously, carmofur is administered orally, thus making it very plausible that treatment leads to a concentration of carmofur in the human gut that is high enough to affect microbial enzymes.

Experimental Section

Bacterial strains and culture conditions: This work used *S. aureus* strains USA300 LAC, USA300 JE2 and their isogenic mutants as summarized in Table 2. All strains were routinely cultured on tryptic soy agar (TSA) or TSA with 100 mM $MgCl_2$ (TSAMg) or Difco tryptic soy broth (TSB). All bacterial strains were incubated at 37 °C and liquid cultures were aeriated by shaking at 180 rpm unless indicated otherwise.

Table 2. Bacterial strains used in this study.

Strain	Description	Ref./ source
S. aureus USA300 LAC	wild-type USA300 Los Angeles County (LAC) clone; multilocus sequence type 8, SCCmec type IV cured of antibiotic resistance plasmid	[41]
LAC_*gehA*: Tn	transposon insertion mutant in LAC SAUSA300_2603 (SAL1); Ery^R, $Linc^R$	[8]
LAC_*gehB*: Tn	transposon insertion mutant in LAC SAUSA300_0320 (SAL2); Ery^R, $Linc^R$	[8]
LAC_*fphA*: Tn	transposon insertion mutant in LAC SAUSA300_2396 (*fphA*); Ery^R, $Linc^R$	[8]
LAC *fphB*: Tn	transposon insertion mutant in LAC SAUSA300_2473 (*fphB*); Ery^R, $Linc^R$	[8]
LAC_*fphC*: Tn	transposon insertion mutant in LAC SAUSA300_1194 (*fphC*); Ery^R, $Linc^R$	[8]
LAC_*fphD*: Tn	transposon insertion mutant in LAC SAUSA300_2148 (*fphD*); Ery^R, $Linc^R$	[8]
LAC_*fphE*: Tn	transposon insertion mutant in LAC SAUSA300_2518 (*fphE*); Ery^R, $Linc^R$	[8]
LAC_*fphF*: Tn	transposon insertion mutant in LAC SAUSA300_2564 (*fphF*); Ery^R, $Linc^R$	[8]
LAC_*fphG*: Tn	transposon insertion mutant in LAC SAUSA300_1733 (*fphG*); Ery^R, $Linc^R$	[8]
LAC_*fphH*: Tn	transposon insertion mutant in LAC SAUSA300 0763 (*fphH*); Ery^R, $Linc^R$	[8]
S. aureus USA300 JE2	a plasmid-cured derivative of USA300 LAC and Parent strain of Nebraska Transposon Mutant Library	[33]
JE2_*purH*: Tn	transposon insertion mutant in JE2 SAUSA300_0975 (*purH*); Ery^R, $Linc^R$	[33]
JE2_*fmtA*: Tn	transposon insertion mutant in JE2 SAUSA300_0959 (*fmtA*); Ery^R, $Linc^R$	[33]

Probes and inhibitors: The carmofur probes **1** and **2** were available from a previous study and their synthesis had been described.[9] Carmofur and 5-FU were purchased from Sigma.

Labeling with fluorescent ABP (1): After overnight growth on TSAMg plate or in liquid culture as indicated, bacteria were suspended to the desired density in TSB and added to microtubes in a final volume of 50–100 μL. For competitive ABPP experiments, the inhibitors (carmofur and 5-FU) were added from 100x-concentrated stock solutions in DMSO and pre-incubated with the cells for 60 min (37 °C, 300 rpm) prior to ABP-labeling. Compound **1** (1 μM) was added from a 100x stock solution in DMSO and cells were incubated for 60 min, at 37 °C, 300 rpm. After probe labeling, bacterial suspensions were transferred to 2 mL screw-cap tube filled with 30–50 μL of 4x SDS-Loading buffer and ca. 60–100 μL of 0.1 mm glass beads and lysed by bead-beating.

SDS-PAGE analysis of fluorescently labeled proteins: After adding the 4x SDS sample buffer (40% glycerol, 240 mM Tris·HCl pH 6.8, 8% SDS, 0.04% bromophenol blue, 5% β-mercaptoethanol), lysates of probe-labeled bacteria were boiled at 95 °C for 10 min and separated by SDS-PAGE gel. The gels were scanned for fluorescence in the Cy2 (488 nm) channel on a Amersham™ Typhoon™ 5 (cytiva).

Labeling with biotinylated probes and sample preparation for mass spectrometry: *S. aureus* USA300 JE2 cultures were grown on TSAMg for 24 h and resuspended to an OD_{600} ~20 in 3 mL TSB. For each biological replicate, 1 mL aliquots were transferred to a 1.5 mL tube and either carmofur–biotin (probe **2**; 2 μM) or an equal concentration of carmofur (as a control for nonspecific biological effects of the probe) were added, and cells were incubated for 60 min at 37 °C, 700 rpm before samples were spun down at 4500 *g* for 5 min at 4 °C, and the supernatant was aspirated. The cell pellets were resuspended in 1.2 mL RIPA lysis buffer (50 mM Tris, 150 mM NaCl, 0.1% SDS, 0.5% sodium deoxycholate, 1% Triton X-100) and lysed by bead-beating. Samples were centrifuged for 5 min at 10000 *g* at 4 °C. Protein concentration in the supernatant was adjusted to 1.0 mg mL^{-1}. Proteins were stored at −20 °C prior to sample preparation. For each sample, 50 μL streptavidin magnetic beads were washed twice with 1 mL RIPA lysis buffer and incubated with 1 mg protein from each sample with an additional 500 μL RIPA lysis buffer at 4 °C for overnight at 18 RPM rotator. After enrichment, beads were pelleted using a magnetic rack, and washed twice with RIPA lysis buffer (1 mL, 2 min at RT), once with 1 M KCl (1 mL, 2 min at RT), once with 0.1 M Na_2CO_3 (1 mL, ~10 s), once with 2 M urea in 10 mM Tris·HCl (pH 8.0; 1 mL, ~10 s), and twice with RIPA lysis buffer (1 mL per wash, 2 min at RT). After the final wash, the beads were transferred in 1 mL RIPA lysis buffer to fresh protein Lo-Bind tubes. Then, beads were washed three times in 500 μL 2 M/4 M urea, 50 mM ammonium bicarbonate (Ambic) with shaking for 7 min. Finally, beads were washed 3x with 500 μL of 50 mM Ambic with shaking for 7 min, each time transferring the samples to a new tube in-between washes. For on-bead digestion, 150 μL 50 mM Ambic, 3 μL 1 mM $CaCl_2$, 0.75 μL 1 M DDT, 4.5 μL 500 mM IAA and 6 μL MS grade trypsin solution were added and samples were incubated at 37 °C overnight at 800 rpm. Tryptic peptide digests were separated, and beads were washed with 70 μL 50 mM Ambic. For each sample, to the combined eluates received 20 μL of formic acid were added, and the samples were kept at −20 °C until analysis via LC–MS/MS.

LC–MS analysis: Varian's OMIX C18 tips were employed to perform sample cleanup and concentration. Peptide mixtures that comprised 0.1% formic acid were loaded onto a Thermo Fisher Scientific EASY-nLC1200 system (C_{18}, 2 μm, 100 Å, 50 μm, 50 cm) and subjected to fractionation by using a 5–80% acetonitrile gradient in 0.1% formic acid at a flow rate of 300 nL min^{-1} for a duration of 60 min. The peptides that were separated were examined using a Thermo Scientific Orbitrap Exploris 480. Data was acquired in a data-dependent mode with the aid of a Top20 method. The raw data were processed by using the Proteome Discoverer 2.5 software, and the fragmentation spectra were searched against (*S. aureus* 300 LAC). Peptide mass tolerances of 10 ppm and a fragment mass tolerance of 0.02 Da were employed during the search. Peptide ions were filtered using a false discovery rate (FDR) set at 5% for peptide identifications. To ensure accuracy, the filter criterion of two unique peptides was used, and three replicates were conducted for all samples. The protein abundance obtained from Proteome Discoverer was averaged across replicates, and the ratio of the ABPP-enriched sample versus the control tryptic digestion sample was calculated. Proteins enriched more than 1.5-fold by the biotinylated probe were selected. ABPP-enriched and other pull-down experiments are significantly limited by nonspecific binding.[36,37] The enrichment of these nonspecific proteins may be due to various reasons, such as naturally biotinylated proteins (e.g., carboxylase family proteins) and ribosomal proteins being enriched by streptavidin beads, as well as proteins with an affinity for hydrophilic beads being enriched. However, proteins exhibiting the latter two types of nonspecific binding were excluded. The mass spectrometry proteomics data have been deposited to the ProteomeXchange Consortium via the PRIDE[38] partner repository with the dataset identifier PXD043275.

Antimicrobial activity testing: To determine the MIC, stock solutions of carmofur and 5-Fluorouracil were prepared at a concentration of 200 μM in sterile distilled water. These solutions were then diluted 1:2 in 96-well microtiter plates and inoculated with *S. aureus* strains at approximately 5×10^5 CFU mL^{-1} in 100 μL. The 96-well microtiter plates were incubated overnight (18 h) to determine the MIC.[39]

Time–kill assay of carmofur/5-fluorouracil: A time–kill study was performed according to the Clinical and Laboratory Standards Institute guidelines following a method previously described.[40] In brief, 4×MIC (20 μM) of carmofur/5-fluorouracil was used to detect differences in time-dependent killing. Overnight cultures of *S. aureus* USA 300 JE2 were grown in Mueller–Hinton (MH) broth at 37 °C until the exponential phase was reached, indicated by OD_{600} = 0.4. The cells were then diluted to yield a final concentration of approximately 2×10^6 cells per mL and transferred to a 50 mL tube containing 20 mL of MH broth, followed by the addition of appropriate concentrations of carmofur and 5-fluorouracil. Tubes were then incubated at 37 °C, and aliquots were removed at 0, 2, 4, 6, 24, 48, and 72 h for the determination of viable counts. Serial dilutions were prepared in sterile PBS and plated according to the method previously described. Colonies were counted after incubation of TSA plates at 37 °C for 16–22 h, with a detection level of 1×10^2 CFU mL^{-1}.

Supporting Information

The authors have included Supporting Dataset 1 in the Supporting Information.

Acknowledgements

Mass spectrometry-based proteomic analyses were performed by UiT Proteomics and Metabolomics Core Facility (PRiME). This facility is a member of the National Network of Advanced Proteomics Infrastructure (NAPI), which is funded by the Research Council of Norway INFRASTRUKTUR-program (project number: 295910). We thank Jack-Ansgar Bruun and Toril Anne Grønset at PRimE for help with conducting LC–MS/MS analysis. The project was funded through a start-up grant by the Centre for New Antibacterial Strategies (CANS) to CSL. We thank Marius Haugland for helpful discussions.

Conflict of Interests

The authors declare no conflict of interest.

Data Availability Statement

The mass spectrometry proteomics data have been deposited to the ProteomeXchange Consortium via the PRIDE partner repository with the dataset identifier PXD043275.

Keywords: *S. aureus* · activity-based protein profiling · biofilm carmofur · 5-fluorouracil

[1] A. C. M. van Esbroeck, A. P. A. Janssen, A. B. Cognetta III, D. Ogasawara, G. Shpak, M. van der Kroeg, V. Kantae, M. P. Baggelaar, F. M. S. de Vrij, H. Deng, M. Allarà, F. Fezza, Z. Lin, T. van der Wel, M. Soethoudt, E. D. Mock, H. den Dulk, I. L. Baak, B. I. Florea, G. Hendriks, L. De Petrocellis, H. S. Overkleeft, T. Hankemeier, C. I. De Zeeuw, V. Di Marzo, M. Maccarrone, B. F. Cravatt, S. A. Kushner, M. van der Stelt, *Science.* **2017**, *356*, 1084–1087.
[2] S. I. Van Kasteren, B. I. Florea, H. S. Overkleeft, *Methods Mol. Biol.* **2017**, *1491*, 1–8.
[3] S. Chakrabarty, J. P. Kahler, M. A. T. Van de Plassche, R. Vanhoutte, S. H. L. Verhelst in *Recent Advances in Activity-Based Protein Profiling of Proteases*, (Eds.: B. F. Cravatt, K.-L. Hsu, E. Weerapana), Springer International, Cham, **2019**, pp. 253–281.
[4] C. S. Lentz, *Biol. Chem.* **2020**, *401*, 233–248.
[5] H. J. Benns, C. J. Wincott, E. W. Tate, M. A. Child, *Curr. Opin. Chem. Biol.* **2021**, *60*, 20–29.
[6] M. Garland, J. J. Yim, M. Bogyo, *Cell Chem. Biol.* **2016**, *23*, 122–136.
[7] Y. Liu, M. P. Patricelli, B. F. Cravatt, *Proc. Natl. Acad. Sci. USA* **1999**, *96*, 14694–14699.
[8] C. S. Lentz, J. R. Sheldon, L. A. Crawford, R. Cooper, M. Garland, M. R. Amieva, E. Weerapana, E. P. Skaar, M. Bogyo, *Nat. Chem. Biol.* **2018**, *14*, 609–617.
[9] C. M. J. Ouairy, M. J. Ferraz, R. G. Boot, M. P. Baggelaar, M. van der Stelt, M. Appelman, G. A. Van der Marel, B. I. Florea, J. M. F. G. Aerts, H. S. Overkleeft, *Chem. Commun.* **2015**, *51*, 6161–6163.
[10] D. Pizzirani, C. Pagliuca, N. Realini, D. Branduardi, G. Bottegoni, M. Mor, F. Bertozzi, R. Scarpelli, D. Piomelli, T. Bandiera, *J. Med. Chem.* **2013**, *56*, 3518–3530.
[11] N. B. Doan, H. Alhajala, M. M. Al-Gizawiy, W. M. Mueller, S. D. Rand, J. M. Connelly, E. J. Cochran, C. R. Chitambar, P. Clark, J. Kuo, K. M. Schmainda, S. P. Mirza, *Oncotarget* **2017**, *8*, 112662–112674.
[12] J. Shelton, X. Lu, J. A. Hollenbaugh, J. H. Cho, F. Amblard, R. F. Schinazi, *Chem. Rev.* **2016**, *116*, 14379–14455.
[13] M. M. Islam, S. P. Mirza, *Drug Dev. Res.* **2022**, *83*, 1505–1518.
[14] W. B. Wang, Y. Yang, Y. P. Zhao, T. P. Zhang, Q. Liao, H. Shu, *World J. Gastroenterol.* **2014**, *20*, 15682–15690.
[15] D. B. Longley, D. P. Harkin, P. G. Johnston, *Nat. Rev. Cancer* **2003**, *3*, 330–338.
[16] S. Sato, T. Ueyama, H. Fukui, K. Miyazaki, M. Kuwano, *Gan to Kagaku Ryoho* **1999**, *26*, 1613–1616.
[17] N. Realini, C. Solorzano, C. Pagliuca, D. Pizzirani, A. Armirotti, R. Luciani, M. P. Costi, T. Bandiera, D. Piomelli, *Sci. Rep.* **2013**, *3*, 1035.
[18] A. Dementiev, A. Joachimiak, H. Nguyen, A. Gorelik, K. Illes, S. Shabani, M. Gelsomino, E. E. Ahn, B. Nagar, N. Doan, *J. Med. Chem.* **2019**, *62*, 987–992.
[19] N. Coant, W. Sakamoto, C. Mao, Y. A. Hannun, *Adv Biol Regul.* **2017**, *63*, 122–131.
[20] A. Rangel-Vega, L. Bernstein, E.-A. Mandujano Tinoco, S.-J. García-Contreras, R. García-Contreras, *Front. Microbiol.* **2015**, *6*, 282.
[21] N. S. Torres, J. J. Abercrombie, A. Srinivasan, J. L. Lopez-Ribot, A. K. Ramasubramanian, K. P. Leung, *Antimicrob. Agents Chemother.* **2016**, *60*, 5663–5672.
[22] A. Rangel-Vega, L. R. Bernstein, E. A. Mandujano-Tinoco, S. J. García-Contreras, R. García-Contreras, *Front. Microbiol.* **2015**, *6*, 282.
[23] C. Attila, A. Ueda, T. K. Wood, *Appl. Microbiol. Biotechnol.* **2009**, *82*, 525–533.
[24] C. Attila, A. Ueda, T. K. Wood, *Appl. Microbiol. Biotechnol.* **2009**, *82*, 525–533.
[25] F. Sedlmayer, A. K. Woischnig, V. Unterreiner, F. Fuchs, D. Baeschlin, N. Khanna, M. Fussenegger, *Nucleic Acids Res.* **2021**, *49*, e73.
[26] Y. N. Kang, A. Tran, R. H. White, S. E. Ealick, *Biochemistry* **2007**, *46*, 5050–5062.
[27] J. A. Brannigan, G. Dodson, H. J. Duggleby, P. C. E. Moody, J. L. Smith, D. R. Tomchick, A. G. Murzin, *Nature* **1995**, *378*, 416–419.
[28] M. Fellner, C. S. Lentz, S. A. Jamieson, J. L. Brewster, L. Chen, M. Bogyo, P. D. Mace, *ACS Infect. Dis.* **2020**, *6*, 2771–2782.
[29] V. Dalal, P. Kumar, G. Rakhaminov, A. Qamar, X. Fan, H. Hunter, S. Tomar, D. Golemi-Kotra, P. Kumar, *J. Mol. Biol.* **2019**, *431*, 3107–3123.
[30] M. M. Rahman, H. N. Hunter, S. Prova, V. Verma, A. Qamar, D. Golemi-Kotra, *mBio* **2016**, *7*, e02070–02015.
[31] K. Wu, Y. Xiu, P. Zhou, Y. Qiu, Y. Li, *Front. Pharmacol.* **2019**, *10*, 818.
[32] J. C. Powers, J. L. Asgian, O. D. Ekici, K. E. James, *Chem. Rev.* **2002**, *102*, 4639–4750.
[33] P. D. Fey, J. L. Endres, V. K. Yajjala, T. J. Widhelm, R. J. Boissy, J. L. Bose, K. W. Bayles, *mBio* **2013**, *4*, e00537–00512.
[34] M. Gélinas, L. Museau, A. Milot, P. B. Beauregard, *Microbiol. Spectr.* **2021**, *9*, e0080421.
[35] L. Maier, M. Pruteanu, M. Kuhn, G. Zeller, A. Telzerow, E. E. Anderson, A. R. Brochado, K. C. Fernandez, H. Dose, H. Mori, K. R. Patil, P. Bork, A. Typas, *Nature* **2018**, *555*, 623–628.
[36] S. Wang, Y. Tian, M. Wang, M. Wang, G.-b. Sun, X.-b. Sun, *Front. Pharmacol.* **2018**, *9*.
[37] S. E. Tully, B. F. Cravatt, *J. Am. Chem. Soc.* **2010**, *132*, 3264–3265.
[38] Y. Perez-Riverol, J. Bai, C. Bandla, D. García-Seisdedos, S. Hewapathirana, S. Kamatchinathan, D. J. Kundu, A. Prakash, A. Frericks-Zipper, M. Eisenacher, M. Walzer, S. Wang, A. Brazma, J. A. Vizcaíno, *Nucleic Acids Res.* **2022**, *50*, D543-d552.
[39] G. Kahlmeter, D. F. J. Brown, F. W. Goldstein, A. P. MacGowan, J. W. Mouton, I. Odenholt, A. Rodloff, C. J. Soussy, M. Steinbakk, F. Soriano, O. Stetsiouk, *Clin. Microbiol. Infect.* **2006**, *12*, 501–503.
[40] F. Silva, O. Lourenço, J. A. Queiroz, F. C. Domingues, *J. Antibiot. (Tokyo).* **2011**, *64*, 321–325.
[41] B. Arsic, Y. Zhu, D. E. Heinrichs, M. J. McGavin, *PLoS One* **2012**, *7*, e45952.

Manuscript received: June 23, 2023
Revised manuscript received: August 7, 2023
Accepted manuscript online: August 8, 2023
Version of record online: August 29, 2023

Supplementary Dataset 1. Target proteins of carmofur-probe (2) in *S.aureus* USA300 JE2

#	Accession	Protein	Description	Protein family	Protein family/molecular function	active site nucleophile	Gene Name	Mol weight [kDa]	Unique Peptides	Abundance: biotin R1	Abundance: biotin R2	Abundance: biotin R3	Abundance: ctrl R1	Abundance: ctrl R2	Abundance:ctrl R3	Average Abundance: biotin	Average Abundance: Ctrl	Abundance Ratio: (biotin) / (ctrl)	Abundance Ratio P-Value
1	QPB88705.1	FphF	Carboxylesterase[31]	α/β hydrolase	Hydrolase, α/β hydrolase fold family	Ser	*estA/fph F* [8, 31]	29.1	2	66473.3	217223.1	435598.7				239765.0	1.0	100.0	1E-17
2	WP_001146763.1	AhpD	Alkyl hydroperoxide reductase	Oxidoreductase	Peroxidase, Acting on a peroxide as acceptor	Cys	*ahpD*	16.5	5	1028771.2	1722907.3	1699798.8	114322.8	126236.9	203441.4	1483825.7	148000.3	10.0	7.344E-12
3	QPB88396.1	YndB	SRPBCC domain-containing protein	Chaperone-like protein	Activator of Hsp90 ATPase homolog 1-like protein	Unknown	*YndB*	20.1	2	210257.2	178770.2	243453.0	38925.9	44698.6	26171.6	210826.8	36598.7	5.8	0.0008609
4	WP_001184005.1	AcuC	acetoin utilization protein	Hydrolases	Hydrolases, Acting on carbon-nitrogen bonds, other than peptide bonds	Lys	*acuC*	44.6	5	938998.9	726315.4	1069997.0	133308.7	137501.2	315150.5	911770.4	195320.1	4.7	0.0035692
5	WP_000379821.1	OatA	acetyltransferase	SGNH_hydrolase	SGNH_hydrolase_yrhL_like , the active site resembles the typical Ser-His-Asp(Glu) triad from other serine hydrolases	Ser	*oatA*	69.1	7	701670.5	276402.8	985381.2	278818.1	213157.6	189722.7	654484.8	227232.8	2.9	0.000793
6	QPB87247.1	PyrF	orotidine-5'-phosphate decarboxylase	Lyase	Lyase, carbon-oxygen lyases	Lys	*pyrF*	25.6	7	2596459.3	1516035.2	2944252.0	951521.4	835070.6	765111.4	2352248.8	850567.8	2.8	0.025706
7	WP_000728763.1	SpA	staphylococcal protein A	Non-enzymatic	Gram-positive cocci surface proteins LPxTG/LYSM	none	*spa*	55.5	12	4095135.2	5092316.0	13947671.5	2990051.9	3767970.5	1833766.1	7711707.6	2863929.5	2.7	0.001222
8	WP_000058383.1	MaeB	NAD-dependent malic enzyme 4	Lyase	Decarboxylase	Lys	*maeB*	44.2	3	213673.0	120221.7	572089.0	181421.5	83256.0	82236.6	301994.6	115638.0	2.6	0.0108281
9	QPB88680.1	BetB	betaine-aldehyde dehydrogenase	Oxidoreductase	Oxidoreductase, Acting on the aldehyde or oxo group of donors	Cys	*betB*	54.6	3	275429.1	207907.1	404351.6	209148.1	112809.0	82387.1	295896.0	134781.4	2.2	0.013202
10	QPB86902.1	Eno	phosphopyruvate hydratase	Lyase	Lyase, carbon-oxygen lyases	Lys, Glu	*eno*	47.1	6	1371007.7	602889.0	1277412.9	760894.4	404141.2	509625.1	1083769.9	558220.2	1.9	0.0243337
11	QPB88514.1	ApbA	2-dehydropantoate 2-reductase	Oxidoreductase	Oxidoreductase, acting on the CH-OH group of donors	Lys, Glu	*apbA*	34.4	4	993749.9	353182.7	1121246.3	361368.0	577090.9	374541.9	822726.3	437666.9	1.9	0.0322089
12	WP_001178942.1	CshA	DEAD/DEAH box helicase	Hydrolase	Hydrolase, acting on acid anhydrides	water/unknown	*cshA*	56.9	24	36539823.0	17762673.2	44969009.0	19276498.6	19577795.4	14422330.6	33090501.7	17758874.9	1.9	0.0098863
13	QPB87344.1	FphC	hydrolase, α/β hydrolase fold family	α/β hydrolase	Hydrolase, α/β hydrolase fold family	Ser	*SAUSA300_1194 / fphC* [8]	35.2	9	2149048.0	1862392.8	1768078.3	1063110.4	1166949.5	1082514.6	1926506.4	1104191.5	1.7	0.0022939
14	QPB87474.1	CvfC	virulence factor C	Non-enzymatic	Contributes to the production of a protease and nuclease via an agr-independent pathway	none	*cvfC*	43	3	269888.6		359833.3	184058.5	180657.3		314860.9	182357.9	1.7	0.0018011
15	WP_001248939.1	YvcK	YvcK family protein	Transferase	Binds UDP-GlcNAc, a precursor of peptidoglycan and also called called a gluconeogenesis factor	Unknown	*yvcK*	36.2	5	1799491.0	1241971.9	1581613.1	863095.7	1130954.3	741161.8	1541025.3	911737.3	1.7	0.0340661
16	QPB87084.1	GNAT	GNAT family N-acetyltransferase	Transferase	Transferases,transferring groups other than amino-acyl groups	Unknown	*SAUSA300_0943*	21.3	6	2122604.9	1366731.6	2312459.0	762990.7	1681667.7	989260.2	1933931.8	1144639.5	1.7	0.0294157
17	QPB87049.1	YjbK	CYTH domain-containing protein	Hydrolase	CYTH-like phosphatases 1	metal dependent	*yjbK*	23.4	2	425156.6	405312.4	94215.8	399540.4	74374.6	82627.2	308228.3	185514.1	1.7	0.0326473
18	WP_001549158.1	Map	extracellular adherence protein	Non-enzymatic	Extracellular adherence protein	none	*Map*	65.5	17	11938012.0	10183990.6	15474997.0	7793899.7	10646533.6	4876968.4	12532333.2	7772467.2	1.6	0.0175591
19	QPB86868.1	PepT	peptidase T	Hydrolase	Hydrolase, acting on peptide bonds	metal dependent	*pepT*	45.8	12	4730594.9	3647833.0	4817123.6	2212161.6	2996053.9	3007430.6	4398517.2	2738548.7	1.6	0.0224451
20	WP_001281145.1	Alr	alanine racemase	Isomerase	Isomerases, acting on amino acids and derivatives	Lys	*alr*	42.8	3	298519.4		303010.3	220528.7	177614.0	174990.9	300764.8	191044.5	1.6	0.010524
21	QPB88602.1	FphB	Carboxylesterase [8]	α/β hydrolase	Hydrolase, α/β hydrolase fold family	Ser	*SAUSA300_2473 / fphB* [8]	36.8	10	9323874.3	8311485.5	9412396.7	7565700.7	5784317.3	4133797.0	9015918.8	5827938.3	1.5	0.0387642
22	QPB87101.1	FmtA	teichoic acid D-Ala esterase	Hydrolase	Hydrolase, acting on ester bonds	Ser	*fmtA*	46	3	95695.2	39416.0	151284.2	63980.7	64403.9	60139.4	95465.1	62841.3	1.5	0.0389844
23	QPB87118.1	PurH	IMP cyclohydrolase	NTN hydrolase	Hydrolase, acting on carbon-nitrogen bonds, other than peptide bond	Cys	*purH*	54.3	26	94656309.3	96966807.0	111214235.2	78563253.4	61363890.4	64096856.2	100945783.8	68008000.0	1.5	0.0114217

Paper II

Activity-Based Protein Profiling Identifies an Alpha-amylase Family Protein Contributing to the Virulence of Methicillin-Resistant *Staphylococcus aureus*

Md Jalal Uddin[1*], Hermen S. Overkleeft[2], Mona Johannessen[1] and Christian S. Lentz[1*]

1. Department of Medical Biology (IMB), UiT—The Arctic University of Norway, 9019 Tromsø, Norway
2. Department of Bioorganic Synthesis, Leiden Institute of Chemistry, Leiden University Einsteinweg 55, 2333 CC Leiden, The Netherlands

*To whom correspondence should be addressed: Christian S. Lentz, Christian.s.lentz@uit.no and Md Jalal Uddin jalal.uddin@uit.no

Abstract

Glycosidases fulfill crucial functions in all life forms contributing to diverse biological processes such as metabolism, cell signaling, or pathogen-host interactions. In search for new putative targets for antimicrobial drugs, we here aimed to identify and characterize retaining glycosidase activities in the bacterial pathogen *Staphylococcus aureus*. Using activity-based protein profiling with a panel of 7 fluorescent covalent probes we initially screened for the activities of diverse retaining glycosidase families in *S. aureus* JE2 under different growth conditions. Biotinylated probe analogs were then used for target enrichment and identification by mass-spectrometry-based. Three glycosidase family proteins were identified: 6-phospho-β-glucosidase (BglA), α-amylase family protein trehalase C (TreC), and autolysin (Atl). The physiological relevance of the previously uncharacterized glycosidases BglA and TreC were addressed using CRISPRi-induced gene silencing. Whereas both enzymes were dispensable for *in vitro* growth in Tryptic Soy Broth, silencing of *tre*C, but not *bgl*A, led to reduced virulence in a *Galleria mellonella* infection model, warranting future investigations into the biochemical function and physiological role of this enzyme.

Introduction

Staphylococcus aureus is a Gram-positive opportunistic pathogen that colonizes the nose and/or pharynx, skin, and intestine in appr one-third of the human adult populations. Facilitated by its unique ability to adapt to diverse environments, manipulate host cells and evade the immune system system[1], it can cause a range of infections, from mild skin infections to life-threatening diseases, including bacteremia, endocarditis, osteomyelitis, and device-related infections[2-5]. Antibiotic resistant strains such as Methicillin-resistant *S. aureus* (MRSA) are spreading rapidly and contribute significantly to the unfolding of the antimicrobial resistance crisis, urging the development of novel treatment options[6].

One putative class of drug target enzymes that has not been systematically explored in *S. aureus* are glycoside hydrolases (GH or glycosidase). By catalyzing the cleavage of glycosidic bonds, GHs fulfill important functions in all life forms, and some are considered as drug targets for e.g., diabetes mellitus and cancer (reviewed in [7] and[8]) or as biomarker for precision medicine[9]. Recently, also enzymes involved in the degradation of peptidoglycan are gaining interest as drug targets. *S. aureus* cell envelope consists of a variety of glycan structures including peptidoglycan (murein), capsule polysaccharide, and teichoic acids. Enzymes involved in the biosynthesis of peptidoglycan such as the penicillin-binding proteins are targeted by β-lactam antibiotics. Autolysin is a *S. aureus* peptidoglycan hydrolase with both N-acetylmuramyl-L-alanine amidase and endo-β-N-acetylglucosaminidase activity.[10] This enzyme plays a role in cell envelope remodeling, virulence, biofilm formation[11] and is the target of novel type V glycopeptide antibiotics[12, 13]. Recent studies have also demonstrated the importance of wall teichoic acid (WTA) glycopolymers for the interactions with host epithelial cells [14]. Specific glycosylation patterns of WTA on the *S. aureus* surface affect recognition recognized by human Langerin cells [15] and affect their susceptibility to vancomycin [16]. Enzymes that would dynamically cleave and modulate these glycosides have – to the best of our knowledge not been reported to date. In addition, bacterial pathogens are continuously exposed to host-derived glycans which they could cleave for use as a nutrient source, to promote invasion or immune evasion.[17, 18,19] We therefore hypothesized that *S. aureus* GHs with putative roles in cleaving endogenous or exogenous glycans remain uncharacterized.

Activity-based protein profiling (ABPP) is a powerful chemoproteomic technique that uses functionalized covalent and irreversible inhibitors (called activity-based probes, ABP) to detect, enrich, and identify active species of an enzyme family of interest in a biological sample. Previously,

we have utilized fluorophosphonate- and carmofur-derived ABPs to identify uncharacterized serine hydrolases in *S. aureus*, which play important roles in bacterial virulence and stress response [20-22]. We have been seeking to expand these studies to other enzyme families. Since retaining glycosidases cleave their substrate in a mechanism that involves a covalent glycosyl-enzyme intermediate[23], these enzymes can be targeted with covalent inhibitors, such as cyclophellitol or its aziridine analogs. Thus, analogs of these inhibitors functionalized with a fluorophore, biotin or click-handles serve as covalent ABPs for detection of active GHs.[24, 25,26] GHs generally have a high degree of substrate selectivity and act on either α- or β-glycosidic bonds, discriminate between configurational isomers and differ in their preference of cleaving bonds in the end or in the middle of glycan chains[27]. Thus, there is no universal broad-spectrum probe for retaining glycosidases with diverse substrate specificities. However, a diverse panel of GH probes has been developed to target α- and β-glycosidases with diverse substrate specificities and allowing for targeting both retaining exo- and endo-glycosidases.[28, 29] These probes have been instrumental in detecting GHs enzymes in human cells/tissues[30, 31] plants[32] and microbes[9, 33-37]

In this study, we set out to identify active GHs in *S. aureus* using ABPP. Initially screened a panel of fluorescent glycosidase ABPs to detect active GHs in *S. aureus* under diverse growth conditions. We continued to use a combination of 3 pooled biotinylated probes for target enrichment and identification by mass spectrometry. We report the identification of two previously uncharacterized enzymes the putative 6-phospho-β-glucosidase (BglA) and the α-amylase family protein trehalase C (TreC). The functional relevance of these enzymes was investigated during *in vitro* growth in rich media and in an *in vivo* infection of *Galleria mellonella* larveae using CRISPRi knock-downs strains. In conclusion our data support a role of TreC, but not BglA, in bacterial virulence during *G. mellonella* infection.

Materials and Methods

Bacterial strains and culture conditions

This study utilized *S. aureus* strains USA300 LAC, USA300 JE2, and their respective isogenic mutants, as summarized in Table **1**. All strains were cultured routinely on Tryptic Soy Agar (TSA), Blood Agar or BHI agar or TSA supplemented with 100 mM $MgCl_2$ (TSAMg), or in Difco Tryptic Soy Broth (TSB). Incubation of all bacterial strains was carried out at 37°C, and liquid cultures were aerated by shaking at 180 rpm unless specified otherwise.

Labeling with fluorescent activity-based probes

Bacterial cultures grown overnight on agar plates or in liquid culture were adjusted to the desired cell density in TSB and transferred to microtubes, with a final volume of 50-100 µL. Glycosidase ABPs were then added (from 100x stock solutions in DMSO) to a final concentration 1 µM and the cells were incubated for an additional 60 min at 37°C and 300 rpm. Following probe labeling, bacterial suspensions were transferred to 2 mL screw-cap tubes containing 30-50 µL of 4x SDS-Loading buffer (40% glycerol, 240mM Tris/HCl at pH 6.8, 8% SDS, 0.04% bromophenol blue, and 5% β-mercaptoethanol) and approximately 60-100 µL of 0.1 mm glass beads, and the bacteria were lysed by bead-beating.

SDS-PAGE analysis of fluorescently labeled proteins

Upon addition of the 4x SDS sample buffer, the probe-labeled bacterial lysates were boiled at 95 °C for 10 min and separated by SDS-PAGE gel. The resulting gels were scanned for fluorescence in the Cy5 (635nm) and Cy2 (488nm) channel, utilizing the Amersham™ Typhoon™ 5 (cytiva) imaging system.

Labeling with biotinylated probes and sample preparation for mass-spectrometry

S. aureus USA300 JE2 cultures were cultivated on TSAMg plates for 24 hours and resuspended to an approximate OD600 of 20 in 3 mL of TSB. For each biological replicate, 1 mL aliquots were transferred to 1.5 mL tubes, and either a biotin-tagged ABP (2 µM) or DMSO as control was added. The cells were incubated for 60 minutes at 37°C and 700 rpm before samples were centrifuged at 4,500 ×g for 5 min at 4°C, and the supernatant was removed. The cell pellets were resuspended in 1.2 mL of RIPA Lysis buffer (50 mM Tris, 150 mM NaCl, 0.1% SDS, 0.5% sodium deoxycholate,

1% Triton X-100) and lysed by bead-beating. Samples were centrifuged for 5 min at 10,000 ×g at 4°C, and the protein concentration in the supernatant was adjusted to 1.0 mg/mL. Proteins were subsequently stored at -20°C until sample preparation.

For each sample, 50 µL of streptavidin magnetic beads (Thermo fisher, 88817) were washed twice with 1 mL of RIPA lysis buffer, and the beads were then incubated with 1 mg of protein from each sample in an additional 500 µL of RIPA lysis buffer at 4°C overnight on a rotator with an 18 RPM speed. After enrichment, the beads were pelleted using a magnetic rack, and washed twice with RIPA lysis buffer (1 mL, 2 min at room temperature), once with 1 M KCl (1 mL, 2 min at room temperature), once with 0.1 M Na_2CO_3 (1 mL, ~10 seconds), once with 2 M urea in 10 mM Tris-HCl (pH 8.0) (1 mL, ~10 seconds), and twice with RIPA lysis buffer (1 mL per wash, 2 minutes at room temperature). After the final wash, the beads were transferred to fresh protein Lo-Bind tubes with 1 mL of RIPA lysis buffer. The beads were then washed three times with 500 µL of 4M urea in 50 mM ammonium bicarbonate (Ambic) with shaking for 7 min each time to remove non-specifically enriched proteins. Finally, the beads were washed three times with 500 µL of 50 mM Ambic with shaking for 7 min, changing the tube between these washes.

For on-bead digestion, 150 µL of 50 mM Ambic, 3 µL of 1 mM $CaCl_2$, 0.75 µL of 1 M dithiothreitol (DTT), 4.5 µL of 500 mM iodoacetamide (IAA), and 6 µL of MS-grade trypsin solution were added to the protein Lo-Bind tube. The samples were incubated at 37°C overnight on a shaker at 800 rpm. After overnight incubation, samples were spun down, and the supernatant containing the tryptic digests was collected, and the remaining beads were washed with 70 µL of 50 mM Ambic. For each sample, 20 µL of formic acid were added to the combined eluates, and the samples were then stored at a temperature of -20°C until their analysis via LC-MS/MS.

Liquid chromatography–mass spectrometry analysis

Varian's OMIX C18 tips were used for sample cleanup and concentration. Peptide mixtures containing 0.1% formic acid were loaded onto a Thermo Fisher Scientific EASY-nLC1200 system equipped with a C18 column (2 µm, 100 Å, 50µm, 50 cm) and subjected to fractionation using a 5-80% acetonitrile gradient in 0.1% formic acid at a flow rate of 300 nL/min for 60 minutes. The separated peptides were analyzed on a Thermo Scientific Orbitrap Exploris 480 instrument, employing a data-dependent mode with a Top20 method. Raw data was processed using Proteome Discoverer 2.5 software, and fragmentation spectra were searched against the *S. aureus* 300 LAC

database. The search employed peptide mass tolerances of 10 ppm and a fragment mass tolerance of 0.02 Da. A false discovery rate (FDR) of 5% was applied for peptide identification. To ensure accuracy, the filter criterion of two unique peptides was used, and three replicates were performed for each sample. Protein abundance obtained from Proteome Discoverer was averaged across replicates, and the ratio of the ABPP-enriched sample versus mock-treated control sample was calculated. Proteins enriched more than 1.5-fold by the biotinylated probe were selected. While performing ABPP-enriched and other pull-down experiments, enrichment of nonspecific binding is a limitation[38, 39]. To minimize false positives, any ribosomal proteins, proteins with known affinity for hydrophilic beads, as well as endogenously biotinylated proteins (e.g., carboxylase family proteins) that interact with streptavidin-beads regardless of ABP-labeling, were excluded from the dataset. The mass spectrometry proteomics data have been deposited to the ProteomeXchange Consortium via the PRIDE[40] partner repository with the dataset identifier PXD052286.

Construction of *S. aureus* CRISPRi strains

The CRISPRi system in *S. aureus* includes two plasmids. One plasmid harbors the dCas9 under the control of an IPTG-inducible promoter, and a second plasmid continuously expresses the sgRNA[41]. To construct CRISPRi strains in *S. aureus* USA 300 LAC, the bacteria were first equipped with a plasmid carrying dCas9. The sgRNA plasmids were then created/engineered into the pVL2336 plasmid using oligonucleotides that contain the sgRNA sequence. The pVL2336 plasmid is designed to facilitate the insertion of gene-specific sgRNAs through Golden Gate cloning using the *Bsm*BI restriction enzyme. The sgRNA oligonucleotides are composed of a 20-nucleotide (nt) sequence that pairs with the non-template DNA strand of the target gene near the 5' end and adjacent to a PAM (Protospacer Adjacent Motif) sequence. These oligonucleotides also include a 4-base pair (bp) overhang that matches the overhang region generated by *Bsm*BI digestion. The resulting sgRNA plasmids then allow for the expression of sgRNAs that consist of a 20 bp gene-specific sequence, the Cas9 handle, and a transcriptional terminator under the control of a constitutive promoter. The plasmid pVL2336 was digested using restriction enzyme *Bsm*BI and then ligated with the chosen sgRNA oligonucleotide using T4 DNA ligase. This assembled plasmid was then transformed into *E. coli* IM08B and, following that, into *S. aureus* LAC. To identify successful transformants, selection was initially carried out using plates containing erythromycin (5 µg/ml) and chloramphenicol (10 µg/ml) antibiotics, followed by verification through PCR and sequencing.

Growth curve

Growth curves were generated using 96-well microtiter plates. Cultures grown overnight were diluted in fresh medium at a 1:100 ratio, and 200 µl of the diluted culture was transferred to each well of the 96-well plate. The plates were then incubated at 37°C, with the optical density at 600 nm (OD600) being recorded every 10 minutes using a Synergy H1 Hybrid Reader (BioTek)) instrument. When necessary, antibiotics erythromycin (5µg/ml) and chloramphenicol (10µg/ml) were used for selection purposes. To induce dCas9 expression, 250 µM IPTG was added.

Infection of *S. aureus* in *G. mellonella* larvae

Larvae of *G. mellonella* were sourced from Reptilutstyr AS (Norway). For the infection experiments, *S. aureus* strains were cultured overnight in TSB, supplemented with the necessary antibiotics and/or IPTG as required. For the depletion of the gene of interest, CRISPRi strains were grown with the addition of 250 µM IPTG. After overnight incubation, the bacterial cultures were washed with PBS and then suspended in PBS to achieve a concentration of 1.0×10^6 CFU/mL. For the infection, 10 µL of this bacterial suspension was injected into the right hind proleg using a 30G syringe microapplicator (0.30 mm (30G) × 8 mm, BD Micro-Fine Demi). A control group of 10 larvae received 10 µL of PBS to verify that mortality was not due to the injection process. The larvae were then placed in 9.2 cm Petri dishes, incubated at 37°C in darkness, and survival was monitored over 48 hours. Each experiment was independently replicated at least three times.

Results

Gel-based activity-based protein profiling using fluorescent glycosidase ABPs

To profile retaining glycosidase activities in *S. aureus* we initially used a panel of fluorescent ABPs developed previously to selectively target α-glucosidases[42] (ABP **1**), β-glucosidases[43] (ABP **2**), α-galactosidases[44] (ABP **3**), β-galactosidases[45] (ABP **4**), α-fucosidases[46, 47] (ABP **5**), β-glucuronidases[31] (ABP **6**), and α-iduronidases[48] (ABP **7**), the structures of which are shown in Scheme **1**.

As a bacterial model strain, we used JE2, which is a derivative of the clinically-relevant methicillin-resistant MRSA lineage USA300 and for which availability of a transposon mutant library[49] facilitates target validation. Initially, we applied this set of probes to profile active enzymes during liquid culture in TSB. After labeling of live cells, samples were fractionated to separate cell culture supernatant including secreted proteins and the cell pellet, which was lysed prior to SDS-PAGE and in-gel fluorescence scanning. The only probe that labelled a band in the culture supernatant was ABP **1**-Cy5, revealing a putative α-glucosidase with a size of approx. 60-70 kDa (Fig. 1A). The same probe also labelled a target protein in the cell pellet (Fig. 1A). In the cell pellet, two additional bands of a size <102 kDa and <52 kDa were labelled indiscriminately by all seven fluorescent probes.

We continued to profile retaining glycosidase activity to growth of live cells on agar, where we tested, diverse solid media including tryptic soy agar (TSA), TSAMg, which promotes biofilm formation[50], as well as Brain-Heart-Infusion and Blood Agar, which both contain host-tissue derived factors that might include physiologically more relevant substrates for glycosidases. In general, we observed that the activity profiles revealed by the various probes were rather similar across the different growth media. Under all conditions, the band at 60-70 kDa labelled by ABP **1** was the most prominent band (Fig. 1B, C). However, upon growth on agar, ABPs **2**, **4** and **5** labelled a variety of additional unique bands with a diverse size from approx. 24 to >102 kDa (Fig. 1B, C). Labeling of probes **1**, **4** and **5** was dose-dependent, and a concentration of 1 μM was necessary for robust labeling (Fig. 1D).

To determine whether the labeling profiles by ABPs **1**, **4** and **5** (on TSAMg) resulted from specific binding to the active site, we examined the effect of pre-incubation with unlabeled parent inhibitors

(Chris021, TB562 and JJB330) in a competitive ABPP setup (Fig. 2B). Pre-incubation with Chris021 (1–10 μM) resulted in reduced labeling of the most pronounced bands at >55 kDa, suggesting that Chris021 competes with ABP **1**. In contrast, pre-incubation with TB562 and JJB330 did not alter the labeling patterns for ABP **4** and **5**, respectively, up to a concentration of 10 μM. This outcome could be indicative of a non-specific labeling mechanism of ABP **4** and **5**, but it might also be explained by limited potency of the inhibitor potentially requiring a much higher excess of the unlabelled inhibitor.

Target Identification by chemoproteomics

To identify putative enzymatic targets of ABPs **1**, **4** and **5** we used biotinylated analogs of these probes for mass-spectrometry based ABPP. In analogy to previous studies[20, 21] bacteria were cultivated on TSAMg, where the fluorescent analogs of these probes gave robust, differential labeling profiles (Fig. 1B). Cells were labelled with a pool of the biotinylated probes **1**, **4** and **5** or treated with vehicle (DMSO) as a control, cells were lysed, and labelled proteins were enriched using a streptavidin resin. Enriched, trypsinized samples were then subjected to analysis by Liquid Chromatography-Tandem Mass Spectrometry (LC-MS/MS).

10 proteins were significantly enriched in the biotin-ABP-pool treated samples compared to the vehicle-treated control dataset (p-value < 0.05, enrichment > 1.5-fold) (Table **2** and Supporting Dataset **1**, data are available from ProteomeXchange with identifier PXD052286). Three of these proteins were are annotated as putative GH family proteins: 6-phospho-β-glucosidase (BglA), the α-amylase family protein trehalase C (TreC) and autolysin (Atl).

Gel-based target validation

To confirm whether these putative GHs are specific targets of one of these probes, we determined the labeling profile of the fluorescent probes in transposon mutants with insertions in either of these genes. No obvious changes in the labeling patterns of either of the fluorescent ABPs **1**, **4** or **5** were seen for the *bgl*A-mutant. A faint band that matches the molecular weight of autolysin (137 kDa) and a 51 kD fragment that may correspond to its cleaved glucosaminidase domain[10] was detected by ABP **1** and more weakly by ABP **4** in WT cells. These bands were absent in the *atl*-deficient transposon mutant (Fig. 3A, B). For the *tre*C-mutant, we observed that the 60-70 kDa band labeled by ABP **1**, which matches the predicted molecular weight of TreC (63.5 kDa), was reduced in intensity, but it was not absent (Fig. 3A, B). We hypothesized that this outcome might be explained

by three different scenarios: 1. TreC may be overlapping with another protein of similar size. 2. The band does not correspond to TreC and the reduced band intensity is caused by secondary effects due to the inactivation of TreC. 3. The band corresponds to TreC, but compensatory upregulation of another glycosidase of similar weight in the *treC* mutant may confound the analysis. Since the latter two explanations would be connected to limitations of the validation in mutant strains, we sought an alternative way of validation and developed IPTG-inducible CRISPRi interference strains in the MRSA strain USA300 LAC, allowing for conditional knock-down of the *tre*C, *bgl*A and *atl* genes, respectively. In stationary phase on TSB, the cell-associated band of 60-70 kDa was reduced after silencing of the *tre*C and *bgl*A genes, whereas the corresponding band in the supernatant was absent after silencing of *tre*C. These results suggest that TreC is the molecular target of ABP **1** in the stationary phase culture supernatant, whereas the cell-associated band might be comprised of TreC in combination with BglA and/or putatively other unidentified targets.

Functional validation of the glycosidase hydrolases

Finally, we aimed to determine whether the newly identified glycosidases TreC and BglA are relevant for bacterial growth or virulence. First, we compared the growth of CRISPRi-strains in TSB with or without the presence of IPTG to induce silencing of target genes. Regardless of the presence of inducer, constructs targeting *bgl*A, *tre*C or *atl* all showed similar growth curves, suggesting that silencing of these genes does not affect *in vitro* growth in TSB (Fig. 4 A,B). Subsequently, we used a *Galleria mellonella* infection model to test whether these enzymes contribute to the virulence of *S. aureus*. We treated the corresponding CRISPRi strains with IPTG *in vitro* to silence *tre*C or *bgl*A, respectively, before infecting *G. mellonella* larvae and compared the resulting mortality of the larvae with that achieved after infection with non-IPTG-induced control and WT *S. aureu*s cells. Upon infection with 10^6 CFU of wild-type (WT) *S. aureus*, all larvae died within 24 hours (Fig. 4C). Larvae infected with the uninduced CRISPRi constructs for *bgl*A and *tre*C were killed more slowly indicating that carriage of the CRISPRi plasmids infers a fitness cost in this infection model. Of note larvae that were infected with *tre*C-silenced, but not *bgl*A-silenced *S. aureus*, led to a significantly higher larval survival rate with approximately 40% of the larvae remaining alive even after 48 hours ($p < 0.001$). These data establish a role for the previously uncharacterized α-amylase family protein TreC in the virulence of *S. aureus*.

Discussion

Here, we present the first ABPP study on identification of retaining glycosidases in a bacterial pathogen. Since glycosidases have a high degree of substrate selectivity and no broad-spectrum probe is available, we first profiled a set of 7 different glycosidase-reactive ABPs by gel-based ABPP and then used biotinylated analogs of the most promising probe candidates in probe cocktail-based strategy[51] for MS-based target identification. Using a cocktail of probes with selectivity for α-glucosidases (ABP **1**), β-galactosidases (ABP **4**) and α-fucosidases (ABP **5**) we identified three putative glycosidases; the putative α-amylase family protein phosphotrehalase (TreC), 6-phospho-β-glucosidase (BglA), and the previously characterized autolysin (Atl).[11-13] The annotation of these enzymes in combination with experimental validation using transposon mutants and CRISPRi mutant suggest that these targets have been enriched predominantly by the cyclophellitol-aziridine probe ABP **1**. For the β-galactosidase probe ABP **4** and the α-fucosidase probe ABP **5**, we conclude that the gel-based labeling patterns are most likely non-specific (with exception of the faint bands that presumably correspond to Atl labelled by ABP **4**). This notion is supported by competitive ABPP with unlabeled inhibitors that did not give evidence for a specific active site-directed binding that would lead to competition with the probe.

In gel-based ABPP experiment with a *tre*C-silencing CRISPRi stain, we confirmed TreC as a target of ABP**1** and found the protein both secreted in the culture supernatant and in the cell-associated fraction. Identification of this enzyme with ABP **1** is not surprising, since the probe is based on an α-configurated cyclophellitiol aziridine inhibitor known to target retaining α-glucosidases [42]. Of note, *S. aureus* also harbors a 58 kDa α-amylase[52]. This enzyme was not enriched in the MS-dataset, which we hypothesize could be due to a lack of expression under the conditions tested. Since the parent inhibitor cyclophellitol is also known to interact with beta-glycosidases (although with lower affinity[42]), it seems plausible that the β-glucosidase BglA and β-glucosaminidase Atl have been enriched through ABP **1**. BglA is 10 kD smaller than TreC, but apparently runs at the same height in the SDS-PAGE. This might be due to post-translational modification of BglA resulting in increased size, but this remains to be established. Still, such a difference in expected size in SDS-PAGE was previously observed in an ABPP study on serine hydrolases.[20] Heterologous expression of these enzymes will be necessary to unambiguously address the question of the reactivity of the

alpha-cyclophellitol aziridine-ABP **1** to this enzyme, and a biochemical characterization of both BglA and TreC is necessary to assess whether their current functional annotation is correct.

Besides the three putative glycosidases discussed above, our MS-based ABPP dataset also included 7 additional proteins that were enriched after treatment with the probe cocktail. Some of these proteins are hydrolytic enzymes (phosphate acyltransferase and phosphate acetyltransferase) which might have active site residues reactive to the aziridine electrophile, whereas others seem to have an affinity for sugars (pectate lyase, fructose-1,6,bisphosphatase and the sugar phosphotransferase system *mur*P). The molecular basis for these interactions remains to be determined.

Functional validation of the newly identified enzymes using CRISPRi gene silencing revealed that TreC, but not BglA, contributes to bacterial virulence in a *Galleria mellonella* model, whereas silencing of neither gene affected growth in TSB. Since the application of IPTG in the wax moth larvae *in vivo* is challenging, dCas9 expression was already induced (and *tre*C knocked down) during the pre-culture period before infection. Thus, bacteria may overcome this knock-down through *de novo* expression of *tre*C, during the 48h experiment, suggesting TreC is functionally important early in the infection process. The physiological relevance of TreC and BglA under other conditions, e.g. during biofilm formation and in other infection models remains to be determined.

Bioinformatics analysis indicates that *tre*C encodes an alpha-amylase that belongs to GH13, the largest family of glycoside hydrolases according to CAZy data[53]. The biochemical activity and physiological substrates of this enzyme will be addressed in future studies.

Of note, we performed the chemoproteomic profiling in this study under simplistic *in vitro* conditions in which probably not all infection-relevant glycosidase enzymes are expressed. Similar profiling studies performed in more complex models for infection, host-interaction and microbe-microbe interactions may identify additional relevant, uncharacterized enzymes that could act on substrates derived from host factors or microbial competitors.

Acknowledgements

The study was funded by a Centre for New Antibacterial Strategies (CANS) starting-grant through the Trond-Mohn Foundation to C.S.L. LC-MS/MS analyses were carried out at the UiT Proteomics and Metabolomics Core Facility (PRiME). The PRiME is part of the National Network of Advanced Proteomics Infrastructure (NAPI), funded by the Research Council of Norway INFRASTRUKTUR-program (project number: 295910). We thank Roni Miah for help with CRISPRi strain construction. We also thank Morten Kjos for kindly providing us the pVL2336 plasmid and *E.coli* IM08B strain.

Keywords: chemoproteomics · activity-based probe · biofilm· virulence

Author contributions

Conceptualization: C.S.L., M.J.U. Investigation: M.J.U., Data analysis: All authors, Supervision: C.S.L. and M. J., Funding acquisition: C.S.L., Writing – original draft: M.J.U., Writing – Editing: All author

References

[1] P. Piewngam, M. Otto *Lancet Microbe*. **2024**.
[2] T. Jin, M. Mohammad, R. Pullerits, A. Ali *Pathogens*. **2021**, *10*.
[3] V. Thammavongsa, H. K. Kim, D. Missiakas, O. Schneewind *Nat Rev Microbiol*. **2015**, *13*, 529-543.
[4] S. Y. Tong, J. S. Davis, E. Eichenberger, T. L. Holland, V. G. Fowler, Jr. *Clin Microbiol Rev*. **2015**, *28*, 603-661.
[5] N. I. Samia, A. Robicsek, H. Heesterbeek, L. R. Peterson *Scientific Reports*. **2022**, *12*, 17007.
[6] M. Shoaib, A. I. Aqib, I. Muzammil, N. Majeed, Z. A. Bhutta, M. F. Kulyar, M. Fatima, C. F. Zaheer, A. Muneer, M. Murtaza, M. Kashif, F. Shafqat, W. Pu *Front Microbiol*. **2022**, *13*, 1067284.
[7] N. Kaur, V. Kumar, S. K. Nayak, P. Wadhwa, P. Kaur, S. K. Sahu *Chem Biol Drug Des*. **2021**, *98*, 539-560.
[8] H. Martin, L. R. Lázaro, T. Gunnlaugsson, E. M. Scanlan *Chem Soc Rev*. **2022**, *51*, 9694-9716.
[9] P. B. Jariwala, S. J. Pellock, D. Goldfarb, E. W. Cloer, M. Artola, J. B. Simpson, A. P. Bhatt, W. G. Walton, L. R. Roberts, M. B. Major, G. J. Davies, H. S. Overkleeft, M. R. Redinbo *ACS Chem Biol*. **2020**, *15*, 217-225.
[10] T. Oshida, M. Sugai, H. Komatsuzawa, Y. M. Hong, H. Suginaka, A. Tomasz *Proc Natl Acad Sci U S A*. **1995**, *92*, 285-289.
[11] P. Houston, S. E. Rowe, C. Pozzi, E. M. Waters, J. P. O'Gara *Infect Immun*. **2011**, *79*, 1153-1165.
[12] E. J. Culp, N. Waglechner, W. Wang, A. A. Fiebig-Comyn, Y. P. Hsu, K. Koteva, D. Sychantha, B. K. Coombes, M. S. Van Nieuwenhze, Y. V. Brun, G. D. Wright *Nature*. **2020**, *578*, 582-587.
[13] A. C. Leonard, M. I. Goncheva, S. E. Gilbert, H. Shareefdeen, L. E. Petrie, L. K. Thompson, C. M. Khursigara, D. E. Heinrichs, G. Cox *Proc Natl Acad Sci U S A*. **2023**, *120*, e2301414120.
[14] V. Winstel, P. Kühner, F. Salomon, J. Larsen, R. Skov, W. Hoffmann, A. Peschel, C. Weidenmaier *mBio*. **2015**, *6*, 10.1128/mbio.00632-00615.
[15] A. Hendriks, R. van Dalen, S. Ali, D. Gerlach, G. A. van der Marel, F. F. Fuchsberger, P. C. Aerts, C. J. C. de Haas, A. Peschel, C. Rademacher, J. A. G. van Strijp, J. D. C. Codée, N. M. van Sorge *ACS Infectious Diseases*. **2021**, *7*, 624-635.
[16] M. Hort, U. Bertsche, S. Nozinovic, A. Dietrich, A. S. Schrötter, L. Mildenberger, K. Axtmann, A. Berscheid, G. Bierbaum *Microbiol Spectr*. **2021**, *9*, e0052821.
[17] L. V. Hooper, J. I. Gordon *Science*. **2001**, *292*, 1115-1118.
[18] J. Sjögren, M. Collin *Future Microbiol*. **2014**, *9*, 1039-1051.
[19] Y. Kim, J. Y. Ko, W. H. Yang *BMB Rep*. **2021**, *54*, 541-544.
[20] C. S. Lentz, J. R. Sheldon, L. A. Crawford, R. Cooper, M. Garland, M. R. Amieva, E. Weerapana, E. P. Skaar, M. Bogyo *Nat Chem Biol*. **2018**, *14*, 609-617.
[21] M. J. Uddin, H. S. Overkleeft, C. S. Lentz *ChemBioChem*. **2023**, *24*, e202300473.
[22] M. Fellner, A. Walsh, S. Dela Ahator, N. Aftab, B. Sutherland, E. W. Tan, A. T. Bakker, N. I. Martin, M. van der Stelt, C. S. Lentz *ACS Infectious Diseases*. **2023**, *9*, 2119-2132.
[23] V. Notenboom, C. Birsan, M. Nitz, D. R. Rose, R. A. Warren, S. G. Withers *Nat Struct Biol*. **1998**, *5*, 812-818.
[24] K. Y. Li, J. Jiang, M. D. Witte, W. W. Kallemeijn, W. E. Donker-Koopman, R. G. Boot, J. M. Aerts, J. D. Codée, G. A. van der Marel, H. S. Overkleeft *Org Biomol Chem*. **2014**, *12*, 7786-7791.
[25] T. M. Gloster, R. Madsen, G. J. Davies *Organic & Biomolecular Chemistry*. **2007**, *5*, 444-446.
[26] L. I. Willems, J. Jiang, K.-Y. Li, M. D. Witte, W. W. Kallemeijn, T. J. N. Beenakker, S. P. Schröder, J. M. F. G. Aerts, G. A. van der Marel, J. D. C. Codée, H. S. Overkleeft *Chemistry – A European Journal*. **2014**, *20*, 10864-10872.
[27] G. Davies, B. Henrissat *Structure*. **1995**, *3*, 853-859.
[28] L. Wu, Z. Armstrong, S. P. Schröder, C. de Boer, M. Artola, J. M. F. G. Aerts, H. S. Overkleeft, G. J. Davies *Current Opinion in Chemical Biology*. **2019**, *53*, 25-36.

[29] S. P. Schröder, J. W. van de Sande, W. W. Kallemeijn, C.-L. Kuo, M. Artola, E. J. van Rooden, J. Jiang, T. J. M. Beenakker, B. I. Florea, W. A. Offen, G. J. Davies, A. J. Minnaard, J. M. F. G. Aerts, J. D. C. Codée, G. A. van der Marel, H. S. Overkleeft *Chemical Communications*. **2017**, *53*, 12528-12531.
[30] L. I. Willems, T. J. Beenakker, B. Murray, S. Scheij, W. W. Kallemeijn, R. G. Boot, M. Verhoek, W. E. Donker-Koopman, M. J. Ferraz, E. R. van Rijssel, B. I. Florea, J. D. Codée, G. A. van der Marel, J. M. Aerts, H. S. Overkleeft *J Am Chem Soc*. **2014**, *136*, 11622-11625.
[31] L. Wu, J. Jiang, Y. Jin, W. W. Kallemeijn, C. L. Kuo, M. Artola, W. Dai, C. van Elk, M. van Eijk, G. A. van der Marel, J. D. C. Codée, B. I. Florea, J. Aerts, H. S. Overkleeft, G. J. Davies *Nat Chem Biol*. **2017**, *13*, 867-873.
[32] A. M. Husaini, K. Morimoto, B. Chandrasekar, S. Kelly, F. Kaschani, D. Palmero, J. Jiang, M. Kaiser, O. Ahrazem, H. S. Overkleeft, R. A. L. van der Hoorn *Plant Physiol*. **2018**, *177*, 24-37.
[33] J. B. Simpson, J. J. Sekela, A. L. Graboski, V. B. Borlandelli, M. M. Bivins, N. K. Barker, A. A. Sorgen, A. L. Mordant, R. L. Johnson, A. P. Bhatt, A. A. Fodor, L. E. Herring, H. Overkleeft, J. R. Lee, M. R. Redinbo *Gut Microbes*. **2022**, *14*, 2107289.
[34] C. Schmerling, L. Sewald, G. Heilmann, F. Witfeld, D. Begerow, K. Jensen, C. Bräsen, F. Kaschani, H. S. Overkleeft, B. Siebers, M. Kaiser *Commun Biol*. **2022**, *5*, 1254.
[35] N. G. S. McGregor, C. de Boer, Q. P. O. Foucart, T. Beenakker, W. A. Offen, J. D. C. Codée, L. I. Willems, H. S. Overkleeft, G. J. Davies *ACS Cent Sci*. **2023**, *9*, 2306-2314.
[36] N. J. Reichart, A. K. Steiger, E. M. Van Fossen, R. McClure, H. S. Overkleeft, A. T. Wright *ISME Commun*. **2023**, *3*, 106.
[37] T. Klaus, S. Ninck, A. Albersmeier, T. Busche, D. Wibberg, J. Jiang, A. G. Elcheninov, K. S. Zayulina, F. Kaschani, C. Bräsen, H. S. Overkleeft, J. Kalinowski, I. V. Kublanov, M. Kaiser, B. Siebers *Front Microbiol*. **2021**, *12*, 734039.
[38] S. Wang, Y. Tian, M. Wang, M. Wang, G.-b. Sun, X.-b. Sun *Frontiers in Pharmacology*. **2018**, *9*.
[39] S. E. Tully, B. F. Cravatt *Journal of the American Chemical Society*. **2010**, *132*, 3264-3265.
[40] Y. Perez-Riverol, J. Bai, C. Bandla, D. García-Seisdedos, S. Hewapathirana, S. Kamatchinathan, D. J. Kundu, A. Prakash, A. Frericks-Zipper, M. Eisenacher *Nucleic acids research*. **2022**, *50*, D543-D552.
[41] G. A. Stamsås, I. S. Myrbråten, D. Straume, Z. Salehian, J.-W. Veening, L. S. Håvarstein, M. Kjos *Molecular Microbiology*. **2018**, *109*, 615-632.
[42] J. Jiang, C.-L. Kuo, L. Wu, C. Franke, W. W. Kallemeijn, B. I. Florea, E. van Meel, G. A. van der Marel, J. D. C. Codée, R. G. Boot, G. J. Davies, H. S. Overkleeft, J. M. F. G. Aerts *ACS Cent Sci*. **2016**, *2*, 351-358.
[43] M. Artola, C. L. Kuo, L. T. Lelieveld, R. J. Rowland, G. A. van der Marel, J. D. C. Codée, R. G. Boot, G. J. Davies, J. Aerts, H. S. Overkleeft *J Am Chem Soc*. **2019**, *141*, 4214-4218.
[44] K. Kytidou, J. Beekwilder, M. Artola, E. van Meel, R. H. P. Wilbers, G. F. Moolenaar, N. Goosen, M. J. Ferraz, R. Katzy, P. Voskamp, B. I. Florea, C. H. Hokke, H. S. Overkleeft, A. Schots, D. Bosch, N. Pannu, J. Aerts *J Biol Chem*. **2018**, *293*, 10042-10058.
[45] L. I. Willems, T. J. M. Beenakker, B. Murray, B. Gagestein, H. van den Elst, E. R. van Rijssel, J. D. C. Codée, W. W. Kallemeijn, J. M. F. G. Aerts, G. A. van der Marel, H. S. Overkleeft *European Journal of Organic Chemistry*. **2014**, *2014*, 6044-6056.
[46] J. Jiang, T. J. M. Beenakker, W. W. Kallemeijn, G. A. van der Marel, H. van den Elst, J. D. C. Codée, J. M. F. G. Aerts, H. S. Overkleeft *Chemistry – A European Journal*. **2015**, *21*, 10861-10869.
[47] J. Jiang, W. W. Kallemeijn, D. W. Wright, A. van den Nieuwendijk, V. C. Rohde, E. C. Folch, H. van den Elst, B. I. Florea, S. Scheij, W. E. Donker-Koopman, M. Verhoek, N. Li, M. Schürmann, D. Mink, R. G. Boot, J. D. C. Codée, G. A. van der Marel, G. J. Davies, J. Aerts, H. S. Overkleeft *Chem Sci*. **2015**, *6*, 2782-false.
[48] M. Artola, C.-L. Kuo, S. A. McMahon, V. Oehler, T. Hansen, M. van der Lienden, X. He, H. van den Elst, B. I. Florea, A. R. Kermode, G. A. van der Marel, T. M. Gloster, J. D. C. Codée, H. S. Overkleeft, J. M. F. G. Aerts *Chemistry – A European Journal*. **2018**, *24*, 19081-19088.

[49] P. D. Fey, J. L. Endres, V. K. Yajjala, T. J. Widhelm, R. J. Boissy, J. L. Bose, K. W. Bayles *mBio*. **2013**, *4*, e00537-00512.
[50] G. Koch, A. Yepes, K. U. Förstner, C. Wermser, S. T. Stengel, J. Modamio, K. Ohlsen, K. R. Foster, D. Lopez *Cell*. **2014**, *158*, 1060-1071.
[51] S. A. Sieber, S. Niessen, H. S. Hoover, B. F. Cravatt *Nat Chem Biol*. **2006**, *2*, 274-281.
[52] H. P. Lakshmi, U. V. Prasad, S. Yeswanth, V. Swarupa, O. H. Prasad, M. L. Narasu, P. V. Sarma *Bioinformation*. **2013**, *9*, 281-285.
[53] M. R. Stam, E. G. J. Danchin, C. Rancurel, P. M. Coutinho, B. Henrissat *Protein Engineering, Design and Selection*. **2006**, *19*, 555-562.
[54] B. Arsic, Y. Zhu, D. E. Heinrichs, M. J. McGavin *PLOS ONE*. **2012**, *7*, e45952.

Table **1.** Bacterial strains used in this study

Strain	Description	Reference/Source
S.aureus USA300 LAC	Wild-type USA300 Los Angeles County (LAC) clone; multilocus sequence type 8, SCCmec type IV cured of antibiotic resistance plasmid	[54]
sgRNA *(atl)*	USA300 LAC carrying pLOW-P*lac*-d*cas*9, pVL2336-sgRNA(*atl*), Ery^R , cm^R	This study
sgRNA *(bglA)*	USA300 LAC carrying pLOW-P*lac*-d*cas*9, pVL2336-sgRNA(*bglA*), Ery^R , cm^R	This study
sgRNA *(treC)*	USA300 LAC carrying pLOW-P*lac*-d*cas*9, pVL2336-sgRNA(*treC*), Ery^R , cm^R	This study
S.aureus USA300 JE2	A plasmid-cured derivative of USA300 LAC and Parent strain of Nebraska Transposon Mutant Library	[49]
JE2_*atl*: Tn	Transposon insertion mutant in JE2 SAUSA300_0955 (*atl*); Ery^R , $Linc^R$	[49]
JE2_*bglA*: Tn	Transposon insertion mutant in JE2 SAUSA300_0260 (*bglA*); Ery^R , $Linc^R$	[49]
JE2_*treC*: Tn	Transposon insertion mutant in JE2 SAUSA300_0449 (*treC*); Ery^R , $Linc^R$	[49]

Table 2. LC-MS/MS-based target proteins identifications of glycosidases-biotin probe **1**, **4**, and **5** in *S.aureus* USA300 JE2

Accession number	Protein	Description	Gene name	Unique Peptides	Mol weight [kDa]	Abundance Ratio: (biotin) / (ctrl)	P-Value
WP_000974460.1	OsmC	Organic hydroperoxide resistance protein	*osmC*	2	15,3	3,5	1,97144E-05
WP_000159750.1	MurP	PTS transporter subunit EIIC	*murP*	6	50,6	3,3	0,052059494
QPB86698.1	EutD	Phosphate acetyltransferase	*eutD*	4	34,9	1,8	4,95726E-07
WP_000163988.1	BglA	6-phospho-beta-glucosidase	*bglA*	2	54,7	1,8	1,85817E-07
WP_000275730.1	PfbA	Pectate lyase	*pfbA*	7	40,7	1,7	0,015415869
QPB87272.1	PlsX	Phosphate acyltransferase PlsX	*plsX*	4	35,4	1,5	6,43444E-10
WP_000031515.1	TreC	Alpha,alpha-phosphotrehalase	*treC*	6	63,5	1,5	5,94054E-06
QPB88486.1	GpmA	2,3-diphosphoglycerate-dependent phosphoglycerate mutase	*gpmA*	4	26,7	1,5	4,57359E-05
QPB88582.1	Fbp	Fructose-1,6-bisphosphatase	*fbp*	4	76,1	1,5	1E-17
WP_001074556.1	Atl	Glucosaminidase domain-containing protein	*atl*	29	137,3	1,5	0,022711654

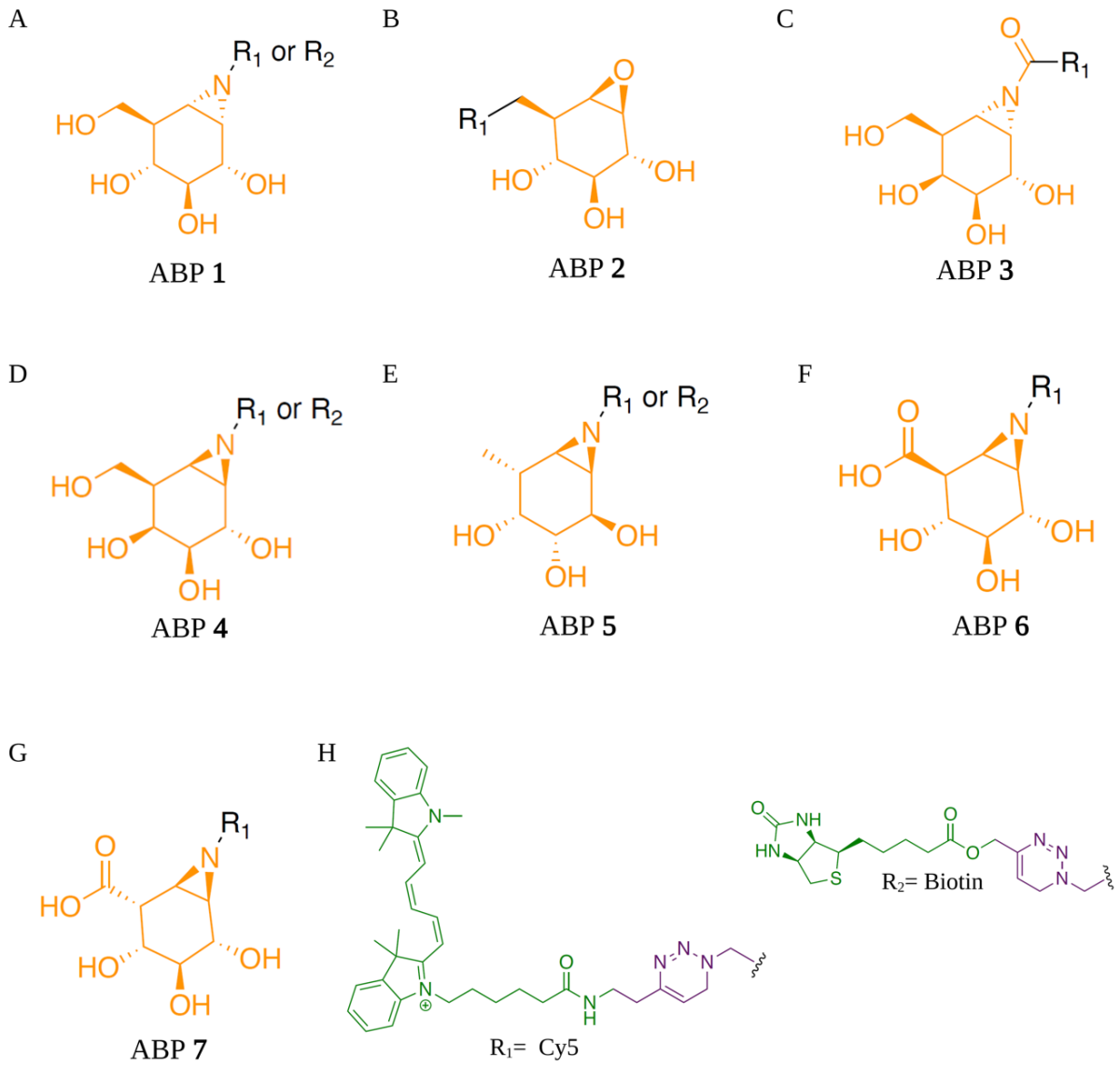

Scheme 1. Chemical structures of glycosidase-targeting activity-based probes used in this study. **A**) ABP **1** (α-glucosidases), **B**) ABP **2** (β-glucosidase), **C**) ABP **3** (α-galactosidase), **D**) ABP **4** (β-galactosidase), **E**) ABP **5** (α-fucosidases), **F**) ABP **6** (β-glucuronidase), **G**) ABP **7** (α-iduronidases), and **H**) equipped with Cy3 (R1) or biotin moieties (R2).

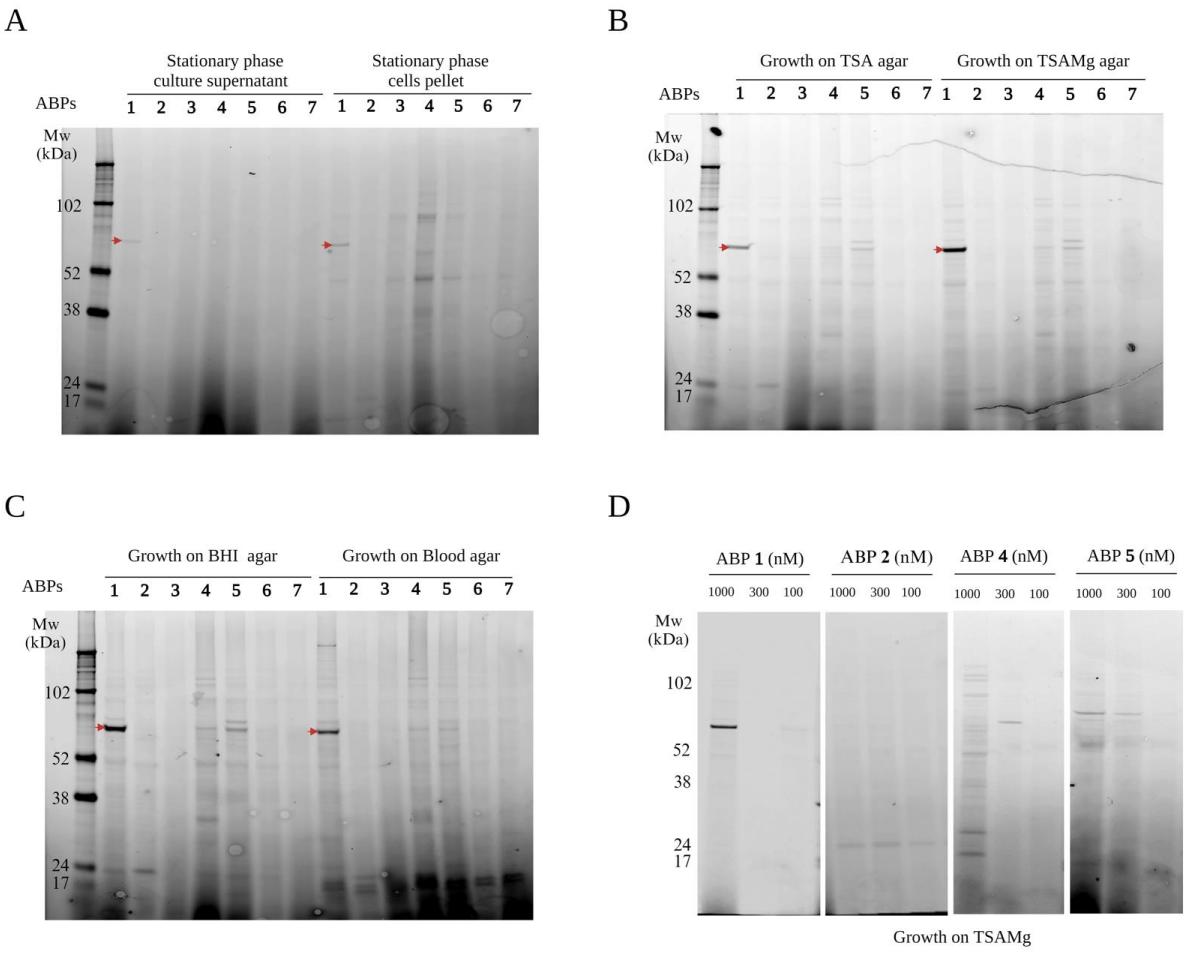

Figure 1. Fluorescent ABP-labeling profiles in *S. aureus* USA300 JE2 using glycosidase ABPs. Live bacteria were subjected to labeling with 1µM of the glycosidase ABPs (1-**7**) for 60 minutes at 37ºC, followed by cell lysis and subsequent SDS-PAGE analysis. The graph illustrates the results with fluorescent scans captured in the Cy5 channel (635nm wavelength) using the Amersham™ Typhoon™ 5 (cytiva) imaging system. **A)** Live cells were grown to stationary phase culture in TSB and fractionated into supernatant (SN) and cell pellet (P). **B**) Live bacteria were labeled after cultivation on TSA or TSAMg. **C**) Labeling profile of *S. aureus* USA300 JE2 live cells, either from grown on BHI agar or Blood agar. Arrowheads indicate the most prominent band labeled by ABP **1** in all conditions. **D**) Dose-dependent labeling profile with ABPs **1**, **4**, and **5**. of *S. aureus* USA300 JE2 cells harvested from TSAMg.

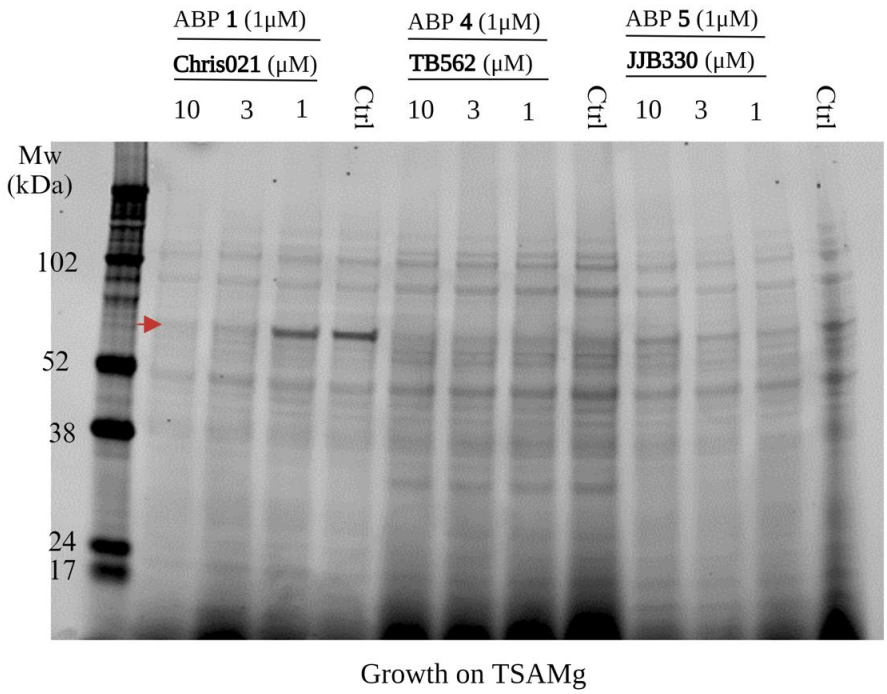

Figure 2. Competitive Activity-Based Protein Profiling (ABPP) in *S. aureus* USA300 JE2. The cells were pre-incubated with non-fluorescent inhibitors related to ABP **1 (Chris021),** ABP **4 (TB562),** and ABP **5 (JJB330)** at the indicated concentrations for 60 min before the addition of ABP **1,** ABP **4,** and ABP **5**. The graph shows fluorescent scans captured in the Cy5 (635nm) channel using the Amersham™ Typhoon™ 5 (cytiva) imaging system.

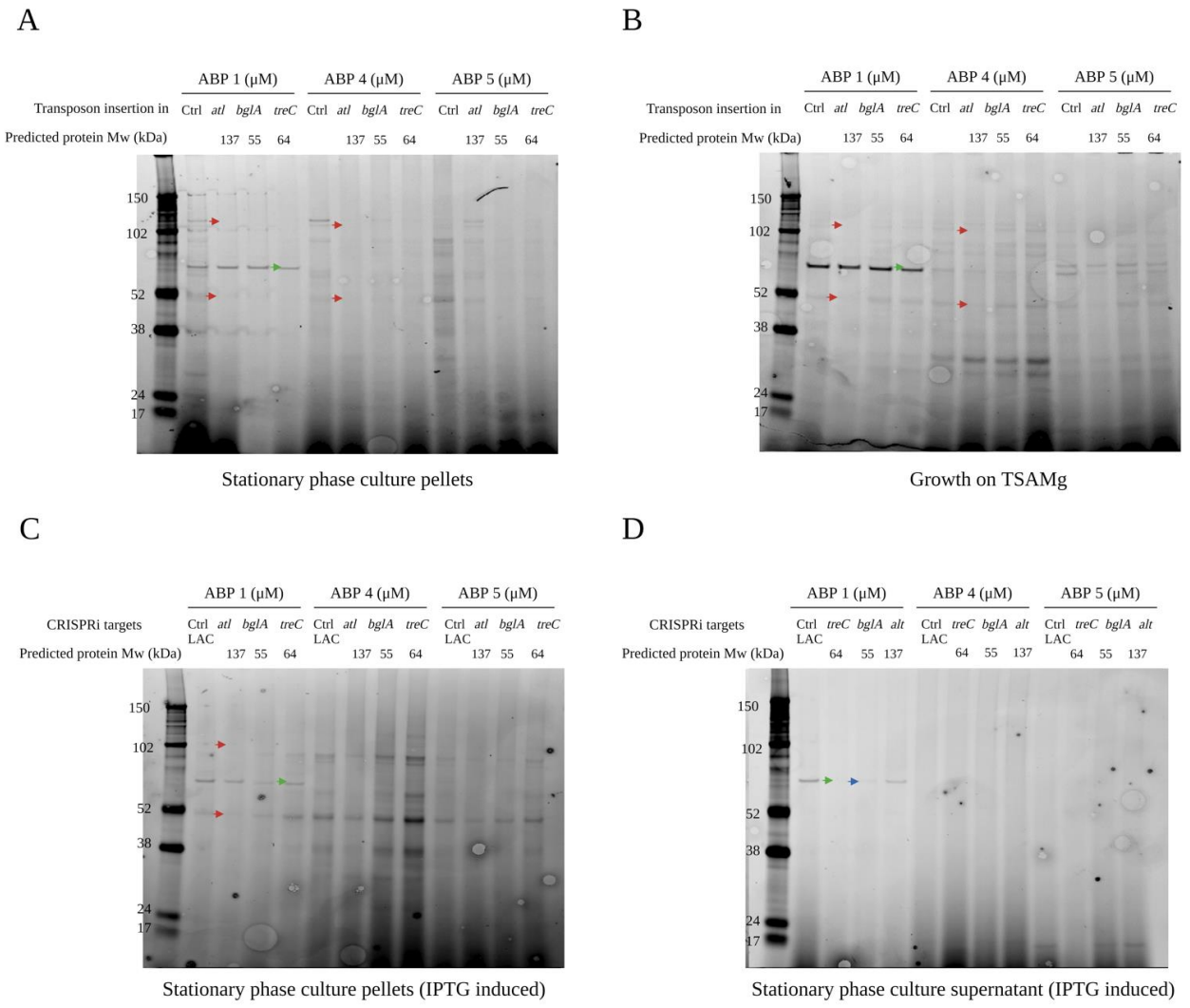

Figure 3. Fluorescent glycosidases ABPs labelling profiles of *S. aureus* USA 300 JE2 transposon mutant strains with insertions of glycosyl hydrolases genes, *atl*, *bglA*, and *treC*. The bacterial cells were labelled under two different conditions: **A**) cells grown to stationary phase culture in TSB, followed by fractionation into cell pellets, and **B**) The cells were harvested in TSAMg. Labeling profiles of *S. aureus* USA 300 LAC CRISPRi constructs targeting the glycosyl hydrolase genes, *atl*, *bglA*, and *treC*. The cells were cultivated in stationary phase culture in TSB supplemented with 250 μM IPTG to induce dCas9 expression and fractionated into a cell pellet (**C**) and culture supernatant (**D**). Arrowheads indicate the labeled proteins disappearing in individual mutant strains.

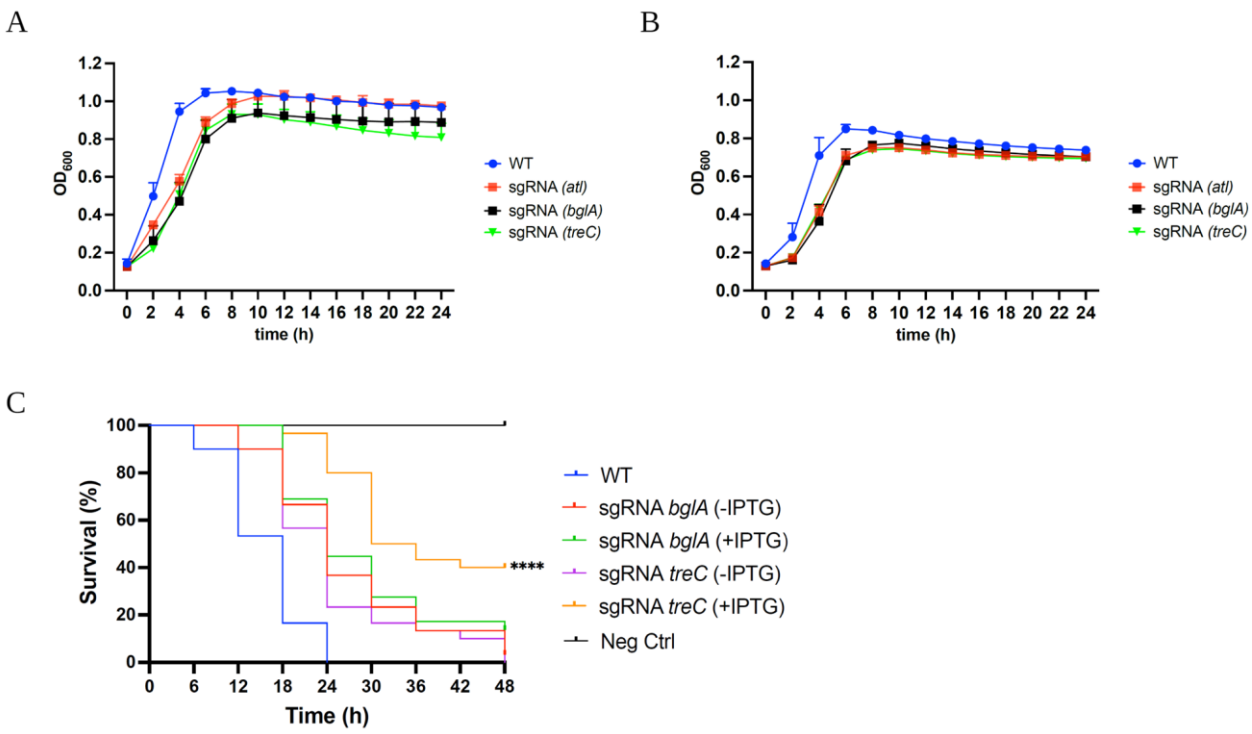

Figure 4. **Functional validation of *S. aureus* CRISPRi knockdown strains**. Growth curves of *S. aureus* LAC (WT) and LAC with CRISPRi constructs (with the indicated sgRNAs) in TSB supplemented with 250 µM IPTG (**A**) or without 250 µM IPTG (**B**). The curves show means ± standard deviation of n= 3 independent biological replicates. **C**) Kaplan–Meier (KM) survival plots of *G. mellonella* larvae after inoculation with *S. aureus* LAC (WT) and CRISPRi strains. Precultures were grown overnight without IPTG as controls or with 250 µM IPTG to induce dCas9 expression and silencing of the target gene. The plots indicate the average of n=3 independent biological replicates (i.e. bacterial cultures originating from 3 different colonies), that were each used to infect 10 larvae per group. Mortality was monitored every 6 hours for 48 hours (N=180). Larvae injected with PBS served as a negative control.). The asterisks in the graph indicates significant difference in survival of IPTG-induced *treC* compared to non-IPTG-induced (**** $p < 0.0001$). All mutants displayed a significant difference in survival compared to the WT, as determined by the log-rank (Mantel–Cox) test($p < 0.0001$).

Supporting dataset 1. Proteins identified in *S. aureus* USA300 JE2 by MS-ABPP

Accession	Description	# Unique Peptides	# AAs	MW [kDa]	Gene Name	LFQ intensity FP-biotin R1	LFQ intensity FP-biotin R2	LFQ intensity FP-biotin R3	LFQ intensity Cntrl R1	LFQ intensity Cntrl R2	LFQ intensity Cntrl R3	Average Abundance: biotin	Average Abundance: ctrl	Abundance Ratio: (biotin) / (ctrl)	Abundance Ratio P-Value: (biotin) / (ctrl)
QPB86653.1	class I SAM-dependent methyltransferase [Staphylococcus aureus LA	3	202	22.7	ORF202; rsmC	175231.4219	110041.0859	148123.6875				144465.3984	1	100	1E-17
WP_000666761.1	MULTISPECIES: shikimate dehydrogenase [Staphylococcus]	3	268	29.9	aroE	79957.24219		100133.625				90045.43359	1	100	1E-17
QPB86366.1	3-hydroxyacyl-CoA dehydrogenase/enoyl-CoA hydratase family prot	13	753	84.6	fadB	617032.6328	1053172.023	1036410.203	262021.4531	148328.7344	271859.1484	902204.9531	227403.112	3.967425711	0.907169673
WP_000974460.1	MULTISPECIES: organic hydroperoxide resistance protein [Staphylo	2	140	15.3			401097.6133	290330.6563	112167.9453	134325.4219	48518.79297	345714.1348	98337.38672	3.515592048	1.97144E-05
WP_000159750.1	MULTISPECIES: PTS transporter subunit EIIC [Staphylococcus]	6	484	50.6	murP	26048375.11		21747957.44	614976.2188	20640069.13	185805.7656	23898166.27	7146950.37	3.343827092	0.052059494
QPB86592.1	dTMP kinase [Staphylococcus aureus LAC]	7	205	23.4	tmk; tmk_2	113382711.3	255468980.7	274154936.7	66195239.13	76944787.5	71233190.12	214335542.9	71457738.91	2.999472781	0.010307358
QPB88197.1	transcription termination factor Rho [Staphylococcus aureus LAC]	21	438	49.9	rho; rho_2	3332177.781	17396466.98	3876896.998	3734484.355	1449847.039	3125748.203	8201847.252	2770026.533	2.960927325	0.434495498
WP_000142049.1	MULTISPECIES: TIGR01741 family protein [Staphylococcus]	2	163	19.7	essG; yezG_1	42285.11719	380980.125	348131.0313	45983.00781	45874.65625	187443.4609	257132.0911	93100.375	2.761880295	0.436961473
QPB88304.1	50S ribosomal protein L18 [Staphylococcus aureus LAC]	5	119	13.1	rplR; rplR_2	952399.4961		1467272.383	338775.9375	217320.9375	797261.4453	1209835.939	451119.4401	2.681852813	0.000395406
QPB86784.1	response regulator transcription factor [Staphylococcus aureus LAC]	5	224	26.1	graR	863044.1719		654730.9922	87519.72656	646058.9375	131231.2813	758887.582	288269.9818	2.63255847	0.09849835
WP_001071717.1	MULTISPECIES: anaerobic ribonucleoside-triphosphate reductase [	10	616	70.4	nrdD	416018.3672	288741.3438	1096592.391	346138.4688	59520.90234	279118.6953	600450.7005	228259.3555	2.630563375	0.008485481
WP_000562498.1	MULTISPECIES: class 1b ribonucleoside-diphosphate reductase sul	16	323	37.5	nrdF; nrdF1; rir2	6237509.688	4051720.242	56551061.23	10469091.19	7309062.43	9636566.688	22280097.05	9138240.102	2.438116837	0.148503411
WP_001001228.1	MULTISPECIES: DNA-3-methyladenine glycosylase I [Staphylococc	3	186	21.4	tag	697974.0625	293553.1875	629662.2188	683486.75	97629.55469	89424.20313	540396.4896	290180.1693	1.862279187	0.263502083
WP_000260118.1	dihydrolipoyl dehydrogenase [Staphylococcus aureus]	8	468	49.4	lpdA; pdhD	3310935.141	3602210.594	3814818.375	3278208.281	1996711.516	579361.2813	3575988.036	1951427.026	1.832498981	0.975594328
WP_001190829.1	MULTISPECIES: anti-sigma B factor RsbW [Staphylococcus]	4	159	17.9	rsbW	472567.4844		259091.875	185125.0625		218630.625	365829.6797	201877.8438	1.812133877	0.00466176
QPB86698.1	phosphate acetyltransferase [Staphylococcus aureus LAC]	4	328	34.9	eutD; pta	370495.5313	577035.5	409554.25	317733	267879.375	173633.7969	452361.7604	253082.0573	1.787411424	4.95726E-07
WP_000163988.1	MULTISPECIES: 6-phospho-beta-glucosidase [Staphylococcus]	2	478	54.7	bglA	1103340.625	376206.5938		184147.4063	442209.75	620265.9375	739773.6094	415541.0313	1.780266096	1.85817E-07
QPB88420.1	alpha/beta hydrolase [Staphylococcus aureus LAC]	10	306	35.5	mlhB_1; mlhB_2	186014.2656		2614453.344	990294.9922		603212.6406	1400233.805	796753.8164	1.757423405	0.655564983
WP_000375864.1	MULTISPECIES: helix-turn-helix transcriptional regulator [Bacteria]	6	154	17.8		662642.7031		857044.4805	632566.75	334568.8242	334253.1719	759843.5918	433796.2487	1.751614022	0.470973305
WP_000275730.1	MULTISPECIES: pectate lyase [Staphylococcus]	7	365	40.7	pfbA	1670671.266	1346004.859	3387405.781	1274717.109	1453209.125	982221.8438	2134693.969	1236716.026	1.726098736	0.015415869
WP_000154228.1	MULTISPECIES: transcription-repair coupling factor [Staphylococcu	12	1168	134.1	mfd	4465285.672	3495884.264	2046782.266	4003198.529	1093099.457	768637.4766	3335984.067	1954978.488	1.706404489	0.505572922
WP_000954810.1	MULTISPECIES: nitric oxide dioxygenase [Staphylococcus]	11	381	42.9	hmp	300045.7266	305342.2813	1603817.313	637298.4297	169806.5898	525248.8125	736401.7734	444117.944	1.65812209	0.299921816
QPB87945.1	GAF domain-containing sensor histidine kinase [Staphylococcus aure	2	370	41.9	vraS_1; vraS_2; vraS_3;	685740.5625	545841.1875	2019382.75	753109.875		601572.125	1083654.833	677341	1.599865996	0.172496945
WP_001173201.1	MULTISPECIES: mannose-6-phosphate isomerase, class I [Staphyl	3	312	35.4	manA; manA2; pmi	122834.6484		322500.7188	161216.6406	161467.2656	106977.1484	222667.6836	143220.3516	1.554720968	0.676823391
QPB87272.1	phosphate acyltransferase PlsX [Staphylococcus aureus LAC]	4	328	35.4	plsX	760012.0625	641120.5	1176025.594	944767.4219		164431.2031	859052.7188	554599.3125	1.548961024	6.43444E-10
WP_000717381.1	MULTISPECIES: CHAP domain-containing protein [Staphylococcus	8	267	29.3	ssaA; ssaA2; ssaA2_1; ss	197264030	297158791.9	216430968.6	185885844.9	163642222.5	118642950.1	236951263.5	156057005.8	1.518363512	0.777492539
WP_000031515.1	MULTISPECIES: alpha,alpha-phosphotrehalase [Staphylococcus]	6	546	63.5	treC		952744.9375	141421.2813	171459.2188	330197.9375	579410.25	547083.1094	360355.8021	1.518174832	5.94054E-06
WP_000035767.1	MULTISPECIES: DNA translocase FtsK [Staphylococcus]	8	789	88.1	ftsK; ftsK_3		185816.2188	635835.6563	413433.875	188410.6875	213226.4844	410825.9375	271690.349	1.512110898	0.562414922
QPB88486.1	2,3-diphosphoglycerate-dependent phosphoglycerate mutase [Staphy	4	228	26.7	gpmA; pgm_2	89450.39844	90433.64063	115291.9141	78508.30469	51945.875		98391.98438	65227.08984	1.50845277	4.57359E-05
QPB88582.1	fructose-1,6-bisphosphatase [Staphylococcus aureus LAC]	4	654	76.1	fbp		96476.26953	45744.36753	47158.88281			71110.31853	47158.88281	1.507888107	1E-17
WP_001074556.1	MULTISPECIES: glucosaminidase domain-containing protein [Staph	29	1256	137.3	atl; atl_2	39251076.25	32704027.26	31648574.95	25332714.83	18733787.59	24961863.38	34534559.49	23009455.27	1.500885575	0.022711654
QPB87716.1	U32 family peptidase [Staphylococcus aureus LAC]	3	307	35.9	yhbU_1; yhbU_2; yhbU_4	170412.7656	329917.4375	189372.6719	142562.9063	167238.4063		229900.9583	154900.6563	1.484183243	0.011492945
QPB87035.1	ABC transporter ATP-binding protein [Staphylococcus aureus LAC]	3	360	40.2	oppD; oppD_1	113539.6328	74989.42188	142997.9219	77171.89844			110508.9922	77171.89844	1.431984886	0.024298382
WP_000382904.1	MULTISPECIES: ATP-binding cassette domain-containing protein [E	5	231	25.8	ecsA_2; ecsA_3	812569.9297	735871.8398	1884710.773	1182468.438	632169.7031	601802.1563	1144384.181	805480.099	1.420747927	0.822253627
WP_001126603.1	MULTISPECIES: type I glutamate--ammonia ligase [Staphylococcus	14	446	50.8	glnA; glnA_2	32659522	22767503.85	21477010.48	12890040.35	13004111.52	29517575.43	25634678.78	18470575.77	1.387865711	0.016020545
QPB87813.1	septation ring formation regulator EzrA [Staphylococcus aureus LAC	12	564	66.2	ezrA	2077903.961	1676344.547	1322405.891	1882121.109	402507.5313	1379330.141	1692218.133	1221319.594	1.385565368	0.005029705
QPB86906.1	ribonuclease R [Staphylococcus aureus LAC]	11	790	90.4	rnr	1647132.438	693296.375	3845712.688	1471395.75	1507405.063	1549955.059	2062047.167	1509585.29	1.365969303	0.034046377
A3EZ82	TREMBL:A3EZ82;Q32W66 Tax_Id=9606 Gene_Symbol=DMKN De	3	476	47.1	DMKN	2400631	2523397.25	1202758.5	1381120.5	1607415.063	1573142.125	2042262.25	1520559.229	1.343099441	1.21874E-05
WP_001019337.1	MULTISPECIES: acetyl-CoA carboxylase biotin carboxyl carrier prot	4	149	16.8	accB; accB_2	75825806.45	62186534.78	210431017.5	93138980.71	81735544.97	84579448.23	116147786.3	86484657.97	1.342987172	0.512242969
WP_001096577.1	MULTISPECIES: 50S ribosomal protein L30 [Bacteria]	2	59	6.6	rpmD; rpmD_2	312868.7813	238936	357550.0625	284871.9688	186747.0469	213823.0469	303118.2813	228480.6875	1.326669158	0.001532073
QPB86644.1	NYN domain-containing protein [Staphylococcus aureus LAC]	3	174	20.2		418651.6953		297323.2891	82672.4375	262110.3438	465966.7188	357987.4922	270249.8333	1.324653887	0.738657537
QPB87339.1	DNA mismatch repair endonuclease MutL [Staphylococcus aureus LA	12	669	76.8	mutL	233374.875	300621.5547		155563.1094	234858.5156	214390.7891	266998.2148	201604.138	1.324368723	0.11122967
QPB87344.1	alpha/beta hydrolase [Staphylococcus aureus LAC]	6	304	35.2		462628.8672		853242.7344	653517.5	248216.5234	593441.8125	657935.8008	498391.9453	1.320117243	0.536259872
QPB87775.1	50S ribosomal protein L20 [Staphylococcus aureus LAC]	4	118	13.7	rplT; rplT_2	33947239.59	28986478.34	20484687.84	19397430.97	14497751.78	29450107.44	27806135.26	21115096.73	1.316884105	0.147673324
WP_000650082.1	MULTISPECIES: transcriptional regulator NrdR [Staphylococcus]	7	156	18.2	nrdR; nrdR_2	1151743.781	683519.4688	1670138.781	1022931.492	104062.5469	1539352.789	1168467.344	888782.276	1.314683444	0.723528995
WP_000175746.1	MULTISPECIES: dihydrofolate reductase [Staphylococcus]	2	159	18.2	dfrA; dfrB; folA	4005647.5	3759064.336	6057320.266	5383876	1721091.625	3532492.828	4607344.034	3545820.151	1.299373301	0.032624931
QPB86318.1	acyl-CoA/acyl-ACP dehydrogenase [Staphylococcus aureus LAC]	6	343	38.5		86431.27344	69673.16406	303508.875	118026.9844			153204.4375	118026.9844	1.298045852	0.330602428
QPB88861.1	type II toxin-antitoxin system PemK/MazF family toxin [Staphylococc	4	237	27.8		202984.4609		132816.625	129549.4844			167900.543	129549.4844	1.29603405	0.777196789
QPB86294.1	bifunctional acetaldehyde-CoA/alcohol dehydrogenase [Staphylococ	17	869	94.9	adhE	3404537.781	113470.2539	411396.5859	2013848.805	562316.5469	492524.1172	1309801.54	1022896.49	1.280482975	0.861544974
QPB87498.1	ATP-dependent helicase DinG [Staphylococcus aureus LAC]	10	897	104.2	dinG	286026701.3	230931279.1	160131367.8	177601485.5	203115170.6	148900393.9	225696449.4	176539016.7	1.278450813	0.093724967
WP_000238227.1	MULTISPECIES: exonuclease SbcCD subunit D [Staphylococcus]	6	398	46.2	yhaO	653907	142138.5625	509412.9688	596928.625	187735.3594	270171.6563	435152.8438	351611.8802	1.237594257	0.619168393
QPB87459.1	response regulator transcription factor ArlR [Staphylococcus aureus	3	219	25.5	arlR; arlR_2	101783.2813	60794.63281	195548.5156	123631.9766	77614.0625	88953.03906	119375.4766	96733.02604	1.234071562	0.565684013
WP_000863479.1	MULTISPECIES: signal recognition particle protein [Staphylococcus	13	455	50.7	ffh	21005005.63	15176800.35	28259450.69	15924343.48	17082769.97	19700404.12	21480418.89	17569172.52	1.22261984	0.999782909
QPB87079.1	glycosyltransferase [Staphylococcus aureus LAC]	9	493	57.2	tagE_1; tagE_3; tarM	496670.7031		469036.9922	1026304.867	152689.75	18959.58398	482853.8477	399318.0671	1.209196096	0.942941677
QPB86806.1	hypothetical protein HUW68_03640 [Staphylococcus aureus LAC]	2	227	26.7		3579117.5	3118603.25	5104600.344	3947662.938	2747065.813	3105943.25	3934107.031	3266890.667	1.204235903	0.139614932

Paper III

Activity-Based Protein Profiling Identifies *Klebsiella pneumoniae* Serine Hydrolases with Potential Roles in Host-Pathogen Interactions

Md Jalal Uddin[1*], George Randall[2], Jiyun Zhu[3], Tulsi Upadhyay[3], Laura van Eijk[4], Paul B. Stege[4], Frerich M. Masson[4], Marco C. Viveen[4], Matthew Bogyo[3], Matthias Fellner[2], Marcel R. de Zoete [4], Mona Johannessen[1] and Christian S. Lentz [1*]

1. Centre for New Antibacterial Strategies (CANS) and Department of Medical Biology (IMB), UiT-The Arctic University of Norway, 9019 Tromsø, Norway
2. Biochemistry Department, School of Biomedical Sciences, University of Otago, Dunedin 9054, New Zealand
3. Department of Pathology, Stanford University School of Medicine, Stanford, California 94305, United States
4. Department of Medical Microbiology, UMC Utrecht, Utrecht, 3584 CX, The Netherlands

*To whom correspondence should be addressed: Christian S. Lentz, Christian.s.lentz@uit.no and Md Jalal Uddin jalal.uddin@uit.no

Abstract

Klebsiella pneumoniae is a normal resident of the human gastro-intestinal tract and an opportunistic, critical priority pathogen that can cause a variety of severe systemic infections. Due to emerging multi-drug resistance of this pathogen, the discovery and validation of novel targets for the development of new treatment options is an urgent priority. Here, we explored the family of serine hydrolases, a highly druggable and functionally diverse enzyme family which is uncharacterized in *K. pneumoniae*. Using functionalized covalent fluorophosphonate inhibitors as activity-based probes we identified 10 serine hydrolases by mass spectrometry-based activity-based protein profiling, 7 of which were previously uncharacterized. Functional validation using transposon mutants deficient in either of the putative lysophospholipase PldB, esterase YjfP and patatin-like phospholipase YchK revealed severe growth defects in human colonic organoid co-culture models and reduced virulence during *Galleria mellonella* infection. Mutants deficient in the PldB and YjfP, but not YchK show increased susceptibility to killing by complement and the antimicrobial peptide antibiotic polymyxin B, suggesting a role in maintaining cell envelope integrity. Biochemical characterization and structural analysis of recombinant YjfP suggest this protein is a deacetylase. This study gives important insights into the molecular mechanisms underlying virulence and cell physiology of *K. pneumoniae* at the host-pathogen interface and it positions PldB, YjfP and YchK as potential antimicrobial or anti-virulence target candidates, inhibition of which might synergize with existing antibiotics and human immune defenses.

Introduction

The Gram-negative enterobacterium *Klebsiella pneumoniae* is an opportunistic pathogen that naturally resides in the gastrointestinal tract of healthy humans and animals but can cause a variety of severe extra-intestinal infections, including urinary tract, bloodstream, and lung infections[1]. This bacterium is also known for its ability to produce extended-spectrum beta-lactamases (ESBLs) and carbapenemases enzymes that confer resistance to many antibiotics, including the carbapenems, which are often used as last-resort antibiotics [2,3]. This makes the infections caused by *K. pneumoniae* difficult to treat and increases the risk of mortality [4]. Carbapenemase-producing *K. pneumoniae* are critical priority pathogens on the list of multi-drug resistant (MDR) pathogens by the World Health Organization (WHO). Therefore research and development of new therapeutics need to be prioritized to prevent entry into a post-antibiotic era[5]. Beyond multi-drug resistance the emergence and global spread of hypervirulent *K. pneumoniae* strains, which are common causes of liver abscesses and other systemic infections are of great concern [6,7].

In the light of the spread of multi-drug resistant strains of this pathogen, it is essential to understand the molecular factors that contribute to its pathogenicity and validate their potential as drug targets. One particularly attractive family of putative target enzyme are the serine hydrolases (SHs), a large and diverse enzyme class with roles in various cellular processes, from metabolism, to signaling, and regulation of gene expression, and can be putative drug targets for a variety of diseases [8-10]. Due to their conserved mechanism and active site architecture, many SHs share reactivity towards the same active site-directed inhibitors, such as fluorophosphonates. This can be exploited by a chemoproteomic technique called activity-based protein profiling (ABPP) that uses functionally-tagged active site-directed covalent enzyme inhibitors (activity-based probes, ABPs) to detect active enzyme species under physiological conditions in complex samples of interest [11-14]. Fluorescent fluorophosphonate (FP)-probes can be used to detect SHs in gel-based ABPP, whereas FP-biotin allows for pull-down and identification of targets by liquid chromatography-mass spectrometry (LC-MS) (Schematically illustrated in **Fig. 1A, B**). In this way, SH activities have been profiled in diverse biological samples including animal tissues[15], human cell lines [16], and more recently bacterial pathogens including *Staphylococcus aureus* [17], *S. epidermidis* [18], *Mycobacterium tuberculosis* [19-21], and *Vibrio cholerae* [22], the gut commensal *Bacteroides thetaiotaomicron*[23] and archaea [24]. In our recent chemoproteomic study on *S. aureus*, we identified a family of ten largely uncharacterized fluorophosphonate-binding serine hydrolases FphA-J several of which have roles in pathogenesis [17] and bacterial stress responses [25]. These enzymes can be targeted by specific small molecule inhibitors and probes holding promise as anti-virulence [17] and pathogen-specific imaging targets[26].

Surprisingly, very few serine hydrolases of *K. pneumoniae* have been described or functionally characterized. A mutant of the periplasmic HtrA-like serine protease DegP showed higher susceptibility to complement-mediated killing and reduced levels of capsule polysaccharide [27]. However, it remains unclear how this protease mediates these effects. In *E. coli*, the two HtrA-serine proteases DegP and DegS have described functions in extracytoplasmic protein quality control and stress responses (reviewed in[28]).

Another serine hydrolase, the phospholipase Tle1 has been described as a secreted effector of the type 6 secretion system (T6SS) in a hypervirulent *K. pneumoniae* strain[29,30]. Due to toxic effects of T6SS effectors on both bacterial competitors and host tissues, the *K. pneumoniae* T6SS is important for both long-term colonization of the gut[30] as well as intestinal barrier dysfunction and bacterial translocation from the gut[31] .

Here, we performed a systematic analysis of serine hydrolase activities in *K. pneumoniae* using a broad spectrum serine hydrolase probe. Seven out of 10 identified hydrolases were poorly annotated and previously uncharacterized. Functional characterization using transposon mutants in colonization/infection assays involving HT29-MTX cells, human-derived 2D colonic organoids, and *Galleria mellonella* infection suggest crucial roles for at least three of these hydrolases during infection and/or colonization. Our data suggest that the cell membrane-associated putative lysophospholipase PldB and esterase YjfP contribute to cell envelope integrity and contribute to resistance to antimicrobial peptides and complement, whereas the putatively secreted patatin-like phospholipase YchK may contribute to *K. pneumoniae* virulence by degrading mucus or host-cell derived phospholipids. Biochemical and structural analysis of recombinant YjfP suggest that this enzyme functions as a deacetylase.

Materials and Methods

Bacterial strains and culture conditions

Strains of *K. pneumoniae* MKP103 and its isogenic mutants are summarized in **Supplementary Table 1**. All strains were routinely cultured on Blood agar or Luria-Bertani broth (LB broth). The bacterial strains were incubated at 37°C, and liquid cultures were aerated by shaking at 180 rpm, except when intended for co-incubation with mammalian cells or organoids (described in their respective sections below).

Bacterial labeling with fluorophosphonate-tetramethylrhodamine (FP-TAMRA)

After overnight growth on either an agar plate or in liquid culture, as indicated, the bacteria were adjusted to the desired density in LB/MH broth and added to microtubes in a final volume of 50-100 µL. ActivX™ TAMRA-FP (ThermoFisher Scientific) (at a concentration of 1 µM) was added from 100X stock solutions in DMSO and the cells were incubated for 60 minutes at 37 °C and 300 RPM. Following probe labeling, bacterial suspensions were transferred to 2 mL screw-cap tubes filled with 30-50 µL of 4x SDS-Loading buffer (comprising 40% glycerol, 240 mM Tris/HCl at pH 6.8, 8% SDS, 0.04% bromophenol blue, and 5% beta-mercaptoethanol) and 60-100 µL of 0.1 mm glass beads, and then lysed using bead-beating (3×30s, 6500 rpm, with 60s pause in-between) (Precellys® Evolution homogenizer (Bertin Technologies) and centrifuge samples at 6000g for 5 min at 4°C to remove the debris.

SDS-PAGE analysis of fluorescently labeled proteins

After adding 4x SDS sample buffer, the samples were subjected to boiling at 95 °C for 10 minutes and subsequently separated using SDS-PAGE gel electrophoresis. The resulting gels were scanned for fluorescence scanning in the Cy3 (532nm) channel, utilizing the Amersham™ Typhoon™ 5 imaging system (cytiva).

FP -biotin labeling of *K. pneumoniae* and sample preparation for mass-spectrometry

K. pneumoniae MKP103 cultures were grown on a blood plate for 24 hours and resuspended to an OD_{600} ~20 in 3 mL MH broth. For each biological replicate, 1 mL aliquots were transferred to a 1.5 mL tube and either FP-Biotin (3 µM) or DMSO was added, and the cells were then incubated for 60 min at 37°C and 700 rpm before samples were centrifuged at 4,500 ×g for 5 minutes at 4°C, and the supernatant was removed. The cell pellets were resuspended in 1.2 mL RIPA Lysis buffer (50 mM Tris, 150 mM NaCl, 0.1% SDS, 0.5% sodium deoxycholate, 1% Triton X-100) in 2 mL screw-cap tube filled with ca. 200 µL of 0.1 mm glass beads and lysed by bead-beating (3×30s, 6500 rpm, with 60s pause in-between, performed two to three times with one min interval on ice). After centrifugation for 5 minutes at 10,000 ×g at 4°C, the protein concentration in the supernatant was adjusted to 1.0 mg/mL, and the proteins were stored at -20°C until the sample preparation.

For each sample, 50 µL of streptavidin magnetic beads were washed twice with 1 mL of RIPA lysis buffer. The streptavidin beads were then incubated with 1 mg of protein from each sample in an additional 500 µL of RIPA lysis buffer at 4°C overnight on a rotator set at 18 RPM. After enrichment, the beads were collected using a magnetic rack and washed with RIPA lysis buffer twice (1 mL, 2 minutes at room temperature), followed by a wash with 1 M KCl (1 mL, 2 minutes at room temperature), a wash with 0.1 M Na_2CO_3 (1 mL, ~10 seconds), a wash with 2 M urea in 10 mM Tris-HCl (pH 8.0) (1 mL, ~10 seconds), and two washes with RIPA lysis buffer (1 mL per wash, 2 minutes at room temperature). After the final wash, the beads were transferred to fresh protein Lo-Bind tubes

with 1 mL of RIPA lysis buffer and washed three times with 500 µL of 4M Urea in 50 mM Ammonium bicarbonate (Ambic) with shaking for 7 minutes each time to remove nonspecific enrichments. Lastly, the beads were washed three times with 500 µL of 50 mM Ambic with shaking for 7 minutes, changing the tube between these washes.

For on-bead digestion, 150 µL of 50mM Ambic, 3 µL of 1mM CaCl2, 0.75 µL of 1M DDT, 4.5 µL of 500mM IAA, and 6 µL of MS-grade trypsin solution were added to the protein Lo-Bind tube, and samples were incubated at 37 °C overnight with a shaker running at 800 rpm. After digestion, tryptic peptide digests were separated, and beads were washed with 70 µL of 50 mM Ambic. For each sample, 20 µL of formic acid was added to the combined eluates. The samples were stored at -20°C until LC-MS/MS analysis. The sample preparation was conducted using the same method previously described[32].

Liquid chromatography–mass spectrometry analysis

Sample cleanup and concentration were performed using OMIX C18 tip (A5700310, Varian). For the LC-MS analysis, the concentrated samples were dissolved in 15 µl of 0.1% formic acid. Then, 0.5 µg of peptides from each sample were injected for analysis. Peptide mixtures containing 0.1% formic acid were loaded onto EASY-nLC1200 system (Thermo Fisher Scientific) with a C18 column (2 µm, 100 Å, 50 µm, 50 cm), and fractionation was performed using a 5-80% acetonitrile gradient in 0.1% formic acid at a flow rate of 300 nL/min for 60 minutes. The fractionated peptides were analyzed using a Orbitrap Exploris 480 mass spectrometer (Thermo Fisher Scientific). Data acquisition was carried out in a data-dependent mode employing a Top20 method. Raw data was processed using Proteome Discoverer 3.1 software with the CHIMERYS, and the fragmentation spectra were matched against the (*Klebsiella pneumoniae* subsp. pneumoniae KPNIH1, Taxonomy ID: 1087440) database. A peptide mass tolerance of 10 ppm and a fragment mass tolerance of 0.02 Da were employed during the search. Peptide ions were filtered using a false discovery rate (FDR) set at 5% for accurate peptide identifications. To ensure precision at least three biological replicates were conducted for all samples. Statistical analysis was conducted using Perseus software (version 2.03.0) [33]. Potential contaminants, reverse hits, and proteins identified by side only were excluded. The intensities from label-free quantification were converted using a log2 transformation. We applied imputation based on a normal distribution (width, 0.3; down-shift, 1.8) to handle missing values. The p-values were determined through a two-sided, two-sample t-test. Proteins identified as significantly enriched serine hydrolases had at least a threefold change (equivalent to a log2 fold-change of 1.58) and a minimum P value of 0.05 (corresponding to a −log10 value of 1.30). The mass spectrometry proteomics data have been deposited to the ProteomeXchange Consortium via the PRIDE[34] partner repository with the dataset identifier PXD052404.

Bioinformatic analyses

The 10 putative serine hydrolases were analyzed using both uniport[35] and the web-based InterPro tool (https://www.ebi.ac.uk/interpro/) to predict proteins structures. The subcellular localization of serine hydrolases in *K. pneumoniae* was predicted with the web-based tools PSORTb v3.0 (https://www.psort.org/psortb/index.html)[36]. Furthermore, homology of *K. pneumoniae* serine hydrolases was identified by querying the full-length protein sequences against the non-redundant protein sequences database for gut commensal bacteria and *Homo sapiens* using Blastp with an E value cutoff of 10^{-10} for all identified homologs.

Growth analyses

Growth curves were monitored using 96-well microtiter plates. Overnight cultures of *K. pneumoniae* MKP103 WT and its transposon mutants were diluted 1:100 in fresh medium or in medium supplemented with polymyxin B at a concentration of 8 µg/mL. A 200 µL aliquot of these diluted cultures was transferred to each well of the 96-well plate as the initial culture. The plates were then incubated at 37°C, and the optical density at 600 nm (OD600) was measured every 10 minutes using a Synergy H1 Hybrid Reader (BioTek) or a Bioscreen plate reader. The area under growth curve (AUC) was determined by using GraphPad Prism 9 for polymyxin B treatment.

Co-incubation of HT29-MTX cells and *K. pneumoniae*

The HT29-MTX human colorectal adenocarcinoma cell line [37] was grown in Dulbecco's modified Eagle medium (DMEM, supplied by Thermo Fisher) supplemented with 10% heat-inactivated (HI) fetal calf serum (FCS). For coculture experiments, HT-29-MTX cells were seeded at a density of approximately 1 x 10^5 cells per well in 48-well plates and mid-log phase *K. pneumoniae* MKP103 and SH-deficient mutants (with OD600 nm of 0.4) in FBS-free DMEM were added to each well at a multiplicity of infection (MOI) of 20. After centrifugation at 200 x g for 5 minutes, the plates were incubated at 37°C with 5% CO_2 for 2, 4, 6, and 8 hours and samples were collected from the media above host cells for counting the colony-forming units per milliliter (CFU/mL). All experiments were performed in duplicate and repeated independently at least three times.

Organoid line and growth conditions

The clonal human-derived colonic organoid cell line Pt15-70206 was used to grow colonic epithelium, following the protocol described by Vonk *et al*.[38] . Briefly, colonic organoid stocks were thawed, and the organoids were cultured in Matrigel domes with medium containing 15% Advanced DMEM/F12, 1x Glutamax, 100 U/mL Penicillin-Streptomycin, 10 mmol/L HEPES (all Invitrogen), 25% Rspo1 Conditioned Medium, 10% Noggin Conditioned Medium, 0.5nM Wnt Surrogate-FC Fusion Protein (ImmunoPrecise-UCN001), 2% B27 (Invitrogen), 1.25 mM N-acetylcysteine, 10 mM Nicotinamide, 3µM p38 inhibitor SB202190 (all Sigma-Aldrich), 50 ng/mL mEGF (Invitrogen), and 0.5 µM A83-01 (Tocris).

After an average of 4 passages, the organoids were disrupted and used to seed transwells (corning, 3470-clear) to generate confluent colonic epithelium. During the first 24 hours in transwells, the organoid culture medium was supplemented with 10nM rock inhibitor Y-27632 (Sigma-Aldrich). Once the Trans-epithelial Electrical Resistance (TEER) surpassed 100 Ω/cm^2, the culture medium was replaced with differentiation medium[39], excluding Wnt Surrogate-Fc Fusion Protein, nicotinamide, and p38 inhibitor. Differentiation medium was refreshed 24 hours before the adding bacteria for co-culturing, in absence of Penicillin-Streptomycin.

Co-incubation of organoids and *K. pneumoniae*

Overnight *K. pneumoniae* MKP103 and its SH-deficient transposon mutants were diluted 1/100 in fresh medium and cultured in LB at 37°C until reaching the exponential growth phase with an optical density at 600nm of 0.3-0.4. Subsequently, the bacterial suspension was washed in PBS and resuspended in PBS to an OD600 of 0.4. The bacterial suspension was further diluted in organoid medium to achieve~2.5× 10^6 CFU/mL when adding them to the 2D organoid monolayers. The transwells containing the organoids and bacteria were spun down at 250 x g for 2 minutes to ensure cell contact. Finally, the co-culture was incubated at 37°C with 5% CO_2 for 2, 4, 6, 8, and 16 hours and samples were collected from the apical side supernatant for counting the CFUs. To evaluate bacterial replication on the epithelial surface, the monolayer tissue and membrane were removed from the insert and dissociated using 2 mm glass beads in ice-cold PBS through 30 s of vortexing.

Alternatively, after removal from the insert, the cells were lysed using 0.2% Triton X-100. The resulting PBS suspension was serially diluted and plated on LB agar. The agar plates were incubated overnight at 37°C, and CFUs were counted. In parallel, samples were taken from the basolateral compartment, serially diluted, and plated to assess any breach of the monolayer. The CFUs were manually enumerated and expressed as CFU/ml. The epithelial cells were examined for damage with the EVOS FL Auto 2 fluorescent microscopes (ThermoFisher Scientific) at 16 hours.

Visualization of 2D organoid cultures

Organoid 2D cultures were fixed with Methacarn fixation (Methanol-based Carnoy fixation), which causes protein denaturation[40], consisting of 60% methanol, 30% chloroform, and 10% glacial acetic acid, for two hours. After washing away the fixative with 100% methanol, the samples were rehydrated using different ethanol dilutions (100%, 90%, 80%, 70%, 60%, 40%, 20%), with each step lasting ten minutes. The filter of the transwells, with the organoids, was separated from the insert and blocked and permeabilized with a blocking buffer containing 2% Bovine Serum Albumin (BSA) (Serva) and 0.1% saponin (Sigma Aldrich) before incubating with the primary and secondary antibodies at 4°C in dark. The primary antibodies used were Anti-MUC1 21D4 (Sigma Aldrich, 05-652), Anti-MUC2 (Abcam, ab76774), Anti-MUC13 (generous gift by Karin Strijbis), Anti-Sox9 (Merck Millipore, AB5535), Anti-Villin 1D2C3 (Santa Cruz, sc-58897), and Anti-lysozyme (Dako, A099). Then, organoids were stained with Phalloidin Atto-647 (65906-10NMOL) and DAPI and imaged with an SP5 II confocal microscope (Leica TCS).

Membrane permeabilization

Bacteria cultured overnight were diluted 1/100 in fresh medium and grown to an OD600 of 0.4–0.5 at 37°C with shaking. The bacteria were washed with RPMI with 0.05% human serum albumin (HSA, Sanquin, The Netherlands) through centrifugation at 10,000×g for 2 minutes and resuspended to an OD600 of 0.5 in RPMI. For the assay, bacteria were adjusted to an OD600 of 0.05 and mixed with 10 % normal human serum (NHS) (serum was prepared as described in[41]) in the presence of 1 µM SYTOX Green Nucleic Acid stain (ThermoFisher) in RPMI. This mixture was incubated at 37°C with shaking. Fluorescence was measured using a CLARIOstar microplate reader (Labtech) at an excitation wavelength of 490–14 nm and an emission wavelength of 537–30 nm.

Protein Expression and Purification

The full length *yjfP*, *yqiA,* and *pldB* (Uniprot[35] IDs A6THA0, A6TE20, and A6TGK5) DNA sequences were codon optimized for *E. coli* expression (IDT and TISIGNER[42]) and synthesized by IDT with overhangs for ligation-independent cloning[43]. The synthesized DNAs were cloned into a modified pET28a-LIC vector incorporating an N-terminal His_6-tag and a 3C protease cleavage site. Plates were incubated at 37 °C overnight and single colonies were used to inoculate a starter culture of 5 mL LB supplemented with 50 µg/mL kanamycin. The starter culture was used to inoculate 1 L of LB media supplemented with 50 µg/mL kanamycin and incubated at 37°C while shaking at 180 rpm until the OD_{600nm} reached 0.5. The cultures were incubated at 18 °C while shaking at 180 rpm and recombinant protein expression was induced with 1 mM IPTG. Cell pellets were harvested the following day by centrifugation at 5,000 × g for 30 minutes. Cell pellets were either stored at -20°C or lysed right away for protein purification.

A cell pellet was resuspended in lysis buffer (50 mM Tris pH 8.0, 300 mM NaCl, 50 mM imidazole, 10% sucrose, 10% glycerol) and incubated on ice for 10 minutes with 400 µg lysozyme and 200 µg DNase. The cells were subsequently lysed via sonication in an ice bath using Sonifier Heat Systems Ultrasonics, for 5 min using a one second pulse mode. Lysate was cleared by centrifugation

at 15,000 x g for 30 minutes. The supernatant was loaded onto 2.0 mL Ni^{2+}-NTA resin which was pre-washed with lysis buffer. The resin-supernatant mixture was incubated at 4 °C room for 30 min before the resin was washed in lysis buffer. The recombinant protein was eluted via 7 mL of elution buffer (50 mM Tris pH 8.0, 300 mM NaCl, 300 mM imidazole, 10% sucrose, 10% glycerol). For PldB and YjfP, these purified His_6-tagged proteins were used for biochemical analysis described below. To cleave the N-terminal His_6 tag for protein crystallization studies, the eluted fractions of YqiA and YjfP incubated with 5 mM DTT and 3C protease overnight at 4 °C. Recombinant proteins of YjfP and YqiA were finally purified by size exclusion chromatography (gel filtration). Protein samples were concentrated using 10,000 MWCO spin columns to approximately 250 µL and injected onto a size exclusion column (Superdex 75 Increase 10/300 GL column, GE Life Sciences) preequilibrated with size exclusion buffer (25 mM Tris pH 8.0, 150 mM NaCl). Protein purity was assessed by SDS-PAGE and nanodrop. Samples were concentrated to ~10 mg/mL and snap frozen in liquid nitrogen or used immediately for crystallization.

Biochemical assay of PldB, YjfP, and YqiA

Activity tests of purified serine hydrolases on different 4-MU (methylumbelliferyl) substrates were carried out as previously described[44]. Briefly, the reaction was carried out in PBS with 0.02 % v/v Triton X-100 (Fisher Scientific, Fairlawn, NJ). 8 µL enzyme solution (0.625 nM His_6-PldB, 0.625 nM His_6-YjfP, 62.5 nM YqiA (tag-free)) was mixed with 2 µL 5x 4-MU substrate stock solutions (250 µM) to initiate reactions and then the fluorescence signal (λ_{ex}= 335 nm and λ_{em}= 450 nm) was monitored by Cytation 3 Multi-Mode Reader (BioTek, Winooski, VT) at 25 ºC for 1 hour. Turnover rates of the 4-MU substrates in the linear phase of the reaction were calculated in GraphPad Prism9 as RFU/second. The reaction rates were corrected by subtraction of the background hydrolysis in the absence of proteins for each substrate. The substrate preference profile was generated by dividing the corrected reaction rates by enzyme concentrations in each assay.

Protein Crystallisation

YjfP and YqiA were crystallized using sitting drop vapour diffusion and screened for crystallization against several broad screens. 0.2 µL of protein solutions at 10 mg/mL were mixed with 0.2 µL of mother liquor. YjfP appeared as needle-like crystals in several different conditions, however the final structure of YjfP was determined from cubic crystals grown in 0.1 M ammonium sulfate, 35 % w/v PEG 8,000, 0.1 M sodium acetate pH 5.0. A YjfP crystal from this condition was soaked in mother liquor supplemented with 25 % v/v ethylene glycol for one minute before freezing in liquid nitrogen for analysis at the Australian Synchrotron. YqiA crystallized in several conditions that mostly contained either calcium chloride or calcium acetate, a crystal grown in 0.3 M calcium chloride hexahydrate, 10 % w/v PEG 6,000, 0.1 Tris pH 8.0 led to successful structure determination of YqiA. This crystal was soaked in mother liquor supplemented with 25 % v/v glycerol for one minute, before being frozen in liquid nitrogen.

Crystal data collection and Processing

Protein crystals were subject to x-ray diffraction at the Australian Synchrotron MX2 beamline[9]. Datasets were processed in XDS[10], before being merged and scaled using AIMLESS[11] in the CCP4 suite. Phases were determined by molecular replacement in Phenix Phaser[12] using an AlphaFold model[13] of YqiA or YjfP prepared with Phenix Process Predicted Model[14]. The output model underwent iterative building and refinement using COOT[15] and Phenix[16].

Infection of *K. pneumoniae* in *G. mellonella* larvae

Galleria mellonella larvae were obtained from Reptilutstyr AS (Norway). For infection experiments, *K. pneumoniae* MKP103 and its transposon mutants were cultured overnight in LB broth and harvested by centrifugation at 4,500 × g for 10 min at 4°C followed by one wash with PBS. The bacteria were then diluted in PBS to achieve OD600 of 1, approximately 1×10^9 CFU/ml. Each experimental group consisted of n=10 larvae. For infection, 10 µl of a bacterial suspension adjusted to 1×10^5 CFU/ml in PBS was injected into right hid proleg using a 30G syringe microapplicator (0.30 mm (30G) × 8 mm, BD Micro-Fine demi). A separate group of 10 larvae were injected with 10 µl of PBS to ensure that death was not due to injection trauma as negative control. The larvae were placed in 9.2 cm Petri dishes and incubated at 37°C in the dark and survival was monitored for 5 days. Each experiment was independently replicated at least three times.

Statistical analysis

Graphs and statistical analyses were produced using GraphPad Prism 9. Unless specified otherwise, all experiments were conducted using three independent biological replicates. Data for graphs are shown as mean ± standard deviation (SD). To compare wild-type (WT) to mutant strains, either one-way or two-way ANOVA tests were utilized, followed by Dunnett's multiple comparisons test, using the WT strain as the control. Significance levels were denoted as follows: *P < 0.05, **P < 0.01, ***P < 0.001, and ****P < 0.0001.

Results

Identification serine hydrolases in *K. pneumoniae*

We first set out to determine global serine hydrolase (SH) activity profile in *K. pneumoniae* when grown on blood agar using the fluorescent ABP FP-TMR. We selected strain MKP103, a derivative of the multi-drug resistant clinical outbreak strain KPNIH1 for which the carbapenemase-gene has been deleted[45]. KPNIH1 belongs to sequence type ST258 which can cause life-threatening infections in hospitalized individuals and poses a considerable risk to spread multidrug resistance into the community[46 47]. After labeling, the cells were lysed, and the labeled proteins were separated via SDS-PAGE analysis and visualized by in-gel fluorescence scanning. The results revealed that several bands were predominantly labeled at the 1 µM probe concentration (**Fig. 1C**). To identify these SH targets, we then used a biotiynylated probe (FP-biotin) with a chemoproteomic workflow using streptavidin-enrichment and LC-MS/MS analysis (**Fig. 1 Aiii, B**). Using this approach, we identified 10 *K. pneumoniae* SHs that displayed significant enrichment (p-value < 0.05, enrichment > 3.5-fold) when compared to a control dataset that was not treated with FP-biotin (as shown in **Fig. 1B. E** and detailed in **Supplementary Table 2** and **Extended Dataset 1,** data are available from ProteomeXchange with identifier PXD052404). Of the 10 identified SHs, 8 were predicted to possess α,β-hydrolase domains, while the remaining two were annotated as serine proteases with Trypsin-like peptidase domains (**Table 1**). Most of these enzymes are generally not well characterized in *K. pneumoniae* and for many of these enzymes their cellular functions are ill defined. Of the 10 SHs, only the HtrA-protease DegP and the carboxylesterase BioH enzymes have been studied functionally in *K. pneumoniae*. The latter putatively hydrolyze the pimeloyl-acyl carrier protein methyl ester as one of the first steps of biotin biosynthesis.[48] Sequence-based bioinformatic prediction of the subcellular location of the 10 identified SH proteins using PSORTb v3.0[36] suggests that only the patatin-like phospholipase YchK is presumably secreted, whereas the two HtrA-like proteases, DegP and DegQ, were predicted to localize to the periplasmic. YjfP and YqiA were predicted to localize to the cytoplasmic. YbIF and YcfA are unknown. PldB is on the cytoplasmic membrane, and BioH and CatD to the cytosol. Except for DegP, DegQ, YchK and YqiA, most of the *K. pneumoniae* SHs displayed limited or no homology with serine hydrolases from 19 other gut commensals and human (**Fig. 1E, Supplementary Table 3**).

To functionally validate the identified target enzymes, we retrieved transposon mutant strains with insertions in individual serine hydrolase genes (*yfbF, yjfP, yqiA, ychK, degP, pldB, degQ,* and *catD*) from the Manoil Lab Transposon Mutant Library[45]. The library did not contain mutants in *bioH* or *ycfP*. At least for BioH with its presumable role in the biosynthesis of biotin, the absence of viable transposon mutants might indicate essentiality. We first labelled the obtained transposon mutants with FP-TMR labeled protein bands in the gel-based FP-TMR labeling. This allowed us to confirm the identities of *pldB*, *degP*, *ychK*, and *ybfF*, but not *degQ, yjfP*, and *ycfF*, as their corresponding transposon mutants showed similar FP-TMR profiles as the WT (**Fig. 2A**). This lack of labeling in the gel based ABPP assay suggesting that some of the identified enzymes may not be abundant and can only be detected in the more sensitive MS assay. In addition, five fluorescent protein bands could not be assigned to the MS identified serine hydrolases, suggesting that differences in selectivity or cellular permeability of the biotinylated and fluorescent probes might have prevented them from being detected in the proteomics approach (**Fig. 2B**). Based on this outcome, a set of five targets were selected for further functional studies: YfbF, YchK, PldB, DegP and the uncharacterized

esterase YjfP which lacks homologs outside of the *Enterobacteriales* and humans (**Fig. 1E, Supplementary Table 3**)

As a first step, we investigated the growth of the selected transposon mutants in LB, a rich liquid media and found that *ychK, pldB, yjfP, degP* and *ybfF* were all dispensable for growth (**Fig. 2C**). Since the primary niche for *K. pneumoniae* as a commensal is the human gut, we next evaluated growth fitness using *in vitro* models mimicking the host-interface of the gut. We adopted a co-culture model with HT29-MTX cells, a mucus-rich goblet cell line[49]. During an 8 h co-culture period with HT29-MTX cells in DMEM/10% HI-FBS, three of the tested transposon mutants (*pldB*, *ychK*, *yjfP*), showed a notable decrease in fitness compared to the WT MKP103, *degP*:Tn and *ybfF*:Tn strains (**Fig. 2D**). This defect was evident both as a delayed onset of replication in the co-culture model and a reduced growth rate. In comparison, neither WT MKP103, nor any of the Tn-mutants was able to grow in DMEM (**Fig. 2E**), suggesting that interactions with the host cells are crucial to sustain growth in this model and may be key for understanding these phenotypes.

PldB, YchK, and YjfP are important for the initial stages of infection in the gut

To determine whether the lysophospholipase (PldB), patatin-like lipase (YchK), and putative esterase (YjfP), play important roles in host-pathogen interactions in the gut, we used a more physiologically relevant model system that better accounts for the complexity of human colonic epithelia. This model is a 2D-co-culture model using a colonic organoid monolayer derived from human adult tissue stem cell-derived organoids using a previously published protocol [38] (**Fig. 3A**). Unlike 3D organoids which have enclosed apical sides, the monolayered organoids directly exposed their apical sides to the culture medium, facilitating direct interactions between the epithelial surface and the administered bacteria[50,51]. Cellular differentiation was assessed by immunofluorescence microscopy and confirmed the presence of the main cell types characteristic of mature/differentiated human colonic epithelium: mucin-1, mucin-2, and mucin-13 cells, (identified by anti-mucin antibodies, note that mucin-13 was detected with a polyclonal antiserum that might also stain other mucins) (**Fig. 3B**), enterocytes (recognized by anti-villin) and stem cells (anti-sox9 antibody). We also detected lysozyme C (by anti-lysozyme C antibody) that is produced by Paneth cells, even though this cell type is usually present in the small intestine[52] (**Fig. 3C**).

To develop a colonization/infection model of *K. pneumoniae* in these 2D-colonic organoids, we added bacteria to the apical side of the monolayers and assessed bacterial growth by determining CFU numbers over time. We observed that the CFU counts of WT bacteria first dropped by an order of magnitude after 2 hours of co-culture compared to the inoculum. This finding could be due to the bactericidal activities of organoid-derived antimicrobial peptides. After 2 h WT bacteria started growing exponentially and approached a plateau at 8-16 hours (**Fig. 3D**). Since the bacteria were not able to grow in organoid media alone (**Supplementary figure S1**), we assume that access to host-cell derived nutrients is necessary to sustain bacterial growth in the co-culture model. After 16 h of co-culture, bacteria have translocated to the basal side of the transwell chamber suggesting damage of the epithelial barrier (**Fig. 3F**).

Upon co-culture with the organoid monolayer, the *pldB*:Tn, *ychK*:Tn, and *yjfP*:Tn mutants showed fitness defects compared to WT bacteria. The initial drop in CFU at 2 h is more pronounced in *pldB*:Tn, *ychK*:Tn and *yjfP*:Tn cells compared to WT (**Fig. 3D**) Furthermore, we observed that the outgrowth of these transposon mutant cells in the culture supernatant was delayed, but once they have resumed growth, the overall rate of growth of the transposon mutants was similar to that of WT cells. (**Fig. 3D**). From 4 h of co-culture onwards, we also observed a lower number of bacteria attached to

the organoid monolayer for the three tested mutants compared to WT (**Fig. 3E**). After 16 hours of culturing, the *yjfP*:Tn mutants showed similar numbers of bacteria at the basal side as the WT despite reduced number of bacteria at the apical end. For *pldB*:Tn and *ychK*:Tn strains there was a trend towards lower bacterial numbers in the basal compartment that may be indicative of reduced or delayed translocation (**Fig. 3F**).

Sensitivity of serine hydrolases-deficient transposon mutants to cell envelope stressors

We hypothesized that the reduced CFU levels observed in the mutants compared to WT (**Fig. 3**) could be explained by an increased sensitivity to the organoid-produced antimicrobial peptides (AMPs). To test this hypothesis, we evaluated the susceptibility of the different mutant strains to polymyxin B, a membrane-destabilizing AMP that interacts with lipopolysaccharide (LPS)[53]. We observed an increased susceptibility to polymyxin B for both *pldB* and *yjfP* as well as for the *degP* transposon mutant, whereas the mutant deficient in the secreted patatin-like phospholipase *ych*K had a similar susceptibility to the WT (**Fig. 4 A, B**).

In the Gram-negative cell envelope, LPS is not the only the target of AMPs like polymyxin, but it also plays a crucial role in resistance to complement-mediated killing[54]. A *degP* mutant was previously reported to be more sensitive to complement-mediated killing than the parent strain[55]. To test the effects of complement mediated killing, we treated each of the mutant lines with serum and heat-inactivated serum in which components of complement are inactivated. We found that serum induced higher killing effect in the *pldB*:Tn, *yjfP*:Tn and *degP*:Tn mutants compared to control or treatment with heat killed serum (**Fig. 4C, D)**. These results suggest a role of YjfP and PldB in shaping envelope integrity, which in turn may affect susceptibility to complement and antimicrobial peptides.

Loss of PldB, YchK, and YjfP reduced *K. pneumoniae* virulence in *G. mellonella* larvae

The *Galleria mellonella* infection model (**Fig. 5A**) is a simple, cost-effective and easily accessible animal model that allows us to assess the effects of serine hydrolases on virulence [56,57]. We found that upon infection with 10^5 CFU WT *K. pneumoniae*, approximately 75% of *G. mellonella* larvae died within 2 days, whereas larvae infected with the *pld*B:Tn, *ychK*:Tn, and *yjfP*:Tn strains showed significantly higher survival rates ($p < 0.0001$) (**Fig. 5B**) and approx. 65% of the larvae remained alive even after 5 days. The *ybfF*:Tn and y*qiA*:Tn mutants showed similar virulence as the WT *K.pneumoniae* MKP103 whereas, the *degP*:Tn mutant displayed reduced virulence compared to WT.

However, phenotypic results achieved by testing of the transposon mutants might be confounded by secondary mutations or polar effects. To rule out secondary mutations that may account for these phenotypes, we retrieved additional mutants from the Manoil *K. pneumoniae* 3-allele transposon mutant library representing individual clones where the transposons were localized within the same gene, but at a different location. Assessment of the virulence of different transposon mutants with insertions in *pldB* (n=3 available strains), *yjf*P (n=3) and *ychK* (n=2) (**Supplementary Figure S2**) all showed similar phenotypes, suggesting that transposon insertion in the respective gene accounts for the observed phenotype rather than secondary mutations. In conclusion, assessment of virulence of the *ych*K, *pld*B, and *yjf*P mutants supports a role of these enzymes in virulence of *K. pneumoniae*.

Biochemical and structure characteristics of YjfP and other serine hydrolases

Of the seven uncharacterized serine hydrolases that we identified in our ABPP proteomics studies, we were able to purify YjfP, YqiA, and PldB (**Supplementary figure S3**). To assess the substrate preference of recombinantly expressed and purified YjfP, YqiA, and PldB, we examined their ability

to cleave various commercially available fluorogenic substrates (**Fig. 6 A, B, C**). Our results indicated that YjfP effectively hydrolyzes saturated lipid esters with chain lengths from C2 to C4, showing a strong preference for the short-chain C2 acetate substrate (**Fig. 6A**). YqiA cleaved a variety of artificial substrates ranging from C2 to C10, with the highest activity observed for the C7 heptanoate substrate (**Fig. 6B**). PldB hydrolyzed saturated lipid esters ranging in chain length from C2 to C8, showing a particularly strong preference for the C2 and C4 chain lengths (**Fig. 6B**).

We also determined the crystal structures of YjfP and YqiA to 1.3 Å and 1.5 Å, respectively (**Fig. 6D, E, F, G, Suppl. Tables S4 and S5, Suppl. Figures S5, S6**), but we were unable to crystalize purified PldB protein. YjfP has the canonical α/β-hydrolase fold which is typical of serine hydrolases[58], with a catalytic triad conserved at residues Ser116, Asp187, and His221 (**Fig. 6D).** An 8-stranded β-sheet is central to the α/β-hydrolase fold, sandwiched between α-helices 1 and 8, and α-helices 2-7 **(Supplementary Figure S5).** Serine hydrolases often contain a flexible lid region between α-helices 4 and 5 that mediates substrate specificity[59]. However, this is absent in YjfP, which instead has a short loop connecting α-helices 4 and 5. Consistent with our gel filtration results (**Supplementary Figure S4**), the asymmetric unit of the YjfP crystal contains a homodimer that creates a closed cavity around the catalytic triad. Submission of the YjfP structure to PISA, an online tool to analyse protein interfaces, predicts the dimer interface to be biologically relevant, scoring a maximum CSS of 1.0[60]. The dimer interface covers 11 % of each protein surface area and is mediated mostly through β-strand 1 and α-helix 1. At the top of this interface, Asp188 and Arg220 from one chain form salt bridges with Arg220 and Asp188 from the second chain. These residues are on the same loops as Asp187 and His221 from the catalytic triad, forming a roof above the putative substrate binding site. Inside the substrate binding cavity there is discontinuous density, potentially corresponding to a cleaved substrate that may have co-purified (**Fig. 6E**). This density approaches a hydrophobic face within the cavity that would not accommodate longer carbon chains than butyrate, explaining the sharp drop-off in activity for C7 and longer chain substrates (**Fig. 6A**).

Similar to YjfP, YqiA has a canonical α/β hydrolase fold[58], with a conserved catalytic triad of residues Ser69, Asp147, and His172 (**Fig. 6F**). However, there are several features in YqiA that differ from YjfP. Firstly, the asymmetric unit contains a monomer, consistent with gel filtration results (**Supplementary Figure S4**), and PISA predicts there are no crystal contacts that are likely to create a dimer[60]. Unlike YjfP, the YqiA active site is much more open despite the presence of a small lid region. Within the oxyanion hole there is a chlorine atom and a hydrophobic face is formed around the active site (**Fig. 6G**). This hydrophobic, open face likely directs substrate specificity towards hydrophobic carbon chains. Since the lid region is small and removed from the active site, it might not accommodate the 4MU leaving group of the fluorogenic substrates well, which might explain the much lower activity rates of YqiA compared to YjfP.

Together, the substrate profiling and structural characterization of YjfP and YqiA suggest they are short-chain esterases. Giving an explanation for the observed substrate selectivity (**Fig. 6A), t**he YjfP structure showed that an acetate group would fit well into the small hydrophobic pocket near the active site Ser116, whereas chains longer than butyrate would not, thus). Our data suggest that YjfP may function as a deacetylase.

Discussion

Serine hydrolases play important roles in various biological processes of both bacteria and host cells yet our understanding of these enzymes in *K. pneumoniae* remains limited. Using a chemical proteomic approach, we have identified 10 previously uncharacterized serine hydrolases. Using transposon mutants of the hydrolases PldB, YchK, and YjfP we observed growth defects in co-culture models with HT29-MTX cells, human colonic organoids and in a *Galleria mellonella* infection model, suggesting putative roles in both gut colonization and infection. In the *G. mellonella* infection model, alternative clones with transposon insertion in the same gene displayed the same phenotype suggesting its specificity.

Based on previous annotation and bioinformatic analysis, the previously uncharacterized PldB, is a lysophospholipase L2 located at the cytoplasmic membrane. YjfP is annotated as a putatively cytosolic esterase. YchK which possesses a patatin-like phospholipase domain is predicted to be secreted. Of note, despite similarities of the phenotypes in the complex organoid and *G. mellonella* infection models, we observed some important differences that might give clues about the underlying molecular functions of these enzymes. Both the *pldB* and *yjfP*-deficient strains showed an increased susceptibility to AMPs, whereas the *ychK* mutant did not.

AMPs are short amphiphilic peptides that, in general, act by disrupting bacterial membranes. Polymyxin B was shown to exert its membrane-destabilizing effect by binding to the lipid A anchor of LPS in the outer membrane of Gram-negative bacteria[61]. AMPs produced by human cells, e.g., the defensins, are considered to act by similar mechanisms. In the human gut, the specialized secretory Paneth cells in the small intestine produce alpha-defensins (as reviewed by Bevins and Salzman[62]), whereas epithelial cells contribute through production of beta-defensins (see review by Gallo and Hooper[63]). In our colonic stem-cell derived organoid model, the presence of Paneth cells was indirectly detected, and we therefore assume that bacteria in the organoid-model are exposed to both alpha- and beta-defensins. Human beta-defensin 1 is expressed by HT29 cells[64] and thus may affect bacterial growth in the HT29-MTX co-culture model. Of note, AMPs are also important effectors of insect innate immunity (as reviewed by Stacek[65]), and *G. mellonella* has been shown to mount pathogen-specific AMP responses upon infection with diverse bacteria and fungi[66]. Thus, an increased susceptibility to AMPs could be detected in both organoid and HT29-MTX co-culture models as well as in the *G. mellonella* infection model.

The most pronounced increase in polymyxin B-sensitivity was observed for the *degP*-mutant, which is consistent with a previous study[27]. This mutant, however, did not show any fitness defect in the HT29-MTX model (and was hence not tested in organoids) and the reduction in virulence in the *G. mellonella* model was less pronounced (and less stable across different clones) compared to the *pldB* and *yjfP* mutants. This discrepancy could be explained by differences in the susceptibility to polymyxin B compared to the AMPs that are endogenously produced in the co-culture and infection models. However, this outcome might also indicate that a reduced susceptibility to AMPs might contribute to the phenotypes in the co-culture and infection models, but on its own is not sufficient to explain them. It is possible that the putative deficiency in cell envelope integrity in the *pld*B and *yjf*P mutants leads to multiple downstream effects that collectively contribute to reduced virulence and fitness.

We can only speculate about which mechanism PldB and YjfP may affect cell envelope integrity, but roles in membrane remodeling, tailoring modifications of LPS cell wall components, or posttranslational modifications of proteins that are involved in cell wall and LPS synthesis could be plausible. Of note, secondary acylation of LPS in *K. pneumoniae* affects susceptibility to polymyxin B and several other AMPs[67], suggesting that remodeling of the lipid A anchor through previously

unidentified hydrolases or transferases could affect cell membrane integrity and AMP susceptibility. However, cleavage of lipid substrates with longer chain fatty acid esters does not appear a likely physiological function of YjfP. The narrow substrate profile and structural characterization of this enzyme suggest that is a deacetylase, that may act on a small molecule, peptide or protein. PldB, in contrast accepts a broader range of substrates cleaving synthetic fluorogenic substrates up to C8 chain length. The interesting phenotypes associated with these SH mutants and the architecture of the YjfP (and YqiA) active sites, warrant further investigation into the native substrates of each enzyme.

The *pldB* and *yjfP* mutant also showed increased sensitivity to complement killing. Since complement activation involves pore formation in the outer membrane and complement resistance is mediated by the protective effects of LPS or capsule polysaccharide [68], these results support the notion that PldB and YjfP might also be partially responsible for the modulation of LPS production and/or constructing the outer membrane. Recently, another chemoproteomic study identified BT4193, a homolog of human dipeptidyl peptidase 4, in the Gram-negative gut commensal *Bacteroides thetaiotaomicron* [23]. Due to its periplasmic location, the authors suspected a role in cell envelope integrity and observed that a BT4193 mutant displayed increased sensitivity for killing by both vancomycin and polymyxin B. However, treatment of WT cells with a BT4193 inhibitor did not phenocopy these deficiencies, so the authors concluded that the phenotype of the ΔBT4193 mutant might be caused by a structural role of this protein rather than by its enzymatic function[23] . Whether the putative role of PldB and YjfP on AMP and complement susceptibility will be due to its enzymatic functions as a lipases or esterase or due to structural roles, remains to be determined.

In contrast to the cell-membrane associated putative lysophospholipase PldB and putative esterase YjfP, the putative phospholipase YchK is predicted to be secreted. As may be expected for a secreted phospholipase, the YchK-mutant did not show any phenotype related to susceptibility to AMP and envelope integrity. Secreted lipases have been described as virulence factors for a number of bacterial pathogens and their hydrolytic function mostly associated with the destruction of defense barrier and toxicity [69-71]. One interesting observation that we made is that *K. pneumoniae* is unable to grow in organoid media alone or in the DMEM medium alone used in the HT29-MTX culture. This means that to sustain growth in the organoid co-culture model, bacteria need to access nutrients from the host cell layers. Both the colon organoid and HT29-MTX monolayer produce a pronounced mucus layer. In the gut, the mucus layer, which is predominantly composed of glycoproteins, is an essential part of human colonic epithelia and acts as the primary defense against bacteria residing in the colon[72-74]. In the human gut, the mucus layer of colonic epithelia has a surface layer of phosphatidylcholine (PC) which contributes to barrier function and immune regulation [75]. Bacterial phospholipases in this layer can convert PC into lyso-PC, thereby disturbing the integrity and protective function of the mucus structure and enabling damage to epithelial cells [75-77]. For the gastric pathogen *H. pylori* secreted lipases are responsible for breaching a mucus-associated defensive phospholipid layer, allowing the pathogen to partially invade the gastric mucus [78,79]. A similar role is plausible for the putatively secreted patatin-like phospholipase YchK of *K. pneumoniae*. Its hydrolytic activity could enable either direct access to phospholipid-derived nutrients or contributing to the break-down of defense barriers that might facilitate cell invasion and extraction of nutrients. However, the origin of the surface layer of PC in the human colon is unclear (Review by [75]) and it might be derived from the ileum or jejunum. It thus remains to be determined if a similar PC layer is in fact found in our organoid model. An alternative role for YchK at the host-pathogen interface in the organoid model as well as in *Galleria infection* model could be that it directly acts on host cell membranes.

Our results indicate that PldB, YjfP and YchK are promising targets for further evaluation as anti-virulence targets. One of the last-resort antibiotics for treatment of infections with carbapenemase producing *K. pneumoniae* is the AMP colistin[80] . The emergence of colistin-resistance in the clinic is therefore of great concern[81] and strategies to reverse colistin resistance are being explored[82]. The

sensitization to AMPs observed for *pld*B, *yjf*P and *deg*P mutants is a significant finding and we suggest that inhibitors of either of these enzymes should be tested for synergy with colistin and other AMP antibiotics.

Another potential drug target that was identified in our dataset but was not validated further, is the carboxylesterase *Bio*H. This enzyme has a putative role in the biosynthesis of biotin[48] and the absence of viable mutants within the Manoil Lab transposon mutant library suggests that it might be essential. Of note, in *Mycobacterium tuberculosis,* biotin metabolism is already considered a viable antibacterial drug target pathway[83 84] , and efforts to target its three bioH isoenzymes are underway[85] . For ABPP, enzyme targets are identified through covalent interaction with a small molecule probe, thus focusing the set of targets that are often likely to be druggable and provides direct assays for development of target-specific inhibitors. There is an increasing pool of serine-hydrolase-reactive chemotypes that continue to produce target-specific inhibitors that can be used as tools to further investigate biological function while also sometime serving as antimicrobial drug candidates. The structural information of YjfP provided in this work may enable structure-based design of specific YjfP inhibitors. Alternatively, inhibitors may be identified through traditional target-based screening approaches[44], or through competitive ABPP which simultaneously assesses the selectivity profile of candidate inhibitors against all of the active serine hydrolase targets in a sample[17,20,86-88]. Importantly, if performed on live cells, as in the current study, cell-based competitive ABPP, can also confirm the accessibility of the targets to small molecule inhibitors[17,86].

We believe that further functional characterizations of the uncharacterized serine hydrolases identified will significantly enhance our understanding of *K. pneumoniae* pathogenesis and colonization and provide the basis for their validation as anti-virulence and antibacterial drug candidates that are urgently needed in times of emerging multidrug resistance of this critical priority pathogen.

Acknowledgements

This work was funded by a Centre for New Antibacterial Strategies (CANS) starting-grant through the Trond-Mohn Foundation to C.S.L. We are grateful for additional financial support through the Aurora Outstanding Career Development program at UiT through C.S.L. The research stay of M. J. U. at UMC Utrecht was generously supported by The National Graduate School in Infection Biology and Antimicrobials (IBA). LC-MS/MS analyses were carried out at the UiT Proteomics and Metabolomics Core Facility (PRiME). The PRiME is part of the National Network of Advanced Proteomics Infrastructure (NAPI), funded by the Research Council of Norway INFRASTRUKTUR-program (project number: 295910). We also thank Fernanda Paganelli for her support during the initial establishment of the organoid model, Janetta Top, Rob Willems and Bart W. Bardoel for helpful discussions, Coco Duizer for discussions in the lab, and Karin Strijbis for generously providing the Anti-MUC13 antibody, all from UMC Utrecht. Some of this work was supported by the New Zealand China - Maurice Wilkins Centre Collaborative Research Programme (to M.F.) and was conducted during tenure of The Sir Charles Hercus Health Research Fellowship of the Health Research Council of New Zealand (to M.F.). This research was undertaken in part using the MX2 beamline at the Australian Synchrotron, part of ANSTO, and made use of the ACRF detector.

Keywords: Virulence · Chemoproteomics · Organoids · *Galleria mellonella* · Bacterial colonization ·Lipases · Deacetylase

Ethics declaration

The organoids used were obtained from the Foundation Hubrecht Organoid Biobank (Utrecht, The Netherlands) under TC-Bio protocol number 14-008 and used according to informed consent.

Human blood was isolated after informed consent was obtained from all subjects in accordance with the Declaration of Helsinki. Approval was obtained from the medical ethics committee of the UMC Utrecht, The Netherlands

Competing interests

The authors declare no competing interests.

Author contributions

Conceptualization: C.S.L., M.J.U., Investigation: M.J.U., G.R., J.Z., T.U., L.v.E, P.H., F.M.; M.C.V., Data analysis: M.J.U., G.R., J.Z., T.U., L.v.E, P.H., M.C.V., M.B., M.F., M.R.d.Z., M.J., C.S.L., Supervision: C.S.L., M.J., M.R.d. Z., M.F., M. B., Funding acquisition: C.S.L., Writing – Original manuscript draft: M.J.U. and C.S.L., Writing - Editing: All authors.

References

1. Martin, R.M. & Bachman, M.A. Colonization, Infection, and the Accessory Genome of *Klebsiella pneumoniae*. *Frontiers in Cellular and Infection Microbiology* **8**(2018).
2. Navon-Venezia, S., Kondratyeva, K. & Carattoli, A. *Klebsiella pneumoniae*: a major worldwide source and shuttle for antibiotic resistance. *FEMS Microbiology Reviews* **41**, 252-275 (2017).
3. Gupta, A., Ampofo, K., Rubenstein, D. & Saiman, L. Extended Spectrum β Lactamase-producing *Klebsiella pneumoniae* Infections: a Review of the Literature. *Journal of Perinatology* **23**, 439-443 (2003).
4. Xu, L., Sun, X. & Ma, X. Systematic review and meta-analysis of mortality of patients infected with carbapenem-resistant *Klebsiella pneumoniae*. *Ann Clin Microbiol Antimicrob* **16**, 18 (2017).
5. WHO (2017). Fact Sheet on Antimicrobial Resistance. https://www.who.int/news-room/detail/27-02-2017-who-publishes-list-of-bacteria-for-which-new-antibiotics-are-urgently-needed.
6. Shon, A.S., Bajwa, R.P.S. & Russo, T.A. Hypervirulent (hypermucoviscous) *Klebsiella pneumoniae*. *Virulence* **4**, 107-118 (2013).
7. Lam, M.M.C. et al. Population genomics of hypervirulent *Klebsiella pneumoniae* clonal-group 23 reveals early emergence and rapid global dissemination. *Nature Communications* **9**, 2703 (2018).
8. Kluge, A.F. & Petter, R.C. Acylating drugs: redesigning natural covalent inhibitors. *Current opinion in chemical biology* **14**, 421-427 (2010).
9. Thornberry, N.A. & Weber, A.E. Discovery of JANUVIA™(Sitagliptin), a Selective Dipeptidyl Peptidase IV Inhibitor for the Treatment of Type2 Diabetes. *Current topics in medicinal chemistry* **7**, 557-568 (2007).
10. Bachovchin, D.A. & Cravatt, B.F. The pharmacological landscape and therapeutic potential of serine hydrolases. *Nature Reviews Drug Discovery* **11**, 52-68 (2012).
11. van Kasteren, S.I., Florea, B.I. & Overkleeft, H.S. Activity-Based Protein Profiling: From Chemical Novelty to Biomedical Stalwart. *Methods in molecular biology (Clifton, N.J.)* **1491**, 1-8 (2017).
12. Cravatt, B.F. Activity-Based Protein Profiling – Finding General Solutions to Specific Problems. *Israel Journal of Chemistry* **63**, e202300029 (2023).
13. Killinger, B.J., Brandvold, K.R., Ramos-Hunter, S.J. & Wright, A.T. Chemoproteomic Analyses by Activity-Based Protein Profiling. in *Mass Spectrometry-Based Chemical Proteomics* 67-99 (2019).
14. Fang, H. et al. Recent advances in activity-based probes (ABPs) and affinity-based probes (AfBPs) for profiling of enzymes. *Chemical Science* **12**, 8288-8310 (2021).
15. van Rooden, E.J. et al. Chemical Proteomic Analysis of Serine Hydrolase Activity in Niemann-Pick Type C Mouse Brain. *Frontiers in Neuroscience* **12**(2018).
16. Jessani, N., Liu, Y., Humphrey, M. & Cravatt, B.F. Enzyme activity profiles of the secreted and membrane proteome that depict cancer cell invasiveness. *Proceedings of the National Academy of Sciences* **99**, 10335-10340 (2002).
17. Lentz, C.S. et al. Identification of a *S. aureus* virulence factor by activity-based protein profiling (ABPP). *Nat Chem Biol* **14**, 609-617 (2018).

18. Keller, L.J. et al. Characterization of Serine Hydrolases Across Clinical Isolates of Commensal Skin Bacteria *Staphylococcus epidermidis* Using Activity-Based Protein Profiling. *ACS Infect Dis* **6**, 930-938 (2020).
19. Ortega, C. et al. Systematic Survey of Serine Hydrolase Activity in *Mycobacterium tuberculosis* Defines Changes Associated with Persistence. *Cell Chem Biol* **23**, 290-298 (2016).
20. Li, M. et al. Identification of cell wall synthesis inhibitors active against *Mycobacterium tuberculosis* by competitive activity-based protein profiling. *Cell Chem Biol* **29**, 883-896.e5 (2022).
21. Babin, B.M. et al. Identification of covalent inhibitors that disrupt *M. tuberculosis* growth by targeting multiple serine hydrolases involved in lipid metabolism. *Cell Chem Biol* **29**, 897-909.e7 (2022).
22. Hatzios, S.K. et al. Chemoproteomic profiling of host and pathogen enzymes active in cholera. *Nature chemical biology* **12**, 268-274 (2016).
23. Keller, L.J. et al. Chemoproteomic identification of a DPP4 homolog in Bacteroides thetaiotaomicron. *Nat Chem Biol* **19**, 1469-1479 (2023).
24. Zweerink, S. et al. Activity-based protein profiling as a robust method for enzyme identification and screening in extremophilic Archaea. *Nature Communications* **8**, 15352 (2017).
25. Fellner, M. et al. Biochemical and Cellular Characterization of the Function of Fluorophosphonate-Binding Hydrolase H (FphH) in *Staphylococcus aureus* Support a Role in Bacterial Stress Response. *ACS Infectious Diseases* **9**, 2119-2132 (2023).
26. Jo, J. et al. Development of Oxadiazolone Activity-Based Probes Targeting FphE for Specific Detection of *Staphylococcus aureus* Infections. *Journal of the American Chemical Society* **146**, 6880-6892 (2024).
27. Cortés, G., de Astorza, B., Benedí, V.J. & Albertí, S. Role of the htrA gene in *Klebsiella pneumoniae* virulence. *Infect Immun* **70**, 4772-6 (2002).
28. Meltzer, M. et al. Structure, function and regulation of the conserved serine proteases DegP and DegS of *Escherichia coli*. *Res Microbiol* **160**, 660-6 (2009).
29. Russell, A.B. et al. Diverse type VI secretion phospholipases are functionally plastic antibacterial effectors. *Nature* **496**, 508-12 (2013).
30. Merciecca, T. et al. Role of *Klebsiella pneumoniae* Type VI secretion system (T6SS) in long-term gastrointestinal colonization. *Sci Rep* **12**, 16968 (2022).
31. Nakamoto, N. et al. Gut pathobionts underlie intestinal barrier dysfunction and liver T helper 17 cell immune response in primary sclerosing cholangitis. *Nat Microbiol* **4**, 492-503 (2019).
32. Uddin, M.J., Overkleeft, H.S. & Lentz, C.S. Activity-Based Protein Profiling in Methicillin-Resistant *Staphylococcus aureus* Reveals the Broad Reactivity of a Carmofur-Derived Probe. *Chembiochem* **24**, e202300473 (2023).
33. Tyanova, S. et al. The Perseus computational platform for comprehensive analysis of (prote)omics data. *Nat Methods* **13**, 731-40 (2016).
34. Perez-Riverol, Y. et al. The PRIDE database resources in 2022: a hub for mass spectrometry-based proteomics evidences. *Nucleic acids research* **50**, D543-D552 (2022).
35. UniProt: the Universal Protein Knowledgebase in 2023. *Nucleic Acids Res* **51**, D523-d531 (2023).

36. Yu, N.Y. et al. PSORTb 3.0: improved protein subcellular localization prediction with refined localization subcategories and predictive capabilities for all prokaryotes. *Bioinformatics* **26**, 1608-1615 (2010).
37. Lesuffleur, T. et al. Differential expression of the human mucin genes MUC1 to MUC5 in relation to growth and differentiation of different mucus-secreting HT-29 cell subpopulations. *Journal of Cell Science* **106**, 771-783 (1993).
38. Vonk, A.M. et al. Protocol for Application, Standardization and Validation of the Forskolin-Induced Swelling Assay in Cystic Fibrosis Human Colon Organoids. *STAR Protoc* **1**, 100019 (2020).
39. Zomer-van Ommen, D.D. et al. Comparison of ex vivo and in vitro intestinal cystic fibrosis models to measure CFTR-dependent ion channel activity. *J Cyst Fibros* **17**, 316-324 (2018).
40. Howat, W.J. & Wilson, B.A. Tissue fixation and the effect of molecular fixatives on downstream staining procedures. *Methods* **70**, 12-9 (2014).
41. Heesterbeek, D.A. et al. Bacterial killing by complement requires membrane attack complex formation via surface-bound C5 convertases. *Embo j* **38**(2019).
42. Bhandari, B.K., Lim, C.S. & Gardner, P.P. TISIGNER.com: web services for improving recombinant protein production. *Nucleic Acids Research* **49**, W654-W661 (2021).
43. Luna-Vargas, M.P. et al. Enabling high-throughput ligation-independent cloning and protein expression for the family of ubiquitin specific proteases. *J Struct Biol* **175**, 113-9 (2011).
44. Jo, J. et al. Development of Oxadiazolone Activity-Based Probes Targeting FphE for Specific Detection of *S. aureus* Infections. *bioRxiv*, 2023.12.11.571116 (2023).
45. Ramage, B. et al. Comprehensive Arrayed Transposon Mutant Library of *Klebsiella pneumoniae* Outbreak Strain KPNIH1. *J Bacteriol* **199**(2017).
46. Chen, L., Mathema, B., Pitout, J.D., DeLeo, F.R. & Kreiswirth, B.N. Epidemic *Klebsiella pneumoniae* ST258 is a hybrid strain. *mBio* **5**, e01355-14 (2014).
47. Pitout, J.D., Nordmann, P. & Poirel, L. Carbapenemase-Producing *Klebsiella pneumoniae*, a Key Pathogen Set for Global Nosocomial Dominance. *Antimicrob Agents Chemother* **59**, 5873-84 (2015).
48. Wang, L. et al. Structural insight into the carboxylesterase BioH from *Klebsiella pneumoniae*. *Biochem Biophys Res Commun* **520**, 538-543 (2019).
49. Lesuffleur, T. et al. Differential expression of the human mucin genes MUC1 to MUC5 in relation to growth and differentiation of different mucus-secreting HT-29 cell subpopulations. *J Cell Sci* **106 (Pt 3)**, 771-83 (1993).
50. In, J. et al. Enterohemorrhagic *Escherichia coli* reduce mucus and intermicrovillar bridges in human stem cell-derived colonoids. *Cell Mol Gastroenterol Hepatol* **2**, 48-62.e3 (2016).
51. Sato, T. et al. Long-term expansion of epithelial organoids from human colon, adenoma, adenocarcinoma, and Barrett's epithelium. *Gastroenterology* **141**, 1762-72 (2011).
52. Yu, S. et al. Paneth Cell-Derived Lysozyme Defines the Composition of Mucolytic Microbiota and the Inflammatory Tone of the Intestine. *Immunity* **53**, 398-416.e8 (2020).
53. Domingues, M.M. et al. Biophysical characterization of polymyxin B interaction with LPS aggregates and membrane model systems. *Biopolymers* **98**, 338-44 (2012).

54. Merino, S., Camprubí, S., Albertí, S., Benedí, V.J. & Tomás, J.M. Mechanisms of *Klebsiella pneumoniae* resistance to complement-mediated killing. *Infect Immun* **60**, 2529-35 (1992).
55. Cortés, G., Astorza, B.d., Benedí, V.J. & Albertí, S. Role of the htrA Gene in *Klebsiella pneumoniae* Virulence. *Infection and Immunity* **70**, 4772-4776 (2002).
56. Ménard, G., Rouillon, A., Cattoir, V. & Donnio, P.-Y. Galleria mellonella as a Suitable Model of Bacterial Infection: Past, Present and Future. *Frontiers in Cellular and Infection Microbiology* **11**(2021).
57. Bruchmann, S., Feltwell, T., Parkhill, J. & Short, F.L. Identifying virulence determinants of multidrug-resistant *Klebsiella pneumoniae* in Galleria mellonella. *Pathog Dis* **79**(2021).
58. Ollis, D.L. et al. The alpha/beta hydrolase fold. *Protein Eng* **5**, 197-211 (1992).
59. Nardini, M., Lang, D.A., Liebeton, K., Jaeger, K.E. & Dijkstra, B.W. Crystal structure of pseudomonas aeruginosa lipase in the open conformation. The prototype for family I.1 of bacterial lipases. *J Biol Chem* **275**, 31219-25 (2000).
60. Krissinel, E. & Henrick, K. Inference of macromolecular assemblies from crystalline state. *J Mol Biol* **372**, 774-97 (2007).
61. Trimble, M.J., Mlynárčik, P., Kolář, M. & Hancock, R.E. Polymyxin: Alternative Mechanisms of Action and Resistance. *Cold Spring Harb Perspect Med* **6**(2016).
62. Bevins, C.L. & Salzman, N.H. Paneth cells, antimicrobial peptides and maintenance of intestinal homeostasis. *Nature Reviews Microbiology* **9**, 356-368 (2011).
63. Gallo, R.L. & Hooper, L.V. Epithelial antimicrobial defence of the skin and intestine. *Nat Rev Immunol* **12**, 503-16 (2012).
64. O'Neil, D.A. et al. Expression and regulation of the human beta-defensins hBD-1 and hBD-2 in intestinal epithelium. *J Immunol* **163**, 6718-24 (1999).
65. Stączek, S., Cytryńska, M. & Zdybicka-Barabas, A. Unraveling the Role of Antimicrobial Peptides in Insects. *International Journal of Molecular Sciences* **24**, 5753 (2023).
66. Mak, P., Zdybicka-Barabas, A. & Cytryńska, M. A different repertoire of *Galleria mellonella* antimicrobial peptides in larvae challenged with bacteria and fungi. *Developmental & Comparative Immunology* **34**, 1129-1136 (2010).
67. Clements, A. et al. Secondary acylation of *Klebsiella pneumoniae* lipopolysaccharide contributes to sensitivity to antibacterial peptides. *J Biol Chem* **282**, 15569-77 (2007).
68. Doorduijn, D.J., Rooijakkers, S.H., van Schaik, W. & Bardoel, B.W. Complement resistance mechanisms of *Klebsiella pneumoniae*. *Immunobiology* **221**, 1102-9 (2016).
69. Schmiel, D.H., Wagar, E., Karamanou, L., Weeks, D. & Miller, V.L. Phospholipase A of Yersinia enterocolitica Contributes to Pathogenesis in a Mouse Model. *Infection and Immunity* **66**, 3941-3951 (1998).
70. Sitkiewicz, I. et al. Emergence of a bacterial clone with enhanced virulence by acquisition of a phage encoding a secreted phospholipase A₂. *Proceedings of the National Academy of Sciences* **103**, 16009-16014 (2006).
71. Istivan, T.S. & Coloe, P.J. Phospholipase A in Gram-negative bacteria and its role in pathogenesis. *Microbiology* **152**, 1263-1274 (2006).
72. Braun, A., Stremmel, W. & Ehehalt, R. The Role of Phospholipids Within the Intestinal Mucosal Barrier. *Z Gastroenterol* **49**, A11 (2011).
73. Swidsinski, A. et al. Mucosal flora in inflammatory bowel disease. *Gastroenterology* **122**, 44-54 (2002).

74. Stremmel, W. et al. Mucosal protection by phosphatidylcholine. *Dig Dis* **30 Suppl 3**, 85-91 (2012).
75. Ehehalt, R., Braun, A., Karner, M., Füllekrug, J. & Stremmel, W. Phosphatidylcholine as a constituent in the colonic mucosal barrier—Physiological and clinical relevance. *Biochimica et Biophysica Acta (BBA) - Molecular and Cell Biology of Lipids* **1801**, 983-993 (2010).
76. Stremmel, W. et al. Phosphatidylcholine passes through lateral tight junctions for paracellular transport to the apical side of the polarized intestinal tumor cell-line CaCo2. *Biochimica et Biophysica Acta (BBA) - Molecular and Cell Biology of Lipids* **1861**, 1161-1169 (2016).
77. Tannaes, T., Bukholm, I.K. & Bukholm, G. High relative content of lysophospholipids of *Helicobacter pylori* mediates increased risk for ulcer disease. *FEMS Immunology & Medical Microbiology* **44**, 17-23 (2005).
78. Goggin, P.M. et al. Surface hydrophobicity of gastric mucosa in Helicobacter pylori infection: effect of clearance and eradication. *Gastroenterology* **103**, 1486-90 (1992).
79. Mauch, F., Bode, G., Ditschuneit, H. & Malfertheiner, P. Demonstration of a phospholipid-rich zone in the human gastric epithelium damaged by *Helicobacter pylori*. *Gastroenterology* **105**, 1698-704 (1993).
80. Munoz-Price, L.S. et al. Clinical epidemiology of the global expansion of *Klebsiella pneumoniae* carbapenemases. *Lancet Infect Dis* **13**, 785-96 (2013).
81. van Duin, D. & Doi, Y. Outbreak of Colistin-Resistant, Carbapenemase-Producing *Klebsiella pneumoniae*: Are We at the End of the Road? *J Clin Microbiol* **53**, 3116-7 (2015).
82. Han, R. et al. The antihelminth drug rafoxanide reverses chromosomal-mediated colistin-resistance in *Klebsiella pneumoniae*. *mSphere* **8**, e0023423 (2023).
83. Park, S.W. et al. Target-based identification of whole-cell active inhibitors of biotin biosynthesis in *Mycobacterium tuberculosis*. *Chem Biol* **22**, 76-86 (2015).
84. Salaemae, W., Booker, G.W. & Polyak, S.W. The Role of Biotin in Bacterial Physiology and Virulence: a Novel Antibiotic Target for *Mycobacterium tuberculosis*. *Microbiol Spectr* **4**(2016).
85. Xu, Y. et al. Three enigmatic BioH isoenzymes are programmed in the early stage of mycobacterial biotin synthesis, an attractive anti-TB drug target. *PLoS Pathog* **18**, e1010615 (2022).
86. Chen, L., Keller, L.J., Cordasco, E., Bogyo, M. & Lentz, C.S. Fluorescent Triazole Urea Activity?Based Probes for the Single?Cell Phenotypic Characterization of *Staphylococcus aureus*. 5699-5703 (Weinheim ; [New York] :, 2019).
87. Prothiwa, M. & Böttcher, T. Competitive profiling for enzyme inhibitors using chemical probes. *Methods Enzymol* **633**, 49-69 (2020).
88. Baggelaar, M.P. & Van der Stelt, M. Competitive ABPP of Serine Hydrolases: A Case Study on DAGL-Alpha. *Methods Mol Biol* **1491**, 161-169 (2017).

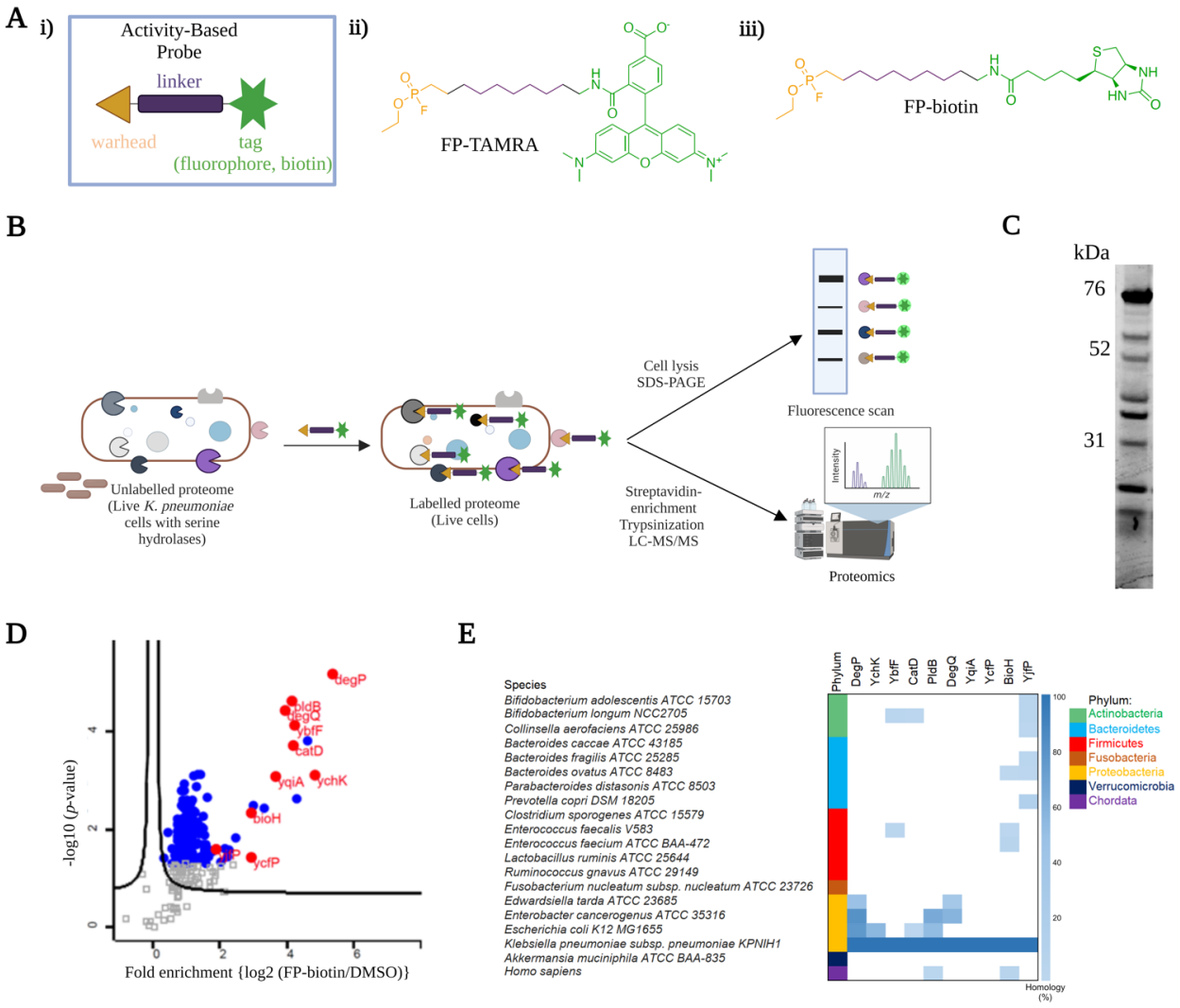

Figure 1. **Chemoproteomic identification of serine hydrolases in *K. pneumoniae*. A)** Schematic drawing of the features of Activity-based probes (ABPs) (i) and the chemical structures of the ABPs FP-TAMRA (ii) and FP-biotin (iii) that were used in this study. **B**) Schematic overview of general workflow for activity-based protein profiling (ABPP) of serine hydrolases in live *K. pneumoniae*. Fluorophosphonate-based ABPs selectively bind to accessible and active serine hydrolase species. Fluorescently tagged ABPs allow their visualization by SDS-PAGE analysis and fluorescence scanning, whereas biotinylated probes are used for streptavidin-enrichment and identification via LC-MS/MS or they can be visualized using a fluorescent tag through SDS-PAGE and in-gel fluorescence analysis. **C)** SDS-PAGE analysis of *K. pneumoniae* MKP103 live cells labeled with FP-TMR for 60 min at 37°C. The graph depicts fluorescent scans in the Cy3 (520nm) channel utilizing the Amersham™ Typhoon™ 5 (cytiva) imaging system. **D)** Volcano plot of *K. pneumoniae* proteins identified by LC-MS/MS that were enriched after FP-biotin treatment compared to a vehicle-treated control dataset. A two-tailed two-sample t-test was conducted to compare cells labeled with DMSO and FP-biotin. Significantly enriched hits are highlighted with blue dots, significantly enriched 10 SHs are indicated with red dots, and enriched but not significant hits are marked with grey rectangles. **E)** Heatmap of homologs of *K. pneumoniae* serine hydrolases across 20 representative gut commensal bacterial species and in humans (Chordata), as sourced from the Human Microbiome Project Reference Genomes for the Gastrointestinal Tract database using BLAST-P. In the heatmap, each filled cell indicates that the species has a homolog of the *K. pneumoniae* SHs, as determined by a threshold e-value of 1×10^{-10}; white background denotes the absence of a homolog.

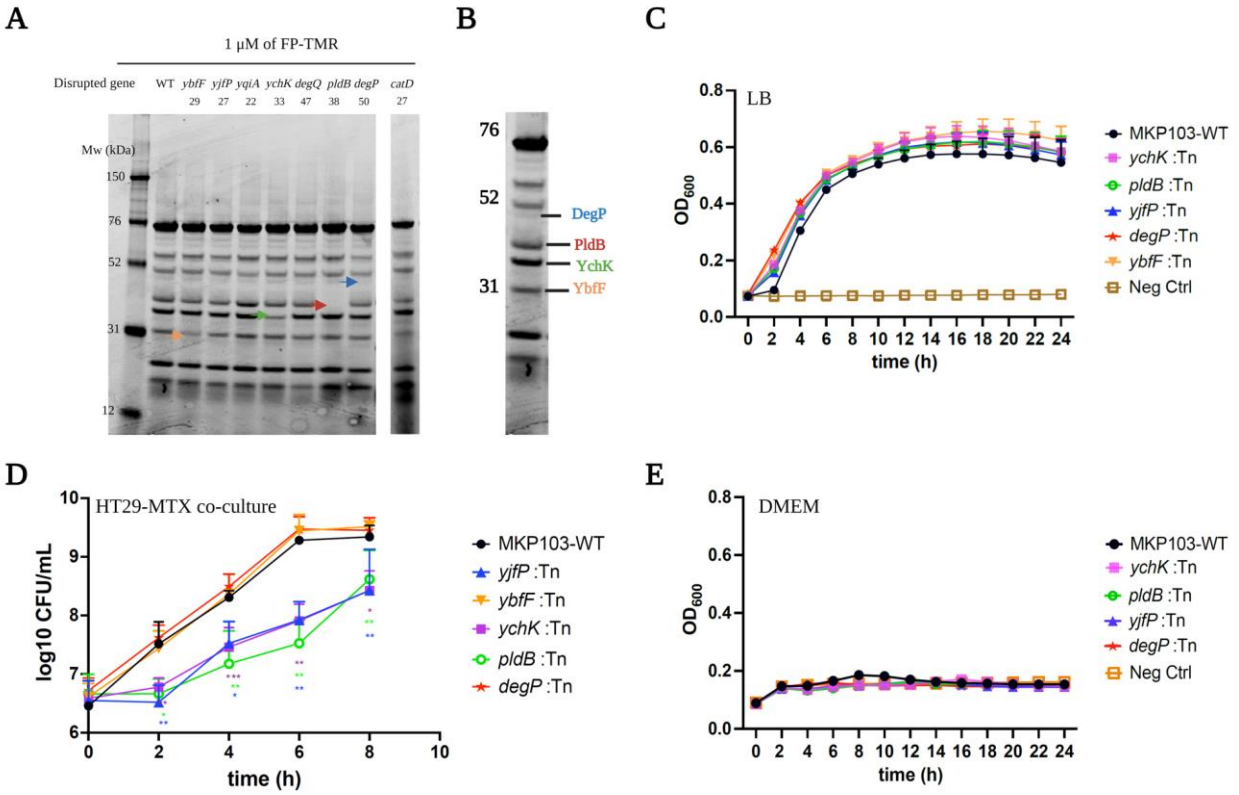

Figure 2. **Functional validation of *K. pneumoniae* transposon mutant strains**. **A)** FP-TMR labeling profiles of *K. pneumoniae* transposon mutant strains with insertions in the indicated serine hydrolase genes. Live cells were labelled with FP-TMR and lysed prior to SDS-PAGE analysis and fluorescence scanning. Arrowheads indicate labeled proteins disappearing in individual mutant strains (Red arrowhead: PldB, blue arrowhead: DegP, green arrowhead: YchK, and orange arrowhead: YbfF). The experiment was performed three times with similar results. B**)** Annotated FP-TAMRA profile of *K. pneumoniae* indicating four identified probe targets. **C)** Growth curves of *K. pneumoniae* WT and SH-deficient transposon mutants in LB media, n=3 biologically independent samples. **D)** Analysis of bacterial growth in HT29-MTX co-culture model. The graph shows bacterial CFUs (log10 CFU/mL) at different time points (0, 2, 4, 6, and 8 hours) after adding *K. pneumoniae* WT and SH-deficient transposon mutants to HT29-MTX cells at an MOI of 20. Statistical significance was assessed using two-way ANOVA test with post hoc Dunnet''s multiple comparisons tests compared with wild type (*p < 0.05, **p < 0.01, ***p < 0.001). **E**) Growth curves of *K. pneumoniae* WT and SH-deficient transposon mutants in DMEM media without FBS. Growth curves in B-E show means ± standard deviation of n=3 independent biological culture replicates.

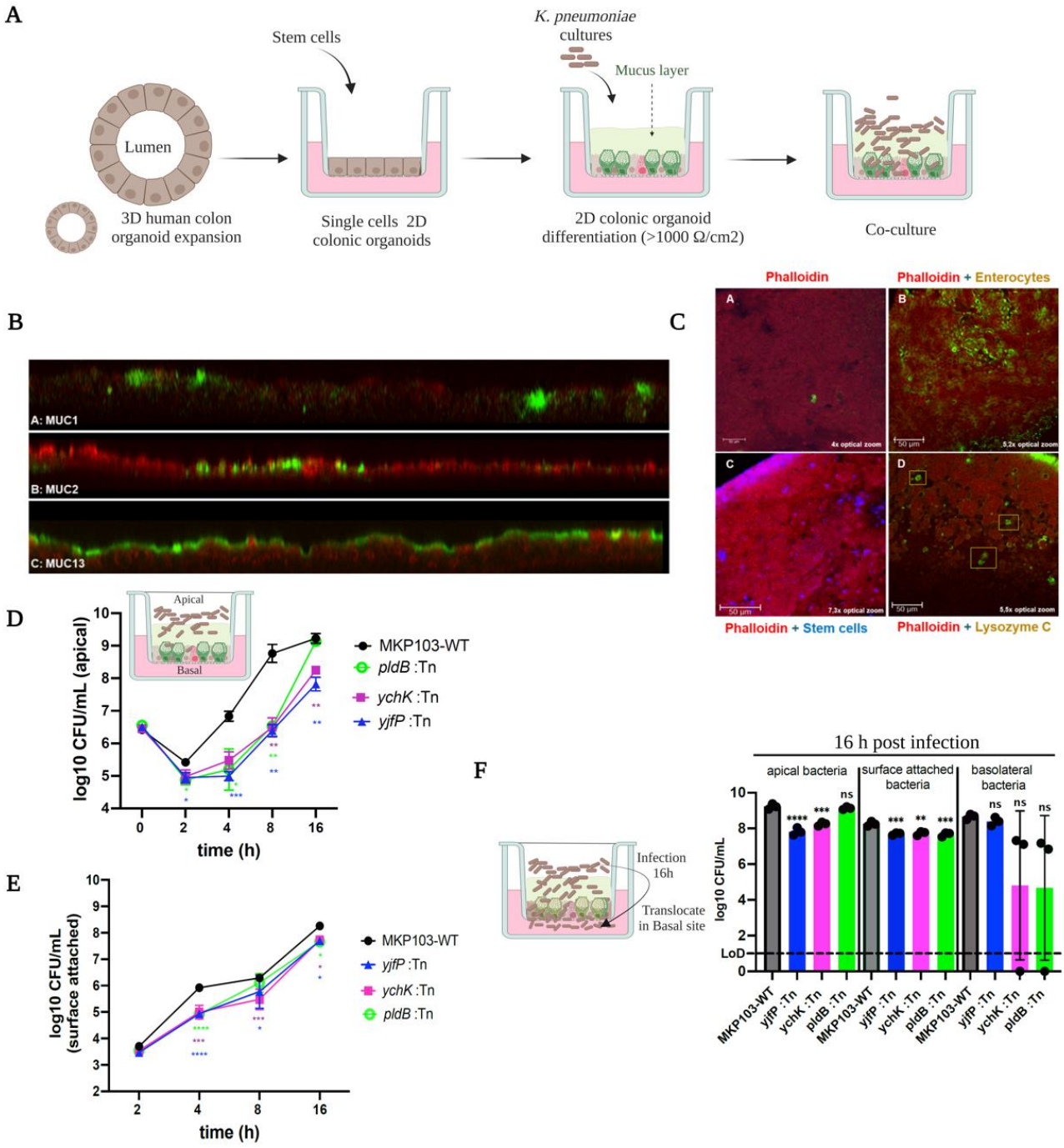

Figure 3. Assessment of SH-deficient *K. pneumoniae* mutants in 2D colonic organoid co-culture model. **A)** Schematic representation of the establishment and differentiation of 2D organoid cultures, including co-culturing with *K. pneumoniae* cultures. **B)** Sideview of Methacarn fixed organoid stained with Wheat Germ Agglutinin conjugated to Alexa fluorTM647 and anti-MUC antibodies combined with Alexa fluorTM488goat anti-mouse or Alexa fluorTM488 goat anti-rabbit. WGA (red) labels the cell layer as well as the mucus layer. (A) Anti-MUC1 (green) binds to the MUC1 mucin, present in the organoid samples in a relatively low abundance. The side view shows co-localization of WGA and MUC1, mainly visible at the ends of the picture. (B) Anti-MUC2 and WGA co-localize,

visible in the middle part of the side view. (C) Anti-MUC13 (green) binds to the MUC13 mucin present in these organoid samples. WGA and anti-MUC13 co-localize, visible primarily on the right end of the image, where the red and green signal are at the same height. 40x magnification. **C)** Methacarn-fixed organoid cultures stained with antibodies against villin, sox9 and lysozyme C. Scale bar to represent size. (A) Negative control stained with only Phalloidin-iFluor 633 (red), Alexa fluorTM488 goat anti-mouse and Alexa fluorTM488 goat anti-rabbit (green) and Alexa fluorTM405 goat anti-rabbit (blue). 10x magnification, 4x optical zoom. (B) Organoids stained with Phalloidin-iFluor 633 to visualize the F-actin filaments of the cells (red) and anti-villin with Alexa fluorTM 488 goat anti-mouse(green) to stain villin cells. 10x magnification, 5,2x optical zoom. (C) Organoids stained with Phalloidin-iFluor 633 to visualize the F-actin filaments of the cells (red) and anti-sox9 with Alexa fluorTM 405goat anti-rabbit (blue) to stain stem cells. 10x magnification, 7,3x optical zoom. (D) Organoids stained with Phalloidin-iFluor 633 to visualize the F-actin filaments of the cells (red) and DAKOA099 with Alexa fluorTM 488 goat anti-rabbit (green) to stain lysozyme C which is secreted by Paneth cells. Yellow boxes show individual Paneth cells. 10x magnification, 5,5x optical zoom. **D)** Bacterial counts (log10 CFU/mL) in the apical part of organoid co-cultures measured at 0, 2, 4, 8, and 16 h following incubation with *K. pneumoniae* WT and SH-deficient mutants on a 2D organoid monolayer. A two-way ANOVA test with Dunnett's multiple comparisons test was used to compare with the wild type (*$p < 0.05$, **$p < 0.01$, ***$p < 0.001$). **E)** Bacterial counts (log10 CFU/mL) for surface-attached bacteria to the organoid co-cultures, were measured at 0, 2, 4, 8 and 16 h following incubation with *K. pneumoniae* WT and SH-deficient mutants on a 2D organoid monolayer. A two-way ANOVA test with Dunnett's multiple comparisons test was used, comparing mutants to the wild type, with significance levels noted as *$p < 0.05$, **$p < 0.01$, ***$p < 0.001$, ****$p < 0.0001$. **F)** *K. pneumoniae* WT and SH-deficient mutants counts (log10 CFU/mL) in the apical part, surface-attached and the basolateral compartments 16 h post infection. LoD is the lower limit of detection level. Dunnett's one-way ANOVA was used for comparison to the WT (**$p < 0.01$, ***$p < 0.001$, ****$p < 0.0001$, ns indicates no significant difference).

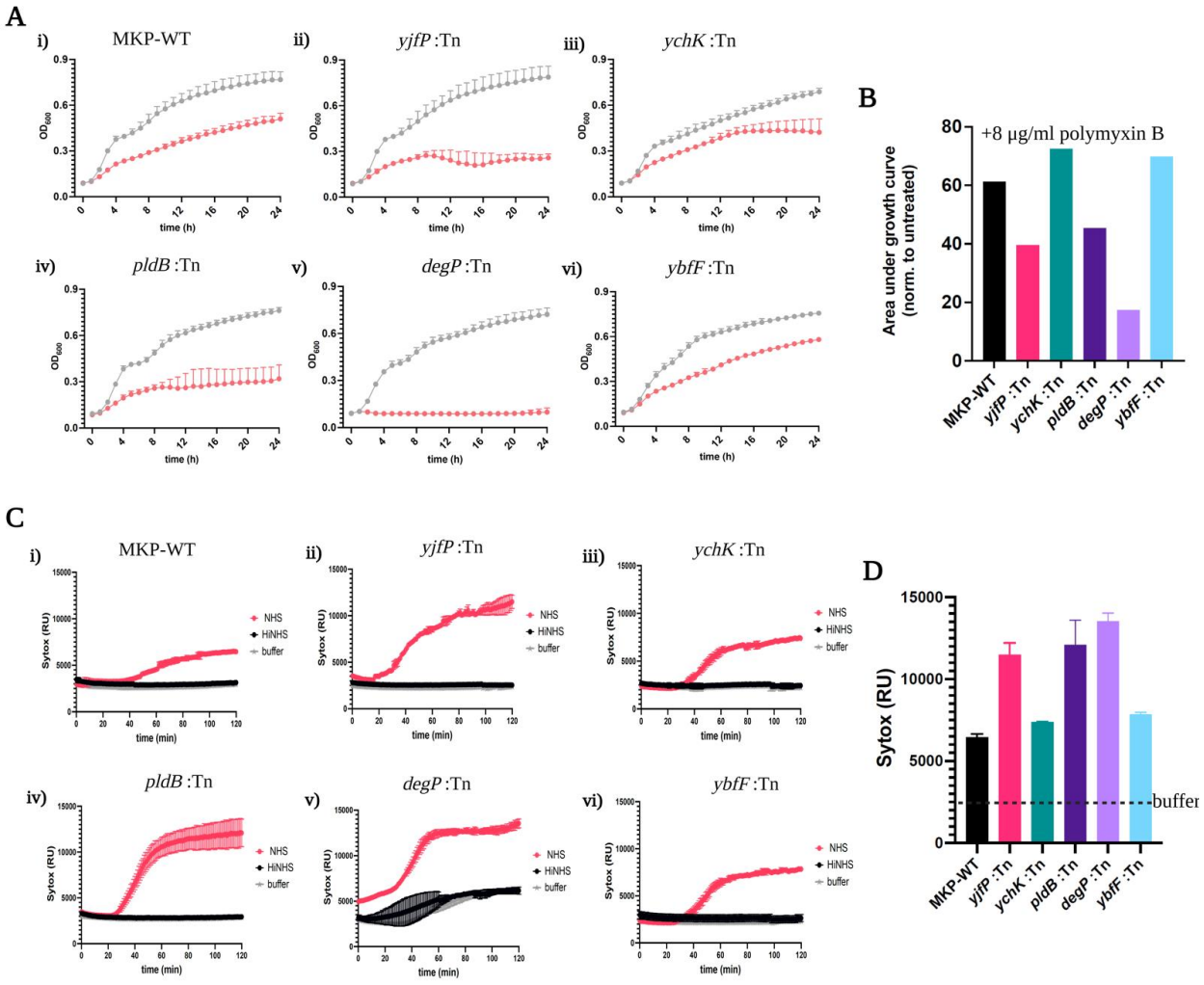

Figure 4. **PldB, YjfP, and DegP confers resistance to envelope stressor polymyxin B and to complement killing**. **A)** The growth of *K. pneumoniae* strains in absence (grey) or presence of 8 mg/ml polymyxin B (red) (mean ± s.e.m.; n = 5 independent replicates). B) Quantification of the area under the growth curve for treatment with polymyxin B was normalized to the growth curve of untreated cultures. **C)** Inner membrane permeabilization was evaluated in *K. pneumoniae* WT and its transposon mutants exposed to either 10% normal human serum (NHS) or 10% heat-inactivated NHS (HiNHS). The bacteria were incubated at 37°C with 1 µM SYTOX Green nucleic acid stain and SYTOX fluorescence intensity was monitored at 1 min intervals for 120 min using a microplate reader. The presented data are the mean ± standard deviation from two independent experiments. **D)** SYTOX Green fluorescence intensity, measured after 120 min of exposure to 10% NHS as described in C. The data are presented as mean ± standard deviate on from two independent experiments. The dashed line refers to buffer permeabilization signal (RPMI + SytoxGreen).

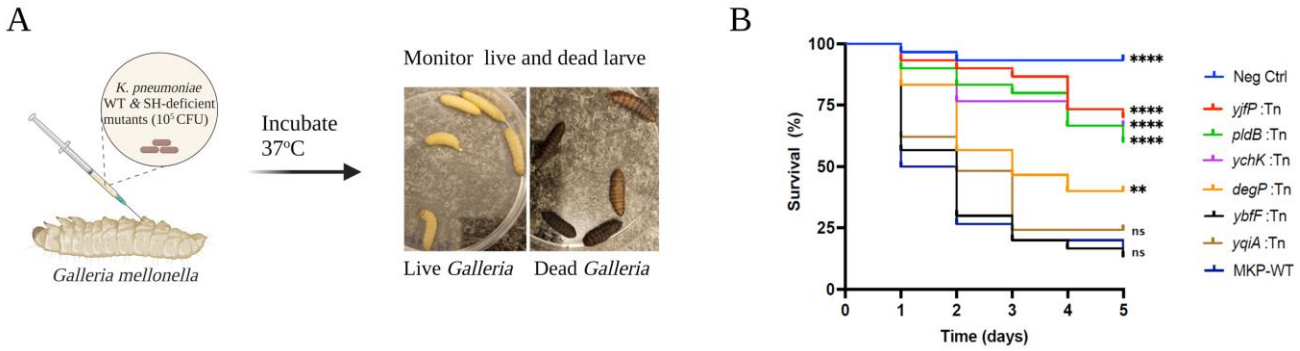

Figure 5. **Infection of *G. mellonella* with *K. pneumoniae* strains.** **A)** Schematic diagram illustrating the experimental process: Groups of *G. mellonella* larvae were injected with *K. pneumoniae* WT or SH-deficient transposon mutants and incubated at 37 °C for up to 5 days. Bacterial virulence was evaluated by monitoring of live and dead larvae. **B)** Kaplan–Meier (KM) survival plots of *G. mellonella* larvae after inoculation of the *K. pneumoniae* WT and SH-deficient mutants. Plots show an average of 3 independent experiments with 10 larvae per group with mortality monitored daily for 5 day (N= 210). Larvae injected with PBS were used as negative control. Mutants displaying a significant difference in survival compared to the WT were determined by the log-rank (Mantel–Cox) test and are denoted (**** $p < 0.0001$, ** $p < 0.05$, ns = not significantly different).

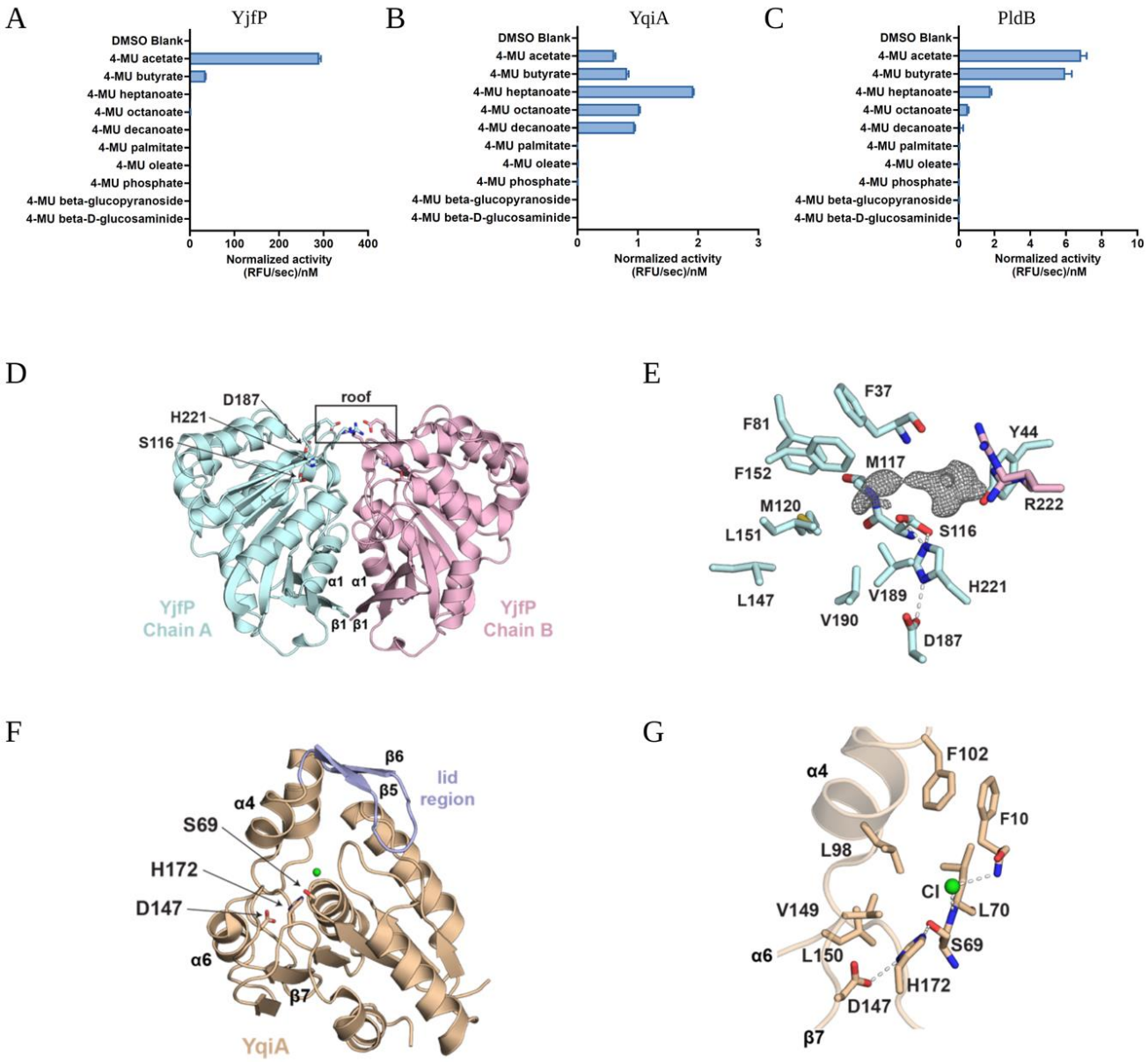

Figure 6. Biochemical characterization of YjfP, YqiA, and PldB and structure of hydrolases YjfP and YqiA. Normalized cleavage rate (, in relative fluorescent unit (RFU)/s per nM of protein) of 4-methylumbelliferone (4-MU) substrates by YjfP (**A**), by YqiA (**B**), and by PldB. (**C**). The presented bars represent the mean ± standard deviation (n = 3 technical replicates). **D**) YjfP crystallised as a dimer (cyan and pink), where the dimer interface is mediated by connections across β strands 1 and α helices 1 from each chain. Two salt bridges are formed at the top of the dimer, creating a roof above a putative substrate binding cavity. This cavity contains the catalytic triad; Ser116, Asp187, and His221. **E**) Interactions are shown between side chains of the catalytic triad (modelled in two conformations). Displayed around Ser116 is the mFo-DFc map contoured at 3.5 for a putative ligand. This putative ligand likely interacts with a hydrophilic portion of the active site (Tyr44, Ser116, and Arg222 modelled in two conformations). Part of the density is in the oxyanion hole, coordinated by backbone amides from Met117 and Phe37. Beyond the oxyanion hole, several hydrophobic side chains are shown. **F**) YqiA (beige) crystallised as a monomer, where β strands 4 and 5 form a lid region. The catalytic triad (Ser69, Asp147, His172) is more exposed than in the YjfP structure. **G**) Interactions between side chains of the catalytic triad are shown. A chlorine atom (green) is modelled in the oxyanion hole coordinated by backbone amides of Leu70 and Phe10. Several hydrophobic side residues on α helix 4 and a loop between β strand 7 and α helix 6 are likely important for substrate recognition.

Table 1. Overview of serine hydrolases identified in *Klebsiella pneumoniae subsp. pneumoniae* KPNIH1. Refer to Supplementary Dataset **1** and Supplementary Table **2**.

	Gene name	**Functional Annotation (putative) (Pfam)**	**Predicted location (Putative) (PSORTb)**	**% Homology with *H. sapiens* protein**	**MW [kDa]**
KPSH 1	*degP*	Trypsin-like peptidase	Periplasmic	-	49.5
KPSH 2	*ychK*	Patatin-like phospholipase	Extracellular	-	33.3
KPSH 3	*ybfF*	AB_Hydrolase 6	Unknown	-	28.5
KPSH 4	*catD*	Hydrolase 4	Cytoplasmic	-	27.3
KPSH 5	*pldB*	Hydrolase 4	Cytoplasmic membrane	25%	38.2
KPSH 6	*degQ*	Trypsin-like peptidase	Periplasmic	-	47.2
KPSH 7	*yqiA*	UPF0227	Cytoplasmic	-	21.5
KPSH 8	*ycfP*	UPF0227	Cytoplasmic	-	21.1
KPSH 9	*bioH*	AB_Hydrolase 1	Cytoplasmic	30%	28.3
KPSH 10	*yjfP*	Peptidase S9	Unknown	-	26.5

Supporting Information

Activity-Based Protein Profiling Identifies *Klebsiella pneumoniae* Serine Hydrolases with Potential Roles in Host-Pathogen Interactions

Md Jalal Uddin[1], George Randall[2], Jiyun Zhu[3], Tulsi Upadhyay[3], Laura van Eijk[4], Paul B. Stege[4], Frerich M. Masson[4], Marco C. Viveen[4], Matthew Bogyo[3], Matthias Fellner[2], Marcel R. de Zoete [4], Mona Johannessen[1] and Christian S. Lentz [1]

1. Centre for New Antibacterial Strategies (CANS) and Department of Medical Biology (IMB), UiT—The Arctic University of Norway, 9019 Tromsø, Norway

2. Biochemistry Department, School of Biomedical Sciences, University of Otago, Dunedin 9054, New Zealand

3. Department of Pathology, Stanford University School of Medicine, Stanford, California 94305, United States

4. Department of Medical Microbiology, UMC Utrecht, Utrecht, 3584 CX, The Netherlands

Table of Contents

Supplementary tables

Table S1. List of bacterial strains used in this study.

Strain	Description	Reference/Source
K. pneumoniae MP103	KPNIH1 derivative with the KPC-3 carbapenemase-encoding gene deleted and Parent strain of Moinul Transposon Mutant Library	[1]
degP:Tn	Transposon insertion mutant in MKP103 KPNIH1_04540	
ychK:Tn	Transposon insertion mutant in MKP103 KPNIH1_15760	
ybfF:Tn	Transposon insertion mutant in MKP103 KPNIH1_07725	
catD:Tn	Transposon insertion mutant in MKP103 KPNIH1_12245	
pldB:Tn	Transposon insertion mutant in MKP103 KPNIH1_00895	
degQ:Tn	Transposon insertion mutant in MKP103 KPNIH1_23755	
yjfP:Tn	Transposon insertion mutant in MKP103 KPNIH1_02230	

Table S2. List of serine hydrolases identified in *K. pneumoniae* by MS-ABPP

Gene	Previous annotation	MW [kDa]	Strain KPNIH1 locus tag
degP	Serine endoprotease	49,5	KPNIH1_04540
ychK	Patatin-like phospholipase	33,3	KPNIH1_15760
ybfF	Acyl-CoA esterase	28,5	KPNIH1_07725
catD	3-oxoadipate enol-lactonase	27,3	KPNIH1_12245
pldB	Lysophospholipase L2	38,2	KPNIH1_00895
degQ	Serine endoprotease	47,2	KPNIH1_23755
YqiA	Esterase	21,5	KPNIH1_22780
YcfP	Esterase	21,1	KPNIH1_09915
bioH	Pimeloyl-ACP methyl ester esterase	28,3	KPNIH1_24570
yjfP	Esterase	26,5	KPNIH1_02230

Table S3. The homology percentage data used for Figure 1E.

All BLASTp results for a homolog of the K. pneumoniae SHs are provided in a separate Excel file

	DegP	YchK	YbfF	CatD	PldB	DegQ	YqiA	YcfP	bioH	YjfP
Bifidobacterium adolescentis ATCC 15703	0	0	0	0	0	0	0	0	0	28.4
Bifidobacterium longum NCC2705	0	0	26.6	24.3	0	0	0	0	0	27.4
Collinsella aerofaciens ATCC 25986	0	0	0	0	0	0	0	0	0	24.8
Bacteroides caccae ATCC 43185	0	0	0	0	0	0	0	0	0	
Bacteroides fragilis ATCC 25285	0	0	0	0	0	0	0	0	0	25.7
Bacteroides ovatus ATCC 8483	0	0	0	0	0	0	0	0	20.0	24.4
Parabacteroides distasonis ATCC 8503	0	0	0	0	0	0	0	0	0	
Prevotella copri DSM 18205	0	0	0	0	0	0	0	0	0	41.3
Clostridium sporogenes ATCC 15579	0	0	0	0	0	0	0	0	0	0
Enterococcus faecalis V583	0	0	26.6	0	0	0	0	0	23.6	0
Enterococcus faecium ATCC BAA-472	0	0	0	0	0	0	0	0	29.3	0
Lactobacillus ruminis ATCC 25644	0	0	0	0	0	0	0	0	0	0
Ruminococcus gnavus ATCC 29149	0	0	0	0	0	0	0	0	0	0
Fusobacterium nucleatum subsp. nucleatum ATCC 23726	0	0	0	0	0	0	0	0	0	0
Edwardsiella tarda ATCC 23685	77.9	0	0	0	0	62.0	0		0	0
Enterobacter cancerogenus ATCC 35316	91.9	0	0	0	84.9	82.0	0	90.0	0	0
Escherichia coli K12 MG1655	90.2	81.1	0	24.7	79.7	0	0	0	0	0
Klebsiella pneumoniae subsp. pneumoniae KPNIH1	100.0	100.0	100.0	100.0	100.0	100.0	100.0	100.0	100.0	100.0
Akkermansia muciniphila ATCC BAA-835	0	0	0	0	0	0	0	0	0	0
Homo sapiens	0	0	0	0	25.2				30.2	

Table S4. Collection statistics of x ray crystallography datasets used to determine the structures of YjfP and YqiA. Values in parentheses refer to the high-resolution shell.

	YjfP	**YqiA**
Beamline	Australian Synchrotron MX2	Australian Synchrotron MX2
Wavelength (Å / keV)	0.954 / 13.00	0.954 / 13.00
Detector	DECTRIS EIGER X 16M	DECTRIS EIGER X 16M
Space group	*C* 2	*P* 3_2 2
a, b, c (Å)	102.71 68.20 65.36	62.46 62.46 80.36
α, β, γ (°)	90.00 77.16 90.00	90.00 90.00 120
Rotation range (°)	250	310
Resolution (Å)	45.11-1.30 (1.32-1.30)	44.87-1.50 (1.53-1.50)
Total Reflections	513,218 (23,779)	507,705 (23,786)
Unique Reflections	106,974 (5,160)	29,609 (1,434)
Multiplicity	4.8 (4.6)	17.1 (16.60)
Completeness (%)	99.2 (97.4)	100.00 (100.00)
I/σ(I)	9.6 (1.7)	13.8 (1.7)
$CC_{1/2}$	0.998 (0.369)	0.999 (0.568)
R_{merge}	0.115 (2.702)	0.121 (5.951)
R_{pim}	0.088 (2.083)	0.043 (2.148)

Table S5. Refinement and validation statistics of YjfP and YqiA crystal structures.

	YjfP	**YqiA**
PDB ID	9BD4	9BI7
Resolution Range (Å)	45.11-1.30	44.87-1.50
Reflections, working	101,407	28,024
Reflections, free	5,336	1,528
R_{work} (%)	16.13	17.46
R_{free} (%)	17.48	21.31
Number of residues	479	192
Number of waters	305	94
Ligand		2 Ca, 1 Cl
Average *B* factors (Å^2)	16.22	30.84
Ligands		23.88
Waters	25.01	33.35
RMSD		
Bonds (Å)	0.006	0.009
Angles (°)	0.89	1.00
Ramachandran		
Favoured (%)	97.89	98.42
Outliers (%)	0	0
Rotamer outliers (%)	0.25	0
Molprobity score	0.88	1.08

Supplementary figures

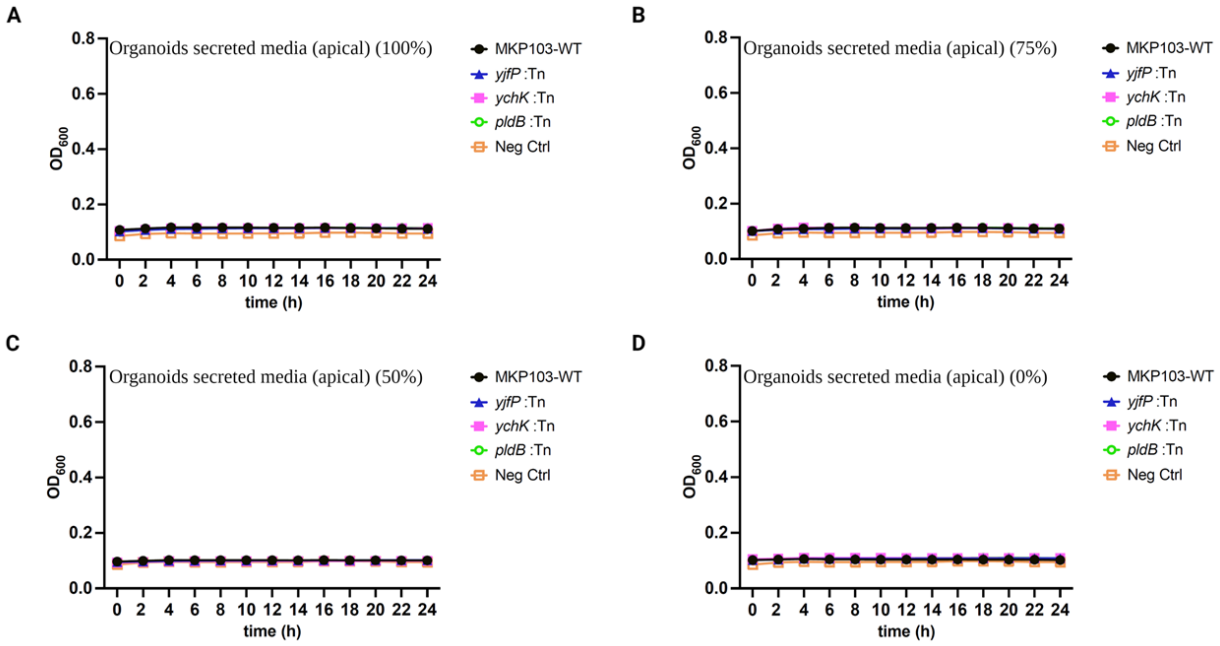

Figure S1. **Growth curves of *K. pneumoniae* MKP103 and isogenic SH-deficient transposon mutant on organoids secreted substances**. The growth curves of *K. pneumoniae* and SH-deficient mutants were measured over 24 hours in: **A**) media containing 100% secretions from organoid monolayers (collected from the apical side), **B**) media with 75% organoid secretions, **C**) media with 50% organoid secretions, and **D**) media without organoid secretions (consisting only of differentiated organoid media). Growth curves in A-D show means standard deviation of n=3 independent biological culture replicates

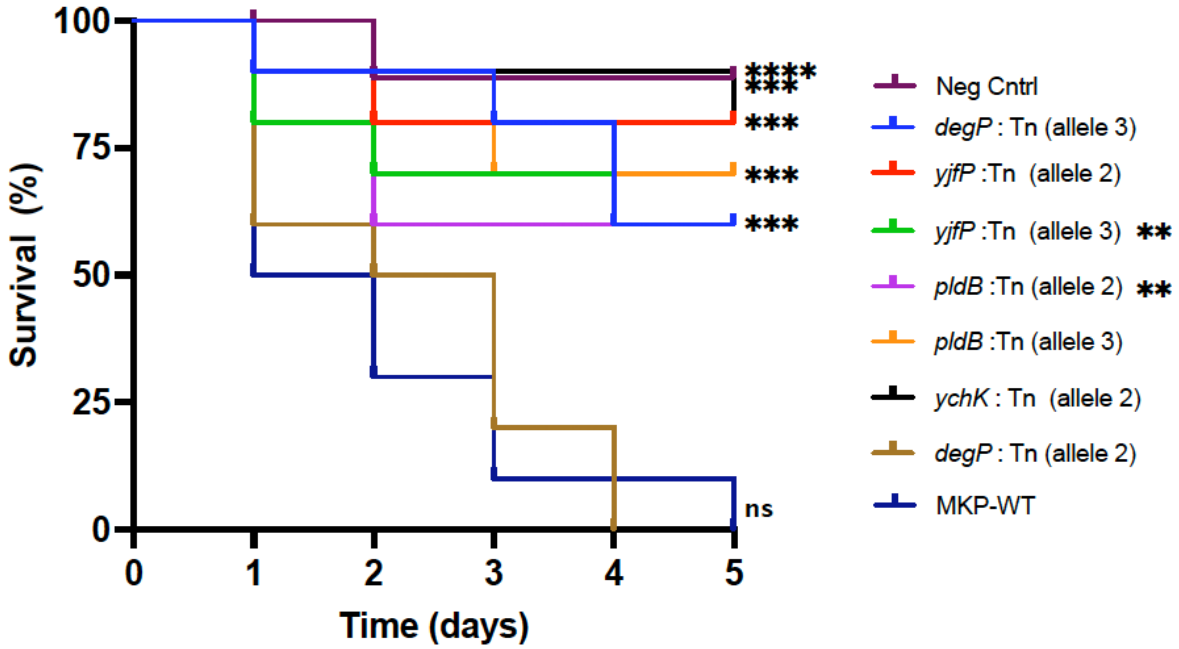

Figure S2. **Infection of *G. mellonella* with *K. pneumoniae.*** Kaplan–Meier (KM) survival plots of *G. mellonella* larvae after inoculation of the *K. pneumoniae* WT and SH-deficient mutants. Different transposon mutants allele displaying a significant difference in survival compared to the WT were determined by the to log-rank (Mantel–Cox) test and are denoted (**** $p < 0.0001$, **** $p < 0.001$, ** $p < 0.05$, ns = not significantly different).

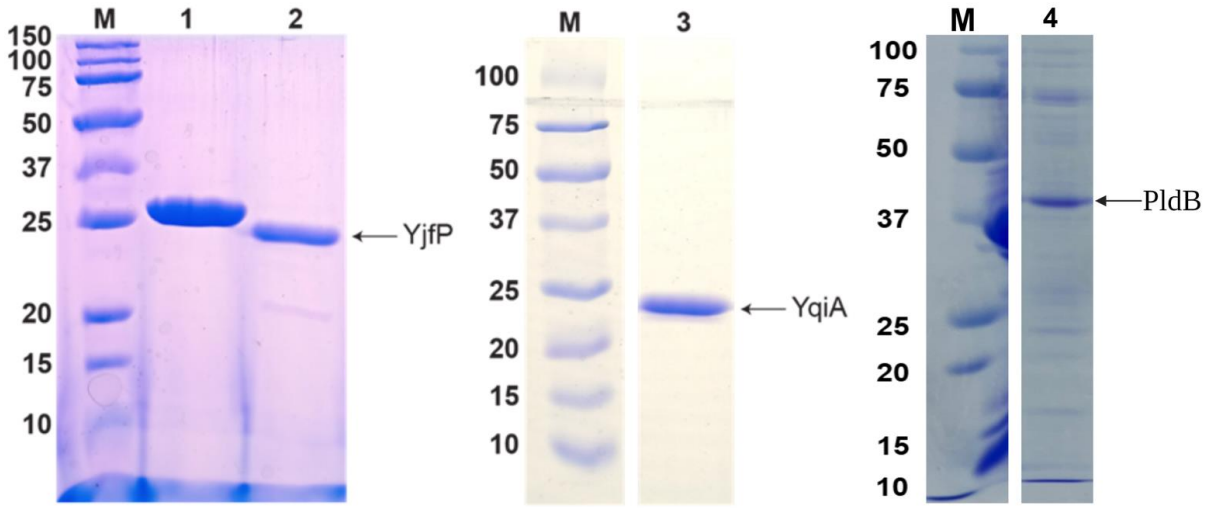

Figure S3. SDS PAGE of purified YjfP, YqiA, and His6-PldB. YjfP, YqiA, and PldB purity were assessed by loading onto SDS PAGE gels of 12 % polyacrylamide. Molecular weight markers are in lanes labelled M and labelled by their size in kDa. His6 YjfP was loaded into lane 1, YjfP after 3C cleavage loaded into lane 2, YqiA loaded into lane 3, and His6-PldB loaded into lane 4. The predicted masses after cleavage of YjfP, YqiA, and PldB are 27 kDa, 22 kDa, and 38 kDa, respectively.

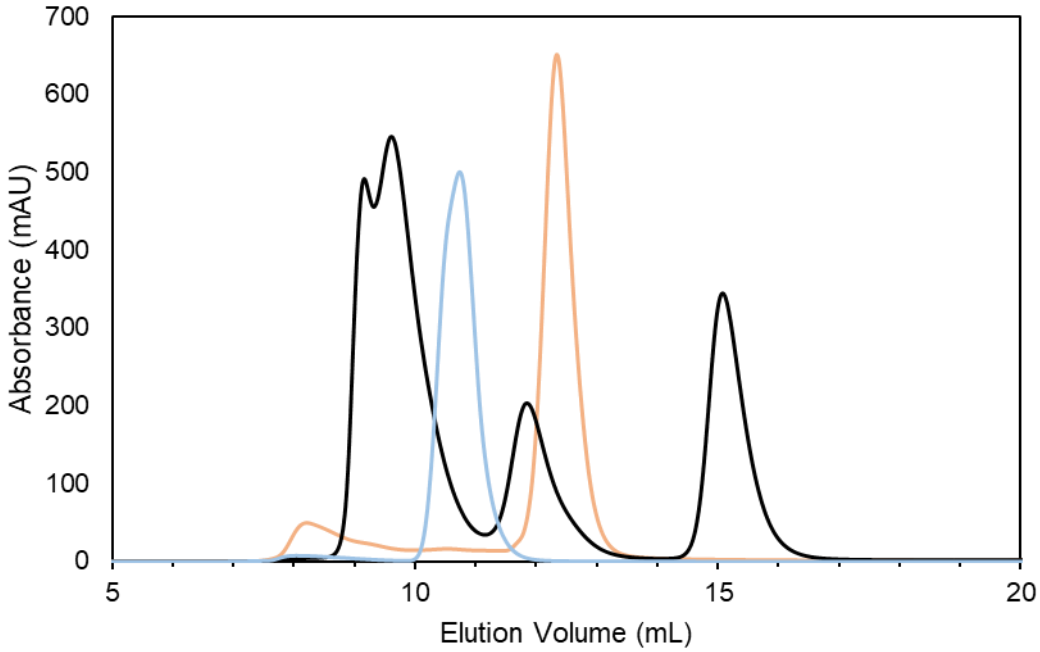

Figure S4. **Gel-filtration chromatogram of YjfP and YqiA**. Gel filtration of YjfP (cyan), YqiA (orange), and protein standards (black). The protein standards run include thyroglobulin (670 kDa), bovine gamma globulin (158 kDa), chicken ovalbumin (44 kDa), and equine myoglobin (17 kDa). YjfP elutes after bovine gamma globulin and before chicken ovalbumin, consistent with a 54 kDa homodimer. YqiA elutes after chicken ovalbumin consistent with a 22 kDa monomer.

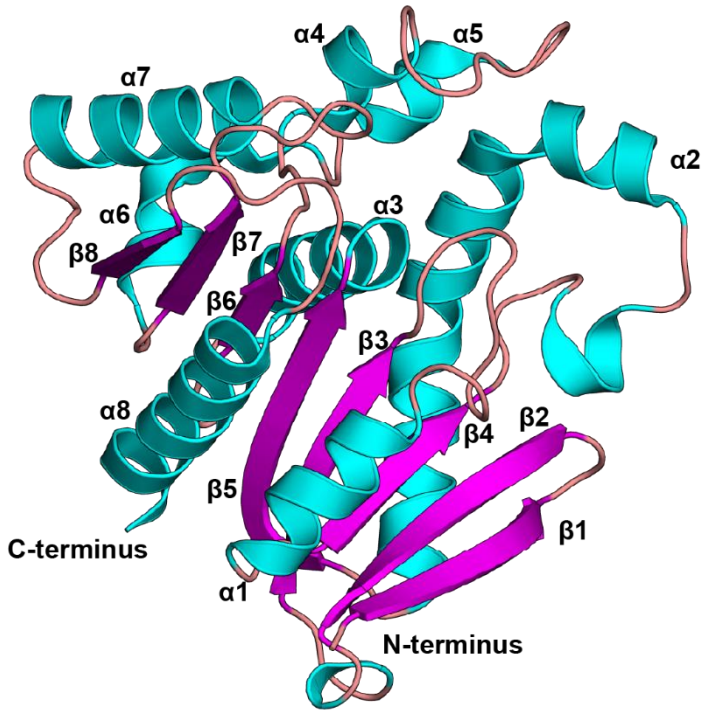

Figure S5. **Secondary structures of YjfP**. Secondary structure elements are displayed as follows: α helices (cyan), β sheets (magenta), and loops (beige).

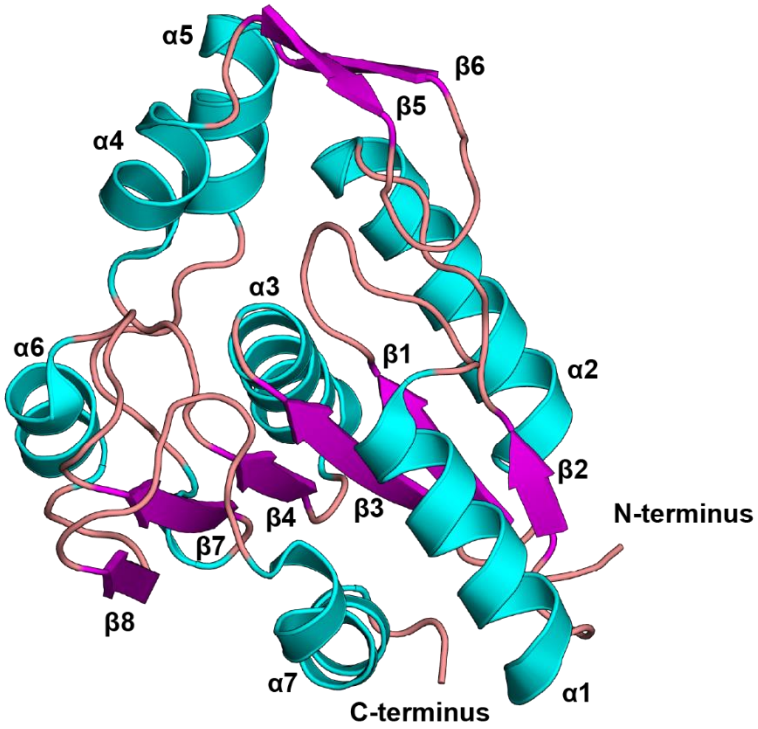

Figure S6. **Secondary structures of YqiA.** Secondary structure elements are displayed as follows: α helices (cyan), β sheets (magenta), and loops (beige).

Supplementary references

1. Ramage, B. et al. Comprehensive Arrayed Transposon Mutant Library of *Klebsiella pneumoniae* Outbreak Strain KPNIH1. *J Bacteriol* **199**(2017).

Extended Data Table **1**_Proteins identified in *K. pneumoniae* BY MS-ABPP

AIE21537.1	serine endoprotease [Klebsiella pneumoniae subsp. pneumoniae KPNIH1]	*degP*	18	49,5	477	5,35315195719401	5,1995646401629	+
AIE23660.1	hypothetical protein KPNIH1_15760 [Klebsiella pneumoniae subsp. pneumoniae KPNIH1]	*ychK;rssA*	4	33,3	300	4,79131126403809	4,6511859628720	+
AIE22089.1	lipid A palmitoyltransferase [Klebsiella pneumoniae subsp. pneumoniae KPNIH1]	*pagP*	2	19,8	172	4,6234302520752	4,4409811548193	+
AIE24131.1	NADH dehydrogenase [Klebsiella pneumoniae subsp. pneumoniae KPNIH1]	*nuoG*	9	99,5	908	4,30469004313151	4,1516488675805	+
AIE22135.1	acyl-CoA esterase [Klebsiella pneumoniae subsp. pneumoniae KPNIH1]	*ybfF*	11	28,5	257	4,2124195098877	3,8065980732798	+
AIE22988.1	3-oxoadipate enol-lactonase [Klebsiella pneumoniae subsp. pneumoniae KPNIH1]	*catD;pcaD*	2	27,3	254	4,18239816029867	3,7324841066015	+
WP_002883412.1	MULTISPECIES: Lysophospholipase L2 [Klebsiella]	*pldB*	5	38,2	330	4,10370381673177	3,1350218873905	+
AIE25182.1	serine endoprotease DegQ [Klebsiella pneumoniae subsp. pneumoniae KPNIH1]	*degQ*	5	47,2	455	3,9325491587321	3,1290556758313	+
WP_002916845.1	MULTISPECIES: esterase YqiA [Klebsiella]	*yqiA*	2	21,5	191	3,61993885040283	3,1138094971165	+
WP_004152192.1	MULTISPECIES: Gfo/Idh/MocA family oxidoreductase [Klebsiella]	*iolG*	4	36,7	337	3,30878893534342	3,1079559562713	+
WP_002913801.1	MULTISPECIES: phosphoribosylaminoimidazolesuccinocarboxamide synthase [Klebsiella]	*purC*	1	26,9	237	2,98962593078613	3,0882646122766	+
AIE22542.1	hypothetical protein KPNIH1_09915 [Klebsiella pneumoniae subsp. pneumoniae KPNIH1]	*ycfP*	2	21,1	180	2,92133935292562	2,9253748038605	+
WP_002920511.1	MULTISPECIES: pimeloyl-ACP methyl ester esterase BioH [Klebsiella]	*bioH*	2	28,3	257	2,91468588511149	2,8709136157757	+
WP_002913195.1	MULTISPECIES: acetate kinase [Klebsiella]	*ackA;ackA_1*	5	43,2	400	2,482697168986	2,7934068908219	+
WP_004152306.1	MULTISPECIES: DNA-directed RNA polymerase subunit beta [Klebsiella]	*rpoB*	10	150,4	1342	2,27951812744141	2,7818199337782	+
AIE25518.1	L-threonine 3-dehydrogenase [Klebsiella pneumoniae subsp. pneumoniae KPNIH1]	*tdh*	1	37,2	341	2,23174222310384	2,6637127743650	+
AIE23453.1	glutaredoxin [Klebsiella pneumoniae subsp. pneumoniae KPNIH1]	*grxD;ydhD*	1	12,9	115	2,14313666025798	2,6307709315405	+
AIE24214.1	PTS system glucose-specific transporter subunit IIA [Klebsiella pneumoniae subsp. pneumo	*crr;crr_1;crr_2*	6	18,2	169	2,02749570210775	2,6102106489190	+
WP_004152017.1	MULTISPECIES: esterase [Klebsiella]	*yjfP*	2	26,5	238	1,86300214131673	2,6046615921897	+
WP_002913178.1	MULTISPECIES: NADH-quinone oxidoreductase subunit NuoB [Enterobacteriaceae]	*nuoB*	3	25,5	224	1,77300516764323	2,5919402950943	+
WP_002914281.1	MULTISPECIES: lipid A hydroxylase LpxO [Klebsiella]	*lpxO*	5	35,4	300	1,68659528096517	2,5705620235051	+
AIE23973.1	tyrosine protein kinase [Klebsiella pneumoniae subsp. pneumoniae KPNIH1]	*wzc*	2	79,5	718	1,67021115620931	2,5489630702262	+
WP_002895841.1	MULTISPECIES: DNA starvation/stationary phase protection protein Dps [Bacteria]	*dps*	8	18,7	167	1,63348770141602	2,5329544399516	+
WP_002910026.1	MULTISPECIES: threonine--tRNA ligase [Klebsiella]	*thrS*	6	73,9	642	1,61337534586588	2,5311412724365	+
WP_002892069.1	MULTISPECIES: multidrug efflux RND transporter permease subunit AcrB [Klebsiella]	*acrB;acrB_3;*	15	113,2	1048	1,59889157613118	2,4864567628767	+
WP_004151337.1	MULTISPECIES: trigger factor [Klebsiella]	*tig*	4	48,1	432	1,58440780639648	2,4744171774973	+
WP_002922402.1	MULTISPECIES: hypothetical protein [Klebsiella]	*yibT*	2	8,7	74	1,54890314737956	2,4653567338905	+
AIE24636.1	CTP synthetase [Klebsiella pneumoniae subsp. pneumoniae KPNIH1]	*pyrG;pyrG_1*	14	60,1	545	1,5426165262858	2,4489549127555	+
AIE24213.1	phosphoenolpyruvate-protein phosphotransferase [Klebsiella pneumoniae subsp. pneumoni	*ptsI;ptsI_3*	4	63,2	575	1,52599143981934	2,4486984755392	+
WP_002888841.1	MULTISPECIES: 3-methyl-2-oxobutanoate hydroxymethyltransferase [Klebsiella]	*panB*	2	28	263	1,51685078938802	2,4402405018112	+
AIE24391.1	elongation factor 4 [Klebsiella pneumoniae subsp. pneumoniae KPNIH1]	*lepA*	5	66,4	599	1,51402982076009	2,4261473583918	+
AIE22963.1	fumarate hydratase [Klebsiella pneumoniae subsp. pneumoniae KPNIH1]	*fumC*	6	49,8	466	1,50342877705892	2,4196944493164	+
WP_002885424.1	MULTISPECIES: aspartate ammonia-lyase [Klebsiella]	*aspA*	4	52	478	1,50018628438314	2,4031932504195	+
AIE22939.1	glutamate dehydrogenase [Klebsiella pneumoniae subsp. pneumoniae KPNIH1]	*gdhA_1*	11	46,4	424	1,48799514770508	2,3870691059525	+
AIE25280.1	elongation factor G [Klebsiella pneumoniae subsp. pneumoniae KPNIH1]	*fusA;fusA_1;*	15	77,5	704	1,44711875915527	2,3792962229932	+
WP_002916061.1	MULTISPECIES: aldo/keto reductase family oxidoreductase [Klebsiella]	*ydbC*	5	31,5	292	1,40972646077474	2,3547897772901	+
WP_002883222.1	MULTISPECIES: ATP-dependent RNA helicase RhlB [Bacteria]	*rhlB*	12	47,1	421	1,39920171101888	2,3402617693602	+
AIE21456.1	cell division protein FtsZ [Klebsiella pneumoniae subsp. pneumoniae KPNIH1]	*ftsZ*	6	40,3	383	1,35885047912598	2,3402142738609	+
AIE24873.1	arginine decarboxylase [Klebsiella pneumoniae subsp. pneumoniae KPNIH1]	*speA*	5	73,8	658	1,35690561930338	2,3138095946857	+
WP_002916505.1	MULTISPECIES: class II fructose-bisphosphate aldolase [Klebsiella]	*fbaA;fbaA_1*	4	39,1	359	1,34550539652507	2,2729242646898	+
WP_002918252.1	MULTISPECIES: transcription termination factor NusA [Klebsiella]	*nusA*	11	54,9	495	1,3229185740153	2,253597433394	+
AIE21373.1	molecular chaperone DnaJ [Klebsiella pneumoniae subsp. pneumoniae KPNIH1]	*dnaJ*	2	41	377	1,30420430501302	2,2437852882644	+
WP_002895068.1	MULTISPECIES: peptidoglycan-associated lipoprotein Pal [Enterobacteriaceae]	*pal*	6	18,9	174	1,29813448588053	2,2209504008413	+
WP_002889381.1	MULTISPECIES: acetyl-CoA carboxylase carboxyl transferase subunit alpha [Klebsiella]	*accA*	4	35,3	319	1,28511683146159	2,2074274768520	+
WP_004144997.1	MULTISPECIES: F0F1 ATP synthase subunit beta [Klebsiella]	*atpB;atpD*	6	50,2	460	1,28271420796712	2,2068961128046	+
WP_000729185.1	MULTISPECIES: 50S ribosomal protein L24 [Bacteria]	*rplX*	3	11,3	104	1,26590347290039	2,1984079917769	+
AIE21202.1	hypothetical protein KPNIH1_02790 [Klebsiella pneumoniae subsp. pneumoniae KPNIH1]		1	38,5	336	1,24973996480306	2,1880344131087	+
AIE20865.1	proline dipeptidase [Klebsiella pneumoniae subsp. pneumoniae KPNIH1]	*pepQ*	4	50,1	443	1,23647244771321	2,1859758004624	+
WP_002910036.1	MULTISPECIES: fructosamine kinase family protein [Klebsiella]	*yniA*	2	33,3	290	1,23516432444254	2,1675197239768	+
AIE21546.1	ribosome recycling factor [Klebsiella pneumoniae subsp. pneumoniae KPNIH1]	*frr*	1	20,6	185	1,2296126683553	2,1645025329742	+
AIE23966.1	dTDP-4-dehydrorhamnose reductase [Klebsiella pneumoniae subsp. pneumoniae KPNIH1]	*rmlD*	9	32,1	296	1,21847025553386	2,1616516852314	+
WP_002898162.1	MULTISPECIES: 30S ribosomal protein S1 [Klebsiella]	*rpsA;rpsA_2*	11	61,1	557	1,21178754170736	2,1241307514013	+
AIE21043.1	molecular chaperone GroEL [Klebsiella pneumoniae subsp. pneumoniae KPNIH1]	*groEL;groL;g*	22	57,1	548	1,18901443481445	2,1234459870689	+
AIE24180.1	multifunctional fatty acid oxidation complex subunit alpha [Klebsiella pneumoniae subsp. pne	*fadJ*	5	77,4	714	1,1822083791097	2,1177107952577	+
WP_004159719.1	MULTISPECIES: thiamine pyrophosphate-binding protein [Klebsiella]	*ipdC*	17	60	553	1,18163172403971	2,0982851645973	+
AIE22565.1	transcriptional regulator [Klebsiella pneumoniae subsp. pneumoniae KPNIH1]	*phoP;phoP_1*	3	25,4	223	1,18142604827881	2,0962204376362	+
AIE24346.1	nucleoside diphosphate kinase [Klebsiella pneumoniae subsp. pneumoniae KPNIH1]	*ndk*	2	15,5	143	1,17601458231608	2,0927625203907	+
AIE23763.1	amino acid dehydrogenase [Klebsiella pneumoniae subsp. pneumoniae KPNIH1]	*dadA;soxB_1*	9	47,3	432	1,16553052266439	2,0861676839247	+
WP_002916796.1	MULTISPECIES: 2,5-didehydrogluconate reductase DkgA [Klebsiella]	*dkgA*	12	30,7	275	1,16539319356282	2,0804824610735	+
AIE21728.1	transcription antiterminator NusB [Klebsiella pneumoniae subsp. pneumoniae KPNIH1]	*nusB*	2	15,8	139	1,16211255391439	2,0762756372798	+
WP_002893003.1	MULTISPECIES: SIS domain-containing protein [Klebsiella]	*frlB_2*	3	36,7	328	1,1593189239502	2,065816691069	+
WP_002889299.1	MULTISPECIES: 30S ribosomal protein S2 [Klebsiella]	*rpsB*	10	26,7	241	1,15743700663248	2,0478228668651	+
WP_002916299.1	MULTISPECIES: lysine--tRNA ligase [Klebsiella]	*lysS;lysS_1*	11	57,5	505	1,15595499674479	2,0430478072030	+
AIE22163.1	succinyl-CoA synthetase subunit alpha [Klebsiella pneumoniae subsp. pneumoniae KPNIH1]	*sucD;sucD_1*	7	29,8	289	1,13977559407552	2,0413373426995	+
WP_004146997.1	MULTISPECIES: molecular chaperone DnaK [Klebsiella]	*dnaK;dnaK_3*	12	69,1	638	1,13864008585612	2,0257802529472	+
AIE24248.1	transaldolase [Klebsiella pneumoniae subsp. pneumoniae KPNIH1]	*tal;talA*	7	35,5	318	1,13556416829427	2,0236386533162	+
WP_002910443.1	MULTISPECIES: redox-regulated ATPase YchF [Klebsiella]	*engD;ychF*	6	39,6	363	1,1190128326416	2,0168297787283	+
AIE23043.1	transposase [Klebsiella pneumoniae subsp. pneumoniae KPNIH1]	*insH_4;tnp*	2	37,8	326	1,11879285176595	2,0133219169673	+
AIE22520.1	ribonuclease E [Klebsiella pneumoniae subsp. pneumoniae KPNIH1]	*rne*	27	119,1	1077	1,11472829182943	2,0127645353969	+
WP_002908860.1	MULTISPECIES: major outer membrane lipoprotein [Bacteria]	*lpp*	3	8,4	78	1,11410776774089	2,0127544315287	+
WP_002883293.1	MULTISPECIES: transcription termination factor Rho [Bacteria]	*rho*	7	47	419	1,10973612467448	2,0096175918424	+
WP_004143804.1	MULTISPECIES: S-(hydroxymethyl)glutathione dehydrogenase/class III alcohol dehydroger	*adhC;frmA*	2	39,2	372	1,10933303833008	2,0021384153119	+
WP_002901243.1	MULTISPECIES: glyceraldehyde-3-phosphate dehydrogenase [Klebsiella]	*gapA*	7	35,4	331	1,10328038533529	1,9883825235471	+
AIE25265.1	30S ribosomal protein S17 [Klebsiella pneumoniae subsp. pneumoniae KPNIH1]	*rpsQ*	2	9,7	84	1,09935124715169	1,9762621215827	+
WP_004142209.1	MULTISPECIES: 2-oxoglutarate dehydrogenase complex dihydrolipoyllysine-residue succin	*sucB*	9	44,2	408	1,09821446736654	1,9693063334781	+
AIE20761.1	ATP-dependent protease ATP-binding subunit HslU [Klebsiella pneumoniae subsp. pneumo	*hslU*	12	49,7	444	1,09618822733561	1,9516692702552	+
AIE24011.1	fructose-bisphosphate aldolase [Klebsiella pneumoniae subsp. pneumoniae KPNIH1]	*fbaB*	7	37,9	350	1,09402656555176	1,9289654564612	+
AIE21358.1	TorR family transcriptional regulator [Klebsiella pneumoniae subsp. pneumoniae KPNIH1]	*arcA;arcA_1;*	7	27,3	238	1,07928276062012	1,9250595332162	+
WP_002909055.1	MULTISPECIES: phosphoenolpyruvate synthase [Klebsiella]	*ppsA*	13	87	792	1,0784797668457	1,9218124953920	+
WP_004152222.1	MULTISPECIES: 2-oxoglutarate dehydrogenase E1 component [Klebsiella]	*sucA*	20	105,1	935	1,07613372802734	1,9209511560036	+
AIE22083.1	alkyl hydroperoxide reductase [Klebsiella pneumoniae subsp. pneumoniae KPNIH1]	*ahpC*	8	20,8	187	1,06162897745768	1,9161620562775	+
AIE21088.1	exoribonuclease R [Klebsiella pneumoniae subsp. pneumoniae KPNIH1]	*rnr*	26	91,8	810	1,06152534484863	1,9157047036238	+
WP_004152033.1	MULTISPECIES: cytosol nonspecific dipeptidase [Klebsiella]	*pepD*	7	52,4	485	1,04026667277018	1,9132361251804	+
WP_002911423.1	MULTISPECIES: bifunctional 4-hydroxy-2-oxoglutarate aldolase/2-dehydro-3-deoxy-phospl	*eda*	2	22,2	213	1,03105481465657	1,9092947577376	+
AIE22209.1	kinase inhibitor [Klebsiella pneumoniae subsp. pneumoniae KPNIH1]	*ybhB*	3	16,9	158	1,03088569641113	1,9050438867868	+
AIE22573.1	isocitrate dehydrogenase [Klebsiella pneumoniae subsp. pneumoniae KPNIH1]	*icd;icd_2;icdA*	17	45,7	416	1,03027788798014	1,9013701955992	+
AIE21133.1	fructose 1,6-bisphosphatase [Klebsiella pneumoniae subsp. pneumoniae KPNIH1]	*fbp*	5	36,7	332	1,02050145467122	1,9002284837267	+
WP_002882755.1	MULTISPECIES: ribosome-dependent GTPase TypA [Klebsiella]	*bipA;typA*	9	67,2	607	1,01906585693359	1,8839079530321	+

AIE22746.1	adenylyltransferase [Klebsiella pneumoniae subsp. pneumoniae KPNIH1]	*aadA;aada2;*	5	29,5	263	1,01704788208008	1,8727370914342	+
WP_002884034.1	MULTISPECIES: 50S ribosomal protein L11 [Enterobacteriaceae]	*rplK*	5	14,9	142	1,01577313741048	1,86168340730205	+
WP_002906030.1	MULTISPECIES: OsmC family protein [Enterobacteriaceae]	*osmC*	1	15,1	143	1,01553853352864	1,85338029017304	+
WP_002898148.1	MULTISPECIES: formate C-acetyltransferase [Klebsiella]	*pflB*	13	85,1	760	1,01324462890625	1,85151250644457	+
WP_002886682.1	MULTISPECIES: 50S ribosomal protein L9 [Klebsiella]	*rplI*	8	15,8	149	1,01255861918132	1,85017988355284	+
WP_002888541.1	MULTISPECIES: division/cell wall cluster transcriptional repressor MraZ [Klebsiella]	*mraZ*	5	17,3	152	1,01088841756185	1,82919037980666	+
AIE21086.1	adenylosuccinate synthetase [Klebsiella pneumoniae subsp. pneumoniae KPNIH1]	*purA*	6	47,1	432	1,01017697652181	1,82308750067807	+
AIE24170.1	3-oxoacyl-ACP synthase [Klebsiella pneumoniae subsp. pneumoniae KPNIH1]	*fabB*	10	42,4	406	1,00581359863281	1,82181772687297	+
AIE23773.1	cell division inhibitor MinD [Klebsiella pneumoniae subsp. pneumoniae KPNIH1]	*minD;minD_1*	9	29,6	270	1,00563812255859	1,80797545329888	+
WP_002918642.1	MULTISPECIES: metalloprotease TldD [Klebsiella]	*tldD*	1	51,2	481	1,00554021199544	1,80557646800886	+
AIE24349.1	3-mercaptopyruvate sulfurtransferase [Klebsiella pneumoniae subsp. pneumoniae KPNIH1]	*sseA*	1	31,2	285	1,00546296437581	1,80439050606551	+
AIE25511.1	preprotein translocase subunit SecB [Klebsiella pneumoniae subsp. pneumoniae KPNIH1]	*secB*	2	17,2	155	1,00445048014323	1,79997916832151	+
AIE25269.1	50S ribosomal protein L22 [Klebsiella pneumoniae subsp. pneumoniae KPNIH1]	*rplV*	5	12,2	110	1,00431187947591	1,7973764907707	+
WP_004152116.1	MULTISPECIES: heat shock survival AAA family ATPase ClpK [Enterobacterales]	*clpB;clpC;clp*	28	102,4	931	1,00391705830892	1,78623832357585	+
WP_002895144.1	MULTISPECIES: galactokinase [Klebsiella]	*galK*	4	41,3	382	1,00375620524089	1,76164016643081	+
WP_004152345.1	MULTISPECIES: class I SAM-dependent DNA methyltransferase [Enterobacterales]	*hsdM*	5	76,2	675	1,00333404541016	1,75362900027894	+
AIE20874.1	transcription antiterminator NusG [Klebsiella pneumoniae subsp. pneumoniae KPNIH1]	*nusG*	2	20,5	181	1,00322469075521	1,75344276366331	+
WP_002898206.1	MULTISPECIES: asparagine--tRNA ligase [Klebsiella]	*asnS*	3	52,5	466	1,00165112813314	1,75172258201615	+
AIE24401.1	methyltransferase [Klebsiella pneumoniae subsp. pneumoniae KPNIH1]	*yfiF*	10	39,6	361	0,996184031168617	1,7484080859232	+
AIE25257.1	30S ribosomal protein S5 [Klebsiella pneumoniae subsp. pneumoniae KPNIH1]	*rpsE*	10	17,6	167	0,996012369791668	1,7463951214431	+
AIE25179.1	50S ribosomal protein L13 [Klebsiella pneumoniae subsp. pneumoniae KPNIH1]	*rplM*	7	16,1	142	0,993878682454429	1,73122594995855	+
WP_004150945.1	translation initiation factor IF-2 [Klebsiella pneumoniae]	*infB*	10	98,1	896	0,992155075073242	1,7284801329242	+
AIE20944.1	hypothetical protein KPNIH1_01455 [Klebsiella pneumoniae subsp. pneumoniae KPNIH1]	*yjbJ*	2	8,3	69	0,989467620849609	1,72525843013364	+
AIE22137.1	phosphoglucomutase [Klebsiella pneumoniae subsp. pneumoniae KPNIH1]	*pgm;pgm_1*	5	58,4	546	0,98927942911784	1,72427695854116	+
AIE23317.1	ethanol-active dehydrogenase/acetaldehyde-active reductase [Klebsiella pneumoniae subsp	*adhP*	11	35,3	336	0,987907409667969	1,71571895422705	+
AIE22661.1	succinylglutamate desuccinylase [Klebsiella pneumoniae subsp. pneumoniae KPNIH1]	*astE*	2	36,5	321	0,981499354044598	1,71315716254433	+
AIE23593.1	cysteine desulfurase [Klebsiella pneumoniae subsp. pneumoniae KPNIH1]	*sufC*	3	27,7	248	0,978995005289713	1,70380274431924	+
AIE22382.1	pyruvate formate lyase-activating enzyme 1 [Klebsiella pneumoniae subsp. pneumoniae KP	*pflA;pflA_1;p*	2	28,3	246	0,977008183797203	1,69567411376267	+
WP_002920113.1	MULTISPECIES: 30S ribosomal protein S7 [Enterobacteriaceae]	*rpsG*	7	17,6	156	0,974309921264648	1,68924981367095	+
WP_002888700.1	MULTISPECIES: pyruvate dehydrogenase (acetyl-transferring), homodimeric type [Klebsiel	*aceE*	33	99,4	887	0,968114852905273	1,68660152256215	+
WP_002895039.1	MULTISPECIES: ADP-forming succinate--CoA ligase subunit beta [Klebsiella]	*sucC*	12	41,5	388	0,967112223307293	1,67352475285483	+
AIE25259.1	50S ribosomal protein L6 [Klebsiella pneumoniae subsp. pneumoniae KPNIH1]	*rplF*	10	18,8	177	0,965184529622398	1,67189317052273	+
AIE21348.1	ABC transporter ATP-binding protein [Klebsiella pneumoniae subsp. pneumoniae KPNIH1]	*ettA;yjjK*	21	62,2	555	0,963148752848308	1,67119360087334	+
WP_002910105.1	MULTISPECIES: UTP--glucose-1-phosphate uridylyltransferase GalU [Klebsiella]	*galU;galU_2*	7	32,6	300	0,955865224202476	1,6591127679037	+
WP_002914082.1	MULTISPECIES: ATP-dependent RNA helicase SrmB [Klebsiella]	*srmB*	12	49,7	443	0,951261520385742	1,65821737895606	+
WP_002885145.1	MULTISPECIES: acetate--CoA ligase [Klebsiella]	*acs;acsA*	14	72	652	0,951038996378578	1,64388225157527	+
AIE21058.1	elongation factor P [Klebsiella pneumoniae subsp. pneumoniae KPNIH1]	*efp*	1	20,6	188	0,948328018188477	1,63975015877254	+
AIE20896.1	DNA-binding protein [Klebsiella pneumoniae subsp. pneumoniae KPNIH1]	*hupA*	3	9,5	90	0,946093877156574	1,63530326699105	+
AIE25144.1	50S ribosomal protein L27 [Klebsiella pneumoniae subsp. pneumoniae KPNIH1]	*rpmA*	3	9,1	85	0,944968541463215	1,63447286112435	+
WP_002882753.1	MULTISPECIES: glutamate--ammonia ligase [Klebsiella]	*glnA*	1	51,8	469	0,942733128865559	1,63050969528153	+
WP_002884036.1	MULTISPECIES: 50S ribosomal protein L1 [Enterobacteriaceae]	*rplA*	12	24,7	234	0,939916610717773	1,62648152623186	+
WP_001207203.1	MULTISPECIES: 50S ribosomal protein L10 [Bacteria]	*rplJ*	6	17,8	165	0,939062118530273	1,62286980377353	+
AIE25275.1	30S ribosomal protein S10 [Klebsiella pneumoniae subsp. pneumoniae KPNIH1]	*nusE;rpS10;r*	5	11,8	103	0,937534968058269	1,62175871415939	+
AIE22126.1	glucosamine-6-phosphate deaminase [Klebsiella pneumoniae subsp. pneumoniae KPNIH1]	*nagB;nagB_1*	3	29,7	266	0,935902913411457	1,61417145135939	+
AIE21192.1	inosose dehydratase [Klebsiella pneumoniae subsp. pneumoniae KPNIH1]	*iolE*	6	33,3	299	0,928174336751304	1,61195488117814	+
AIE25203.1	acetyl-CoA carboxylase [Klebsiella pneumoniae subsp. pneumoniae KPNIH1]	*accB*	6	16,5	155	0,928113301595051	1,61185017011097	+
WP_002913162.1	MULTISPECIES: NADH-quinone oxidoreductase subunit C/D [Klebsiella]	*nuoC;nuoCD*	9	69,1	602	0,927086512247723	1,61048258105564	+
WP_004151336.1	MULTISPECIES: endopeptidase La [Klebsiella]	*lon;lon_1;lon*	19	87,4	784	0,924786249796547	1,61038016076715	+
AIE20872.1	elongation factor Tu [Klebsiella pneumoniae subsp. pneumoniae KPNIH1]	*ef-tu;tuf;tuf_1*	19	43,2	394	0,914241790771484	1,60433890378967	+
AIE25262.1	50S ribosomal protein L5 [Klebsiella pneumoniae subsp. pneumoniae KPNIH1]	*rplE*	11	20,3	179	0,910654067993164	1,59868383188214	+
AIE25282.1	30S ribosomal protein S12 [Klebsiella pneumoniae subsp. pneumoniae KPNIH1]	*rpsL*	5	13,7	124	0,909037907918297	1,59323193144981	+
AIE25536.1	50S ribosomal protein L28 [Klebsiella pneumoniae subsp. pneumoniae KPNIH1]	*rpmB*	3	9	78	0,900881449381512	1,59038403116930	+
WP_002916508.1	MULTISPECIES: phosphoglycerate kinase [Klebsiella]	*pgk*	2	41,1	387	0,89797306060791	1,58820836702939	+
WP_004151551.1	MULTISPECIES: F0F1 ATP synthase subunit alpha [Klebsiella]	*atpA*	17	55,2	513	0,897473017374672	1,58404899373254	+
WP_002913016.1	MULTISPECIES: class 1a ribonucleoside-diphosphate reductase subunit alpha [Klebsiella]	*nrdA*	11	85,6	761	0,892283757527672	1,57928250828413	+
AIE25271.1	50S ribosomal protein L2 [Klebsiella pneumoniae subsp. pneumoniae KPNIH1]	*rplB*	14	29,8	273	0,89194615681966	1,57324851718773	+
AIE21539.1	hypothetical protein KPNIH1_04550 [Klebsiella pneumoniae subsp. pneumoniae KPNIH1]		6	15,1	128	0,891180674235024	1,56973685835920	+
WP_004189469.1	MULTISPECIES: translation initiation factor IF-3 [Klebsiella]	*infC*	4	20,5	180	0,890858332316082	1,56809549230066	+
WP_002919259.1	MULTISPECIES: 30S ribosomal protein S13 [Klebsiella]	*rpsM*	7	13,2	118	0,881100336710613	1,56767533198903	+
WP_002921789.1	MULTISPECIES: ABC transporter substrate-binding protein [Klebsiella]	*dppA;dppA_1*	5	60,1	535	0,879015604654949	1,55985862453633	+
WP_002902877.1	MULTISPECIES: phenylacetate--CoA ligase [Klebsiella]	*paaK*	2	49	438	0,869573911031088	1,55639538625400	+
WP_002914769.1	MULTISPECIES: recombinase RecA [Klebsiella]	*recA*	7	37,9	352	0,869090398152668	1,54387633750339	+
WP_002919766.1	MULTISPECIES: 30S ribosomal protein S3 [Bacteria]	*rpsC*	8	25,8	232	0,866425196329754	1,54325299721539	+
WP_004151361.1	pyruvate dehydrogenase complex dihydrolipoyllysine-residue acetyltransferase [Klebsiella p	*aceF*	17	65,9	632	0,866349538167317	1,53429235516165	+
AIE25264.1	50S ribosomal protein L14 [Klebsiella pneumoniae subsp. pneumoniae KPNIH1]	*rplM;rplN*	5	13,5	123	0,86133639017741	1,53029517519088	+
AIE25260.1	30S ribosomal protein S8 [Klebsiella pneumoniae subsp. pneumoniae KPNIH1]	*rpsH*	8	14,1	130	0,855939229329426	1,52911552775014	+
AIE25274.1	50S ribosomal protein L3 [Klebsiella pneumoniae subsp. pneumoniae KPNIH1]	*rplC*	9	22,2	209	0,853150685628254	1,522377515487	+
WP_004151904.1	enoyl-ACP reductase FabI [Klebsiella pneumoniae]		8	27,9	262	0,853096008300781	1,51857952020514	+
WP_004152486.1	glucose-1-phosphate thymidylyltransferase RfbA [Klebsiella pneumoniae]	*rmlA*	6	32,1	289	0,848490397135414	1,51751471228783	+
AIE23286.1	peroxidase [Klebsiella pneumoniae subsp. pneumoniae KPNIH1]	*katG*	3	78,9	725	0,845319747924805	1,51364959396683	+
WP_000242758.1	MULTISPECIES: cAMP-activated global transcriptional regulator CRP [Enterobacterales]	*cap;crp;crp_1*	11	23,6	210	0,845208485921223	1,49806214752629	+
WP_002896406.1	MULTISPECIES: ubiquinone-dependent pyruvate dehydrogenase [Klebsiella]	*poxB*	10	62	572	0,844914118448894	1,47243841205977	+
WP_000617546.1	MULTISPECIES: 50S ribosomal protein L23 [Bacteria]	*rplW;rplW_40*	1	11,2	100	0,839486440022785	1,47168520049511	+
AIE22158.1	succinate dehydrogenase [Klebsiella pneumoniae subsp. pneumoniae KPNIH1]	*sdhA*	8	64,4	588	0,837594985961914	1,46358565797988	+
WP_002901234.1	MULTISPECIES: protein kinase YeaG [Klebsiella]	*yeaG*	22	74,3	644	0,833330790201821	1,45206867423048	+
WP_002884142.1	MULTISPECIES: 50S ribosomal protein L7/L12 [Bacteria]	*rplL*	2	12,3	121	0,830522537231445	1,44372805199	+
AIE25255.1	50S ribosomal protein L15 [Klebsiella pneumoniae subsp. pneumoniae KPNIH1]	*rl15;rplO*	7	15,1	144	0,828699111938477	1,43947116920915	+
AIE25273.1	50S ribosomal protein L4 [Klebsiella pneumoniae subsp. pneumoniae KPNIH1]	*rplD*	5	22,1	201	0,817341486612957	1,43840294037265	+
WP_002919667.1	MULTISPECIES: 30S ribosomal protein S14 [Bacteria]	*rpsN*	1	11,6	101	0,803735097249348	1,43685938095455	+
WP_001138115.1	MULTISPECIES: 30S ribosomal protein S19 [Bacteria]	*rpsS;rpsS_28*	3	10,4	92	0,800384521484375	1,42672779948477	+
WP_000228469.1	MULTISPECIES: leucine-responsive transcriptional regulator Lrp [Enterobacteriaceae]	*lrp;lrp_1;lrp_2*	4	18,8	164	0,796780904134113	1,42529216236725	+
WP_002919759.1	MULTISPECIES: 50S ribosomal protein L16 [Bacteria]	*rplP*	3	15,2	136	0,794464111328125	1,42502820555577	+
AIE21341.1	phosphopentomutase [Klebsiella pneumoniae subsp. pneumoniae KPNIH1]	*deoB*	10	44,2	407	0,794357299804688	1,41935101162377	+
AIE25251.1	30S ribosomal protein S4 [Klebsiella pneumoniae subsp. pneumoniae KPNIH1]	*rpsD*	10	23,5	206	0,787843068440754	1,41654658786411	+
WP_002918379.1	MULTISPECIES: 50S ribosomal protein L21 [Bacteria]	*rplU*	6	11,6	103	0,783462524414063	1,40396548871027	+
AIE25252.1	30S ribosomal protein S11 [Klebsiella pneumoniae subsp. pneumoniae KPNIH1]	*rpsK*	5	13,9	129	0,783237457275391	1,40328884515379	+
WP_004146678.1	MULTISPECIES: plasmid segregation protein ParM [Klebsiella]	*parM;parM_2*	6	35,2	318	0,781722386678062	1,36903860110486	+
AIE25178.1	30S ribosomal protein S9 [Klebsiella pneumoniae subsp. pneumoniae KPNIH1]	*rpsI*	7	14,8	130	0,777706782023113	1,36532134886377	+
AIE23307.1	oxidoreductase [Klebsiella pneumoniae subsp. pneumoniae KPNIH1]	*yghA*	2	32,4	304	0,763093948364258	1,36444047413997	+
AIE22712.1	aconitate hydratase [Klebsiella pneumoniae subsp. pneumoniae KPNIH1]	*acnA*	37	97,5	890	0,74394416809082	1,36407390582247	+
WP_004222662.1	MULTISPECIES: leu operon leader peptide [Gammaproteobacteria]	*leuL*	1	3,2	28	0,733625411987305	1,36111738383467	+
AIE25124.1	30S ribosomal protein S15 [Klebsiella pneumoniae subsp. pneumoniae KPNIH1]	*rpsO*	2	10,2	89	0,729977925618488	1,36016779665479	+
WP_002919206.1	MULTISPECIES: 50S ribosomal protein L17 [Bacteria]	*rplQ*	6	14,4	128	0,72447903951009	1,35021502578999	+
AIE25777.1	heat-shock protein Hsp20 (plasmid) [Klebsiella pneumoniae subsp. pneumoniae KPNIH1]	*hsp10;hsp20*	10	21,5	189	0,721589406331379	1,34353695009509	+
WP_000124850.1	MULTISPECIES: 50S ribosomal protein L20 [Bacteria]	*ppa;rpl20;rpl7*	6	13,5	118	0,719025293986004	1,33242375306988	+
WP_000358960.1	MULTISPECIES: 50S ribosomal protein L18 [Bacteria]	*rplR*	4	12,8	117	0,70482571919759	1,32424766381966	+
WP_002891359.1	MULTISPECIES: aldo/keto reductase [Klebsiella]	*iolS_1*	10	36,2	324	0,70024299621582	1,31758394954270	+
AIE25422.1	glutathione S-transferase [Klebsiella pneumoniae subsp. pneumoniae KPNIH1]		1	24,7	214	0,681575139363607	1,31476734788723	+
AIE23823.1	pyruvate kinase [Klebsiella pneumoniae subsp. pneumoniae KPNIH1]	*pyk;pykA*	10	51,4	480	0,645804723103844	1,31329200785202	+
AIE23787.1	PTS mannose transporter subunit IIAB [Klebsiella pneumoniae subsp. pneumoniae KPNIH1	*manX;manX*	1	34,9	323	0,572376251220703	1,30810261000775	+
WP_002915033.1	MULTISPECIES: manganese/iron ABC transporter ATP-binding protein [Klebsiella]	*afeB;fhuC_1*	4	29,8	273	0,556459744771322	1,30519521855515	+
WP_000135199.1	MULTISPECIES: 30S ribosomal protein S18 [Bacteria]	*rplU;rpsR*	3	9	75	0,440686543782551	1,30517780026307	+
WP_002920777.1	MULTISPECIES: gluconate operon transcriptional repressor GntR [Klebsiella]	*gntR;gntR_1;*	1	36,6	331	0,319991429646809	1,30514055418307	+

Extended Data Excel_ BLASTp results for a homolog of the *K. pneumoniae* SHs

	DegP				**YchK**				**YbfF**				**CatD**				**PldB**				**DegQ**				**YqiA**				**YcfP**				**bioH**				**YjfP**			
	KPNIH1_04540	Query Cover	e-value	Per. Identity	KPNIH1_15760	Query Cover	e-value	Per. Identity	KPNIH1_07725	QueryCover	e-value	Per. Identity	KPNIH1_12245	Query Cover	e-value	Per. Identity	KPNIH1_00895	Query Cover	e-value	Per. Identity	KPNIH1_23755	QueryCover	e-value	Per. Identity	KPNIH1_22780	QueryCover	e-value	Per. Identity	KPNIH1_09915	QueryCover	e-value	Per. Identity	KPNIH1_24570	Query Cover	e-value	Per. Identity	KPNIH1_02230	Query Cover	e-value	Per. Identity
Bifidobacterium adolescentis ATCC 15703	WP_011742607	58 %	4.00E-53	43.49%													WP_011742599.1	82 %	1.00E-13	25.61%	WP_011742607.1	61 %	1.00E-55	42.52%													WP_011742596.1	55 %	3.00E-04	28.36%
Bifidobacterium longum NCC2705	WP_011068543.1	56 %	5.00E-55	42.36%					WP_007055490.1	92 %	3.00E-09	26.59%	WP_007051340.1	94 %	5.00E-09	24.25%					WP_011068543.1	60 %	1.00E-56	43.55%													WP_011068565.1	55 %	9.00E-03	27.41%
Collinsella aerofaciens ATCC 25986	WP_006234732.1	56 %	7.00E-57	43.42%	WP_006234697.1	53 %	5.00E-11	29.34%													WP_006234732.1	57 %	8.00E-50	42.01%													WP_006236158.1	74 %	4.20E-02	24.77%
Bacteroides caccae ATCC 43185	WP_005678199.1	89 %	3.00E-75	37.17%	WP_005675736.1	93 %	2.00E-42	30.96%													WP_005678199.1	86 %	2.00E-81	39.43%																
Bacteroides fragilis ATCC 25285	WP_005788554.1	89 %	4.00E-71	35.54%	WP_005788931.1	59 %	2.00E-28	29.52%													WP_005788554.1	86 %	6.00E-75	36.24%													WP_010993734.1	49 %	0.003	25.64%
Bacteroides ovatus ATCC 8483	WP_004296667.1	89 %	4.00E-74	37.31%	WP_004297378.1	60 %	6.00E-30	31.13%													WP_004296667.1	86 %	2.00E-80	39.19%									WP_004296987.1	40 %	4.00E-04	22.02%	WP_004298042.1	53 %	0.002	24.41%
Parabacteroides distasonis ATCC 8503	WP_005862015.1	72 %	4.00E-70	40.50%	WP_011967204.1	53 %	1.00E-22	31.25%													WP_005862015.1	76 %	2.00E-69	39.67%																
Prevotella copri DSM 18205	WP_040553047.1	73 %	6.00E-69	39.19%	WP_050758659.1	52 %	1.00E-21	32.63%													WP_040553047.1	95 %	7.00E-72	35.53%													WP_040553047.1	19 %	0.005	41.30%
Clostridium sporogenes ATCC 15579	WP_003488218.1	60 %	1.00E-58	42.52%																	WP_003488218.1	71 %	6.00E-57	38.34%																
Enterococcus faecalis V583	AAO82710.1	76 %	3.00E-47	33.77%					WP_002358908.1	36 %	5.00E-07	26.60%									AAO82710.1	70 %	2.00E-41	33.33%									WP_002358908.1	45 %	3.00E-04	23.58%	WP_011109565.1	98 %	1.00E-36	32.26%
Enterococcus faecium ATCC BAA-472	AFK57873.1	45 %	6.00E-42	42.68%																	AFK57873.1	47 %	6.00E-36	40.00%									WP_002289461.1	43 %	1.00E-07	29.27%	WP_002289259.1	94 %	8.00E-32	30.51%
Lactobacillus ruminis ATCC 25644	WP_003697683.1	57 %	3.00E-38	36.00%													EFZ34801.1	68 %	1.00E-23	27.71%	WP_003697683.1	70 %	5.00E-41	36.57%													WP_003698387.1	99 %	5.00E-28	28.51%
Ruminococcus gnavus ATCC 29149	WP_004844482.1	55 %	9.00E-46	38.06%																	WP_009243941.1	65 %	3.00E-45	34.89%																
Fusobacterium nucleatum subsp. nucleatum ATCC 23726					WP_005904212.1	98 %	2.00E-23	23.55%																																
Edwardsiella tarda ATCC 23685	WP_005289490.1	100 %	0.00E+00	77.78%					WP_003559515.1	98 %	2.00E-95	52.76%	WP_005293620.1	96 %	1.00E-22	29.07%	WP_005290670.1	72 %	1.00E-90	58.33%	WP_005281724.1	98 %	0.00E+00	62.00%	EFE24848.1	99 %	6.00E-116	78.42 %	WP_035594481.1	72 %	3.00E-67	69.47%	WP_005290526.1	73 %	1.00E-82	64.02%	WP_005281220.1	100 %	4.00E-72	47.39%
Enterobacter cancerogenus ATCC 35316	WP_006173627.1	100 %	0.00E+00	91.86%	WP_006175848.1	99 %	1.00E-175	76.59%	WP_006172172.1	99 %	2.00E-166	85.55%	WP_006177897.1	92 %	7.00E-11	25.82%	WP_006179259.1	100 %	0.00E+00	84.85%	WP_006178828.1	100 %	0.00E+00	81.98%	WP_006178565.1	100 %	2.00E-116	83.77 %	WP_006174705.1	100 %	5.00E-128	90.00%	WP_006177897.1	100 %	6.00E-144	73.54%	WP_006178985.1	100 %	3.00E-114	67.08%
Escherichia coli K12 MG1655	WP_000753946.1	100 %	0.00E+00	90.15%	HBP13235.1	100 %	0.0	81.06%	HBP13030325.1	98 %	2.00E-164	85.43%	HBP15585523.1	90 %	2.00E-09	24.69%	WP_000487654.1	100 %	0.00E+00	79.70%	WP_000105733.1	99 %	6.00E-122	83.16%	WP_000105733.1	99 %	6.00E-122	83.16 %	WP_000587933.1	100 %	3.00E-128	91.11%	HBP1284551.1	99 %	2.00E-149	76.95%	HBP1324492.1	100 %	1.00E-96	57.03%
Klebsiella pneumoniae subsp. pneumoniae KPNIH1	WP_002889286.1	100 %	0.00E+00	100.00 %	WP_00210108.1	100 %	0.00E+00	100.00 %	WP_004152229.1	100 %	0.00E+00	100.00%	WP_004151556.1	100 %	0.00E+00	100.00%	WP_002883412.1	100 %	0.00E+00	100.00%	WP_00218566.1	100 %	0.00E+00	100.00%	WP_00216845.1	100 %	8.00E-144	100.00 %	WP_002900775.1	100 %	6.00E-138	100.00 %	WP_002920511.1	100 %	0.00E+00	100.00 %	WP_004152017.1	100 %	5.00E-180	100.00%
Akkermansia muciniphila ATCC BAA-835	ACD04643.1	73 %	9.00E-58	35.75%																	ACD04643.1	88 %	1.00E-52	30.98%																
Homo sapiens	3NZI_A	49 %	1.00E-45	43.03%	BAG573800.1	58 %	1.00E-22	33.88%	NP_683711.2	91 %	3.00E-40	35.63%					3HJU_A	76 %	2.00E-05	25.19%	NP_444272.1	65 %	3.00E-45	37.58%									NP_001378938.1	40 %	3.00E-06	30.17%